ABSTRACT

Title of Document: A PHYSICAL CHEMIST'S GUIDE TO APPLIED COMPUTATIONAL CHEMISTRY: PRACTICAL CALCULATION OF POLYPROTIC ACID PKA VALUES, MERCURY HALIDES, THIOLS, AND METHYLMERCURY ANALOGUES' STABILITIES AND STRUCTURES, AND RAMAN SPECTRA OF MYO-INOSITOL HEXAKIS PHOSPHATE.

Merle McKinley Dickerson Zimmermann, Ph. D., 2011

Directed By: Dr. John Tossell, Chemistry Department

In this thesis, we present both *ab-initio* investigation of the series of compounds $HgCl_x^y$ and the charges of each system running x=(0,1,2,3,4) and y=(+2,+1,0,-1,-2).

We investigate the energies of formation using Gaussian 03 (G03), a quantum chemistry package. In our calculations, $HgCl_3^{-1}$ was most stable in the gas phase, and $HgCl_2^0$ the most stable in the polarizable continuum model water-solvated phase. The addition of a solvent layer of $H_2O$ molecules did not significantly affect the results.

DFT calculations on the series running between $HgCl^+$, through $HgCl_2^0$, and $HgCl_3^{-1}$ compounds done with the Amsterdam Density Functional (ADF) program from Scientific Computing and Modeling (SCM) yielded absolute Hg NMR shieldings with a $\Delta$ of approximately -1000 ppm for each additional atom of Chlorine bonding to the Mercury for the first two additions.

We also investigate $H_3PO_4$, $H_3AsO_4$, and the $HClO_x$ acid series with x=(1,2,3,4). We have succeeded in determining pKas with theoretical quality results within 2 kcal/mol of experimental measurement for the majority of the systems examined by use of a discovered linear correlation between experimental and calculated pKa values.

Finally, we present our contribution to a joint project involving myo-inositol hexakis phosphate with an experimental group, confirming the observed experimental trends seen in the Raman spectra.

# A PHYSICAL CHEMIST'S GUIDE TO APPLIED COMPUTATIONAL CHEMISTRY: PRACTICAL CALCULATION OF POLYPROTIC ACID PKA VALUES, MERCURY HALIDES, THIOLS, AND METHYLMERCURY ANALOGUES' STABILITIES AND STRUCTURES, AND RAMAN SPECTRA OF MYO-INOSITOL HEXAKIS PHOSPHATE.

By

Merle McKinley Dickerson Zimmermann.

Dissertation submitted to the Faculty of the Graduate School of the
University of Maryland, College Park, in partial fulfillment
of the requirements for the degree of
Ph. D.
2011

Advisory Committee:
Professor John Tossell, Chair
Janice Reutt-Robey
Millard Alexander
Wendell T. Hill, III
Yu Huang Wang

# Preface

The following work is presented in the hope that it may inspire further cooperation and collaboration between physical chemistry experimentalists and applied computational theory, and hope that the included successes and suggestions are useful both to new applied computational chemists getting started and physical chemists interested in applying computational chemistry techniques to shed more light on experimental problems.

# Dedication

We would like to dedicate this work to Dr. Tossell, who showed near infinite amounts care and patience as this work was slowly completed under his supervision, and his laboratory, whose focus on applying computational chemistry to environmental and geochemical mysteries shed much useful light and inspiration across the dark world of the unknown. We also would like to acknowledge the invaluable support provided by friends and family, especially S. Vinnikova, whose help with proofreading was indispensable. Thank all of you very much. This would not have been possible without you.

# Acknowledgements

This thesis is the result of support from many different people and groups, to all of whom we would like to extend our highest gratitude.

To begin, we would like to thank our sources of funding and financial support, including NSF Grant EAR0539109, DOE Grant DE-FG02-94ER14467, the NSF-MRSEC at the University of Maryland, College Park DMR#0520471, and an ARCS Foundation's Achievement Awards for College Scientists Fellowship received in 2008 by the author.

We would also like to acknowledge G. R. Helz for suggesting the arsenic system for study, D.A. Dixon and M. H. Alexander for suggesting excellent references, fellow graduate students E. Khaskin, and Liang T. for suggestions and . We would also like to thank L. Heighton for collaborating on the myo-inositol phosphate theoretical study with experimental results. We would also like to acknowledge the invaluable assistance of Parallel Quantum Solutions for both kindly and excellent after-market technical support of their QuantumCube™ chemistry cluster used to calculate the NMR data presented in Chapter 4.

Finally, we also acknowledge S. Vinnikova for her great assistance in proofreading, countless helpful suggestions and moral support during the writing of this thesis.

# Table of Contents

# List of Tables

# List of Figures

# List of Equations

(3.1) $$\hat{H} = -\frac{\hbar^2}{2\mathrm{m}} \sum_{i=1}^{n} \nabla_i^2 - \sum_{i=1}^{n} \frac{Ze'^2}{r_i} + \sum_{i=1}^{n} \sum_{j>i} \frac{e'^2}{r_{ij}}$$

(3.2) $$\hat{H}\psi = E\psi$$

(3.3) $$\varphi = \prod_i s_i(r_i, \theta_i, \varphi_i)$$

(3.3a) $$s_i = \sum_k c_{ik} b_k(r_i, \theta_i, \varphi_i)$$

(3.4) $$V_{ij} = e'^2 \int \frac{|s_j|^2}{r_{ij}} dv_j$$

(3.5) $$V_i(r_i, \theta_i, \varphi_i) = \sum_{j \neq i} e'^2 \int \frac{|s_j|^2}{r_{ij}} dv_j - \frac{Ze'^2}{r_i}$$

(3.6) $$V(r_i) = \frac{\int_0^{2\pi} \int_0^{\pi} V(r_i, \theta, \varphi) \sin\theta \, d\theta \, d\varphi}{\int_0^{2\pi} \int_0^{\pi} \sin\theta \, d\theta \, d\varphi}$$

(3.7) $$[-\frac{\hbar^2}{2\mathrm{m}} \nabla_i + V(r_i)] t_i(1) = \epsilon_i t_i(1)$$

(3.8) $$[-\frac{\hbar^2}{2\mathrm{m}} \nabla_i + V(r_i)] t_i(1) - \epsilon_i t_i(1) = 0$$

(3.9) $$E_{atomic}=\sum_{i=1}^{n}\epsilon_i-\sum_i\sum_{j>i}\int\int\frac{e'^2|s_i(i)|^2|s_j(j)|^2}{r_{ij}}dv_i dv_j$$

(3.10) $$\hat{H}=-\frac{\hbar^2}{2\mathrm{m}}\sum_i\nabla_i^2-\sum_\alpha\sum_{i=1}^{n}\frac{Z_\alpha e'^2}{r_i}+\sum_{i=1}^{n}\sum_{j>i}\frac{e'^2}{r_{ij}}-\frac{\hbar^2}{2\mathrm{m}_\alpha}\sum_\alpha\nabla_\alpha^2+\sum_\alpha\sum_{\beta>\alpha}\frac{Z_\alpha Z_\beta}{r_{\alpha\beta}}$$

(3.11) $$V_{NN}=\sum_\alpha\sum_{\beta>\alpha}\frac{Z_\alpha Z_\beta}{r_{\alpha\beta}}$$

(3.12) $$\hat{H}_{el}=-\frac{\hbar^2}{2\mathrm{m}}\sum_i\nabla_i^2-\sum_\alpha\sum_{i=1}^{n}\frac{Z_\alpha e'^2}{r_i}+\sum_{i=1}^{n}\sum_{j>i}\frac{e'^2}{r_{ij}}$$

(3.13) $$\hat{F}=\hat{H}_{el}+V_{NN}=-\frac{\hbar^2}{2\mathrm{m}}\sum_i\nabla_i^2-\sum_\alpha\sum_{i=1}^{n}\frac{Z_\alpha e'^2}{r_i}+\sum_{i=1}^{n}\sum_{j>i}\frac{e'^2}{r_{ij}}+\sum_\alpha\sum_{\beta>\alpha}\frac{Z_\alpha Z_\beta}{r_{\alpha\beta}}$$

(3.14) $$E_{HF}=\langle D|\hat{F}|D\rangle=\langle D|\hat{H}_{el}+V_{NN}|D\rangle=2\sum_{i=1}^{n/2}h_i+\sum_{i=1}^{n/2}\sum_{j=1}^{n/2}(2\mathrm{J}_{ij}-K_{ij})+V_{NN}$$

(3.15) $$h_i=\langle\varphi_i(1)|-\frac{1}{2}\nabla_i^2-\sum_\alpha\frac{Z_\alpha}{r_{1\alpha}}|\varphi_i(1)\rangle$$

(3.16) $$J_{ij}=\langle\varphi_i(1)\varphi_j(2)|\frac{1}{r_{12}}|\varphi_i(1)\varphi_j(2)\rangle$$

(3.17) $$K_{ij}=\langle\varphi_i(1)\varphi_j(2)|\frac{1}{r_{12}}|\varphi_j(1)\varphi_k(2)\rangle$$

(3.18) $$\hat{F}(1)\varphi_i(1)=\epsilon_i(1)\varphi_i(1)$$

(3.19) $$\varphi_i = \sum_k c_{ki} \chi_k$$

(3.20) $$\hat{F} \varphi_i = \hat{F} \sum_k c_{ki} \chi_k = \sum_k c_{ki} \hat{F} \chi_k = \epsilon_i \sum_k c_{ki} \chi_k$$

(3.21) $$\sum_k c_{ki} (F_{jk} - \epsilon_i S_{jk}) = 0$$

(3.22) $$F_{jk} = \langle \chi_j | \hat{F} | \chi_k \rangle$$

(3.23) $$S_{jk} = \langle \chi_j | \chi_k \rangle$$

(3.24) $$det(F_{jk} - \epsilon_i S\, jk) = \begin{vmatrix} F_{11} - \epsilon_i S_{11} & F_{21} - \epsilon_i S_{21} & \cdots \\ F_{12} - \epsilon_i S_{12} & F_{22} - \epsilon_i S_{22} & \cdots \\ \vdots & \vdots & \ddots \end{vmatrix} = 0$$

(3.25) $R(\mathbf{r}) = \mathbf{r}^{n-1} e^{-\zeta \mathbf{r}}$ ($\mathbf{r}$ = radial distance to the nucleus)

(3.26) $E_n = E_{CBS} + An^{-3}$

(4.1) $E_n = E_{CBS} + An^{-3}$

(4.2) $E_{CBS} = E_n - An^{-3}$

(4.3) $E_{CBS} = (27/19)E_3 - (8/19)E_2$

(5.1) $$K_a = \frac{[H+][A-]}{[HA]}$$

(5.2) $$pK_a = -\log K_a = -\log\left(\frac{[H+][A-]}{[HA]}\right)$$

(5.3) $$pH = -\log [H+]$$

(6.1) $\Delta G_{rxn} = \Delta G(A^-_{gas}) - \Delta G(AH_{gas}) + \Delta G_s(AH) - \Delta G_s(AH) - 269.0$ kcal/mol

(6.2) $pKa_{expt} = 0.429\ pKa_{CBS\text{-}QB3\ CPCM\ w/H2O} - 0.233$

(7.1) $pKa_{fitted} = 0.429\ pKa_{CBS\text{-}QB3} - 0.233$

(11.1) $pKa_{expt} = 0.429\ pKa_{CBS\text{-}QB3\ CPCM\ w/H2O} - 0.233$

# Chapter 1: General Overview

## *1.1 Background*

Theoretical chemistry as a science has continued to develop as the years have passed and computational technology has advanced. At the current time, it is possible to apply computational chemistry to analyze many physical chemistry situations which were not within reach in the past. While a dedicated theoretician is essential for detailed study, it is also possible for a general physical chemistry laboratory to do calculations on their on or in conjunction with a theoretical group.

We hope in this thesis to promote further collaboration between experimental and theoretical groups, and to encourage experimental groups without access to a dedicated theorist to consider the possibilities of adding such calculations to their repertoire of scientific tools.

We therefore present the following, where we show an example of theoretical chemistry as applied to computational analysis of molecules including mercury (with Gaussian 03[1], for example), and present it as a safe way to explore these hazardous compounds [2] and supplement experimental results with less risk to the scientific group.

Our selection of mercury as our focus of study was twofold.

Mercury pollution from human sources is ongoing, and an improved understanding of the chemistry of the chemical will provide opportunities for us to deal with the consequences of an industrialized society in a logical and well-informed manner. We discuss some of the anthropological consequences of mercury chemistry in Chapter 2.

And in a pure scientific point of view, there are several notable things about mercury chemistry which are unique to this particular element:

- Mercury depletion during spring in the Arctic[3-8] is a notable phenomenon which has several successful computational contributions[3, 4], but with additional knowledge of mercury's stability and behavior could be further explained.
- Methylmercury compounds[1], especially as environmental pollutants, are one of the most recognized dangerous forms of mercury available in the environment[2, 9-21].
- Biological consequences of mercury pollution are well understood from a symptomatic side[2, 18, 19, 21, 22]. However, deeper understanding of the reasons why particular body systems are targeted by the compound would be useful in developing possible treatments.
- Solvation effects on relevant Mercury compounds. As we will show later, the

[1] Sadly, medical journals are quite vague about the particular formulae of the methylmercury compounds they mention. Presumably dimethylmercury, and $CH_3Hg^+Cl^-$ compounds are to blame.

change in chemical environment for a particular set of HgCl compounds going between the gas phase and the aqueous solution is enough to change which species is the most thermodynamically stable.

Modeling and understanding how mercury compounds behave in solution in addition to the gas phase is doubly important because most biological systems involve solvated phases (both aqueous and organic). We would suggest a future study examining how mercury compounds behave in a variety of common organic solvents aside from water, such as octanol, methanol, ethanol, THF, or ether[2].

We have modeled a variety of likely mercury compounds for a selection of the above listed situations via software: GAUSSIAN 03[1] and ADF[34-36] in particular were in use for these explorations.

In order to further understand the quality and reliability of the results of the mercury calculations which did not have experimental results readily available for comparison, we conducted a series of computations on the acidities of a variety of triply and doubly protonated polyprotic acid systems as well. Our goal in this case was to predict the deprotonation behavior of unknown polyprotic acids.

These systems were chosen with both light phosphorus central atoms and moderately

[2] We acknowledge Eugene Khaskan from Dr. Vedernikov's laboratory for suggesting most of these solvents from his work with catalysts in a discussion in early 2006.

heavy arsenic central atoms, to introduce d-shell electrons to the calculation and to show the behavior of our solvation methods on elements moving towards the part of the periodic table where mercury appears at atomic number 80.

Finally, the calculations on the phosphoric acid systems were extended by a collaboration with an experimental lab in calculating a set of spectra on Myo-Inositol hexakis phosphates to provide further insight into their identification and behavior and further demonstrate the contributions that applied theory can bring to an experimental problem.

*1.2 Overview*

*For a guide to computational chemistry terms used in the discussion below, please see Chapter 3,* ***An Overview of Computational Chemistry Techniques****, where they are defined in sections 3.2 to 3.4 and discussed at further length.*

There were five main things which we explored in the production of this thesis.

Our primary goal was a study of mercury-halogen compounds in solvated systems. These calculations were most successful on the chloride compounds, which became our focus, and appear in Chapter 4.

We also discuss a series of Mercury thiol compounds for their application to undersea

sulfuous vents where mercury and sulfur would both be present naturally, and a number of methylated mercury compounds (methylmercury having been shown to be one of the most hazardous forms of the heavy metal). Our results in these areas appear in Chapter 8 and 9, after our discussion of the polyprotic acids, which were used as a measuring-stick to estimate the accuracy of the results in this type of theoretical calculation and appear in the thesis in Chapters 5 through 7.

Finally, we discuss the *ab inito* calculations on the pH dependence of Myo-Inositol Hexakis Phosphate's Raman Spectra, which appear in Chapter 10.

In each case, we present the set-up for our selected problem and discuss possible future calculations which would expand upon what we presented here.

Finally, we discuss a few of the initial results which we produced for the mercury chloride systems discussed at length in Chapter 4.

### 1.2.1 – Mercury-Chloride Compounds in Solution

The main species of interest in this series were as follows:

$Hg^{+2}$, $HgCl^{+}$, $HgCl_2$, $HgCl_3^{-}$, $HgCl_4^{-2}$, and $Cl^{-}$.

We planned to use CCSD[24] with a CEP-121G basis[25, 26] to run the calculations. The CCSD method is advantageous to us because we expect that mercury will show significant electron correlation effects because of the large number of near-valence electrons. Our preferred choice of basis set is CEP-121G, since mercury exhibits relativistic effects and the core effective potential basis allows us to take some of these into account implicitly. We also intended to conduct a selection of these calculations using MP2 and B3LYP as well.

B3LYP[27] is a hybrid method that allows for higher quality results than Hartree-Fock, but at a more modest computational cost than corresponding higher-level methods (such as Gaussian-1[28]). This method has been shown [29] to provide reasonable results in comparison to CCSD(T) calculations for some Hg complexes already.

Second, after running each calculation in the gas phase, we will calculate the stabilization energy of hydration using a polarizable continuum model, CPCM with a reduced basis set. This type of model accounts for solvation energies by placing the calculated electron density in a cavity of an infinite dielectric modeled to match the characteristics of the solvent. The solvation energy depends on electron density, and we assume here, based upon unpublished internal lab experience, that it converges spatially to a scale where those numbers are stable at a level of theory. In many cases, we also modeled the CCSD or B3LYP calculations in the polarizable

continuum model. Explicit water molecules were also used for solvation in some cases.

Third, we use ADF[34-36] to calculate NMR shieldings[37-39] on the HgCl compounds after the Gaussian calculations are done. In ADF, we will use the Zeroth Order Relativistic Approximation[30] to take into account the effects of relativity on the inner shell electrons of Mercury in our all-electron calculations of the compounds.

Finally, we run portions of the above series of calculations with $F^-$, $Br^-$, and $I^-$ substituted for $Cl^-$. This extension provides us with a better understanding of the differences in halogen chemistry exhibited by mercury. We also did a variety of Complete Basis Set extrapolations for the four systems.

In some cases calculations with the solvating water molecules were not conducted due to limited time. The completed calculations are described in the appropriate chapters. The remainder of the systems mentioned above, but not explored, would be an ideal project for further explorations.

A future effort would definitely include additional solvation calculations with polarizable continuums tuned to the properties of the other solvent compounds. This would allow us to compare the effects of different solvents on the equilibria of the compounds above, and if time allowed, we would also substitute the alcohols and

other solvating agents mentioned in the introduction for water in some of the smaller complexes (the larger ones, we calculate with B3LYP instead of CCSD).

Explicit solvation could also be further explored via use of a molecular dynamics study. In the future, calculations with the CPMD [23] molecular dynamics package, for example, could be used to conduct further calculations. Its direct support of periodic boundary conditions would allow sampling of many different explicit bonding situations and the collection of statistical mechanics information about the behavior of the complexes. A possible plus is that the high computational cost of this kind of calculation will be less of an expense in the future, as this kind of model scales well with the number of CPUs working on the problem and it appears that increasing parallelization is the direction that computer system development is currently taking.

### 1.2.2 – Mercury-Thiol Complexes

Another project was to examine $Hg(SH)_2$ complex formation, geometries, and the resulting energetics of each different type of complex using B3LYP, MP2, CCSD, MP3, and MP4 with the CEP-121G basis set and the differences between these approaches compared to each other.

### 1.2.3 – Methylmercury compounds

One of the main goals of this segment of research was to do a variety of calculations upon methylmercury compounds, which have a (well-deserved) reputation for being dangerous to experimenters handling them. In a recent occurrence written up in

1998, a researcher at Dartmouth was conducting NMR research on mercury compounds and was exposed to a dimethylmercury standard through her latex gloves, which did not provide protection against the compound [33]. The slight exposure lead to a condition of mental degeneration which rapidly progressed over the course of a year, resulting in the researcher's death. Chelation therapy treatments were unfortunately not effective enough to prevent the scholar's fate.

We conducted a number of stability and structure calculations on methylmercury halides, described in Chapter 4, with the goal of demonstrating it is currently possible to safely investigate the behavior of these hazardous compounds via theoretical chemistry.

However, the calculations on the mercury compounds are of charged ion species, which stresses the theory applied to produce their results. We therefore started a side project to further confirm the quality of those other results by proceeding with calculations on a few systems which have been exhaustively explored in experiments. In this way, the quality of the results in the mercury calculations can be measured practically by comparing the quality of the similar systems against experimental results.

### 1.2.4 – Polyprotic Acid pKa Calculations: phosphoric, arsenic, and others

We selected a variety of polyprotic acids to investigate to address this concern. These

would give us a system which both matched the mercury ones in having moderately sized ionic species of different total charges such as the phosphoric acids, as well as having moderately heavier central atoms in the case of the As-based systems.

As arsenic appears in the middle of the periodic table with 33 electrons, the accuracy of the results calculated on it will give a better feel for the 80-electron mercury atom calculations than results on lighter atoms.

To begin, we did a number of calculations on $H_3PO_4$ in detail to reproduce experimental pKa values for the multiply deprotonated ion. pKa values depend strongly on the free energy of the ion, to the order of 1 kcal/mol, which is approximately 0.0015 Hartrees. Therefore, a study of pKa values and their relation to the experimental measurements of the same would be a good "acid" test of the accuracy of our chosen models.

We therefore calculated optimized geometries and single point energies for $H_3PO_4$, $H_2PO_4^-$, $HPO_4^{2-}$, and $PO_4^{3-}$ using the CBS-QB3 model chemistry, MP2 with the CBSB7 basis set, and CPCM polarizable continuum calculations done both separately (on the gas phase geometries of the species) and in conjunction (during the CBS-QB3 and MP2 calculations) with the two computational methods. We also did solvation calculations with an explicit $Na^+$ counterion which was used to reduce dependence on the CPCM model for finding the stabilized energy.

The CPCM single point stabilization energies were calculated in the gas phase conditions with self-consistent electron cloud geometries found from HF calculations at the gas phase geometries with three different basis sets, 6-31G, 6-31G**, and G-31+G**.

Overall, the energies found from the solvation calculations with explicit Na+ counterions were closest to experimental measurement, although there were issues with converging the geometries in some cases.

Possible future calculations might include molecular dynamics (MD) calculations with each species and $Na^+$ counterions to sample their statistical behavior. Anticipated difficulties would of course include the usual concern with MD, where the size of the periodic boundary conditions causes an effective concentration of the analyte that is not realistic, but future advances in computer speeds as well as the inherent parallelizability of MD methods should allow for easy calculations in sufficiently large reaction volumes that the concentration of the acid would be quite reasonable in the near future.

Another possible avenue of exploration would be to do more modeling using the CBS-QB3 model chemistry with additional explicit solvent molecules. This would provide more opportunities for directly calculated solute-solvent interactions rather

than the simpler and less computationally expensive solvation models such as the polarizable continuum (used extensively in our work here), which have some shortcomings such as not allowing for hydrogen bonding.

We continued demonstration of the quality of the calculations by doing some more in a similar direction on a variety of arsenic compounds.

Arsenic compounds were chosen for several reasons. First, they are important both environmentally, due to their easy availability in the geosphere, and the ease by which arsenic compounds can affect the human condition. A semi-metal of atomic number 33, arsenic is a good way down the periodic table towards mercury (atomic number 80). Arsenic has a full 3d orbital while mercury compounds usually has three filled d shells. Arsenic was therefore a middle step in going from the light P atoms to the heavy Hg atoms in similar chemical conditions.

Therefore, we followed up our calculations on phosphoric acid with similar ones on some common arsenic and arsenous acids. The species of interest were $H_3AsS_3$, $H_3AsS_4$, $H_3AsO_3$, $H_3AsO_4$, $H_3PO_4$, $H_3SO_4$. Later we also did calculations on the deprotonations of $H_3SO_3$ species.

Methods used were CBS-QB3, CCSD, and CCSD(T). The CBS-QB3 model chemistry included geometry optimization and vibrational frequency calculations, and

the CCSD and CCSD(T) calculations were done with these as well.

Hydration was modeled in several ways. Arguably the most successful in this case was conducted with a single explicit water molecule and the CPCM solvation model applied to the system at the same time as the geometry optimizations. Solvation calculations were done with and without the explicit water molecule's presence and either with the geometry optimization done with the solvation model present or the solvation energy estimated at the gas phase geometry of the system.

Optimization with the CPCM therefore produced B3LYP/CBSB7 CPCM optimized geometries in the case of the CBS-QB3, as the geometry optimization step in that method uses the B3LYP hybrid density-functional model.

The final results for the $H_3PO_4$ and $H_3AsO_4$ and $H_3AsO_3$ were then compared to available experimental data, and we noticed a distinct correlation between the theoretical calculations and the measurements. This led us to construct a linear fit between the two sets of data which was then checked against $H_3SO_3$ theoretical calculations and experimental measurements conducted later. The results for $H_3SO_3$ were not used to construct the fit.

Finally, a series of the same sort of calculations were conducted on HClO, $HClO_2$, $HClO_3$, and $HClO_4$ with counterions.

The quality of the data before and after the fit can be used to evaluate some of the assumptions made for the mercury calculations. We can see that although before fitting our calculated trends were OK for the highly charged anions, the higher the charge the lower the quality of the results, very much so when compared to the ones with neutral or singly-charged species.

### 1.2.5 – Raman Spectra of Myo-Inositol Phosphates

The final project was to calculate theoretical Raman (and IR) spectra of different forms of Myo-Inositol hexakis phosphate (IHP) to compare and shed light on an experimental study of the compound[40] conducted across a variety of pH conditions from strongly acidic to neutral to strongly basic. In this case we decided to begin with Hartree-Fock (HF) calculations done with a minimal 6-31G basis due to the size of IHP, followed by higher level methods. Raman and IR spectra from the HF calculations as well as some B3LYP IR spectra were ready as of the time of this writing, and they are presented here. The results were favorable, reproducing the experimental trends presented at ACS[40], and further calculations currently in progress as well as those described here will be the subject of a future joint paper.

*1.3 Initial Results and Discussion*

As was presented at the NOBCChE Conference in 2006, many of our first calculations on the $HgCl_x$ series of species were completed using GAUSSIAN 03 (G03) and ADF. Interpretations of the raw results (which are summarized in Tables 1.1 and 1.2) are in the following *Conclusions* section.

GAUSSIAN 03 (G03) calculations were set up with starting geometries slightly differing from the highest symmetry, to allow for possible asymmetric bond distances to develop or be extinguished as the geometry optimizations saw fit. This avoided some cases which appeared when symmetric starting geometries were chosen accidentally on saddle points, such as appeared in some of the

Table 1.1 summarizes the G03 calculations, and appears below. They were run using CCSD with the CEP-31G and CEP-121G basis sets. The CEP-121G calculations showed less of an apparent basis set overlap error than the CEP-31G calculations; the energies of the smaller complexes were closer to that of the larger ones.

Hydration energy calculations are done with HF and the CEP-31G basis at the single point of the final geometry. We used the Conducting Polarizable Continuum Method, CPCM, to run the self-consistent reaction field (SCRF) calculation.

| HgClx | CCSD Energy | 1 Hartree = 627.5 kcal/mol | | | Delta G |
|---|---|---|---|---|---|
| | CEP-31G | | CEP-121G basis | | Hydration E |
| | Hartrees | kcal/mol | Hartrees | kcal/mol | kcal/mol |
| Cl- (singlet) | -14.873432 | **-9333.0786** | -14.902545 | -9351.34699 | -76.55 |
| Cl0 (doublet) | -14.775784 | -9271.80446 | | | |
| Cl2 (singlet) | -29.613822 | -18582.6733 | | | 1.43 |
| Cl+ (singlet) | -14.252053 | -8943.16326 | | | -68.79 |
| Hg+2 | -152.141721 | **-95468.93** | -152.159227 | -95479.9149 | -407.17 |
| Hg0 | -153.181514 | -96121.4 | | | -0.46 |
| HgCl+ | -167.646138 | **-105197.95** | -167.68025 | -105219.357 | -139.85 |
| HgCl2 0 | -182.87579 | -114754.558 | -182.922266 | -114783.722 | -20.68 |
| HgCl3 - | -197.824502 | -124134.875 | -197.890057 | -124176.011 | -47.26 |
| HgCl4 -2 | -212.636335 | -133429.3 | -212.717105 | -133479.983 | -160.89 |
| | | | | Delta E | |
| CEP-31G | Hg+2 | + Cl- -> | HgCl+ | Sum(Prod.)-Sum(React.) | |
| CCSD E | **-95468.93** | **-9333.0786** | **-105197.95** | -395.943088 | Total Delta E |
| Hydration E | -407.17 | -76.55 | -139.85 | 343.87 | -52.07 |
| | | | | **CEP-121G E=** | **-44.22** |
| CEP-31G | HgCl+ | + Cl- -> | HgCl2 0 | | |
| CCSD E | -105197.952 | -9333.07858 | -114754.558 | -223.52805 | |
| Hydration E | -139.85 | -76.55 | -20.68 | 195.72 | -27.81 |
| | | | | **CEP-121G E=** | **-17.30** |
| CEP-31G | HgCl2 0 | +Cl- -> | HgCl3 - | | |
| CCSD E | -114754.558 | -9333.07858 | -124134.875 | -47.2382 | |
| Hydration E | -20.68 | -76.55 | -47.26 | 49.97 | 2.73 |
| | | | | **CEP-121G E=** | **9.03** |
| CEP-31G | HgCl3 - | +Cl- -> | HgCl4 2- | | |
| CCSD E | -124134.875 | -9333.07858 | -133429.3 | 38.6533725 | |
| Hydration E | -47.26 | -76.55 | -160.89 | -37.08 | 1.57 |
| | | | | **CEP-121G E=** | **10.29** |

Table 1.1: $HgCl_x$ compound energies of reaction in the gas phase and with CPCM hydration.

Calculations were first run with the specified basis sets and the OPT FREQ keywords. On the occasions where the first run was unsuccessful in attaining the final geometry (due to our starting geometries being too distant from equilibria to converge in the default short run length), the geometries were then copied out in Cartesian coordinates, and the software used its standard symmetry detection methods to

accelerate computation.

After the geometry was converged, second calculations with HF 6-31G and SCF=CPCM were executed at the final geometries of the calculation. This schema, recommended by Dr. Tossell from experience and so the results would be compatible with other ones within the Tossell Group, is used to estimate the solvation energy of each complex.

As is outlined in Table 1.1 (where following the bold numbers to illustrates how each figure is calculated), we determine the change in free energy of reaction from our intermediate calculations. The ΔG values are reported in each of the GAUSSIAN results for vibrational spectra calculations as the $\Delta G_{formation}$ of each species.

We would like to suggest that the new GAUSSIAN user read the excellent text *Exploring Chemistry with Electronic Structure Methods*, which we would like to acknowledge for its usefulness in getting familiar with the GAUSSIAN system and its implementation of theoretical chemistry methods.

ADF (Amsterdam Density Functional)[34-36], a program from SCM (Scientific Computing and Modeling), was used to do DFT[31] calculations with a TZ2P basis set without frozen core electrons. The XC was GGA Becke Perdew[32]. The ZORA[30] was used to model relativistic effects on the Hg electrons, and the

calculations were run with and without excitations allowed, and NMR shieldings were calculated[37-39].

Table 1.2, below, summarizes the ADF calculation results.

ADF Calculations on HgClx series

| HgClx with Excitations | Bond Energy LDA+GGA-XC (atomic units) | NMR Shielding (ppm) Hg | Cl |
|---|---|---|---|
| Hg atom (solvated) | 0.52212496 | 9909.5 | |
| HgCl | 0.29870258 | 10077.44 | -867.59 |
| HgCl (solvated) | 0.14661713 | 9109.17 | 618.35 |
| HgCl2 | -0.18954049 | 7306.67 | 807.37 |
| HgCl2 (solvated) | -0.20115095 | 7444.05 | 894.14 |
| HgCl3 | -0.39838704 | 6538.59 | 892.1 |
| HgCl3 (solvated) | -0.47154059 | 6639.91 | 924.4 |
| HgCl4 | -0.47052597 | 6764.95 | 929 |
| HgCl4 (solvated) | -0.73686043 | 6483.6 | 967 |
| | | | |
| HgClx with No Excitations | | | |
| Cl atom | 0.07361672 | | |
| Hg atom | 1.09951364 | 9909.71 | |
| HgCl | 0.29870215 | 10077.22 | -867.23 |
| HgCl (solvated) | 0.14661688 | 9109.25 | 618.29 |
| HgCl - H2O | -0.293957 | 8198.2 | 580.16 |
| HgCl - H2O (solvated) | -0.39646566 | 8055.78 | 792.71 |
| HgCl2 | -0.18954118 | 7306.71 | 807.33 |
| HgCl2 (solvated) | -0.20115224 | 7443.37 | 894.22 |
| HgCl2 - 2H2O | -1.23904561 | 7259.04 | 841 |
| HgCl2 - 2H2O (solvated) | -1.25297228 | 7335.65 | 865 |
| HgCl3 | -0.39838715 | 6538.56 | 892.1 |
| HgCl3 (solvated) | -0.4715399 | 6639.9 | 924.4 |
| HgCl3 - H2O | -0.93251747 | 6571.58 | 2x869, 1x895 |
| HgCl3 - H2O (solv) | -0.99475377 | 6715.55 | 937 |
| HgCl3 - 2H2O (solv) | -1.52886988 | 6651.42 | 910 |
| HgCl4 | -0.47052725 | 6764.95 | 929 |
| HgCl4 (solvated) | -0.7368604 | 6483.76 | 967 |
| HgCl4 - 2H2O | -1.56246352 | 6702.4 | 914 |
| HgCl4 - 2H2O (solvated) | -1.80401526 | 6510.32 | 935 |
| HgCl4 (flat) | 0.47050426 | 6778.92 | 927 |
| HgCl5 | (Geometry did not converge) | | |
| HgCl5 (solvated) | -0.95764149 | 6971.03 | 3x960, 2x810 |
| HgCl6 | (Geometry did not converge) | | |
| HgCl6 (solvated) | -1.17432797 | 7137.75 | 890, 905, and 969 |

Table 1.2: ADF NMR calculation results for compounds in $HgCl_x$ series.

The ADF data include both gas phase and PCM stabilized calculations (with and without explicit water molecules in the case of the calculations without excitations). The results with excitations were similar enough to the corresponding ones without that the author feels he has a reasonable case for confidence in the conclusions of the simpler computation[3]. These results are considered in detail at the end of Chapter 1.

We would like to thank the SCM team for their rather essential ADF-GUI, which was indispensible in setting up all of the jobs used to calculate NMRs.

Table 1.3, below, summarizes the counterpoise correction calculations we conducted at the beginning of the project. In the past, to correct for using smaller basis sets than were optimal, the counterpoise correction was developed to address the problem of the presence of nearby atoms increasing the quality of the basis sets near them. We attempted a number of calculations in GAUSSIAN 03 with ghost atoms in an effort to see the effects on the energy of stabilization by the basis size.

The author wishes to withhold judgment on these counterpoise results, however, since a related experiment which he observed yielded electron distributions well beyond the border of absurdity, having layouts where, for example, ligands' electrons ended up in (otherwise occupied) orbitals of the ghost heavy atom, and the electron clouds for these calculations were not shown to be reasonable.

[3] The simpler also being much easier for the author to converge, as it turned out.

| | **Ghost Atom Calculations** | | | | | |
|---|---|---|---|---|---|---|
| | Sum of electronic and thermal free energies | | | | | |
| Cl- in | | Hartrees | | | | |
| | | | *N Cl atoms | | | |
| HgCl+ | CEP121G | -14.926598 | 1 | -14.926598 | | |
| HgCl+ | CEP31G | -14.91592 | 1 | -14.91592 | | |
| HgCl2 0 | CEP121G | -14.934319 | 2 | -29.868638 | | |
| HgCl2 0 | CEP31G | -14.924157 | 2 | -29.848314 | | |
| HgCl3- | CEP121G | -14.943416 | 3 | -44.830248 | | |
| HgCl3- | CEP31G | -14.92414 | 3 | -44.77242 | | |
| HgCl4-- | CEP121G | -14.938398 | 4 | -59.753592 | | |
| HgCl4-- | CEP31G | -14.939102 | 4 | -59.756408 | | |
| | | | | | | |
| Hg2+ | | Hartrees | | | Actual Calc. | Delta |
| | | | | Sum | Hartrees | Hartrees |
| HgCl+ | CEP121G | -152.167682 | | -167.09428 | -167.68025 | -0.58597 |
| HgCl+ | CEP31G | -152.167631 | | -167.083551 | -167.646138 | -0.562587 |
| HgCl2 0 | CEP121G | -152.173626 | | -182.042264 | -182.922266 | -0.880002 |
| HgCl2 0 | CEP31G | -152.173557 | | -182.021871 | -182.87579 | -0.853919 |
| HgCl3- | CEP121G | -152.182321 | | -197.012569 | -197.890057 | -0.877488 |
| HgCl3- | CEP31G | -152.182305 | | -196.954725 | -197.824502 | -0.869777 |
| HgCl4-- | CEP121G | -152.190814 | | -211.944406 | -212.717105 | -0.772699 |
| HgCl4-- | CEP31G | -152.190793 | | -211.947201 | -212.636335 | -0.689134 |
| | | | | | | |
| | | | | Hg+2 | Cl- | |
| | | Lone Atom | | -152.159227 | -14.902545 | |
| | | Energy | | -152.141721 | -14.873432 | |

Table 1.3: Ghost atom calculations for Counterpoise Correction in $HgCl_2$ system.

The results of the calculation indicated a correction between $HgCl^+$ and $HgCl_2^0$ on the order of 200 kcal/mol (Conversion used: 1 Hartree = 627.5 kcal/mol) worth of apparent false stabilization. Comfortingly, the difference for the two species most interesting to us, $HgCl_2^0$ and $HgCl_3^{-1}$ is much less, being nearly a tenth that number. However, this figure *is* still quite significant, considering that 20kcal/mol is certainly on the scale of the differences in energy we calculated for the species.

To address any concerns about basis set size which may have appeared to be the case in the counterpoise calculation, we increased the basis set size by adding additional diffuse functions to all of the heavy atoms and focusing on the CEP-121G basis

instead of using the smaller CEP-31G.

The results were also assisted by including counterions in some cases, which reduced the total charges of the systems studied, and by showing that similar calculations done on As compounds with similar sizes of basis sets provided reasonable results *without* use of counterpoise corrections.

*1.4 Conclusions*

To summarize the conclusions of the calculations covered here, for the G03 calculations the most stable complex in solution was calculated to be $HgCl_2^0$. $HgCl_3^-$ was the most stable in the gas phase. This is presumably due to the lost hydration energy of the $Cl^-$ ion, which is less easy to hydrate when combined with $HgCl_2$ than alone.

In the ADF calculations, shieldings for Hg decrease by approximately 1000 ppm per $Cl^-$ added up to $HgCl_3^-$. $HgCl_4^{-2}$ does not continue the trend, however. Solvation by both the conducting polarizable continuum model (CPCM) alone and a CPCM system assisted by explicit $H_2O$ molecules yielded the same results as the gas phase ones.

*1.5 References*


1. Frisch, M.J., et al., *Gaussian 03, Revision B.03*. 2003, Gaussian, Inc.: Wallingford CT.
2. Nierenberg, D.W., et al., *Delayed cerebellar disease and death after accidental exposure to dimethylmercury.* New England Journal of Medicine, 1998. **338**(23): p. 1672-1676.
3. Goodsite, M.E., J.M.C. Plane, and H. Skov, *A theoretical study of the oxidation of Hg-0 to HgBr2 in the troposphere.* Environmental Science & Technology, 2004. **38**(6): p. 1772-1776.
4. Tossell, J.A., *Calculation of the energetics for oxidation of gas-phase elemental Hg by Br and BrO.* Journal of Physical Chemistry A, 2003. **107**(39): p. 7804-7808.
5. Khalizov, A.F., et al., *A theoretical study on the reactions of Hg with halogens: Atmospheric implications.* Journal of Physical Chemistry A, 2003. **107**(33): p. 6360-6365.
6. Ariya, P.A. and A. Ryzhkov, *Atmospheric transoformation of elemental mercury upon reactions with halogens.* Journal De Physique Iv, 2003. **107**: p. 57-59.
7. Lindberg, S.E., et al., *Dynamic oxidation of gaseous mercury in the Arctic troposphere at polar sunrise.* Environmental Science & Technology, 2002. **36**(6): p. 1245-1256.

8. Schroeder, W.H., et al., *Arctic springtime depletion of mercury.* Nature, 1998. **394**(6691): p. 331-332.

9. Jitaru, P. and F. Adams, *Toxicity, sources and biogeochemical cycle of mercury.* Journal De Physique Iv, 2004. **121**: p. 185-193.

10. Grigg, J., *Environmental toxins; their impact on children's health.* Archives of Disease in Childhood, 2004. **89**(3): p. 244-250.

11. Bisinoti, M.C. and W.F. Jardim, *Behavior of methylmercury in the environment.* Quimica Nova, 2004. **27**(4): p. 593-600.

12. Tchounwou, P.B., et al., *Environmental exposure to mercury and its toxicopathologic implications for public health.* Environmental Toxicology, 2003. **18**(3): p. 149-175.

13. Clarkson, T.W., L. Magos, and G.J. Myers, *The toxicology of mercury - Current exposures and clinical manifestations.* New England Journal of Medicine, 2003. **349**(18): p. 1731-1737.

14. Ullrich, S.M., T.W. Tanton, and S.A. Abdrashitova, *Mercury in the aquatic environment: A review of factors affecting methylation.* Critical Reviews in Environmental Science and Technology, 2001. **31**(3): p. 241-293.

15. Sweet, L.I. and J.T. Zelikoff, *Toxicology and immunotoxicology of mercury: A comparative review in fish and humans.* Journal of Toxicology and Environmental Health-Part B-Critical Reviews, 2001. **4**(2): p. 161-205.

16. Takizawa, Y., *Understanding minamata disease and strategies to prevent further environmental contamination by methylmercury.* Water Science and Technology, 2000. **42**(7-8): p. 139-146.

17. Satoh, H., *Occupational and environmental toxicology of mercury and its compounds.* Industrial Health, 2000. **38**(2): p. 153-164.

18. Morel, F.M.M., A.M.L. Kraepiel, and M. Amyot, *The chemical cycle and bioaccumulation of mercury.* Annual Review of Ecology and Systematics, 1998. **29**: p. 543-566.

19. Harada, M., *Minamata Disease - Methylmercury Poisoning in Japan Caused by Environmental-Pollution.* Critical Reviews in Toxicology, 1995. **25**(1): p. 1-24.

20. Boffetta, P., E. Merler, and H. Vainio, *Carcinogenicity of Mercury and Mercury-Compounds.* Scandinavian Journal of Work Environment & Health, 1993. **19**(1): p. 1-7.

21. Bakir, F., et al., *Methylmercury Poisoning in Iraq - Interuniversity Report.* Science, 1973. **181**(4096): p. 230-241.

22. Lohman, K., et al., *Sensitivity analysis of mercury human exposure.* Science of the Total Environment, 2000. **259**(1-3): p. 3-11.

23. *CPMD, Copyright IBM Corp 1990-2006, Copyright MPI für Festkörperforschung Stuttgart 1997-2001.*

24. Bartlett, R.J. and G.D. Purvis, *Many-body perturbation theory, coupled-pair many-electron theory, and the importance of quadruple excitations for the correlation problem.* Int. J. Quant. Chem., 1978. **14**(5): p. 561-581.

25. Stevens, W.J., H. Basch, and M. Krauss, *Compact effective potentials and efficient shared-exponent basis sets for the first- and second-row atoms.* J. Chem. Phys., 1984. **81**(12): p. 6026-6033.

26. Stevens, W.J., et al., *Relativistic compact effective potentials and efficient, shared-exponent basis sets for the third-, fourth-, and fifth-row atoms.* Can. J. Chem./Rev. can. chim., 1992. **70**(2): p. 612-630.

27. Becke, A.D., *Density-functional thermochemistry. III. The role of exact exchange.* J. Chem. Phys., 1993. **98**(7): p. 5648-5652.

28. Pople, J.A., M. Head-Gordon, and D.J. Fox, *Gaussian-1 theory: A general procedure for prediction of molecular energies.* J. Chem. Phys., 1989. **90**(10): p. 5622-5629.

29. Riedel, S., M. Straka, and M. Kaupp, *Validation of density functional methods for computing structures and energies of mercury(IV) complexes.* Physical Chemistry Chemical Physics, 2004. **6**(6): p. 1122-1127.

30. van Lenthe, E., E.J. Baerends, and J.G. Snijders, *Relativistic regular two-component Hamiltonians.* J. Chem. Phys., 1993. **99**(6): p. 4597-4610.

31. Perdew, J.P., et al., *Prescription for the design and selection of density functional approximations: More constraint satisfaction with fewer fits.* The Journal of Chemical Physics, 2005. **123**(6): p. 062201.

32. Perdew, J.P., et al., *Atoms, molecules, solids, and surfaces: Applications of the generalized gradient approximation for exchange and correlation.* Phys. Rev. B, 1992. **46**(11): p. 6671-6687.

33. Nierenberg, D.W., et al., *Delayed cerebellar disease and death after accidental exposure to dimethylmercury.* New England Journal of Medicine, 1998. **338**(23): p. 1672-1676.

34. Guerra, C.F., et al., *Towards an order-N DFT method.* Theoretical Chemistry Accounts, 1998. **99**.

35. Velde, G.t., et al., *Chemistry with ADF.* Journal of Compututational Chemistry, 2001. **22**: p. 931.

36. Baerends, E.J., et al., ADF2004.01, SCM, Theoretical Chemistry, Vrije Universiteit, Amsterdam, The Netherlands, http://www.scm.com. 2004.

37. Wolff, S.K., et al., *Density functional calculations of nuclear magnetic shieldings using the zeroth-order regular approximation (ZORA) for relativistic effects: ZORA nuclear magnetic resonance.* Journal of Chemical Physics, 1999. **110**: p. 7689

38. Schreckenbach, G. and T. Ziegler, *The calculation of NMR shielding tensors based on density functional theory and the frozen-core approximation.* International Journal of Quantum Chemistry, 1996. **60**.

39. Schreckenbach, G. and T. Ziegler, *The calculation of NMR shielding tensors using GIAO's and modern density functional theory.* Journal of Physical Chemistry, 1995. **99**.

40. Heighton, L.P. and W.F. Schmidt. *Raman spectra of organic (myo-inositol hexakis phosphate) and inorganic P spectra show pH dependence. in Proceedings of American Chemical Society National Meeting*. 2009. Washington, D.C.

# Chapter 2: Mercury Compounds in the Environment: An Overview of their Human Impact

## *2.1 Background*

The study of mercury is one fraught with hazard and danger. Since mercury is extremely hazardous in some forms, research has been understandably difficult to conduct with safety. The organic forms of mercury, especially methylmercury, are intensely poisonous. Since the death of a researcher at Dartmouth College caused by acute methylmercury poisoning [1], there is even more caution exercised when dealing with this hazardous compound. But although there is less experimentation with organic mercury complexes, it is important to understand them thoroughly, because they are one of the main ways that people are exposed to this toxic metal [2]. Mercury chemistry is also important for other reasons; its behavior in some situations is determined by relativistic quantum effects, such as its liquidity at room temperatures.

There are several current problems which merit more understanding, but which are difficult to approach. Every year, upon polar sunrise, the concentrations of mercury in the atmosphere are observed to drop precipitously in both the arctic [3] / [4] and Antarctic poles [5]. At the same time, a drop in concentration of ozone, another

important environmental chemical, is also observed [6]. The behavior of arctic formaldehyde during this same critical time window is also irregular [7].

These depletion observations are a phenomenon that is not yet fully understood. There are strong suspicions that a reaction with a halide species [8] in a process similar to that known in ozone depletion [9], [10] is involved in the mercury depletions. Computer simulation studies have produced results that confirm an inverse correlation between the concentrations of mercury as well as ozone against several halide species [11]. There have been studies that suggested HgO was formed as a product [5], but this result is disputed by models that indicate that the formation of HgO from BrO and Hg-0 isn't energetically favorable [12], [13]. A later paper suggests that perhaps the species of interest is $HgBr_2$, not HgO [14], and that this species might be the result of reactions with atomic bromine in the atmosphere [15]. Further compounding matters, an earlier study showed that measuring concentrations of $HgCl_2$ using different methods did not produce the same resultant data [16].

Whatever the process, the mercury displaced from the atmosphere ends up primarily in the snowpack on the arctic surface. Modeling indicates that slightly more than 200 tons of mercury could be deposited in the arctic every year [17], which is triple what it was several centuries ago [18]. One laboratory has already developed an instrument for measuring mercury compound concentrations at different depths in the snow [19]. Using this instrument, they determined that the amount of elemental

mercury in the air embedded in the snow increases by approximately a factor of two during the daylight hours, and falls during the nighttime [20]. The same group has also come to the conclusion that the majority of the mercury in the snowpack ends up dissolved in the water when it melts [21], as nearly all (99%) of it is associated with the ice crystals rather than in gaseous form [22].

This observation brings us to our next topic, the prevalence and chemistry of mercury in waterways and lakes. Although the concentrations of mercury in arctic waters weren't observed to be especially higher when compared to concentrations in other nonpopulated areas (one study measured [23] less than half a nanogram of mercury per liter of water), concentrations in excess of 0.5 micrograms per gram of animal muscle tissue were observed in animals living in the arctic in the early 1990s [24]. This factor of a thousand difference in the two concentrations is an example of how biomagnification can increase the concentrations of pollutants where it counts.

It has been observed that the release of mercury from the surfaces of lakes in a study in Sweden occurs at a higher rate during the day than at night, and mercury emission wasn't observed at all when the water was close to 0 degrees Centigrade [25]. This correlates well with the observations in the arctic, where little mercury was observed between the ice crystals in the snowpack [22].

There are three main categories which mercury contamination in waterways falls into: elemental mercury, methylmercury, and ionic compounds with mercury 2+ [26]. Elemental mercury isn't very soluble in water and generally either migrates to the riverbeds, where it ends up converted to HgS(s) and precipitated into the silt, or is released intact into the air above. Mercury 2+ was shown to be present mostly in complexed form in urban wastewater [27], and one eighth to one half of the ions were held extremely tightly, with dissociation constants on the order of $10^{-3}$. Of the three species, methylmercury is probably the most dangerous, since it is readily absorbed and concentrated by fish and other water creatures, and can cross cell walls straightforwardly using existing channels [28]. The same anaerobic bacteria that reduce sulfates can also convert mercury to methylmercury [29], which compounds the problem. Interestingly enough, in conditions where iron would be reduced there is less methylation observed [30].

Luckily, photochemical decomposition of methylmercury, both observed [26] and successfully modeled in simulations [31], helps this situation somewhat, converting it back into elemental mercury, which is less harmful to us.

We can't ignore mercury depositing into the ocean either. Several studies have started to study the dynamics of mercury redistribution in the ocean [32]. Examination of concentrations compared to time show that photochemical oxidation of mercury is important in the dissolution of elemental mercury in the seawater [33].

Studies in the St. Lawrence estuary determined that there, the rate of photo-oxidation increased by a factor of seven when the light used contained UV-A radiation [34]. Concentrations of bromine are also involved in the emission and absorption of mercury over the ocean.

One study of Tuna had some better news, however. The modeling method which they were using indicated that they should have observed an increase in the concentrations of methylmercury in the fish, but this was not seen [35]. This initially surprising result would make some sense upon further review, since the anoxic bacteria which are generally responsible for converting elemental mercury fallout into methylmercury would not be found in the same water that tuna inhabit.

Mercury poisoning can occur to both animals and humans. A very recent study of mercury exposure in zebrafish [36] observed the activations of several genes in fish fed between 0.08 and 13.5 micrograms of methylmercury per gram of food and found, surprisingly, that the brains of the fish did not show greater gene expression in any of the ones they monitored even though they accumulated more than 60 micrograms of mercury per gram of dried fish tissue at the end of their 63 day experiment. This lack of an extraction method might shed some light on the poor clinical performance of human victims of mercury poisoning, who often end up sick for several months after exposure before beginning to improve [2]. Symptoms of Mercury poisoning include progressive deteriorations of the senses, especially visual,

loss of motor control, and death from central nervous system failure [37]. Even with chelation therapy to help the body eliminate mercury, the rate at which methylmercury damages the nervous system can be fast enough that intense treatment after the asymptomatic period (which can last from one half to two months [38]) is over is not enough to effectively save lives [1].

Although the elemental form of mercury isn't as hazardous to people as organic complexes (especially methylmercury), it is still dangerous, as its vapor can enter the body through the lungs, and it can also be converted to methylmercury by the action of anaerobic bacteria. The vapor inhalation of elemental mercury is probably the cause of the mad hatter's ailment, as they used mercury to cure the felt used to make hats in the latter half of the nineteenth century and as such were chronically exposed to mercury vapors.

The chemical industry in Japan caused one of the largest episodes of acute mercury poisoning in the recent past [39]. Nippon Nitrogen Fertilizer Company (now known as Chisso Corporation) released methyl mercury into the waterways near Minamata Bay, and many people there ended up sick or dead—nearly three thousand in total [40]. The first indication that there was something wrong was when cats began acting strange and throwing themselves into the water and drowning, but the people there weren't able to determine the cause of the scourge until much later, although a scientist in the Chisso Company determined what was going on and was silenced by

the corporation until much later. Now, over three thousand people or their families have qualified for reimbursement due to the disaster. Computer modeling [41] has been used to project future conditions of Minamata bay and its environs as well as the Gulf of Trieste. Minamata bay is expected to do no further damage to the environment.

There was a larger disaster in Iraq in the early 1970s, where farmers accustomed to consuming bread made from the grain they were planting caused more than six thousand people to become sick from methylmercury poisoning when the grain they were provided with from the government had been treated with a different variety of fungicide than usual [38]. From the epidemiological data, they determined that deaths only began occurring in earnest once victims ingested more than 200mg of methylmercury, upon which the death rate quickly rose to above 20% at 250mg. Tingling in extremities was observed above 25mg of exposure, and blindness above approximately 100mg. The problem was compounded by the fact that symptoms took a long time to develop, so people who tested the food to see if it was poisonous on animals didn't observe any ill effects until well after they had already exposed themselves and their families to large amounts of the chemical.

Industrial negligence is not the only cause of mercury pollution, however. Coal powered plants and factories are moving significant amounts of the element into the atmosphere as they burn fuel that contains traces of the element [42]. There are

processes being used to remove mercury from the gas emitted by these plants which are successful in removing over half of the chemical [43], and new methods are in development [44], but there is a great challenge presented in removing the relatively non-reactive Hg-0 elemental mercury from the emissions, especially when the temperatures involved are so high (typical coal flue gasses are between 50 and 400 degrees centigrade, although they can be cooled as they are emitted), because mercury has a very high vapor pressure compared to other metals. It is easier to remove other mercury compounds, like $HgCl_2$ [45], although in the quest for more effective solutions there is constant development on new methods and materials [46]. The chemistry of mercury in the unusual environment of combustion products is also novel, and there are multiple studies investigating its behavior there [47]. Some modeling studies suggested that American factories might not be the main source of mercury in the US [48], but they are certainly important here as well as in other countries, such as China [49]. In countries with dry seasons and dust storms, mercury can also reenter the atmosphere seasonally as well [50].

Mercury poisoning wouldn't be so bad if treatment methods existed which were more effective. The body has difficulty removing mercury from its system, leading to individuals ending up continuing to be damaged mentally a long period of time after an initial exposure. Studies on farmers involved with the Iraq event indicated that mercury has a half-life in the body ranging from between forty to one hundred days [38], and the concentrations in the brain are much higher than in other organs.

Unfortunately, although treatment with current known chelating agents can show an increase in excretion by a factor of a thousand (observed in the patient at Dartmouth College), this isn't as helpful as we might like, since the mercury remaining in the body continues to do damage until it is extracted. In the studies in Iraq, they found that multiple treatments with the chelating agents were less effective after the first round. The main obstacle to treating patients with mercury poisoning effectively is that they show a long asymptomatic period, during which the brain concentrates the poison and is continuously being damaged. This span of time is often long enough that the additional length of time necessary to remove the mercury from the patient is great enough that serious permanent damage can occur before the treatment is complete.

Better and less dangerous chelating agents would therefore be a good product to develop, since they could be used to better remove mercury from the body than the current chemicals. In the Iraqi disaster, they used D-penicillamine, N-acetyle-DL-penicillamine, and a thiol resin containing -$CH_3SH$ groups to bind mercury [38]. A better understanding of how mercury interacts with the enzymes in cells might provide much additional impetus towards intelligent medicine design. To date, there have been a number of studies on different sorts of mercury-sulfur complexes. Mercury is suspected to interfere with proper enzyme behavior primarily by binding itself to sulfur atoms.

*2.2 Previous Work*

So far, there have been the many studies published in the literature that used computers to simulate mercury compounds in different situations. The following are a summary of a few additional related mercury papers which were not referred to previously.

The first paper includes calculations on mercury has an analysis based in molecular orbital theory and analyzes many complexes, including tetrahedral $HgS_4^{6-}$ and linear $HgS^{2-}$ mercury complexes. It was published in the early eighties before computational capabilities were strong enough to include relativistic effects and notes that those "may even be quite important" when considering mercury complexes [51].

There were also several later papers by a different laboratory that included early relativistic calculations on mercury: [52], [53], [54], [55], and [56]. In our case we did some calculations with Core Effective Potential basis sets, which include relativistic effects for the core electrons in the basis set.

A later study calculates stretching frequencies and hydrated stabilities using a relativistic effective core potential with additional polarization functions and finds that, as expected, $CH_3HgOH$ is one of the most important species involved in photodecomposition of aqueous methylmercury compounds [31]. A future paper

computes water solvation energies for a variety of divalent complexes, then goes on to determine the energy required to dissolve cinnabar by various species using that same model [57].

Revisiting one of the earlier topics, another paper analyzes the stabilities of HgS-based species in water solution, and concludes that it exists as a strongly hydrated HgSH(OH) molecule when it is in solution instead [58].

Another study manages to reproduce the known spectroscopic properties of gaseous mercury(II) chlorides and bromides successfully [59], and the same group continues by calculating reactions relevant to oxidation of atmospheric elemental mercury [60].

A more recent ab-initio study of mercury-sulfur and other group sixteen ligands calculated results which would seem to imply that previous experimental measurements of the stability of HgS and other similar compounds were greatly overestimated, perhaps because the experiments were being conducted on dimers or mixtures of larger molecules [61].

Preliminary calculations conducted at the beginning of the research suggest that the most stable mercury-sulfur complexes have near-linear angles around the mercury atom, and an approximately 120 degree angle between the sulfurs. It is possible to form ring structures with more stability than the linear open forms so long as the

number of sulfur atoms involved is greater than six, and a bare mercury atom will easily approach and break open a sulfur ring when placed within 4 angstroms of its center when using B3LYP with an extended CEP-31G basis set. Further examination of this phenomenon is indicated for the future.

Suggested future directions that this research should take would also include studies on isotopic fractionation in mercury-sulfur species in both aqueous and solid phases, theoretical studies on where mercury would stably bind to some common well-characterized enzymes, and attempts to run some ab-initio calculations on crystal formations of mercury and sulfur compounds.

*2.3 References*


1. Nierenberg, D.W., et al., *Delayed cerebellar disease and death after accidental exposure to dimethylmercury.* New England Journal of Medicine, 1998. **338**(23): p. 1672-1676.
2. Clarkson, T.W., L. Magos, and G.J. Myers, *The toxicology of mercury - Current exposures and clinical manifestations.* New England Journal of Medicine, 2003. **349**(18): p. 1731-1737.
3. Schroeder, W.H., et al., *Arctic springtime depletion of mercury.* Nature, 1998. **394**(6691): p. 331-332.
4. Ariya, P.A., et al., *The Arctic: a sink for mercury.* Tellus Series B-Chemical and Physical Meteorology, 2004. **56**(5): p. 397-403.

5. Ebinghaus, R., et al., *Antarctic springtime depletion of atmospheric mercury.* Environmental Science & Technology, 2002. **36**(6): p. 1238-1244.

6. Bottenheim, J.W., et al., *Ozone in the Arctic lower troposphere during winter and spring 2000 (ALERT2000).* Atmospheric Environment, 2002. **36**(15-16): p. 2535-2544.

7. Sumner, A.L., et al., *Atmospheric chemistry of formaldehyde in the Arctic troposphere at Polar Sunrise, and the influence of the snowpack.* Atmospheric Environment, 2002. **36**(15-16): p. 2553-2562.

8. Ariya, P.A., A. Khalizov, and A. Gidas, *Reactions of gaseous mercury with atomic and molecular halogens: Kinetics, product studies, and atmospheric implications.* Journal of Physical Chemistry A, 2002. **106**(32): p. 7310-7320.

9. Boudries, H. and J.W. Bottenheim, *Cl and Br atom concentrations during a surface boundary layer ozone depletion event in the Canadian high Arctic.* Geophysical Research Letters, 2000. **27**(4): p. 517-520.

10. Platt, U. and G. Honninger, *The role of halogen species in the troposphere.* Chemosphere, 2003. **52**(2): p. 325-338.

11. Calvert, J.G. and S.E. Lindberg, *A modeling study of the mechanism of the halogen-ozone-mercury homogeneous reactions in the troposphere during the polar spring.* Atmospheric Environment, 2003. **37**(32): p. 4467-4481.

12. Tossell, J.A., *Calculation of the energetics for oxidation of gas-phase elemental Hg by Br and BrO.* Journal of Physical Chemistry A, 2003. **107**(39): p. 7804-7808.

13. Shepler, B.C. and K.A. Peterson, *Mercury monoxide: A systematic investigation of its ground electronic state.* Journal of Physical Chemistry A, 2003. **107**(11): p. 1783-1787.

14. Goodsite, M.E., J.M.C. Plane, and H. Skov, *A theoretical study of the oxidation of Hg-0 to HgBr2 in the troposphere.* Environmental Science & Technology, 2004. **38**(6): p. 1772-1776.

15. Khalizov, A.F., et al., *A theoretical study on the reactions of Hg with halogens: Atmospheric implications.* Journal of Physical Chemistry A, 2003. **107**(33): p. 6360-6365.

16. Sheu, G.R. and R.P. Mason, *An examination of methods for the measurements of reactive gaseous mercury in the atmosphere.* Environmental Science & Technology, 2001. **35**(6): p. 1209-1216.

17. Skov, H., et al., *Fate of elemental mercury in the arctic during atmospheric mercury depletion episodes and the load of atmospheric mercury to the arctic.* Environmental Science & Technology, 2004. **38**(8): p. 2373-2382.

18. Fitzgerald, W.F., et al., *Modern and historic atmospheric mercury fluxes in northern Alaska: Global sources and Arctic depletion.* Environmental Science & Technology, 2005. **39**(2): p. 557-568.

19. Dommergue, A., C.P. Ferrari, and C.F. Boutron, *First investigation of an original device dedicated to the determination of gaseous mercury in interstitial air in snow.* Analytical and Bioanalytical Chemistry, 2003. **375**(1): p. 106-111.

20. Dommergue, A., et al., *Diurnal cycles of gaseous mercury within the snowpack at Kuujjuarapik/Whapmagoostui, Quebec, Canada.* Environmental Science & Technology, 2003. **37**(15): p. 3289-3297.

21. Dommergue, A., et al., *The fate of mercury species in a sub-arctic snowpack during snowmelt.* Geophysical Research Letters, 2003. **30**(12).

22. Ferrari, C.P., et al., *Profiles of Mercury in the snow pack at Station Nord, Greenland shortly after polar sunrise.* Geophysical Research Letters, 2004. **31**(3).

23. Lyons, W.B., K.A. Welch, and J.C. Bonzongo, *Mercury in aquatic systems in Antarctica.* Geophysical Research Letters, 1999. **26**(15): p. 2235-2238.

24. Muir, D.C.G., et al., *Arctic Marine Ecosystem Contamination.* Science of the Total Environment, 1992. **122**(1-2): p. 75-134.

25. Schroeder, W., et al., *Volatilization of Mercury from Lake Surfaces.* Science of the Total Environment, 1992. **125**: p. 47-66.

26. Morel, F.M.M., A.M.L. Kraepiel, and M. Amyot, *The chemical cycle and bioaccumulation of mercury.* Annual Review of Ecology and Systematics, 1998. **29**: p. 543-566.

27. Hsu, H. and D.L. Sedlak, *Strong Hg(II) complexation in municipal wastewater effluent and surface waters.* Environmental Science & Technology, 2003. **37**(12): p. 2743-2749.

28. Bisinoti, M.C. and W.F. Jardim, *Behavior of methylmercury in the environment.* Quimica Nova, 2004. **27**(4): p. 593-600.

29. Baldi, F., *Microbial transformation of mercury species and their importance in the biogeochemical cycle of mercury.* Metal Ions in Biological Systems, Vol 34, 1997. **34**: p. 213-257.

30. Warner, K.A., E.E. Roden, and J.C. Bonzongo, *Microbial mercury transformation in anoxic freshwater sediments under iron-reducing and other electron-accepting conditions.* Environmental Science & Technology, 2003. **37**(10): p. 2159-2165.

31. Tossell, J.A., *Theoretical study of the photodecomposition of methyl Hg complexes.* Journal of Physical Chemistry A, 1998. **102**(20): p. 3587-3591.

32. Hedgecock, I.M. and N. Pirrone, *Chasing quicksilver: Modeling the atmospheric lifetime of Hg-(g)(0) in the marine boundary layer at various latitudes.* Environmental Science & Technology, 2004. **38**(1): p. 69-76.

33. Laurier, F.J.G., et al., *Reactive gaseous mercury formation in the North Pacific Ocean's marine boundary layer: A potential role of halogen chemistry.* Journal of Geophysical Research-Atmospheres, 2003. **108**(D17).

34. Lalonde, J.D., et al., *Photoinduced oxidation of Hg-0 (aq) in the waters from the St. Lawrence estuary.* Environmental Science & Technology, 2004. **38**(2): p. 508-514.

35. Kraepiel, A.M.L., et al., *Sources and variations of mercury in tuna.* Environmental Science & Technology, 2003. **37**(24): p. 5551-5558.

36. Gonzalez, P., et al., *Comparative Effects of Dietary Methylmercury on Gene Expression in Liver, Skeletal Muscle, and Brain of the Zebrafish (Danio rerio).* Environmental Science & Technology, 2005. **ASAP Web Release**.

37. Satoh, H., *Occupational and environmental toxicology of mercury and its compounds.* Industrial Health, 2000. **38**(2): p. 153-164.

38. Bakir, F., et al., *Methylmercury Poisoning in Iraq - Interuniversity Report.* Science, 1973. **181**(4096): p. 230-241.

39. Harada, M., *Minamata Disease - Methylmercury Poisoning in Japan Caused by Environmental-Pollution.* Critical Reviews in Toxicology, 1995. **25**(1): p. 1-24.

40. Takizawa, Y., *Understanding minamata disease and strategies to prevent further environmental contamination by methylmercury.* Water Science and Technology, 2000. **42**(7-8): p. 139-146.

41. Rajar, R., et al., *Application of three-dimensional mercury cycling model to coastal seas.* Ecological Modelling, 2004. **171**(1-2): p. 139-155.

42. Yan, R., D.T. Liang, and J.H. Tay, *Control of mercury vapor emissions from combustion flue gas.* Environmental Science and Pollution Research, 2003. **10**(6): p. 399-407.

43. Tang, S., et al., *Mercury speciation in the flue gas of a small-scale coal-fired boiler in Guiyang, PR China.* Journal De Physique Iv, 2003. **107**: p. 1287-1290.

44. Granite, E.J. and H.W. Pennline, *Photochemical removal of mercury from flue gas.* Industrial & Engineering Chemistry Research, 2002. **41**(22): p. 5470-5476.

45. Sommar, J., O. Lindqvist, and D. Stromberg, *Distribution equilibrium of mercury (II) chloride between water and air applied to flue gas scrubbing.* Journal of the Air & Waste Management Association, 2000. **50**(9): p. 1663-1666.

46. Abu-Daabes, M.A. and N.G. Pinto, *Synthesis and characterization of a nano-structured sorbent for the direct removal of mercury vapor from flue gases by chelation.* Chemical Engineering Science, 2005. **60**(7): p. 1901-1910.

47. Galbreath, K.C. and C.J. Zygarlicke, *Mercury transformations in coal combustion flue gas.* Fuel Processing Technology, 2000. **65**: p. 289-310.

48. Seigneur, C., et al., *Modeling the atmospheric fate and transport of mercury over North America: power plant emission scenarios.* Fuel Processing Technology, 2004. **85**(6-7): p. 441-450.

49. Fang, F.M., et al., *Atmospheric particulate mercury in Changchun City, China.* Atmospheric Environment, 2001. **35**(25): p. 4265-4272.

50. Friedli, H.R., et al., *Mercury in the atmosphere around Japan, Korea, and China as observed during the 2001 ACE-Asia field campaign: Measurements, distributions, sources, and implications.* Journal of Geophysical Research-Atmospheres, 2004. **109**(D19).

51. Tossell, J.A. and D.J. Vaughan, *Relationships between Valence Orbital Binding-Energies and Crystal-Structures in Compounds of Copper, Silver, Gold, Zinc, Cadmium, and Mercury.* Inorganic Chemistry, 1981. **20**(10): p. 3333-3340.

52. Stromberg, D., O. Gropen, and U. Wahlgren, *Non-Relativistic and Relativistic Calculations on Some Zn, Cd and Hg Complexes.* Chemical Physics, 1989. **133**(2): p. 207-219.

53. Stromberg, D., M. Sandstrom, and U. Wahlgren, *Theoretical Calculations on the Structure of the Hexahydrated Divalent Zinc, Cadmium and Mercury Ions.* Chemical Physics Letters, 1990. **172**(1): p. 49-54.

54. Stromberg, D. and U. Wahlgren, *1st-Order Relativistic Calculations on Au2 and Hg-2(2+).* Chemical Physics Letters, 1990. **169**(1-2): p. 109-115.

55. Stromberg, D., A. Stromberg, and U. Wahlgren, *Relativistic Quantum Calculations on Some Mercury Sulfide Molecules.* Water Air and Soil Pollution, 1991. **56**: p. 681-695.

56. Xiao, Z.F., D. Stromberg, and O. Lindqvist, *Influence of Humic Substances on Photolysis of Divalent Mercury in Aqueous-Solution.* Water Air and Soil Pollution, 1995. **80**(1-4): p. 789-798.

57. Tossell, J.A., *Theoretical studies on the formation of mercury complexes in solution and the dissolution and reactions of cinnabar.* American Mineralogist, 1999. **84**(5-6): p. 877-883.

58. Tossell, J.A., *Calculation of the structures, stabilities, and properties of mercury sulfide species in aqueous solution.* Journal of Physical Chemistry A, 2001. **105**(5): p. 935-941.

59. Balabanov, N.B. and K.A. Peterson, *A systematic ab initio study of the structure and vibrational spectroscopy of HgCl2, HgBr2, and HgBrCl.* Journal of Chemical Physics, 2003. **119**(23): p. 12271-12278.

60. Balabanov, N.B. and K.A. Peterson, *Mercury and reactive halogens: The thermochemistry of Hg+{Cl-2, Br-2, BrCl, ClO, and BrO}*. Journal of Physical Chemistry A, 2003. **107**(38): p. 7465-7470.

61. Filatov, M. and D. Cremer, Revision of the dissociation energies of mercury chalcogendies - Unusual types of mercury bonding. Chemphyschem, 2004. 5(10): p. 1547-1557.

# Chapter 3: An Overview of Computational Chemistry Techniques

Computational Chemistry is the study of chemical compounds via computer simulations. As we use it here, it is the application of quantum mechanics and theories based thereupon.

The purpose of this chapter is to provide a bit of background and an easy reference to the terminology and basic methods used in our calculations, aimed towards the physical chemist who has not yet become a specialist in applied theoretical chemistry, beginning with an introduction to the Schrodinger equation used in quantum mechanics and a tour through a low level *ab initio* method, Hartree-Fock theory before going on to discuss the other levels of theory and approaches which we shall be using.

## *3.1 Introduction*

In quantum mechanics, the Schrodinger equation[1] can be used to predict the electronic stability of atoms and small molecules, but solving it is another matter. While it is possible to get precise solutions for smaller systems, such as the H atom[2], which was solved exactly in 1926, there are many chemical problems which involve larger molecules, such as $H_2$, which remain a work in progress[3, 4]. Heavier

elements also call for attention and are currently beyond direct exact solution of the Schrodinger equation due to electron overlap integrals which combine multiple basis functions in a nonintegrable (analytically) way. It is these cases that we take measures to approximate the correct solution with a sufficiently accurate estimate to proceed.

## *3.2 – Key Basics*

***Approximations. Hartree-Fock. Basis Sets (from Linear Algebra). Self-consistency.***

Thus we are forced to accept different approximations in order to make calculations on the larger systems feasible.

The approximations which are essential and widely used in our case include the Hartree-Fock self-consistent field method and basis functions. Before discussing these at length, we will provide a quick overview of the two techniques for dealing with the problem of representing physical chemicals for computational study.

### 3.2.1 – An overview of the Hartree-Fock self-consistent field method

*An Overview of the Hartree-Fock self-consistent field method and basis functions.*

The geometry of the electron cloud is solved for iteratively in this implementation of the Hartree-Fock approach[5]. As the Hartree-Fock method forms the basis from which we build much of the other methods used in our computational chemistry calculations, we will discuss it at length below. Popular methods for conducting this solution include approaches where the electron cloud geometries are kept track of numerically, and approaches where the cloud is divided into smaller, simpler to manipulate functions. These functions are called basis functions and are combined linearly and their total approximates the wavefunction for the electrons.

*Applied linear algebra: representing the electron cloud geometry with a basis set.*

By combining the functions linearly, we can take advantage of properties from Linear Algebra. It is easily proved by linear algebra that if enough functions are combined, they can not just approximate, but equal precisely any arbitrary function of the same variables. Therefore, given a large enough number of basis functions (called all together a "basis set"), we can represent any arbitrary geometry.

However, this is somewhat of an overkill, because at a certain point (which has to be determined via calculations) adding additional basis functions does not significantly improve the final results. When computationally limited resources are in play, such

as higher-level methods which become rapidly expensive as N, the problem size (where N = number of basis functions) increases, it is important to strike a balance between the basis set chosen and the quality of the method, so determining what basis set is required for stable results in a calculation is essential.

### 3.2.2 – The Hartree Fock Method (explained in detail)

*How Hartree-Fock works: Iterating the electron cloud geometry to find a self-consistent geometry.*

The Hartree-Fock method works[5] by iteratively solving for the electron probability wavefunction using a variational method. At each step, the current geometries of the electron wave functions are used to calculate updated energies and new geometry of the electrons across the basis set. As the field is brought to self-consistency, the electron cloud which the basis set and coefficients describe becomes the solution to the method. Further discussion of the mechanisms of Hartree-Fock are described below based on the 1970 textbook exposition by Ira N. Levine [58].

We begin by considering a situation where we are calculating the energetics of a single atom, and after explaining the Hartree-Fock process under those conditions extend it to the molecular situation.

Assuming that the total charge of the nucleus is Z, the mass of the electron is m, and the unit charge is e', then the following Equation 3.1 represents the Hamiltonian needed to calculate the energy of a particular electronic arrangement of n electrons.

(3.1) $$\hat{H} = -\frac{\hbar^2}{2\mathrm{m}} \sum_{i=1}^{n} \nabla_i^2 - \sum_{i=1}^{n} \frac{Ze'^2}{r_i} + \sum_{i=1}^{n} \sum_{j>i} \frac{e'^2}{r_{ij}}$$

The terms are as follows, with the first term being the total kinetic energy of the electrons, the second being the nuclear attraction that each electron feels towards the nucleus of charge Z, and the third term electron-electron repulsion.

This Hamiltonian is applied to the wavefunction representing the electron geometry using the Schrodinger equation as shown Equation 3.2 below.

(3.2) $$\hat{H}\,\psi = E\,\psi$$

This gives the total energy E as an eigenvalue of the wavefunction ψ.

However, the correct ψ is unknown. The Hartree-Fock approach is to start out with a guess or trial wavefunction, φ, which is a product of eigenfunctions $s_i$ of the Hartree-Fock atomic Hamiltonian in polar coordinates $r_i$, $\theta_i$, and $\varphi_i$.

(3.3) $$\varphi = \prod_i s_i(r_i, \theta_i, \varphi_i)$$

These eigenfunctions $s_i$ can be represented as a linear combination of basis functions $b_k$ within the same coordinate system as shown in Equation 3.3a below. The coefficients $c_{ik}$ are varied to make the basis set approximate the exact $s_i$ to the an arbitrarily good precision.

(3.3a) $$s_i = \sum_k c_{ik} b_k(r_i, \theta_i, \varphi_i)$$

In the atomic case, $s_i$ can be further simplified and written as a product of a radial and angular portion to reduce the complexity of the calculation with little loss in accuracy, but as this method does not apply to the molecular calculations which we are primarily interested in explaining, we will omit it for now.

We then begin a repeating process called the Self-Consistent Field method.

The self-consistent field method works by fixing all of the electrons except for one in place, then optimize the remaining free electron's wavefunction to minimize the total energy. This process is repeated for each electron until an equilibrium is reached.

When the electrons are all fixed in place, the electron-electron repulsion term becomes the repulsion between a single electron and the field generated by the other electrons.

We can divide this into a sum of interactions between the single electrons in the field, and can treat them separately.

An individual electron-electron repulsion between an arbitrary electron *i* and *j* is therefore written as $V_{ij}$, shown in Equation 3.4, where e' is the charge on an electron and the integral over all space is done on the expectation value of $s_j$ over $r_{ij}$, which is the distance between the two charges:

$$V_{ij} = e'^2 \int \frac{|s_j|^2}{r_{ij}} dv_j \tag{3.4}$$

And the total electrostatic interaction for electron *i* is the sum of $V_{ij}$ over all of the other electrons, which appears as the first term in Equation 3.5 below, minus the nuclear attraction term for that electron, which is a single term in the case of :

$$V_i(r_i, \theta_i, \varphi_i) = \sum_{j \neq i} e'^2 \int \frac{|s_j|^2}{r_{ij}} dv_j - \frac{Ze'^2}{r_i} \tag{3.5}$$

As mentioned before, in the atomic case here the nuclear attraction term includes only

the contribution for the one point nucleus present. In the molecular system there will be a sum of attractions as the second term in Equation 3.5 to account for nuclear attraction to each individual nucleus.

We also mentioned that in the atomic case we have a spherical symmetry we can take advantage of by applying the Central Field Approximation. This is done by averaging out the two angles in the spherical coordinate system to produce a potential which only depends on $r_i$ as shown in Equation 3.6. In the polyatomic case this approximation would not apply for the possibly bonding valence electrons (those in the outermost orbitals of each atom), but would remain relatively valid for inner shell electrons.

$$V(r_i) = \frac{\int_0^{2\pi}\int_0^{\pi} V(r_i,\theta,\varphi)\sin\theta\, d\theta\, d\varphi}{\int_0^{2\pi}\int_0^{\pi} \sin\theta\, d\theta\, d\varphi} \tag{3.6}$$

This $V(r_i)$ is then substituted into the one electron Schrodinger Equation Equation 3.2, as the potential energy in the one electron Hamiltonian, making it appear as follows in Equation 3.7, where $t_i$ is the unknown optimized eigenfunction with the minimum energy $\varepsilon_i$.

(3.7) $$[-\frac{\hbar^2}{2\mathrm{m}}\nabla_i + V(r_i)]t_i(1) = \epsilon_i t_i(1)$$

Where the Hamiltonian appears in brackets on the left and the eigenfunction $t_i$ yields the minimum energy $\varepsilon_i$. This can be solved for by rearranging it as follows in Equation 3.8:

(3.8) $$[-\frac{\hbar^2}{2\mathrm{m}}\nabla_i + V(r_i)]t_i(1) - \epsilon_i t_i(1) = 0$$

Presuming that $t_i(1)$ is made from a linear combination of the basis functions $b_k$ in our basis set as shown in Equation 3.3a, this is equivalent to a system of linear equations which can be solved for their individual coefficients to determine both the new electron wavefunction $t_i(1)$ for the free electron and the corresponding minimum energy state. The new electron wavefunction for electron i, $t_i$, replaces the original $s_i$, and the process is then repeated for the next electron present on the atom, until a stable configuration is found for all the electrons individually.

At this point, the overall wavefunction $\varphi$, is a product of optimized eigenfunctions $s_i$ of the Hartree-Fock atomic Hamiltonian in polar coordinates $r_i$, $\theta_i$, and $\varphi_i$, and our calculation is complete.

The total energy is then closely related to the sum of the individual electron energies

calculated during the cyclic solution on Equation 3.8, less the double-counted electron repulsion integral which is then subtracted as the second term of the full energy shown as Equation 3.9 below:

$$(3.9) \qquad E_{atomic} = \sum_{i=1}^{n} \epsilon_i - \sum_i \sum_{j>i} \int \int \frac{e'^2 |s_i(i)|^2 |s_j(j)|^2}{r_{ij}} dv_i dv_j$$

However, the above atomic Hartree-Fock only covers situations where there is only one point nucleus present. We can extend it to multiple atoms in a molecule with multiple nuclei with an extended Hamiltonian as shown in Equation 3.10 below:

$$(3.10) \qquad \hat{H} = -\frac{\hbar^2}{2\mathrm{m}} \sum_i \nabla_i^2 - \sum_\alpha \sum_{i=1}^{n} \frac{Z_\alpha e'^2}{r_i} + \sum_{i=1}^{n} \sum_{j>i} \frac{e'^2}{r_{ij}} - \frac{\hbar^2}{2\mathrm{m}_\alpha} \sum_\alpha \nabla_\alpha^2 + \sum_\alpha \sum_{\beta>\alpha} \frac{Z_\alpha Z_\beta}{r_{\alpha\beta}}$$

It is instructive to compare this to our original one-nucleus Hamiltonian shown in Equation 3.1.

The differences are a sum appearing in the second term of the original equation, which now covers all of the positive nuclei $Z_\alpha$ present where previously in the atomic version we only were concerned with a single positive nucleus of charge Z. There are also two new terms on the right which cover the kinetic energy of each nuclei and a nuclear-nuclear repulsion interaction $V_{NN}$ which does not involve the electron cloud wavefunction which we shall show in Equation 3.11.

(3.11) $$V_{NN} = \sum_{\alpha} \sum_{\beta > \alpha} \frac{Z_\alpha Z_\beta}{r_{\alpha\beta}}$$

Before demonstrating the molecular Hartree-Fock system, we shall apply another assumption: the Born-Oppenheimer Approximation, where we assume that the positions of the nuclei are fixed compared to the mobile electron cloud, thereby removing the fourth term from Equation 3.10 which measures the kinetic energy of the nuclei. The remainder is divisible into two parts, the first three terms, which are the electronic Hamiltonian shown in Equation 3.12 below:

(3.12) $$\hat{H}_{el} = -\frac{\hbar^2}{2\mathrm{m}} \sum_i \nabla_i^2 - \sum_{\alpha} \sum_{i=1}^{n} \frac{Z_\alpha e'^2}{r_i} + \sum_{i=1}^{n} \sum_{j>i} \frac{e'^2}{r_{ij}}$$

The Fock Operator is then the total energy found from the sum of the electronic Hamiltonian and the nuclear repulsion energy, as presented in Equation 3.13:

(3.13) $$\hat{F} = \hat{H}_{el} + V_{NN} = -\frac{\hbar^2}{2\mathrm{m}} \sum_i \nabla_i^2 - \sum_{\alpha} \sum_{i=1}^{n} \frac{Z_\alpha e'^2}{r_i} + \sum_{i=1}^{n} \sum_{j>i} \frac{e'^2}{r_{ij}} + \sum_{\alpha} \sum_{\beta>\alpha} \frac{Z_\alpha Z_\beta}{r_{\alpha\beta}}$$

Our expected Hartree-Fock energy, $E_{HF}$ is then the expectation value of these two elements over the electronic wavefunction. Presuming a doubly occupied wavefunction with closed shells D, it appears as shown below in Equation 3.14, with the different parts of the expectation values factored out into separate units:

(3.14) $$E_{HF}=\langle D|\hat{F}|D\rangle=\langle D|\hat{H}_{el}+V_{NN}|D\rangle=2\sum_{i=1}^{n/2}h_i+\sum_{i=1}^{n/2}\sum_{j=1}^{n/2}(2\mathrm{J}_{ij}-K_{ij})+V_{NN}$$

On the right, we introduce some notation to separate out the different calculation types necessary to calculate the energy of the system. The first term, $h_i$, has the parts of the energy which only depend on one electron, seen below in Equation 3.15 for the first electron (1).

(3.15) $$h_i=\langle\varphi_i(1)|-\frac{1}{2}\nabla_i^2-\sum_{\alpha}\frac{Z_\alpha}{r_{1\alpha}}|\varphi_i(1)\rangle$$

Then $J_{ij}$ is the repulsion between the a pair of arbitrary electons (1) and (2), and the $K_{ij}$ is the exchange stabilization gained from switching the same two electrons with each other. $J_{ij}$, and $K_{ij}$ as shown below in Equations 3.16, and 3.17 respectively.

(3.16) $$J_{ij}=\langle\varphi_i(1)\varphi_j(2)|\frac{1}{r_{12}}|\varphi_i(1)\varphi_j(2)\rangle$$

(3.17) $$K_{ij}=\langle\varphi_i(1)\varphi_j(2)|\frac{1}{r_{12}}|\varphi_j(1)\varphi_k(2)\rangle$$

This system of equations is now solved in the same way as the original atomic Hartree-Fock system which we previously showed, with the exception of the additional complexity introduced by the presence of the exchange energies.

Now we fix the wavefunctions of all but one of the electrons in our trial wavefunction φ, and beginning with the first electron minimize the energy ε of that single electron with the one-electron Fock operator in a single electron Schrodinger equation (shown below as Equation 3.18) formatted in the same pattern as the complete Schrodinger equation shown in Equation 3.2.

(3.18) $$\hat{F}(1)\varphi_i(1)=\epsilon_i(1)\varphi_i(1)$$

When we expand the trial single electron wavefunction $\varphi_i$ under a linear basis set of eigenfunctions of the Fock operator χ, as shown in Equation 3.19,

(3.19) $$\varphi_i=\sum_k c_{ki}\chi_k$$

Then we can substitute this in the Fock Schrodinger equation, Equation 3.18, to gain the following system of linear equations as shown in Equation 3.20, which simplifies because the Fock operator is linear to the Fock operator applied to the basis set underneath the original trial wavefunction while remaining equal to the energy eigenvalue.

(3.20) $$\hat{F}\varphi_i=\hat{F}\sum_k c_{ki}\chi_k=\sum_k c_{ki}\hat{F}\chi_k=\epsilon_i\sum_k c_{ki}\chi_k$$

This can then be rearranged by subtracting the right side of Equation 3.20 from the final simplification of the left, which appears in the same form, as Equation 3.21, creating a system of linear equations:

(3.21) $$\sum_k c_{ki}(F_{jk}-\epsilon_i S_{jk})=0$$

Where $F_{jk}$ and $S_{jk}$ are the Fock operator applied to basis functions $\chi_j$ and $\chi_k$, and $S_{jk}$ is the overlap integral between the two basis functions $\chi_j$ and $\chi_k$, as shown below in Equations 3.22 and 3.23.

(3.22) $$F_{jk}=\langle \chi_j|\hat{F}|\chi_k\rangle$$

(3.23) $$S_{jk}=\langle \chi_j|\chi_k\rangle$$

This system of equations can then be written compactly as Equation 3.24, shown for the first two basis functions explicitly:

(3.24) $$det(F_{jk}-\epsilon_i S\,jk)=\begin{vmatrix} F_{11}-\epsilon_i S_{11} & F_{21}-\epsilon_i S_{21} & \cdots \\ F_{12}-\epsilon_i S_{12} & F_{22}-\epsilon_i S_{22} & \cdots \\ \vdots & \vdots & \ddots \end{vmatrix}=0$$

The solution of this system of linear equations for the minimum $\varepsilon_i$ yields the individual coefficients $c_{ij}$ for a particular electron I, and the self-consistent field process can be repeated in the manner presented previously until the electron geometries are no longer changing, leaving them at the energy minima and the energy at a minimum as well.

At this point, if the nuclear geometry is at the equilibrium geometry for the system, our work is done and we have the Hartree-Fock energy.

To do a geometry optimization procedure, we need to take the derivative of the final

energy with respect to the nuclear coordinates and update the nuclear geometies in a fixed average electron cloud, using the assumption that the electrons move fast enough that the nuclei only see their average positions. The cycle of calculating an updated electron wavefunction then repeats using the same process until both sets of geometries have reached stable final coordinates, at which point our Hartree-Fock energy calculation is complete.

### 3.2.3 – Background on Basis Set Selection

*Choice of Basis Functions, Slater-Type Orbitals versus Gaussian-Type Basis-Sets*

Initial calculations used Slater orbitals[6], which corresponded closely to the expected shape of the electron distribution. This allowed for small and very quickly converging basis sets, but also caused another problem.

Because of the form of a Slater orbital (Equation 3.25 below), it is difficult or impossible to do analytical integration for part of the Hartree-Fock solution (as the orbital overlap integral has a product of two of these functions and is integrated over the distance between the two centers)[7].

(3.25) $R(\mathbf{r}) = \mathbf{r}^{n-1} e^{-\zeta \mathbf{r}}$ ($\mathbf{r}$ = radial distance to the nucleus)

This means that for models using Slater orbitals in their basis, although the number of actual integrals needed may be small, the amount of work needed to evaluate the functions would be quite sizable, because the two-electron overlap integrals are impossible to solve analytically with the Slater basis functions. However, this problem was overcome by a clever trick:

*Using a less efficient for representing the geometry but more efficient for calculation Gaussian basis set rather than one with basis functions more similar to actual electron cloud geometries.*

Initially, S. F. Boys (b.1911-d.1972) suggested and worked on forming a groundwork of analytical work that showed a Gaussian approach would be effective in doing calculations on molecular systems[57]. Later, John Pople (b.1925-d.2004) was integral in implementing a system which used Gaussian functions to form its Slater orbital basis set as well[8]. As Gaussian functions do not have the correct kind of radial dropoff this meant that many more basis functions were required to achieve the same quality of basis functions. But at the same time, because the overlap integral could be done analytically, the problem was overall much simpler computationally overall.

Because of the linear algebra methods used in the basis set solution, their properties apply whenever the methods are used, so the difference in function types used in the

expansions would not make any difference if the basis sets were large enough that the set could represent the solutions to the Schrodinger equation. As things turned out, the larger Gaussian basis sets were both more efficient (due to the analytical integration possible) even though more functions were required to reach the same level of quality in the results.

However, the current path of research has come full circle, as the use of higher level methods which scale rapidly towards impossibility as the basis set is increased in size, now the ease of computing numerical integrals is looking like it may eventually be more efficient at attaining accuracy than doing analytical analysis on a Gaussian basis.

## *3.3 – An Overview of Computational Chemistry Methods*

Methods which we used included the following:

- Hartree Fock (HF) (previously discussed)
- Moller-Plesset Perturbation Theory (MP2)
- CCSD (coupled cluster single and double excitations)
- CCSD(T) (single, double, and some triple excitations)
- Density-functional Theory (used with ADF), and
- Hybrid-Density Functional Theory (B3LYP)

- And Model Chemistries such as CBS-QB3 (G2 and G3 are other examples)
- Solvation Methods

We did a number of calculations with Gaussian 03[9] implementing the methods of Hartree-Fock (HF)[5], Moller-Plesset perturbation theory (MP2)[10, 11], CCSD[12] and CCSD(T)[13], B3LYP[14], and a number of model chemistry calculations using CBS-QB3[15, 16]. We also did a series of density-functional theory calculations using ADF[17-19] to find NMR chemical shifts[20-24]. We will discuss each of the methods below.

*Hartree-Fock (HF)*

As previously discussed, the Hartree-Fock method (HF)[5] is a variational theory solution of the Schrodinger equation[1]. It originally was implemented with Slater-type orbitals[6] but was later improved by Pople *et al.* with a Gaussian basis set implementation[8]. The change in basis set allowed for an analytical solution to the overlap integrals between the orbitals.

HF is a computationally light method that scales proportional to the fourth power of the number of basis functions in the calculation, or $N^4$. A doubling in the number of basis functions would increase the length of the calculation by a factor of 16. Other

methods scale at different rates, which can make the computational cost too expensive for a typical group as the size of the system grows.

Although it is faster than the soon-to-be discussed higher level methods, the Hartree-Fock method leaves somewhat to be desired when dealing with hydrogen-bonding interactions, and the bonds it models are generally stiffer than experimentally measured. The cause for this can easily be seen when considering the HF molecular orbitals involved in a bond dissociation, where the model's results are completely incorrect. The dissociation of HF has an electron which ends up divided equally between the atoms after separation, which is nonphysical.

### *Moller-Plesset Perturbation Theory (MP2)*

Moller-Plesset Perturbation Theory[10] is an approach which uses perturbation theory to improve the Hartree-Fock results. A first order Moller-Plesset calculation is equivalent to a Hartree-Fock calculation. MP2[11] consists of a base Hartree-Fock calculation with an additional term which adds some of the correlation energy. There are a series of MP methods which include successively more correlation energy terms. MP2 contains one term beyond HF, while MP3[25] and MP4[26] contain third and fourth order terms as well. The MP2 method is slower than HF, scaling at $N^5$ with the complexity of the calculation.

*Density-functional Theory (used here with ADF)*

Density-functional theory[27] is an alternate way of treating the bonding problem. As opposed to the HF approach of modeling inter-electron interactions directly, DFT operates by modeling the energy directly based upon the spatial electron distribution. This method while being much more efficient (scaling directly with the volume of the system being investigated) also has some shortcomings because, in that one electron density coordinate system, means of finding the precise correlation energy does not yet exist.

The implementation of DFT which we used in ADF works by filling a predefined space with electron probability to a specific resolution instead of placing basis functions on the atoms in the molecules. This approach allows for a lot of parallelism in the calculations, which can take increasing advantages of current computer development trends.

We have used DFT directly in a few cases, in particular in calculating NMR shielding[21, 22, 24] trends for HgCl compounds with the ADF computational package[19].

*Hybrid-Density Functional Theory (B3LYP)*

B3LYP[14] is a combination of a DFT and HF based model which has a similar accuracy as the MP2 method, but at much less computational cost. It works by adding the exchange energy component of the Hartree Fock system to an energy calculated by a DFT method. Enough data has been collected from the B3LYP method to confirm this, but our observed errors in the B3LYP method's energies have a tendency not to have an obvious trend of being either low or high, appearing instead more randomly distributed.

*CCSD (coupled cluster single and double excitations)*

and *CCSD(T) (single, double, and some triple excitations)*

Coupled Cluster theory is another higher level method.

In CCSD[12] the calculation includes contributions from both single and double excitations of the electrons in the system. The energies calculated with CCSD are generally higher in accuracy than MP2 calculations, but the computational cost is much greater. CCSD(T)[13] also includes some triple excitations, but is computationally expensive enough (it scales at $N^7$ with problem size) that it is difficult to calculate geometries under the method, although single point CCSD(T) calculations are good for confirming that the CCSD results are stable, or adding energy corrections to other calculations. We often use CCSD and CCSD(T)

calculations to demonstrate that our results at lower levels such as MP2 or B3LYP are stable.

So to summarize, Hartree Fock theory (HF) scales at $N^4$, MP2 at $N^5$, and CCSD at $N^7$.

*Model Chemistries: CBS-QB3 (G2 and G3 are other examples)*

Model chemistry methods such as Gaussian-2 (G2)[28], G3[29], or the Complete Basis Set method (we used CBS-QB3[15, 16]) are intended to provide the chemist with a general-purpose method for computational assistance. Each method is comprised of a series of calculations with fixed basis sets and methods which, when combined, yield results with well-characterized properties across a set of experimental reference data. Though often computationally expensive, they are very useful in the practical arena as they are designed to provide high quality results in a large variety of situations.

The G2 and G3 methods were developed by Gaussian and were tested on various reference sets of compounds[30-34] which were well known experimentally to confirm that the results have an very good average error – on the order of one or two kcal/mol.

The CBS-QB3 method was designed in particular to tackle the problem of limited basis sets by doing a series of calculations starting with an B3LYP geometry optimization and frequency calculation using the CBSB7 basis set. After this, a series of single point calculations are done at the final geometry, starting with the highest level used, a CCSD(T) calculation, with the smallest electron basis set, a 6-31+G(d') basis. This calculation is followed by a more calculations at lower levels under larger basis sets, starting with an MP4SDQ/CBSB4 calculation and ending with an MP2/CBSB3 calculation. Finally, the results are combined to yield the model chemistry result.

The CBS-QB3 method is in common use today, and has been assessed as similar in quality to the Gaussian model chemistry methods (G2 and G3)[15, 35, 36] with less computational cost. For this reason, and because of its ease of use, we made certain to use the CBS-QB3 method extensively in our acidity calculations discussed in Chapters 5 through 7, so that reproducing similar calculations would be accessible to the novice computational chemist.

### *Solvation Methods*

There are a variety of ways to model solvation effects in theoretical chemistry.

In this work, we concentrated on two main ones: explicit hydration, where additional $H_2O$ molecules are added to the calculation and optimized along with the rest of the system, and CPCM hydration[37-39], a method where the molecule or system of interest is placed in a spherical cavity surrounded by a dielectric to model bulk solvation.

The main difference between these two methods is that in the former case, computational costs grow very rapidly, and solving for reasonable and reproducible final geometries can become a consideration. With the second method, there is no opportunity for solute-solvent interactions such as hydrogen-bonding, which often affects results such as spectra (see Chapter 10, on myo-inositol hexakis phosphate, for an example of this).

*3.4 – An Overview of Basis Sets*

**Key information about basis sets are:**

- Basis set essentials
- Diffuse and Polarization functions[40]
- 6-31G[41, 42] and 6-311G(d,p)[43]
- CEP-type basis sets[44-46]
- cc-pVxZ basis sets[47-49] and complete basis set extrapolation

- CBSB7 basis set[16]
- custom basis set functions
- basis set overlap corrections (counterpoise corrections)

*Basis set essentials*

As we mentioned before, basis sets are used to approximate the ideal of a continuous probability distribution functions which would give the geometry of the electron cloud surrounding our nuclei. An infinite or complete basis set would allow the representation of any probability distribution, but due to computational limits we are restricted to calculating energetics with finite basis sets. Some methods, like the CBS-QB3 model chemistry method, contain a complete basis set extrapolation (although this can also be done separate from the model chemistry; we did a complete basis set extrapolation in another calculations by hand) that attempts to take care of the problems that a limited basis set introduces.

*Diffuse and Polarization functions*

Most small-scale basis sets suffer from a problem where they become dramatically worse when dealing with situations with polarized bonds (between atoms of different electronegativity, the electron geometry is distorted towards the more electronegative atom) or with ionic compounds (with negatively charged ones especially, because the

extra electrons make the cloud much larger than normal). This is where diffuse and polarization functions can help an inadequate basis set become adequate.

Diffuse functions are basis functions with small exponents, making the functions very large. They are most useful in the case of the anionic compounds[50, 51], because they allow the basis set to better represent electron probability distributions that range farther from the nuclei in the system than expected by the basis sets, which were mostly developed for neutral species.

A different problem exists for cations, where the basis functions have a similar error in estimation, only the amount of electron cloud contraction in the cation is less because of repulsion from the inner electrons and can be dealt with in gaussian bases by slewing the electrons towards the inner gaussian functions used to form the basis. This cannot be done for the anions because the size change is much more dramatic.

Polarization functions cover the other case, where the electron cloud is distorted further from spherical symmetry around a nucleus than is usual for the basis set. By adding polarization functions, systems which have polar or ionic internal interactions (such as when we calculate the properties of ion/counterion pairs), can be more accurately calculated.

*6-31G and 6-311G(d,p)*

This type of basis set, currently called a Pople basis set, was based on concepts originally developed by Boys and presented in 1950[59]. The set names list the number of Gaussian basis functions used to form each orbital in the basis set, with 6 Gaussians combined to form each core orbital basis function and multiple basis functions for the valence electrons.

For 6-31G[41, 42] there are two basis functions per valence electron, one made of 3 Gaussian distributions added together and one made with a single Gaussian function. This type of basis set is called a split-valence basis set because the valence orbital's shape can be optimized by adjusting the relative weights of the multiple basis functions in the valence orbitals during the ab-initio step.

The additional (d,p) in the second example, 6-311G(d,p) has 3 functions per valence electron rather than two as in 6-31G. It also adds polarization functions to the s and p orbitals to further improve the quality of the basis. The s type orbital receives an additional p-type basis function and the p orbital receives a d-type orbital.

*CEP basis sets*

The CEP basis sets, CEP-31G and CEP-121G[44-46], are Relativistic Compact Effective Potential basis sets. They replace central core electrons by a single potential which includes relativistic effects, leaving the valence electrons to be

calculated normally by the theory chosen in the calculation. The basis sets were developed to use a reduced number of basis functions but provide the same accuracy as previously developed numerical basis sets. We used these basis sets extensively in our calculations with mercury to save calculation time and allow us to examine larger systems which would otherwise be computationally out of reach.

*cc-pVxZ basis sets and complete basis set extrapolation*

The cc- basis sets, concieved by Dunning, T.H. and later Petersen et al.[47-49], were designed specifically to be correlation-consistent across the different basis set sizes, which means that the energies calculated with each one would be proportional to the energy as calculated with a complete basis set (or with numerical methods to sufficient accuracy). This property allows calculations with a series of cc-pV*Z basis sets (they appear in a series from cc-pVDZ, cc-pVTZ, cc-pVQZ, cc-pV5Z) on the same system to be combined to easily estimate the results which would appear from the complete basis set in a reproducible manner.

An extrapolation function[52] is shown in Equation 3.26 below, and an example of its use appears in Chapter 4 applied to an $HgCl_2$ calculation.

(3.26) $$E_n = E_{CBS} + An^{-3}$$

*CBSB7 basis sets*

Similarly, a basis set was customized by Petersen's group for a model chemistry which they designed called CBS-QB3[15, 16], which does a basis set extrapolation as part of its procedure. The CBSB7[16] basis sets are not necessarily needed outside of the CBS-QB3 method, but they are useful when finding system geometries especially in solvated systems, where the CBS-QB3 method sometimes has difficulties determining a minimum in the potential energy surface for the geometry during its B3LYP optimization step.

*custom basis set functions*

Its quite possible to add custom functions to a basis set, or to define one from scratch entirely, but doing so goes beyond the scope of this paper. In some of our calculations, we added additional basis set functions to the basis sets used to assist in the quality of the calculations. This is discussed in the appropriate sections.

*basis set overlap corrections (counterpoise corrections)*

Inadequate basis sets can introduce an additional error when there are several atoms close together. The additional basis set coverage caused by the presence of the additional atoms can is called basis set superposition error[53], and if the basis set

used was too small, the extra functions significantly improve the possible electron cloud geometries that the simulation can access, causing an artificial lowering of the calculated energy for the system.

This can be corrected in simpler bonding situations (such as diatomic bonding) by applying a counterpoise correction: introducing a "ghost" atom consisting solely of basis functions without an actual nucleus instead of one of the bonding atoms. By substituting a ghost atom for an atom in a system, the additional energy stabilization caused by its extra basis functions can be determined by comparison with a calculation without the ghost atom, and this correction can be applied to the final result. This may introduce its own problems if there are many basis functions which would be fully occupied by the ghost atom's omitted electrons, by overestimating the correction for artificial stabilization.

This approach is most useful on the edge cases where the size of the calculation combined with the choice of method *forces* the use of a smaller basis set than would be ideal. In normal cases, it is best to increase the basis set size until adding additional basis functions does not significantly affect the final energy, and this is what we did for the most part.

### *3.5 – The Importance of Quality*

What is important in quality? Calculations can have varying levels of quality, going from answers which provide qualitative answers ($H_3AsO_4$ is more acidic than $H_3AsO_3$) to quantitative predictions ($H_3AsO_4$ is 6.9 pKa units (more) acidic than $H_3AsO_3$). As the results of most calculations are defined to a high level of precision, but may or may not correspond closely with experimental measurements.

The causes are often unclear, but often fall into several broad categories.

In some cases, the experimental measurements make assumptions which can be demonstrated to be incorrect by the theory, such as in a calculation of oxidation energetics for gas phase $Hg^0$ [54], where the species that had initially been assumed to be the primary mercury compound in the gaseous system was not clearly identified. A series of calculations showed that the assumed reaction was not predicted to be energetically favorable under gaseous conditions, and set forward another species which fit the observed experimental data much better.

Then there are cases where there are large effects which are difficult to treat with theory, such as quantitatively modeling the stabilization of ions in bulk water.[55] In these cases, the theory can often produce a lot of quite valuable information about spectra and other properties of the system, but can not necessarily be used to predict reaction energetics to high accuracy. Although some of the assumptions which we

make to use our methods are less than perfect, there is still a lot of good data to be seen in the results which we calculate.

Finally, there are the cases which fall somewhere in between, where the experimental data is unavailable or unclear and, at the same time, we are pushing the theory in some fashion. We shall seek to explore some of these cases in our study of solvated mercury compounds.

Model chemistry methods like CBS-QB3, G2, or G3 have been designed in order to produce a predictable level of error in normal situations. The term "Model Chemistry" has to do with the fact that the methods can be used as a model for predicting experimental chemistry results, in particular, well characterized gas dissociation energies from a standardized test set. In exchange for possibly requiring more computation than is necessary for solving some simpler conditions, the methods have been tested over a variety of compounds and the approach explained in detail and justified for general use. They also have an advantage over more hands-on methods in that they may be used by physical chemists who are not necessarily dedicated theoretical chemists. Therefore, we considered this type of approach, as embodied by CBS-QB3, in many cases.

*3.6 – Approaches to Verifying Quality*

There are a few ways by which we confirm the quality of a calculation.

By using higher level methods which have been observed to provide more stable, better and higher quality results we can show by comparison that a lower, more computationally easy method has reached a stable answer as well. This approach requires a knowledge of which assumptions are most correct in the tree of methods available to the researcher, so assistance from a dedicated theoretician in constructing a plan would be invaluable in this part of the process even for a stand-alone lab.

For systems in the sizes which we used here, method wise we usually started with an HF or B3LYP calculation to reach initial geometries from starting guesses or molecular mechanics models, followed by MP2 and CCSD (or CCSD(T) calculations, for the smaller systems) could show that the total energy and our measurements of interest had stabilized in one of the lower level steps.

We often do a variety of calculations on each of our compounds of interest at differing levels of theory to get a feel for the level of theory required to get accurate results. For example, as seen in Chapters 5 through 7, we used several different methods to deal with hydration including CPCM, counterions, and explicit hydration to estimate solvation effects on a series of polyprotic acids, comparing the results.

Alternatively, we can use two similar in quality, but different in approach methods to check on the other's result. If both schema yield the same final answer for a dissociation, for example, it makes us confident that that level of theory is sufficient to treat the problem. An example of this might be our calculations using B3LYP and MP2 methods in parallel to explore the behavior of the $HClO_x$ compounds discussed in Chapter 7.

We can apply this same approach to our choice of basis set as well. By doing a set of calculations with a normally sized basis, followed by a few with a much larger basis, we can confirm that the results with the extra large basis set are equivalent to the smaller set, and this gives us confidence that the results have stabilized to the extent that our first set was sufficient to represent the situation we are simulating.

Another factor in our approach is the ordering of the calculations. While it is not very expensive to do hybrid density-functional method calculations such as B3LYP, it is often the case that a B3LYP optimization takes much longer on its own than a less correct Hartree-Fock optimization followed by a B3LYP optimization from the final geometry. Even if a method has known shortcomings it can be a vital part of a good calculation. It is like the story of the lensgrinder who said that it is faster to make a three inch lens then a six inch lens than make a six inch lens right off.

We also used a similar approach when doing our CBS-QB3 calculations, which start out with a B3LYP optimization. We have observed that an initial HF or MP2 optimization of our compound followed by CBS-QB3 requires much less human intervention to reach a stable optimized geometry and we would therefore suggest that this approach of preliminary optimization may be a more efficient use of time and resources than direct application of CBS-QB3.

This method of starting with a medium or small-scale calculation and then bootstrapping the results to reach a higher-level answer more efficently is common in applied computational chemistry. Another tool is to do a calculation a few times using different methods and compare the differences in the results[9] For example, one can, when constructing a spectra, conduct anharmonic and harmonic frequency calculations at a lower level of theory, and compute correction factors from those to apply to a higher-level, simpler calculation of harmonic frequencies. This bootstrapping approach would yield results with higher quality results with less calculation time than attempting a possibly impossible anharmonic calculation under the higher-level model[56].

## *3.7 References*

1. Schrodinger, E., *An Undulatory Theory of the Mechanics of Atoms and Molecules.* Physical Review, 1926. **28**(6): p. 1049.

2. Pauli, W., *Über das Wasserstoffspektrum vom Standpunkt der neuen Quantenmechanik.* Zeitschrift für Physik A Hadrons and Nuclei, 1926. **36**(5): p. 336-363.

3. Adams, W.H., *Solution of Schrodinger Equation for H2 in Terms of a Wave-Function Least Distorted from a Product of Atomic Wave-Functions.* International Journal of Quantum Chemistry, 1973: p. 127-133.

4. Kolos, W. and Wolniewi.L, *IMPROVED THEORETICAL GROUND-STATE ENERGY OF HYDROGEN MOLECULE.* Journal of Chemical Physics, 1968. **49**(1): p. 404-&.

5. Roothaan, C.C.J., *New Developments in Molecular Orbital Theory.* Reviews of Modern Physics, 1951. **23**(2): p. 69-89.

6. Slater, J.C., *Atomic Shielding Constants.* Physical Review, 1930. **36**(1): p. 57.

7. Harris, F.E. and H.H. Michels, *Multicenter Integrals in Quantum Mechanics. II. Evaluation of Electron-Repulsion Integrals for Slater-Type Orbitals.* The Journal of Chemical Physics, 1966. **45**(1): p. 116-123.

8. Hehre, W.J., R.F. Stewart, and J.A. Pople, *Self-Consistent Molecular-Orbital Methods .I. Use of Gaussian Expansions of Slater-Type Atomic Orbitals.* Journal of Chemical Physics, 1969. **51**(6): p. 2657-&.

9. M. J. Frisch, G.W.T., H. B. Schlegel, G. E. Scuseria, M. A. Robb, J. R. Cheeseman, J. A. Montgomery, Jr., T. Vreven, K. N. Kudin, J. C. Burant, J. M. Millam, S. S. Iyengar, J. Tomasi, V. Barone, B. Mennucci, M. Cossi, G. Scalmani, N. Rega, G. A. Petersson, H. Nakatsuji, M. Hada, M. Ehara, K.

Toyota, R. Fukuda, J. Hasegawa, M. Ishida, T. Nakajima, Y. Honda, O. Kitao, H. Nakai, M. Klene, X. Li, J. E. Knox, H. P. Hratchian, J. B. Cross, V. Bakken, C. Adamo, J. Jaramillo, R. Gomperts, R. E. Stratmann, O. Yazyev, A. J. Austin, R. Cammi, C. Pomelli, J. W. Ochterski, P. Y. Ayala, K. Morokuma, G. A. Voth, P. Salvador, J. J. Dannenberg, V. G. Zakrzewski, S. Dapprich, A. D. Daniels, M. C. Strain, O. Farkas, D. K. Malick, A. D. Rabuck, K. Raghavachari, J. B. Foresman, J. V. Ortiz, Q. Cui, A. G. Baboul, S. Clifford, J. Cioslowski, B. B. Stefanov, G. Liu, A. Liashenko, P. Piskorz, I. Komaromi, R. L. Martin, D. J. Fox, T. Keith, M. A. Al-Laham, C. Y. Peng, A. Nanayakkara, M. Challacombe, P. M. W. Gill, B. Johnson, W. Chen, M. W. Wong, C. Gonzalez, and J. A. Pople, *Gaussian 03, Revision C.02*, 2004, Gaussian, Inc., Wallingford CT.

10. Moller, C. and M.S. Plesset, *Note on an Approximation Treatment for Many-Electron Systems.* Physical Review, 1934. **46**(7): p. 618.

11. Head-Gordon, M., J.A. Pople, and M.J. Frisch, *MP2 energy evaluation by direct methods.* Chemical Physics Letters, 1988. **153**(6): p. 503-506.

12. Čížek, J., *On the Use of the Cluster Expansion and the Technique of Diagrams in Calculations of Correlation Effects in Atoms and Molecules*. Advances in Chemical Physics1969: John Wiley & Sons, Inc. 35-89.

13. Pople, J.A., et al., *Electron Correlation Theories and Their Application to Study of Simple Reaction Potential Surfaces.* International Journal of Quantum Chemistry, 1978. **14**(5): p. 545-560.

14. Becke, A.D., *Density-functional thermochemistry. III. The role of exact exchange.* J. Chem. Phys., 1993. **98**: p. 5648-52.

15. Montgomery, J.A., et al., *A complete basis set model chemistry. VII. Use of the minimum population localization method.* Journal of Chemical Physics, 2000. **112**(15): p. 6532-6542.

16. Montgomery, J.A., et al., *A complete basis set model chemistry. VI. Use of density functional geometries and frequencies.* Journal of Chemical Physics, 1999. **110**(6): p. 2822-2827.

17. Velde, G.t., et al., *Chemistry with ADF.* Journal of Compututational Chemistry, 2001. **22**: p. 931.

18. Guerra, C.F., et al., *Towards an order-N DFT method.* Theoretical Chemistry Accounts, 1998. **99**.

19. Baerends, E.J., et al., *ADF2004.01, SCM, Theoretical Chemistry, Vrije Universiteit, Amsterdam, The Netherlands,* http://www.scm.com. 2004.

20. Lenthe, E.v. and E.J. Baerends, *Optimized Slater-type basis sets for the elements 1-118.* Journal of Computational Chemistry 2003. **24**.

21. Schreckenbach, G. and T. Ziegler, *The calculation of NMR shielding tensors using GIAO's and modern density functional theory.* Journal of Physical Chemistry, 1995. **99**.

22. Schreckenbach, G. and T. Ziegler, *The calculation of NMR shielding tensors based on density functional theory and the frozen-core approximation.* International Journal of Quantum Chemistry, 1996. **60**.

23. Lenthe, E.v., A.E. Ehlers, and E.J. Baerends, *Geometry optimization in the Zero Order Regular Approximation for relativistic effects.* Journal of Chemical Physics, 1999. **110**.

24. Wolff, S.K., et al., *Density functional calculations of nuclear magnetic shieldings using the zeroth-order regular approximation (ZORA) for relativistic effects: ZORA nuclear magnetic resonance.* Journal of Chemical Physics, 1999. **110**: p. 7689

25. J. A. Pople, J.S.B., and R. Seeger, *Theoretical Models Incorporating Electron Correlation.* Int. J. Quant. Chem, 1976. **S10**.

26. K. Raghavachari and J. A. Pople, *Approximate 4th-order perturbation-theory of electron correlation energy.* Int. J. Quant. Chem, 1978. **14**: p. 91-100.

27. Yang, R.G.P.a.W., *Density-functional theory of atoms and molecules.*1989, Oxford: Oxford Univ. Press.

28. Curtiss, L.A., et al., *Gaussian-2 Theory for Molecular-Energies of 1st-Row and 2nd-Row Compounds.* Journal of Chemical Physics, 1991. **94**(11): p. 7221-7230.

29. Curtiss, L.A., et al., *Gaussian-3 (G3) theory for molecules containing first and second-row atoms.* Journal of Chemical Physics, 1998. **109**(18): p. 7764-7776.

30. Curtiss, L.A., et al., *Assessment of Gaussian-2 and density functional theories for the computation of ionization potentials and electron affinities.* Journal of Chemical Physics, 1998. **109**(1): p. 42-55.

31. Curtiss, L.A., et al., *Assessment of Gaussian-2 and density functional theories for the computation of enthalpies of formation.* Journal of Chemical Physics, 1997. **106**(3): p. 1063-1079.

32. Curtiss, L.A., P.C. Redfern, and K. Raghavachari, *Assessment of Gaussian-3 and density-functional theories on the G3/05 test set of experimental energies.* Journal of Chemical Physics, 2005. **123**(12): p. -.

33. Curtiss, L.A., et al., *Assessment of Gaussian-3 and density functional theories for a larger experimental test set.* Journal of Chemical Physics, 2000. **112**(17): p. 7374-7383.

34. Redfern, P.C., et al., *Assessment of Gaussian-3 and density functional theories for enthalpies of formation of C-1-C-16 alkanes.* Journal of Physical Chemistry A, 2000. **104**(24): p. 5850-5854.

35. Xiu-Juan, Q., et al., *Assessment of Performance of G3B3 and CBS-QB3 Methods in Calculation of Bond Dissociation Energies.* Chinese Journal of Chemistry, 2005. **23**(2): p. 194-199.

36. Pickard Iv, F.C., et al., *Comparison of CBS-QB3, CBS-APNO, G2, and G3 thermochemical predictions with experiment for formation of ionic clusters of hydronium and hydroxide ions complexed with water.* The Journal of Chemical Physics, 2005. **122**(2): p. 024302-7.

37. Barone, V. and M. Cossi, *Quantum calculation of molecular energies and energy gradients in solution by a conductor solvent model.* Journal of Physical Chemistry A, 1998. **102**(11): p. 1995-2001.

38. Barone, V., M. Cossi, and J. Tomasi, *Geometry optimization of molecular structures in solution by the polarizable continuum model.* Journal of Computational Chemistry, 1998. **19**(4): p. 404-417.

39. Cossi, M., et al., *Energies, structures, and electronic properties of molecules in solution with the C-PCM solvation model.* Journal of Computational Chemistry, 2003. **24**(6): p. 669-681.

40. Frisch, M.J., J.A. Pople, and J.S. Binkley, *Self-Consistent Molecular-Orbital Methods .25. Supplementary Functions for Gaussian-Basis Sets.* Journal of Chemical Physics, 1984. **80**(7): p. 3265-3269.

41. Hehre, W.J., Ditchfie.R, and J.A. Pople, *Self-Consistent Molecular-Orbital Methods .12. Further Extensions of Gaussian-Type Basis Sets for Use in Molecular-Orbital Studies of Organic-Molecules.* Journal of Chemical Physics, 1972. **56**(5): p. 2257-&.

42. Ditchfie.R, W.J. Hehre, and J.A. Pople, *Self-Consistent Molecular-Orbital Methods .9. Extended Gaussian-Type Basis for Molecular-Orbital Studies of Organic Molecules.* Journal of Chemical Physics, 1971. **54**(2): p. 724-&.

43. Mclean, A.D. and G.S. Chandler, *Contracted Gaussian-Basis Sets for Molecular Calculations .1. 2nd Row Atoms, Z=11-18.* Journal of Chemical Physics, 1980. **72**(10): p. 5639-5648.

44. Stevens, W.J., et al., *Relativistic Compact Effective Potentials and Efficient, Shared-Exponent Basis-Sets for the 3rd-Row, 4th-Row, and 5th-Row Atoms.*

Canadian Journal of Chemistry-Revue Canadienne De Chimie, 1992. **70**(2): p. 612-630.

45. Stevens, W.J., H. Basch, and M. Krauss, *Compact Effective Potentials and Efficient Shared-Exponent Basis-Sets for the 1st-Row and 2nd-Row Atoms.* Journal of Chemical Physics, 1984. **81**(12): p. 6026-6033.

46. Cundari, T.R. and W.J. Stevens, *Effective Core Potential Methods for the Lanthanides.* Journal of Chemical Physics, 1993. **98**(7): p. 5555-5565.

47. Wilson, A.K., et al., *Gaussian basis sets for use in correlated molecular calculations. IX. The atoms gallium through krypton.* Journal of Chemical Physics, 1999. **110**(16): p. 7667-7676.

48. Woon, D.E. and T.H. Dunning, *Gaussian-Basis Sets for Use in Correlated Molecular Calculations .3. The Atoms Aluminum through Argon.* Journal of Chemical Physics, 1993. **98**(2): p. 1358-1371.

49. Dunning, T.H., *Gaussian Basis Functions for Use in Molecular Calculations . 1. Contraction of (9s5p) Atomic Basis Sets for First-Row Atoms.* Journal of Chemical Physics, 1970. **53**(7): p. 2823-&.

50. Spitznagel, G.W., et al., *Efficient Diffuse Function-Augmented Basis-Sets for Anion Calculation .4. An Evaluation of the Performance of Diffuse Function-Augmented Basis-Sets for 2nd-Row Elements, Na-Cl.* Journal of Computational Chemistry, 1987. **8**(8): p. 1109-1116.

51. Clark, T., et al., *Efficient Diffuse Function-Augmented Basis-Sets for Anion Calculations .3. The 3-21+G Basis Set for 1st-Row Elements, Li-F.* Journal of Computational Chemistry, 1983. **4**(3): p. 294-301.

52. Halkier, A., et al., *Basis-set convergence of the energy in molecular Hartree-Fock calculations.* Chemical Physics Letters, 1999. **302**(5-6): p. 437-446.

53. Davidson, E.R. and S.J. Chakravorty, *A possible definition of basis set superposition error.* Chemical Physics Letters, 1994. **217**(1-2): p. 48-54.

54. Tossell, J.A., *Calculation of the energetics for oxidation of gas-phase elemental Hg by Br and BrO.* Journal of Physical Chemistry A, 2003. **107**(39): p. 7804-7808.

55. Tossell, J.A., *Calculation of reaction energies in solution: Successes and conundrums.* Abstracts of Papers of the American Chemical Society, 2005. **229**: p. U710-U710.

56. Tossell, J.A. and M.D. Zimmermann, *Calculation of the structures, stabilities, and vibrational spectra of arsenites, thioarsenites and thioarsenates in aqueous solution.* Geochimica Et Cosmochimica Acta, 2008. **72**(21): p. 5232-5242.

57. Boys, S. F., *Electronic Wave Functions. I. A General Method of Calculation for the Stationary States of Any Molecular System*. Proc. R. Soc. Lond. A, 1950, **200**(1063) p. 542-554.

58. Levine, I. N. *Quantum Chemistry*, 3rd ed.; Allyn and Bacon: Massachusetts, 1970.

# Chapter 4: Mercury Chloride Free energies in solution: equilibrium constants from theoretical calculations at the CCSD(T) level and above

*A series of calculations on $HgCl_x$ compounds is conducted using CCSD(T) and correlation-consistent basis sets in the gas phase, and combined with hydration free energies taken at HF/CEP-121G with the CPCM solvation model. NMR shieldings calculated by ADF are also explored for the same series.*

## *4.1 Introduction*

As previously discussed, $Hg^{2+}$ and its compounds, often referred to as Reactive Gaseous Mercury (RGM) in atmospherics studies[1], are of interest to us because of the hazards seen from methylmercury compounds, which have been observed to be converted from other sources of dissolved mercury by sulfur reducing bacteria.

Mercury chloride compounds have been studied before in solution, but the experimental data on hand is from many years ago[2]. An important sink for gaseous mercury is the world's oceans, and these have a relatively high concentration of salt, which could easily interact with any dissolved cationic mercury.

Therefore, we began our calculations by investigating the behavior of chlorinated mercury compounds ($Hg^{2+}$, $HgCl^{+}$, $HgCl_2$, $HgCl_3^{-}$, and $HgCl_4^{-2}$), followed by compounds formed from the other halides expected to be in seawater ($F^{-}$, $Br^{-}$ and, $I^{-}$).

*4.2 Methods*

Gaussian 03[3], a computer quantum chemistry package, was used to conduct the calculations presented in this chapter.

In each case we attempted to follow a systematic series of steps when conducting our calculations. We shall describe those steps here. Although in each stage we used different quantum chemical theories to do the calculations, the basis sets used most often were CEP-31G and CEP-121G. Because of prior experience, we expected the results from CEP-121G to be higher quality than the others, and for both basis sets we included additional diffuse functions to improve the modeling of the anionic forms after reviewing our initial calculations without them. These additional functions for heavy atoms (Hg, halogens, oxygen, etc.) are described as follows in Table 4.1 for each of the atom types:

| Atoms | Function Type | Coefficient |
|---|---|---|
| Hg | F | 0.486 |
| C, S, O | D | 0.700 |
| F, Cl, Br, I | D | 0.650 |

Table 4.1: Extra diffuse functions used in the calculations conducted in this chapter.

Initially, Hartree-Fock geometry optimization and vibrational frequency calculations (for confirming the final geometries were not at saddle points on the potential energy surface) were conducted for each species. These were for the most part successful. As the primary reason for these calculations was to determine geometries for the other methods, the results of most of the HF calculations are not reported here except as noted below.

B3LYP geometry optimization and vibrational frequency calculations were slightly less successful than the HF calculations due to difficulties getting all of the geometries to converge successfully in a timely manner. We observed some compounds oscillating in loops on the potential energy surface, and others where the geometry changed so slowly that convergence was not attained in a reasonable length of time. In the majority of cases we eventually did reach optimized geometries, however, though the occasional troublesome anion remained unsolved. In particular, this optimization problem prevented us from reporting data for reactions involving the $HgCl_4^{2-}$ species.

Finally, CCSD geometry optimization and vibrational frequency calculations were taken from the HF geometries. Although the CCSD calculations were computationally expensive, these calculations were completed successfully for most

of the compounds and the results are presented below and compared with the B3LYP results.

The largest calculations which we ran used the CCSD(T) method, which was combined with multiple Correlation Consistent basis sets from the cc-pV*Z series to do energetics calculations at the CCSD geometries.

### 4.2.1 Basis Set Selection

The Gaussian 03 package[3] included these basis sets for the $Cl^-$, and $Br^-$ calculations, while the Hg and $I^-$ basis sets used were obtained from the Extensible Computational Chemistry Environment Basis Set Database, Version 02/25/04[4].

CCSD(T) calculations were completed for the cc-pVDZ basis, and up to the triply substituted species for Cl, Br, and I anions. In the case of the cc-pVTZ basis, the Cl calculation was also finished to the triply substituted $HgCl_3^-$. For the heavier systems with Br and I, the results were somewhat limited, but included both of the singly substituted ions.

The $Cl^-$ calculations were also done up to $HgCl_2$ with cc-aug-pVDZ and cc-aug-pVTZ, correlation consistent basis sets augmented with extra basis functions to improve accuracy for the ionic species in the calculation.

[4]As developed and distributed by the Molecular Science Computing Facility, Environmental and Molecular Sciences Laboratory which is part of the Pacific Northwest Laboratory, P.O. Box 999, Richland, Washington 99352, USA, and funded by the U.S. Department of Energy. (The Pacific Northwest Laboratory is a multi-program laboratory operated by Battelle Memorial Institute for the U.S. Department of Energy under contract DE-AC06-76RLO 1830. Contact Karen Schuchardt for further information.)

### 4.2.2 Complete Basis Set Extrapolation

With the results from the CCSD(T) calculations it was possible to extrapolate from the cc-pVDZ and cc-pVTZ results using a complete basis set extrapolation function initially developed by Halkier, et al.[4] and applied to CCSD(T) shortly afterwards[5], which appears as Equation (1) below. As expected, with the more extensive aug-cc-pVDZ/aug-cc-pVTZ basis we see a lower raw energy for the $Hg^{2+}$ cation as well as the other species which were looked at with the approach, $Cl^-$, $HgCl^+$ and $HgCl_2$.

The complete basis set energy ECBS can be extrapolated from lower level calculations with correlation consistent basis sets by the following method shown in Equation 4.1, 4.2, and 4.3, where $E_{CBS}$ is the complete basis set energy, $E_n$ is the energy calculated with the corresponding basis set (cc-pVDZ would have n=2, cc-pVTZ would have n=3), and A is a factor which depends on which basis sets are being used in the calculation.

(4.1) $E_n = E_{CBS} + An^{-3}$, or

(4.2) $E_{CBS} = E_n - An^{-3}$, and

(substituting n=2 and n=3 for cc-pVDZ and cc-pVTZ, and solving A and then for $E_{CBS}$)

(4.3) $E_{CBS} = (27/19)E_3 - (8/19)E_2$

The solvation model used throughout this project was the CPCM polarizable continuum method. The energy of solvation for each compound at its final gas phase geometry was calculated, and this stabilizing factor added to the final Gibbs Free Energy when calculating the change in Gibbs Free Energy for each formation reaction to estimate the solvation energy in the solvated phase.

Also examined a system with explicitly solvated clusters of water molecules, to compare the energetics for the following reaction:

$$Hg^{2+} + Cl^{-} \rightarrow HgCl^{+} + H_2O$$

The $Hg^{2+}$ was solvated with six water molecules, and the $HgCl^{+}$ with five. We then calculated the energy using both Hartree-Fock and MP2 approaches.

In future chapters, later calculations including ones with hydration energies calculated during the optimization phases shall be presented. The energies determined from that direct approach will then be compared to energies which were found (additively as described in this chapter) at that point.

*4.3 Results and Discussion*

In each case we see that the CPCM stabilization calculated is dramatically larger for the more charged and smaller species. This is reasonable, because the CPCM method makes a sequestered shell in a continuous dielectric around the compound of interest, and a smaller shell will lead to a much stronger electronic stabilization because of the reduced area that the charge is interacting over.

Therefore, we see that the CPCM hydration energy for $Cl^-$ and $HgCl^{3-}$ are significantly different; -76.55 kcal/mol for $Cl^-$ and only 47.26 kcal/mol for $HgCl^{3-}$. We see a similar, but even larger difference between the calculated hydration energies for $Hg^{2+}$ and $HgCl_4^{2-}$. There, the energy for $Hg^{2+}$ is -407.17 kcal/mol, but the stabilization for $HgCl_4^{2-}$, which is much larger of a species, is -160.89 kcal/mol. This is on the same scale as $HgCl^+$, which has a CPCM stabilization energy of -139.85 kcal/mol.

Comparing the calculations done with CCSD and B3LYP is instructive as well. The CCSD calculations were done with two different basis sets, CEP-31G+ and CEP-121G+. The calculation with the larger basis shows a difference on the order of 3 hundredths of Hartrees for species including the Chlorine atoms. This difference is approximately 19 kcal/mol (627.5 Hartrees are approximately 1 kcal/mol), but it is present in all of the cases so the difference doesn't affect the changes in energy for the chlorination reactions.

For the solvated cluster, we see a more dramatic result from updating the basis set used in the calculation. The total effect on the stability of the clusters is approximately 0.1 Hartrees or 62 kcal/mol. This dramatic change in energy is probably due to the additional wavefunctions on the six water molecules. The difference for the single water molecule is approximately 0.01 Hartrees going between the CEP-31G+ basis set and the CEP-121G+ basis set.

This accounts for about half of the energy difference between the free $Hg^{2+}$ and the singly solvated group $Hg^{2+}$. $6H_2O$ between the two basis sets. The larger basis has an additional stabilization of 0.07 Hartrees, or approximately 44 kcal/mol when the system is calculated under HF conditions. Under the MP2 method, the energy difference caused by the change in basis is only 2 kcal/mol, however.

From the previous measurements, we can find the reaction energetics for each of the following tabulated reactions, shown below in Table 4.2. This table shows the difference in solvation stabilization between the products and the reactants. We see here that, as we might expect, that multiple smaller and more charged species are stabilized more than the single product molecules except in the final case of HgCl42-.

| Reaction | CPCM Stabilization Energy (kcal/mol) |
|---|---|
| $Hg^{2+} + Cl^- \rightarrow HgCl^+$ | +343.87 |
| $HgCl^+ + Cl^- \rightarrow HgCl_2$ | +195.72 |
| $HgCl_2 + Cl^- \rightarrow HgCl_3^-$ | +49.97 |
| $HgCl_3^- + Cl^- \rightarrow HgCl_4^{2-}$ | -37.08 |

Table 4.2: Stabilization Energies for Successive $Cl^-$ addition to $Hg^{2+}$

We see in each case that the solvation stabilization from the gas phase geometries of each compound taken together yields a non-favorable result for the reactions except in the case of the final one where the effect is favorable due to the high charge of the $HgCl_4^{2-}$.

| Reaction | $\Delta G_{rxn}$ Energy (Hartrees) | $\Delta G_{rxn}$ Energy (kcal/mol) | CPCM Stabilization Energy (kcal/mol) | Gas phase geom. + stabilization (kcal/mol) $\Delta G_{rxn}$ |
|---|---|---|---|---|
| $Hg^{2+} + Cl^- \rightarrow HgCl^+$ | -.630985 | -395.94 | +343.87 | -52.07 |
| $HgCl^+ + Cl^- \rightarrow HgCl_2$ | -.356220 | -223.53 | +195.72 | -27.81 |
| $HgCl_2 + Cl^- \rightarrow HgCl_3^-$ | -.075280 | -47.23 | +49.97 | +2.74 |
| $HgCl_3^- + Cl^- \rightarrow HgCl_4^{2-}$ | .061599 | 38.65 | -37.08 | +1.57 |

Table 4.3: CCSD CEP-31G Energy Calculations for Successive $Cl^-$ addition

We report the results here to two decimal places in kcal/mol units. The original Hartree units are reported to more decimals, but it is important to realize that the results of the calculations may be precise to this many decimal places, but we need to show their accuracy against known experimental data as these models contain many assumptions which affect the quality of the results. Care must be taken in assuming that reported experimental measurements are applicable to the conditions presumed in

the calculation, as occasionally the interpretations of experimental measurements change as further research is conducted.

In the *ab initio* calculation with the smallest basis set we observe trends that stay in place throughout the other more computationally expensive methods. Although in the gas phase all but the last $Cl^-$ addition are energetically favorable, the magnitudes of the favorability are comparable with the magnitudes of the hydration energy contributions.

In the gas phase, the results vary from the favorable -394.94 kcal/mol change in energy for the first chlorination to the unfavorable +38.65 kcal/mol energy change for the fourth chlorination. This could be due to the instability of the $Cl^-$ ion in the gas phase, which makes forming the larger anion automatically favorable because it gives the extra electron more room. This means that without solvation, $HgCl_3^-$ would be the last compound formed with excess $Cl^-$ present under normal gas phase conditions. Any $HgCl_4^{2-}$ introduced "bare" into the gas phase would be predicted to dissociate into $HgCl_3^-$ and $Cl^-$ ions by these results as well.

With the contributions from CPCM solvation, we see that the stabilization ranges from -52.07 kcal/mol favorable for the first chlorination to +2.74 kcal/mol unfavorable for the third. To add an additional $Cl^-$ and reach $HgCl_4^{2-}$ would only require another +1.57 kcal/mol of energy.

This would presumably mean the most common species in aqueous solutions would be $HgCl_2$, although with sufficient presence of $Cl^-$ anions one could push through and end up with $HgCl_4^{2-}$.

| Reaction | $\Delta G_{rxn}$ Energy (Hartrees) | $\Delta G_{rxn}$ Energy (kcal/mol) | CPCM Stabilization Energy (kcal/mol) | $\Delta G_{rxn}$ Gas phase geom. + stabilization (kcal/mol) |
|---|---|---|---|---|
| $Hg^{2+} + Cl^- \rightarrow HgCl^+$ | -.625995 | -392.81 | +343.87 | -48.94 |
| $HgCl^+ + Cl^- \rightarrow HgCl_2$ | -.352189 | -221 | +195.72 | -25.28 |
| $HgCl_2 + Cl^- \rightarrow HgCl_3^-$ | -.072343 | -45.40 | +49.97 | +4.57 |
| $HgCl_3^- + Cl^- \rightarrow HgCl_4^{2-}$ | .064210 | +40.29 | -37.08 | +3.21 |

Table 4.4: CCSD CEP-121G+ Calculations for Successive $Cl^-$ addition

Conducting the same calculations with a larger CEP-121G+ basis set, we observe an identical trend in the results. The most favorable step in the solvated system is the initial chlorination of $Hg^{2+}$ to form $HgCl^+$, and the least favorable is the conversion of $HgCl_2$ to $HgCl_3^-$, and we see the same instance in the gas phase system of the larger anion in the $HgCl_2$ to $HgCl_3^-$ system being more favorable.

The most stable solvated species here is $HgCl_2$. Looking at the calculated energetics, this is where the benefits of chlorination in the gas phase system become significantly

smaller. While the first chlorination has a benefit of -392.81 kcal/mol, and the second has one of -221.00 kcal/mol, a difference about half the magnitude of the larger number, the difference in the second case between -221.00 kcal/mol and -45.40 kcal/mol is one quarter of the magnitude of the larger figure. At the same time, the magnitudes of the CPCM stabilization are shrinking by a similar amount. It is the interaction between these two different rates of change that places the solvated $HgCl_2$ system in a balancing place, providing for a different most stable species in the gas phase and in solution. In the gas phase, the ionic system would preferentially form $HgCl_3^-$ rather than $HgCl_2$, because the additional third chlorination is favorable by -45.40 kcal/mol against keeping the free $Cl^-$ ion separate from the cluster.

| Reaction | Energy (Hartrees) $\Delta G_{rxn}$ | Energy (kcal/mol) $\Delta G_{rxn}$ | CPCM Stabilization Energy (kcal/mol) | Gas phase geom. + stabilization (kcal/mol) $\Delta G_{rxn}$ |
|---|---|---|---|---|
| $Hg^{2+} + Cl^- \rightarrow HgCl^+$ | -.633918 | -397.78 | +343.87 | -53.91 |
| $HgCl^+ + Cl^- \rightarrow HgCl_2$ | -.344079 | -215.91 | +195.72 | -20.19 |
| $HgCl_2 + Cl^- \rightarrow HgCl_3^-$ | -.074486 | -46.74 | +49.97 | +3.23 |
| $HgCl_3^- + Cl^- \rightarrow HgCl_4^{2-}$ | .064352 | +40.38 | -37.08 | +3.30 |

Table 4.5: B3LYP CEP-121G+ Energy Calculations of Successive $Cl^-$ addition to $Hg^{2+}$

The B3LYP method has previously been shown to provide reasonable results on the G2 test set, with average errors of 2.4 kcal/mol across the collection[6]. Its performance on this system is similar. The gas phase results indicate that the $HgCl_2$ system will be chlorinated once more with the favorable energy -46.74 kcal/mol, but that this third chlorination is not favorable in the solvated system. The energetics calculated here differ from the CCSD values by about 5 kcal/mol in the first two systems, but the differences between the results in the $HgCl_2$ to $HgCl_3^-$ chlorination and the $HgCl_3^-$ to $HgCl_4^{2-}$ chlorination drop to the order of 1 kcal/mol for the former and less than 1 kcal/mol for the latter.

Once again in this method we see that the most stable $HgCl_x$ species in the gas phase is $HgCl_3^-$ and in the hydrated phase $HgCl_2$. The energies here required to form $HgCl_3^-$ from $HgCl_2$ and $HgCl_4^{2-}$ from $HgCl_3^-$ are approximately equal in magnitude, though this theory calculates that the $HgCl_4^{2-}$ reaction is even less favorable (slightly) than $HgCl_3^-$.

In all three cases, however, the reaction is shown to show the same identical trends. As the B3LYP approach is significantly less computationally expensive than CCSD, this stability of the results both indicates that B3LYP is sufficient and that it has reached a stable answer. We shall look at some further methods of calculation, however, to confirm this.

| Method | Energy (Hartrees) | Energy (kcal/mol) |
|---|---|---|
| HF CEP-31G | -.23827 | -149.51 |
| HF CEP-121G | -.22884 | -143.60 |
| MP2 CEP-31G | -.35487 | -222.68 |
| MP2 CEP-121G | -.35307 | -221.55 |

Table 4.6: Comparison of methods in calculating the $\Delta G_{rxn}$ free energy of reaction for the explicitly Solvated System: $Hg^{2+} . 6H_2O + Cl^- \rightarrow HgCl^+ . 5H_2O + H_2O$

We see here that the change in free energy here is much lower than the gas phase reaction energy. This is because the single solvation layer present in the system can account for a good percentage of the energy stabilization which we previously modeled with the CPCM method as adjusted to provide a solvation environment similar to water.

The cluster calculation done at HF and MP2 levels shows an energy which is in between the gas phase + CPCM stabilized energy calculation for the same reaction and the gas phase energies as expected. The presence of even a single solvation layer of water molecules in a nanocluster demonstratably brought the total energy about 180 kcal/mol closer in the MP2 case and 230 kcal/mol closer in the HF case to the stabilized energies found with the other approaches. In the future, more explicit cluster calculations are clearly indicated for further exploration.

We also conducted a complete basis set extrapolation from CCSD(T) calculated energies, the results of which are shown in Table 4.7 and with supporting data in Table 4.10(a-e) below.

| Reaction | Energy (Hartrees) | Energy (kcal/mol) | CPCM Stabilization Energy (kcal/mol) | Gas Phase geom. + stabilization |
|---|---|---|---|---|
| $Hg^{2+} + Cl^- \rightarrow$ | -.6166878 | -386.97 | +343.87 | -43.10 |
| $HgCl^+$ | -.6291525 | -394.79 | | -50.92 |
| $HgCl^+ + Cl^- \rightarrow HgCl_2$ | -.34507 | -216.53 | +195.72 | -20.81 |
| | -.347219 | -217.88 | | -22.16 |
| $HgCl_2 + Cl^- \rightarrow HgCl_3^-$ | -.06584 | -41.31 | +49.97 | +8.66 |
| $Hg^{2+} + Br^- \rightarrow$ | -.6223905 | -390.55 | | |
| $HgBr^+$ | | | | |

Table 4.7: Complete Basis Set CCSD(T) CBS model results for successive Cl-additions to $Hg^{2+}$. Values on the first rows are with the standard cc-pV*Z basis sets, values beneath them were calculated with the augmented aug-cc-pV*Z basis sets.

This extrapolation lead us to observe the same trends as we did with the limited CEP-31G and CEP-121G+ basis sets; the theoretical methods show that the formation of $HgCl_3^-$ in the gas phase is a favorable reaction, while in the solvated system the last favorable chlorination is converting $HgCl^+$ to $HgCl_2$. The main differences we see

here when compared to the CCSD CEP-121G+ are that except for the $HgCl^+$ formation with the augmented basis set shown on the bottom right of the first line of the table, the energetics calculated with this method are uniformly less favorable than the ones found with the CCSD CEP-121G+ method by around 4 kcal/mol.

We also have calculations for $Hg^{2+}$ + $Br^-$ forming $HgBr^+$. This reaction is favorable on about the same level as the chlorination reaction. Though the hydration energy stabilization for the HgBr system is not presented here, we would expect it to be a similar magnitude as the HgCl system, which would leave the first bromination favorable. Complete basis set calculations on further $HgBr_x$ systems remain an open area of exploration for the future.

*Further discussion of NMR calculations follows after Tables 8-10 below.*

**TABLES:** **Energies of Formation**

| HgCl compound series energy of formation (Gibbs Free Energy) | | | | |
|---|---|---|---|---|
| | CCSD (**Hartrees**) | | B3LYP (**Hartrees**) | CPCM Hyd. ΔG |
| | CEP-31G + | CEP-121G + | CEP-121G+ | **(kcal/mol)** |
| $Cl^-$ | -14.873432 | -14.887522 | -14.987182 | -76.55 |
| $Hg^{2+}$ | -152.141721 | -152.141721 | -152.760699 | -407.17 |
| $HgCl^+$ | -167.646138 | -167.655236 | -168.381799 | -139.85 |
| $HgCl_2$ | -182.87579 | -182.894947 | -183.71306 | -20.68 |
| $HgCl_3^-$ | -197.824502 | -197.854812 | -198.774728 | -47.26 |
| $HgCl_4^{2-}$ | -212.636335 | -212.678124 | -213.697558 | -160.89 |

Table 4.8: HgCl Compound energies of formation

| HgCl formation with explicit single water solvation layer | | | | |
|---|---|---|---|---|
| | HF | | MP2 | |
| | CEP-31G + | CEP-121G + | CEP-31G + | CEP-121G + |
| $Hg^{2+}$ $6H_2O$ | -253.347388 | -253.4749919 | -254.722269 | -254.803736 |
| $Cl^-$ | -14.749066 | -14.7366582 | -14.877519 | -14.890205 |
| $HgCl^+$ $5H_2O$ | -251.488878 | -251.5852034 | -252.929499 | -253.007683 |
| $H_2O$ | -16.845846 | -16.8552933 | -17.025162 | -17.039328 |

Table 4.9: Solvated Cluster Calculation energies of formation for HgCl system.

**(These tables were used to calculated the energetics appearing above.)**

Tables 4.10(a-e): Complete Basis Set Calculation on HgCl series: ($Hg^{2+}$, $Cl^-$, $HgCl^+$, $HgCl_2$, $HgCl_3^-$, $HgCl_4^{2-}$) are presented below.

In Table 10a below we can see that the calculated CCSD(T) stabilization energy is much greater for $Cl^-$ than for $Hg^{2+}$ with the correlation consistent basis sets used. This is because the valence electrons used in calculating the stabilizations are not present in the case of the $Hg^{2+}$. The exercise of comparing the calculated energies for the $Hg^+$ and $Hg^0$ species to illustrate this effect is left for the reader.

| CCSD(T) Calculated Energy, Hartrees<br><br>Basis set: Cl: cc-pV*Z, Hg: cc-pV*Z-PP | | | | |
|---|---|---|---|---|
| | n=2 (pVDZ) | n=3 (pVTZ) | n=4 (pVQZ) | n=5 (pV5Z) |
| $Cl^-$ | -459.6895858 | -459.7851298 | -459.7851298 | |
| $Hg^{2+}$ | -151.9714435 | -151.9714435 | -152.2772938 | -152.3289605 |
| $HgCl^+$ | -612.2979752 | -612.3792635 | -612.7282043 | |
| $HgCl_2$ | -1072.348222 | -1072.514083 | | |
| $HgCl_3^-$ | -1532.120548 | -1532.37006 | | |
| $HgCl_4^{2-}$ | -1991.751637 | | | |

Table 4.10(a): HgCl series cc-pV*Z basis calculated energies

| CCSD(T) Calculated Energy, Hartrees<br><br>Basis set: Cl: aug-cc-pV*Z, Hg: aug-cc-pV*Z-PP | | | | |
|---|---|---|---|---|
| | n=2 (pVDZ) | n=3 (pVTZ) | n=4 (pVQZ) | n=5 (pV5Z) |
| $Cl^-$ | -459.7383021 | -459.8050418 | -459.8272536 | -459.8342742 |
| $Hg^{2+}$ | -151.9948455 | -152.0227306 | -152.2823505 | |
| $HgCl^+$ | -612.351157 | -612.4536232 | | |
| $HgCl_2$ | -1072.427855 | -1072.603270 | | |
| $HgCl_3^-$ | | | | |
| $HgCl_4^{2-}$ | | | | |

Table 4.10(b): HgCl series aug-cc-pV*Z basis calculated energies

| CCSD(T) Calculated Energy, Hartrees<br><br>Basis set: Br: cc-pV*Z, Hg: cc-pV*Z-PP | | | | |
|---|---|---|---|---|
| | n=2 (pVDZ) | n=3 (pVTZ) | n=4 (pVQZ) | n=5 (pV5Z) |
| $Br^-$ | -2572.577998 | -2572.771779 | | |
| $Hg^{2+}$ | -151.9714435 | -151.9714435 | -152.2772938 | -152.3289605 |
| $HgBr^+$ | -2725.190374 | -2725.371107 | -2725.771581 | |
| $HgBr_2$ | -5298.111298 | -5298.476037 | | |
| $HgBr_3^-$ | -2725.190374 | | | |
| $HgBr_4^{2-}$ | | | | |

Table 4.10(c): HgBr series cc-pV*Z basis calculated energies

| CCSD(T) Calculated Energy, Hartrees<br><br>Basis set: I: cc-pV*Z-PP, Hg: cc-pV*Z-PP | | | | |
|---|---|---|---|---|
| | n=2 (pVDZ) | n=3 (pVTZ) | n=4 (pVQZ) | N=5 (pV5Z) |
| $I^-$ | -296.8548199 | -296.9832305 | | |
| $Hg^{2+}$ | -151.9714435 | -151.9714435 | -152.2772938 | -152.3289605 |
| $HgI^+$ | -449.4732538 | -449.5771151 | -450.0288159 | |
| $HgI_2$ | -746.6435659 | | | |
| $HgI_3^-$ | -1043.566473 | | | |
| $HgI_4^{2-}$ | | | | |

Table 4.10(d): HgI series calculated energies with cc-pV*Z-PP basis

| Extrapolated Complete Basis Set CCSD(T) Energies, Hartrees<br><br>Using above pVDZ/pVTZ data to extrapolate via (Equation 1) | | | | |
|---|---|---|---|---|
| | X=Cl, cc-pV*Z* basis | X=Cl, aug-cc-pV*Z* basis | X=Br, cc-pV*Z* basis | X=I, cc-pV*Z-PP basis |
| $X^-$ | -459.8253589 | -459.8331427 | -2572.853371 | -297.0372981 |
| $Hg^{2+}$ | -151.9714435 | -152.0344717 | -151.9714435 | -151.9714435 |
| $HgX^+$ | -612.4134902 | -612.4967669 | -2725.447205 | -449.6208462 |
| $HgX_2$ | -1072.58392 | -1072.677129 | -5298.629611 | |
| $HgX_3^-$ | -1532.475118 | | | |
| $HgX_4^{2-}$ | | | | |

Table 4.10(e): Reaction Energetics with extrapolated CBS from the above mercury halogen compounds $HgCl_x$, $HgBr_x$, and $HgI_x$.

To offer further characterization for these HgX compounds and possibly to identify local structure via NMR measurement, we also conducted a number of NMR calculations[7-9] using the ADF software package[10-12]. Although Hg NMR is challenging due to generally low concentrations, future techniques and current approaches can remedy the sensitivity issues. We therefore present the following results, summarized in Table 4.11 and 4.12 below:

HgClx with Excitations

| | NMR Shielding (ppm) | | | |
|---|---|---|---|---|
| | Hg (solvated) | Hg (gas phase) | Cl (solvated) | Cl (gas phase) |
| Hg atom (solvated only) | 9909.5 | | | |
| HgCl | 9109.17 | 10077.44 | 618.35 | -867.59 |
| HgCl2 | 7444.05 | 7306.67 | 894.14 | 807.37 |
| HgCl3 | 6639.91 | 6538.59 | 924.4 | 892.1 |
| HgCl4 | 6483.6 | 6764.95 | 967 | 929 |

Table 4.11: ADF NMR calculation results for compounds in $HgCl_x$ series calculated with excitations.

HgClx with No Excitations

| | NMR Shielding (ppm) | | | |
|---|---|---|---|---|
| | Hg (solvated) | Hg (gas phase) | Cl (solvated) | Cl (gas phase) |
| Hg atom | | 9909.71 | | |
| HgCl | 9109.25 | 10077.22 | 618.29 | -867.23 |
| HgCl - H2O | 8055.78 | 8198.2 | 792.71 | 580.16 |
| HgCl2 | 7443.37 | 7306.71 | 894.22 | 807.33 |
| HgCl2 - 2H2O | 7335.65 | 7259.04 | 865 | 841 |
| HgCl3 | 6639.9 | 6538.56 | 924.4 | 892.1 |
| HgCl3 - H2O | 6715.55 | 6571.58 | 937 | 2x869, 1x895 |
| HgCl3 - 2H2O (solv. only) | 6651.42 | | 910 | |
| HgCl4 | 6483.76 | 6764.95 | 967 | 929 |
| HgCl4 - 2H2O | 6510.32 | 6702.4 | 935 | 914 |
| HgCl4 (flat) | | 6778.92 | | 927 |
| HgCl5 (solv. only) | 6971.03 | | 3x960, 2x810 | |
| HgCl6 (solv. only) | 7137.75 | | 890, 905, and 969 | |

Table 4.12: ADF NMR calculation results for compounds in $HgCl_x$ series calculated without excitations.

The calculations made with excitations took a significantly longer length of time to complete than the calculations with no excitations, which limited the size of the systems which we could examine in the former case. This allowed us in the latter case, however, to do calculations with both explicit hydration and more Cl atoms in the cluster.

Examining the sections of each table in turn, we see the following trends.

When we consider the solvated HgCl series calculated with excitations as shown in Table 4.11, there is a consistent decrease in NMR shielding for $HgCl_x$ with increasing x in the solvated case, as shown in Figure 4.1 below:

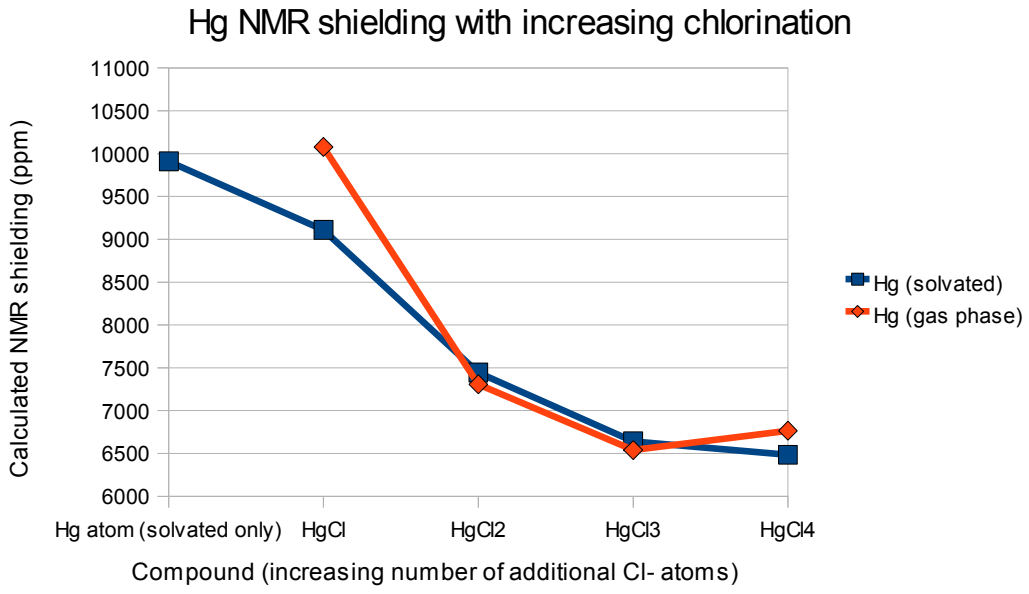


Figure 4.1: $HgCl_x$ series Hg calculated ADF NMR shielding (ppm) (with excitations)

In the gas phase calculations, the trend worked for the first two additional Cl atoms, but after that the shielding stabilized around 6600 ppm.

If we consider the Cl NMR shielding instead, as charted in Figure 4.2 below, we see that there is a similar trend of increasing shielding (ppm) with increasing numbers of Cl atoms present in both the solvated and gas phase cases, although the most major differences appear between $HgCl^+$ and $HgCl_2$.

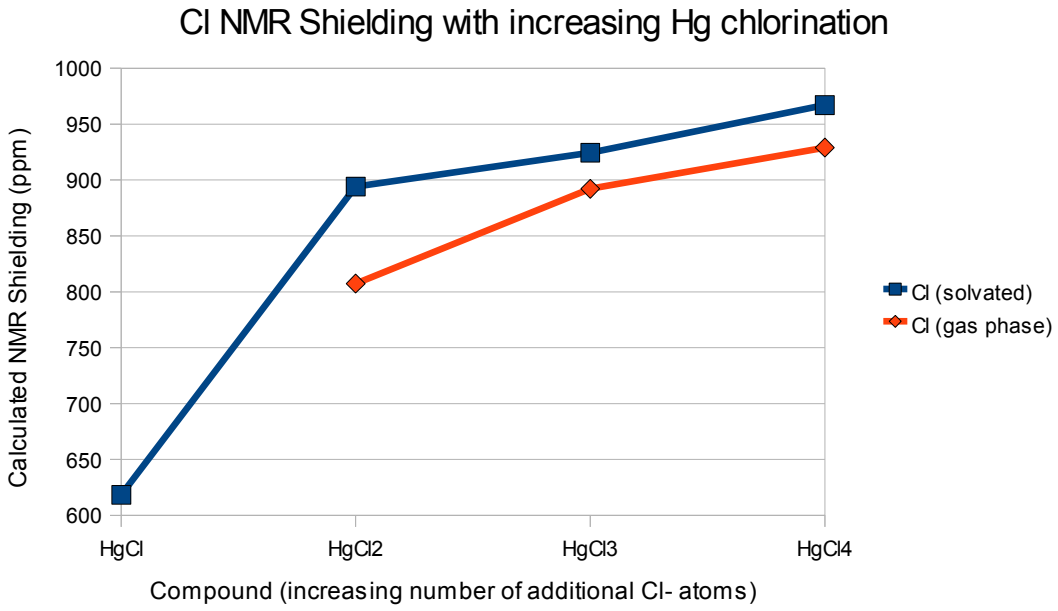


Figure 4.2: $HgCl_x$ series Cl calculated ADF NMR shielding (ppm) (with excitations)

Moving on to the calculations which were done without excitations, we have a greater variety of species which we examined, including all of the ones which we looked at in

the system with excitations and explicitly solvated ones. These are shown in Table 4.12 and Figure 4.3 and 4.4.

Looking at Figure 4.3 first, where we have a chart of the Hg NMR shielding with increasing chlorination, we see that the general trend we observed previously is still present. As more Cl atoms are added to the cluster, the shielding decreases until we have $HgCl_3^-$, where it apparently bottoms out, having similar shieldings through $HgCl_6^{4-}$. We can also see that the presence of water molecules explicitly hydrating the system only has a significant effect on the Hg shielding before the mercury has two Hg-Cl bonds present; the explicitly solvated $HgCl^+$ shows a lower calculated shielding than the plain $HgCl^+$, but otherwise differences are quite minimal. When the Hg has more than 4 Cl atoms attached, the shielding increases again in the solvated calculations which included 5 and 6 Cl atoms.

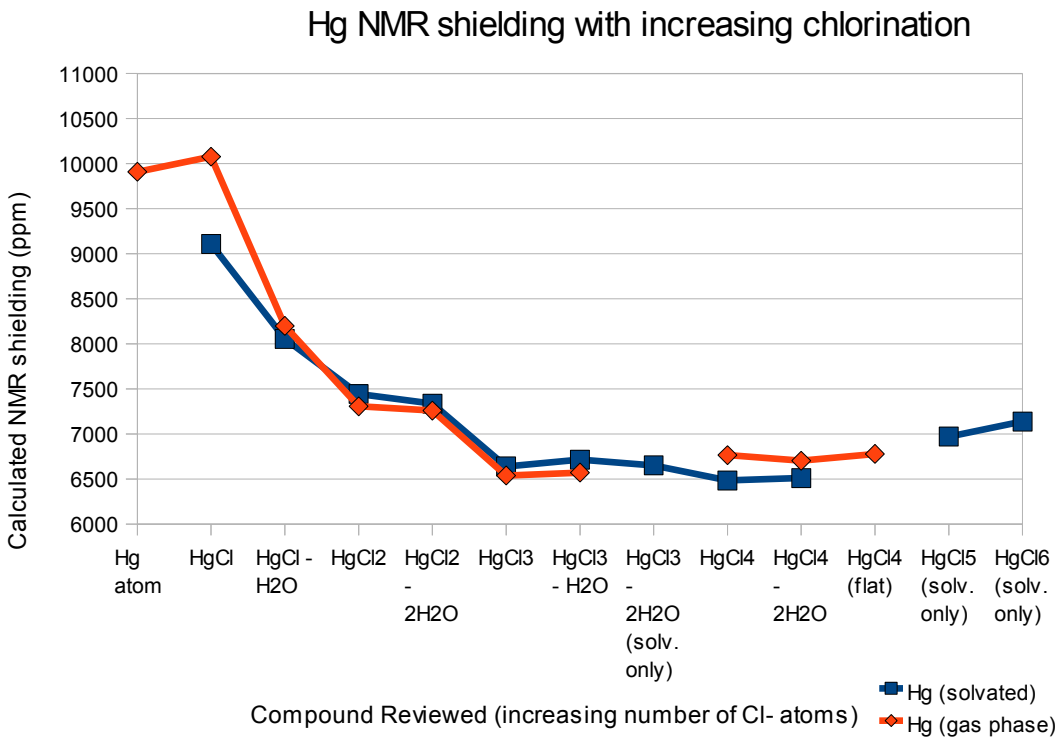


Figure 4.3: $HgCl_x$ series Hg calculated ADF NMR shielding (ppm) (no excitations)

If we examine the Cl shieldings calculated by ADF without excitations, we see less of a pattern, although the tetrahedral $HgCl_3$ . $H_2O$ system can be distinguished from the normal $HgCl_3$ by virtue of an additional NMR peak which appears for Cl. The trend of increasing shielding with increasing substitution holds through $HgCl_3$, but as previously seen in the calculations with excitations, the relative differences between species shrink drastically after the 3rd Cl atom is added to the group. The shielding conditions for $HgCl_5^{3-}$ and $HgCl_6^{4-}$ also do not continue the trend of increasing shielding with increasing substitution.

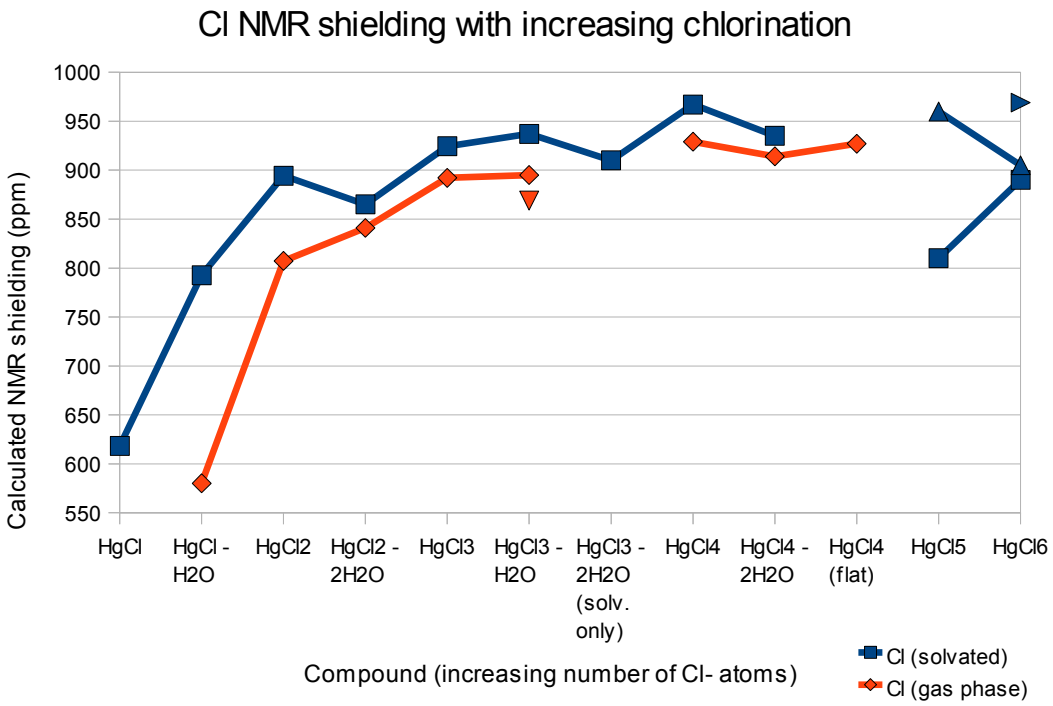


Figure 4.4: $HgCl_x$ series Cl calculated ADF NMR shielding (ppm) (no excitations). Because of the different environments for Cl atoms in the calculated geometries for $HgCl_3 – H_2O$, $HgCl_5$, and $HgCl_6$, there are multiple calculated shieldings in each case.

Overall, we would say that from these calculations, we would predict that on the basis of NMR one could distinguish between species up to $HgCl_2$, and tell them apart from $HgCl_3^-$ and further substituted species, but that the differences between the shieldings for $HgCl_3^-$ and $HgCl_4^{2-}$ would be much less straightforward to tell apart experimentally.

## *4.4 Conclusions*

Through these calculations we demonstrated that the $HgCl_x$ system can be represented with a B3LYP / CEP-121G+ approach with the same overall results as CCSD / CEP-121G+ or the CCSD(T) complete basis set extrapolation.

This is good news, because the relatively low computational cost of B3LYP calculations will allow us to look at larger systems which would be inaccessible with the more computationally expensive CCSD and CCSD(T) calculations.

Through our NMR calculations, we showed that a trend of decreasing shielding with increasing substitution exists for $HgCl_x$ compounds, but that the differences become progressively smaller and might not be useful for telling apart $HgCl_3^-$ and above.

## *4.5 Acknowledgements*

We would like to acknowledge the invaluable assistance of Parallel Quantum Solutions for both kindly and excellent after-market technical support of their QuantumCube™ chemistry cluster used to calculate the NMR data presented in this chapter.

*4.6 References*


1. Sheu, G.R. and R.P. Mason, *An examination of methods for the measurements of reactive gaseous mercury in the atmosphere.* Environmental Science & Technology, 2001. **35**(6): p. 1209-1216.
2. Sillen, L.G., *Electrometric Investigation of Equilibria between Mercury and Halogen Ions .8. Survey and Conclusions.* Acta Chemica Scandinavica, 1949. **3**(5): p. 539-553.
3. M. J. Frisch, G.W.T., H. B. Schlegel, G. E. Scuseria, M. A. Robb, J. R. Cheeseman, J. A. Montgomery, Jr., T. Vreven, K. N. Kudin, J. C. Burant, J. M. Millam, S. S. Iyengar, J. Tomasi, V. Barone, B. Mennucci, M. Cossi, G. Scalmani, N. Rega, G. A. Petersson, H. Nakatsuji, M. Hada, M. Ehara, K. Toyota, R. Fukuda, J. Hasegawa, M. Ishida, T. Nakajima, Y. Honda, O. Kitao, H. Nakai, M. Klene, X. Li, J. E. Knox, H. P. Hratchian, J. B. Cross, V. Bakken, C. Adamo, J. Jaramillo, R. Gomperts, R. E. Stratmann, O. Yazyev, A. J. Austin, R. Cammi, C. Pomelli, J. W. Ochterski, P. Y. Ayala, K. Morokuma, G. A. Voth, P. Salvador, J. J. Dannenberg, V. G. Zakrzewski, S. Dapprich, A. D. Daniels, M. C. Strain, O. Farkas, D. K. Malick, A. D. Rabuck, K. Raghavachari, J. B. Foresman, J. V. Ortiz, Q. Cui, A. G. Baboul, S. Clifford, J. Cioslowski, B. B. Stefanov, G. Liu, A. Liashenko, P. Piskorz, I. Komaromi, R. L. Martin, D. J. Fox, T. Keith, M. A. Al-Laham, C. Y. Peng, A. Nanayakkara, M. Challacombe, P. M. W. Gill, B. Johnson, W. Chen, M. W.

Wong, C. Gonzalez, and J. A. Pople, *Gaussian 03, Revision C.02*, 2004, Gaussian, Inc., Wallingford CT.

4. Halkier, A., et al., *Basis-set convergence of the energy in molecular Hartree-Fock calculations.* Chemical Physics Letters, 1999. **302**(5-6): p. 437-446.

5. Feller, D. and J.A. Sordo, *A CCSDT study of the effects of higher order correlation on spectroscopic constants. I. First row diatomic hydrides.* The Journal of Chemical Physics, 2000. **112**(13): p. 5604-5610.

6. Becke, A.D., *Density-functional thermochemistry. III. The role of exact exchange.* The Journal of Chemical Physics, 1993. **98**(7): p. 5648-5652.

7. Wolff, S.K., et al., *Density functional calculations of nuclear magnetic shieldings using the zeroth-order regular approximation (ZORA) for relativistic effects: ZORA nuclear magnetic resonance.* Journal of Chemical Physics, 1999. **110**: p. 7689

8. Schreckenbach, G. and T. Ziegler, *The calculation of NMR shielding tensors based on density functional theory and the frozen-core approximation.* International Journal of Quantum Chemistry, 1996. **60**.

9. Schreckenbach, G. and T. Ziegler, *The calculation of NMR shielding tensors using GIAO's and modern density functional theory.* Journal of Physical Chemistry, 1995. **99**.

10. Guerra, C.F., et al., *Towards an order-N DFT method.* Theoretical Chemistry Accounts, 1998. **99**.

11. Velde, G.t., et al., *Chemistry with ADF*. Journal of Compututational Chemistry, 2001. **22**: p. 931.

12. Baerends, E.J., et al., ADF2004.01, SCM, Theoretical Chemistry, Vrije Universiteit, Amsterdam, The Netherlands, http://www.scm.com. 2004.

# Chapter 5: Ab Initio Phosphoric acid pKa calculations using CBS-QB3 and MP2 methods

*In this chapter we discuss several approaches to calculating the pKas of phosphoric acid ($H_3PO_4$), a common polyprotic acid which forms several different species in aqueous solution, using the MP2*[1] *and CBS-QB3*[2] *methods and applying an explicit counterion correction to see if the reduction in total ionic charge improves accuracy significantly.*

## *5.1 Introduction*

Phosphoric acid is a common polyprotic inorganic acid which is well-characterized experimentally. Many experimental measurements of its acidities are readily available. However, there are relatively few theoretical studies to date, though recently it has been of more interest, perhaps because of its disarming simplicity[3].

Phosphoric acid is a useful model for multiply charged anions because it is light enough that it is easy to conduct many different higher-level calculations on it than is possible for larger molecules with heavier atoms, which would be considerably more computationally expensive to study in a variety of details.

Our goals were to reproduce experimentally measured acid deprotonation constants (pKa values) if possible, and to show how future laboratories could follow a

straightforward method which we can demonstrate produces reasonably good results of known quality.

Acid deprotonation constants are determined from the deprotonation reactions as follows. For a sample reaction of an acid HA which dissociates in solution to $A^-$ and $H^+$, shown below as (a):

(a) $$HA(aq) \rightarrow H^+(aq) + A^-(aq)$$

The rate of the forward reaction is called the rate constant K. As the acidity of the HA species varies the rate constant will increase or decrease. Normal rate constants are calculated as a ratio of concentrations of products over reactants at equilibrium, which appear as shown below in Equation 5.1 for hypothetical reaction (a).

(5.1) $$K_a = \frac{[H+][A-]}{[HA]}$$

This can then be converted into a pKa by taking the negative logarithm as shown in Equation 5.2:

(5.2) $$pK_a = -\log K_a = -\log\left(\frac{[H+][A-]}{[HA]}\right)$$

pKa values are especially useful because they can be used with pH measurements to predict the form that the acidic chemical HA will take in an aqueous solution of that

acid. pH measurements are determined based on the concentration of the [H+] ion in a solution, as shown in Equation 5.3 below:

(5.3) $$pH = -\log [H+]$$

The problem of phosphoric acid is an interesting and challenging one in part for two main reasons. Although the protonated form is neutral, it can be deprotonated three times, making a significantly negatively charged ion.

Computationally, determining the stability of an ion is generally more difficult than the neutral species, especially if it is being stabilized by a solvent. The electron cloud geometry changes in one of two ways when an ion is formed. If electrons are lost, leaving a positive ion, the electron cloud shrinks slightly towards the nucleus after the highest energy electrons are removed. In this situation the shape and geometry does not change very much. When electrons are added to an ion, the cloud becomes much larger and the probability of finding any of the electrons further from the nucleus becomes much greater. Representing this latter situation with basis sets can require additional basis set functions and other techniques to accurately reproduce the optimal electron probability density distribution.

There are many reactions of ions that can be straightforwardly treated with *ab initio* approaches. In reactions where the total charge on both sides of the reaction is the same, and the square of the individual charges are the same, errors in the solvation

model generally cancel out to a great degree if the ions on both sides are similar in structure.

However, for deprotonation reactions, this balance is lost. This may be why previous calculations[4] focused mainly on the first deprotonation of phosphoric acid and not on further ones.

There are also some technical challenges that crop up because of geometry (B3LYP geometry optimizations, such as are found in the initial steps of CBS-QB3, tend to have difficulty converging to a minima especially when done with PCM solvation) and wavefunction convergence issues (especially in the presence of a strongly interacting counterion) which we will discuss later.

As mentioned earlier, phosphoric acid has several well known experimentally measured pKa values shown in Table 5.1 below.

| pKa | Experimentally Measured Value |
|---|---|
| $pKa_1$ ($H_3PO_4 \rightarrow H_2PO_4^- + H^+$) | 2.2 |
| $pKa_2$ ($H_2PO_4^- \rightarrow HPO_4^{2-} + H^+$) | 7.1 |
| $pKa_3$ ($HPO_4^{2-} \rightarrow PO_4^{3-} + H^+$) | 12.3 |

Table 5.1: Experimentally measured pKa values from William L. Jolly, *Modern Inorganic Chemistry*, 2nd edition.[5]

These values have been tightly characterized and verified by countless generations of undergraduates following their general acceptance in the annals of inorganic chemistry research. The values above were quoted from a standard inorganic chemistry textbook,

More recently, we have a few theoretical studies of $H_3PO_4$ and deprotonated derivatives done by several groups:

D.A. Dixon et al. published a paper on CCSD(T) Complete Basis Set Extrapolations with an excellent treatment of the first deprotonation in 2005[4]. In that work, $H_3PO_4$ was calculated to have a heat of formation of -268.8 kcal/mol, a gas acidity of 322.2 kcal/mol, and a first deprotonation pKa of 2.5. This particular example required the use of several corrections to the energy which would put the approach initially outside the purview of the typical physical chemist not specializing in computational chemistry. However, this excellent project shows what will soon be in reach for smaller laboratories once common computer technology advances a bit further.

E. Tsuchida's paper from 2006[6] covered molecular dynamics calculations using DFT (by way of a PBE functional). It was concerned with studying liquid phase $H_3PO_4$ via molecular dynamics (MD) simulation on a supercomputing cluster, and successfully reproduced both experimental structures and vibrational properties of the

fully protonated compound, although it noted that the MD simulation observed proton exchanges between the $H_3PO_4$ groups.

D. B. Chesnut conducted 31P NMR calculations via sB3LYP and GIAO on $H_3PO_4$[7], and garnered both energetics for hydrogen bonding and absolute NMR shieldings for both $H_3PO_4$ and its deprotonated anions, noting that there were a variety of geometries with multiple $H_3PO_4$ atoms associating with each other and with water, and these lead to a variety of different possible calculated shieldings around the experimental measurement. The results suggested that $H_3PO_4$ . 2 $H_2O$ was the best model for experimental conditions of 85% $H_3PO_4$ 31P NMR measurement.

*5.2 Methods*

Keeping in mind that our goal was to demonstrate a method which would be within reach of experimental physical chemistry groups without necessarily access to a dedicated theorist, we decided to investigate the following different approaches to calculating $H_3PO_4$ energetics.

We calculated the change in Gibbs free energies using Gaussian 03[8] with the CBS-QB3 model chemistry[2] method for each species and MP2/CBSB7[9] free energies as well.

To estimate solvation stabilization we applied several tools. Our main one was the CPCM polarizable continuum model[10-12]. With it, we did independent Hartree-Fock calculations[13] using 6-31+G**, 6-31G**, and 6-31G basis sets. We also applied it in conjunction with the CBS-QB3 calculations as well as with the MP2/CBSB7 calculations.

After these were done, we added $Na^+$ counterions in association with the negatively charged ions in the systems, and did more calculations in the CPCM to determine how the presence of the ion reduced dependence on the CPCM model and whether it would reduce the error in the calculations. While it did improve the results, it caused trouble with the SCF step of the HF calculation, making several results inaccessible.

*5.3 Results*

The results for the first set of calculations is in Table 5.2. These are ones done with the CBS-QB3 gas phase free energy calculations plus CPCM stabilizations calculated under the HF method at those CBS-QB3 geometries (which were found during the B3LYP/CBSB7 optimization step of CBS-QB3). This first estimate approach for finding the values tends not to run into difficulties during the geometry optimization

| | CBS-QB3 Gas phase Free Energies + (basis set) HF CPCM Stabilization at gas phase geometries | | | Experimental Results |
|---|---|---|---|---|
| $H_3PO_4$ | 6-31+G** | 6-31G** | 6-31G | |
| $pKa_1$ | 6.0 | 5.5 | 6.5 | 2.2 |
| $pKa_2$ | 21.8 | 18.7 | 21.5 | 7.1 |
| $pKa_3$ | 24.7 | 14.8 | 17.9 | 12.3 |

Table 5.2: CBS-QB3 Gas Phase Free Energies + CPCM Stabilization (with various basis sets) on phosphoric acid.

In this case the extra + in 6-31+G** is a diffuse function and we observe that the second and third pKas with the most negatively charged anions are uncharacteristically larger compared to calculation with the smaller basis 6-31G** which has only polarization functions. But though the calculations with 6-31G** have results closest to the experimental ones although the reversed trend for the $pKa_2$ and $pKa_3$ are clearly nonphysical.

Noting the unusually high value for the other $pKa_2$s in this case, one thing to consider here might be that the CPCM stabilization in the 6-31G and 6-31G** calculation is smaller than it ought to be for the $HPO_4^{2-}$ species. This would increase the $pKa_2$ while decreasing the $pKa_3$ as was observed here. In our later calculations we used the HF/6-31+G** basis for calculating stabilization of gas phase systems for this reason.

| $H_3PO_4$ | CBS-QB3 plus HF/6-31+G** CPCM energy | CBS-QB3 run in CPCM | MP2/CBSB7 in CPCM | Experimental Results |
|---|---|---|---|---|
| $pKa_1$ | 6.0 | 4.9 | 11.5 | 2.2 |
| $pKa_2$ | 21.8 | 21.1 | 31.8 | 7.1 |
| $pKa_3$ | 24.7 | 29.8 | 45.5 | 12.3 |

Table 5.3: CBS-QB3 and MP2 Calculations on Phosphoric Acid solvated with CPCM

Adding CPCM to the CBS-QB3 run improved the results slightly for the species with lower charges, although the results are still better than the corresponding simple MP2 geometry optimization and calculation.

However, introducing a counterion improves the results significantly for the second and third deprotonation as seen in Table 5.4 below:

| $H_3PO_4$ , $NaH_2PO_4$ , $NaHPO_4^-$, and $NaPO_4^{2-}$ | CBS-QB3 CPCM with $Na^+$ Counterion | CBS-QB3 CPCM calculation without counterion | Experimental Results |
|---|---|---|---|
| pKa1 | N/A | 4.9 | 2.2 |
| pKa2 | 15.6 | 21.1 | 7.1 |
| pKa3 | 24.9 | 29.8 | 12.3 |

Table 5.4: Phosphoric Acid CBS-QB3 calculations with counterion.

There were regrettable failures in calculating the CBS-QB3 energy of the solo $Na^+$ ion ("Not enough resources for E2 calculation.") which prevented us from finding the $pKa_1$ using the method. There were also difficulties with the $NaPO_4^{2-}$ calculation, which experienced several wavefunction convergence failures during the process. However, we could find the second and third deprotonation energies, which were quite a bit closer to the experimental results, going from a factor of three error to a factor of two.

*5.4 Discussion and Conclusions*

Overall, using CBS-QB3 + CPCM with $Na^+$ counterions yielded results closest to experiment. However, the difficulties with the geometry optimization and the

wavefunction convergence were issues that might not be within reach for a laboratory without theoretical assistance.

The results also left a bit to be desired from a quantitative point of view. Although we got much closer to experimental measurements for the second and third deprotonation than previous work, there is still a distance remaining before *ab inito* or hybrid *ab initio*/fitted calculations of pKas can be easily done in experimental labs.

We would conclude that although finding trends in the pKas is possible using CBS-QB3 along with the CPCM model, easy desktop calculation of quantitative pKa and pH values for polyprotic acids remains in the future.

Molecular dynamics calculations should be able to overcome the convergence problem we experienced here from the SCF not converging as they use a different approach with plane waves to representing the electron cloud. However, there may be drawbacks from the method sampling a solution of a unrealistically high concentration of the acid. In the future it would be interesting to do MD calculations on these systems to explore the differences between the two approaches.

More complex solvation models should be able to help as well. If we add explicit water molecules it will increase the cost, but should also take care of some more of the chemical interactions between the solvent and the ion which aren't represented by

the CPCM model at all. In the future, a Car-Parrinello Molecular Dynamics calculation[14] might be effective in this case, as the theory is designed to handle a fixed volume of space with an effective level of quality, and the direction of increasing parallelization in computer design should allow for easy scaling of calculations using the method in the future.

We went on to do calculations with single $H_2O$ molecule explicit solvation and with some acidic arsenic compounds as we worked to find a better approach to get improved results, as detailed in the next section of this chapter.

*5.5 Acknowledgements*

This work was sponsored by NSF Grant EAR0539109, DOE Grant DE-FG02-94ER14467, and the NSF-MRSEC at the University of Maryland, College Park DMR#0520471.

We would also like to acknowledge D.A. Dixon for references to prior work, J.A. Tossell for much advice on the experimental process, and fellow graduate students E. Khaskin, and Liang T. for suggestions given on the presentation this work was based upon.

*5.6 References*


1. Moller, C. and M.S. Plesset, *Note on an Approximation Treatment for Many-Electron Systems.* Physical Review, 1934. **46**(7): p. 618.
2. Montgomery, J.A., J.W. Ochterski, and M.J. Frisch, *An improved complete basis set (CBS) model chemistry.* Abstracts of Papers of the American Chemical Society, 1996. **211**: p. 231-PHYS.
3. Lopez, X., et al., *Theoretical Evaluation of pKa in Phosphoranes: Implications for Phosphate Ester Hydrolysis.* Journal of the American Chemical Society, 2002. **124**(18): p. 5010-5018.
4. Alexeev, Y., et al., *Accurate heats of formation and acidities for H3PO4, H2SO4, and H2CO3 from ab initio electronic structure calculations.* International Journal of Quantum Chemistry, 2005. **102**(5): p. 775-784.
5. Jolly, W.L., *Modern Inorganic Chemistry*. 2nd ed 1991, New York: McGraw Hill. 655.
6. Tsuchida, E., *Ab initio molecular-dynamics simulation of concentrated phosphoric acid.* Journal of the Physical Society of Japan, 2006. **75**(5): p. -.
7. Chesnut, D.B., *A Theoretical Study of 31P NMR Chemical Shielding Models for Concentrated Phosphoric Acid Solution.* The Journal of Physical Chemistry A, 2005. **109**(51): p. 11962-11966.
8. M. J. Frisch, G.W.T., H. B. Schlegel, G. E. Scuseria, M. A. Robb, J. R. Cheeseman, J. A. Montgomery, Jr., T. Vreven, K. N. Kudin, J. C. Burant, J.

M. Millam, S. S. Iyengar, J. Tomasi, V. Barone, B. Mennucci, M. Cossi, G. Scalmani, N. Rega, G. A. Petersson, H. Nakatsuji, M. Hada, M. Ehara, K. Toyota, R. Fukuda, J. Hasegawa, M. Ishida, T. Nakajima, Y. Honda, O. Kitao, H. Nakai, M. Klene, X. Li, J. E. Knox, H. P. Hratchian, J. B. Cross, V. Bakken, C. Adamo, J. Jaramillo, R. Gomperts, R. E. Stratmann, O. Yazyev, A. J. Austin, R. Cammi, C. Pomelli, J. W. Ochterski, P. Y. Ayala, K. Morokuma, G. A. Voth, P. Salvador, J. J. Dannenberg, V. G. Zakrzewski, S. Dapprich, A. D. Daniels, M. C. Strain, O. Farkas, D. K. Malick, A. D. Rabuck, K. Raghavachari, J. B. Foresman, J. V. Ortiz, Q. Cui, A. G. Baboul, S. Clifford, J. Cioslowski, B. B. Stefanov, G. Liu, A. Liashenko, P. Piskorz, I. Komaromi, R. L. Martin, D. J. Fox, T. Keith, M. A. Al-Laham, C. Y. Peng, A. Nanayakkara, M. Challacombe, P. M. W. Gill, B. Johnson, W. Chen, M. W. Wong, C. Gonzalez, and J. A. Pople, *Gaussian 03, Revision C.02*, 2004, Gaussian, Inc., Wallingford CT.

9. Head-Gordon, M., J.A. Pople, and M.J. Frisch, *MP2 energy evaluation by direct methods.* Chemical Physics Letters, 1988. **153**(6): p. 503-506.

10. Cossi, M., et al., *Energies, structures, and electronic properties of molecules in solution with the C-PCM solvation model.* Journal of Computational Chemistry, 2003. **24**(6): p. 669-681.

11. Barone, V., M. Cossi, and J. Tomasi, *Geometry optimization of molecular structures in solution by the polarizable continuum model.* Journal of Computational Chemistry, 1998. **19**(4): p. 404-417.

12. Barone, V. and M. Cossi, *Quantum calculation of molecular energies and energy gradients in solution by a conductor solvent model.* Journal of Physical Chemistry A, 1998. **102**(11): p. 1995-2001.

13. Roothaan, C.C.J., *New Developments in Molecular Orbital Theory.* Reviews of Modern Physics, 1951. **23**(2): p. 69-89.

14. Car, R. and M. Parrinello, *Unified Approach for Molecular Dynamics and Density-Functional Theory.* Physical Review Letters, 1985. **55**(22): p. 2471.

# Chapter 6: Arsenic and Phosphoric Acid pKa calculations using the CBS-QB3 model chemistry and the CPCM SCRF solvation method

*In this chapter we further discuss several different polyprotic acids, continuing the study from the previous chapter and developing an extrapolation which improves the accuracy of the results significantly. Methods used focused on the CBS-QB3 computational chemistry[1] with the CPCM solvation model[2].*

*This section based on* Zimmermann, M. D. and Tossell, J. A. *Acidities of Arsenic(III) and Arsenic(V) Thio- and Oxyacids in Aqueous Solution using CBS-QB3.*[3] *Tables and Figures are reproduced from the same.*

## *6.1 Introduction*

Arsenic chemistry is important because of its dramatic impact on human welfare as well as an element which is widely dispersed around the world. Arsenic poisoning has serious health effects on those exposed to it, causing damage to the immune system and dramatically shortening life expectancies.[4]

It has previously been shown that high level methods can directly calculate pKa values for first deprotonations for small phosphoric acid systems[5], but further deprotonations have fewer results available.

This problem will be shown to be easily addressed systematically by the CBS-QB3 model chemistry[1] and a fitting extrapolation determined from small polyprotic acids with the form $H_3AO_4$ (with A=P,S,As). One of the goals of this part of the research was to make sure that any procedure developed would be both approachable and straightforward enough to be easily accessible to any physical chemist with a computer, and this was attained successfully.

The main compounds analyzed here via *ab-initio* approaches were $H_3AsS_3$, $H_3AsS_4$, $H_3PO_4$, and $H_2SO_4$ and their deprotonated derivatives[5]. These were done in the gas phase and in aqueous solution (either in a PCM modeled uniform dipole system approximating water, or the same with an explicit water molecule present to add hydrogen bonding interactions). In each case we calculated the pKas of each deprotonation step, then made a linear fit, extrapolating the results against known experimentally measured pKa values for $H_3AsO_4$ and $H_3PO_4$.

[5] Although for $HAsS_3^{2-}$ we were unable to locate a stable equilibrium geometry in our CBS-QB3 calculation.

This approach yielded data which corresponded well with the measured values. Of the methods which were attempted in this experiment, the best fits came for the CBS-QB3 calculation performed within the CPCM came the closest to a linear relation.

After completing the calculations, several experimental measurements of $H_2SO_3$ which were not used in determining the extrapolation matched the predicted data excellently. The values for the extrapolation were within 1 pKa unit of the measured experimental values.

*6.2 Methods*

Each compound was examined with the CBS-QB3 method of calculation[1] as implemented in Gaussian 03[6]. CBS-QB3 is a model chemistry like the G2[7] and G3[8] methods which aims to provide a universal approach to modeling chemical compounds. CBS-QB3 uses B3LYP[9] for geometry optimization and CCSD(T) [10], MP4SDQ[11], and MP2 calculations[12] with progressively larger basis sets to determine a complete basis set extrapolation for the compounds examined with the method.

Like the other model chemistries, CBS-QB3 is an easily conducted calculation for a group without a dedicated theoretical support team.

A method for accurately determining pKas which could easily be done by a lab without dedicated theorists would be useful to chemists in all areas of study. Therefore, the approaches which we set forward here were chosen to provide the maximum level of quality with a minimum of expertise required for their use.

To verify that the CBS-QB3 model chemistry is a reasonable choice for this system of chemicals, we conduct additional calculations with CCSD(T), coupled cluster theory with singles, doubles, and some triple excitations, to determine if the results we see are reproduced in the same fashion with two representative species, $H_3AsO_4$ and $H_3PO_4$. The theory is applied with the relativistically corrected CEP-121G basis set to include contributions to the calculated pKas from effects in the core electron shells.

CBS-QB3 uses several different basis sets in its calculations to pick up the contributions from different levels of theory. The initial B3LYP step uses a CBSB7 basis set, while MP2 uses CBSB3, and MP4SDQ CBSB4. With the CCSD(T) step of the calculation, CBS-QB3 uses the 6-31+G(d') basis set, the smallest basis used in CBS-QB3. The progressively smaller basis sets ensure that each step after geometry optimization will take a similar amount of time to complete.

CBS-QB3 produces energetics similar to the G2 and G3 model chemistries, with energies of the order of 1-2 kcal/mol away from the G2 test set's experimental

measurements[13]. However, the arsenic compounds in the G2 test set are $As_2$, AsH, $AsH_2$, and $AsH_3$, while our focus here is arsenic oxides and sulfides.

While conducting the CBS-QB3 calculations we occasionally observed that the initial B3LYP optimization did not converge in a reasonable amount of time, requiring several restarts of the 30 step optimization sequence to bring the systems to final geometries. We found it helpful in the more difficult cases to optimize under the MP2 method, then use that converged geometry as the input for the CBS-QB3 calculation. This approach seemed to strike a better balance between theorist intervention and CPU time required for the calculations.

CPCM[14] is used to determine the total energy of hydration for each compound. The CPCM method is very computationally efficient, and unlike explicit hydration does not add a significant computational cost to the overall calculation. Another advantage of using CPCM instead of full explicit solvation is that changes in the structure of the solvation cluster of explicit solvent molecules can add noise to the data in the results and make it more difficult to easily retrieve useful data from the results of calculations. For example, a change in cluster geometry that adds a hydrogen bond to the overall favorable interactions in a group would change the energy measured by about 4.3 kcal/mol. If not accounted for, this could change a predicted pKa including the data by about 4 pKa units.

One difficulty introduced by using the CPCM method is that converging the B3LYP optimizations is even more difficult than in the gas phase without CPCM. However, we feel the additional quality of the results justifies the extra trouble.

Solvation energy is approached in two different ways which have both been used in the past. A gas phase calculation of the species of interest is completed first, followed by a calculation of the CPCM solvation stabilization energy at that same geometry. We use a HF/6-31+G** single point calculation with a tight optimization of the self consistent field as the basis of our solvation calculation. The SCFVAC and RADII=UAHF tags are also applied to yield direct compatibility with previous experiments in our laboratory. This approach yields a swift, but less accurate estimation of the free energy of solvation.

A logical next step here would be to optimize the solvation shell sizes for each species analyzed, but this would put reproducing our approach out of reach of groups with less theoretical support and was therefore not done in our lab, although it was applied with great success in other experiments[5, 15].

A disadvantage of our approach, however, is that it assumes that the stabilization of the compounds does not change significantly from changes in their geometry caused by placing them in solution. Also, because the CPCM model represents the solvation by a continuous space outside a cavity made to hold the molecule there is no specific

interaction with solvent molecules such as the hydrogen bonding mentioned earlier as an occasional problem with explicit solvation.

These two disadvantages, however, can be ameliorated somewhat by our second approach, which was to do the entire CBS-QB3 procedure in the CPCM. This yielded different geometries, ones which were optimized under B3LYP/CBSB7 CPCM conditions. This approach does not require the assumption that the solvated geometry is the same as the unsolvated one – in fact, it is not – but it also makes the optimization step even less willing to converge than it was in the gas phase setting. This is possibly caused by the much flatter potential energy surface in the latter case.

The total energies of reaction $\Delta G_{rxn}$ can then be determined through the following equation:

(6.1) $\Delta G_{rxn} = \Delta G(A^-_{gas}) - \Delta G(AH_{gas}) + \Delta G_s(AH) - \Delta G_s(AH) - 269.0$ kcal/mol

Where $\Delta G\ (A^-_{gas}) - \Delta G(AH_{gas})$ is the change in energy for deprotonation of the compound in the gas phase calculated with the CBS-QB3 method, $\Delta G_s$ is the free energy of solvation (found either through the first method or the second) and -269.0 kcal/mol is a calculated energy of solvated $H^+$ ion in water as referenced in [16] including corrections for the different gas and solvation reference states for the

proton. In other experiments a value in the neighborhood of -264 kcal/mol has been used and the conversations of state dealt with separately[17-21].

The choice of this particular figure, however, is somewhat arbitrary, because during the following approach we will be applying a linear correction factor which would eliminate any possible errors introduced by a differing constant factor in the free energy calculation.

The pKa of deprotonation can be found from the free energy change by dividing it by 1.3644 kcal/mol.

CCSD(T) calculations from both the final CBS-QB3 gas phase and CPCM CBS-QB3 solvated geometries for $H_3AsO_4$, $H_2AsO_4^-$, $HAsO_4^{2-}$, $H_3PO_4$, $H_2PO_4^-$, $HPO_4^{2-}$, and $PO_4^{3-}$ were done with the aforementioned CEP-121G basis set to check for relativistic effects, the large standard basis set 6-311G(2d,p) used to measure the effects of additional diffuse orbitals, and aug-cc-pVDZ to compare with the CBSB7 and CBSB8 basis sets.

The thermal correction to the Gibbs free energy was estimated in these single point calculations by assuming it would be similar to that calculated from the B3LYP/CBSB7 frequency calculation conducted as part of the CBS-QB3 determination and using that figure to correct the single point energy in each case.

Following these, a last series of calculations was run with one explicit water molecule associated with each species of interest by a hydrogen-bonding interaction. If there was a deprotonated oxygen or sulfur present, the $H_2O$ was positioned to form one HOH ... $^-$OA hydrogen bond. In the two cases of saturated systems, $H_3AsS_3$ and $H_3AsO_3$, the water molecule was positioned initially with one hydrogen bond to its oxygen from the fully protonated acid: AH ... $OH_2$. The two different types of bonding are illustrated in Figure 6.1 and Figure 6.2 below.

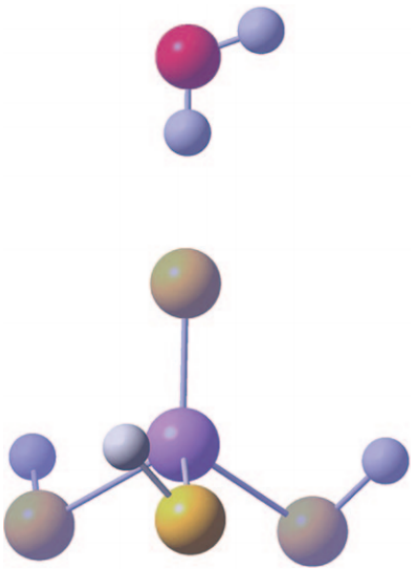

Figure 6.1: $H_3AsO_4$ Hydrogen-bonding from explicit water molecule to the compound.

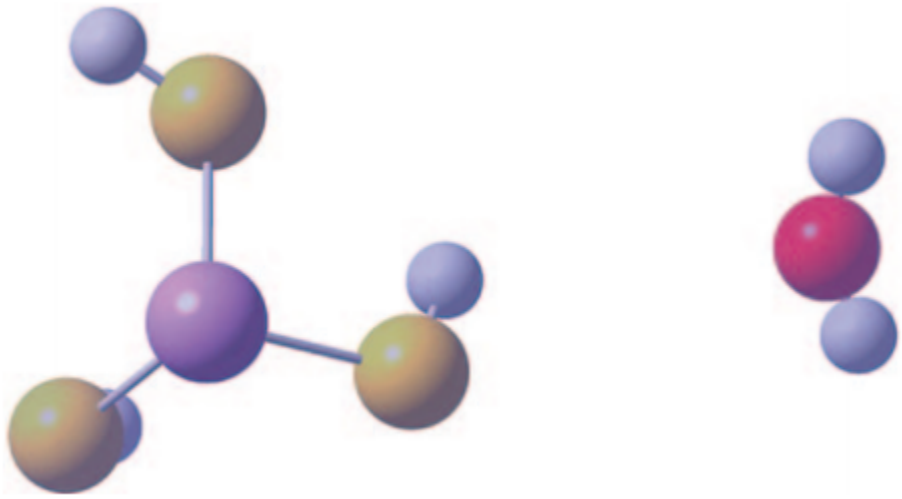

Figure 6.2: $H_3AsO_3$ hydrogen-bonding from acidic hydrogen on arsenic complex to the explicit water molecule.

*6.3 Results and Discussion*

As previously mentioned, we calculated reaction free energy changes with (1). The results from this are tabulated in the Table 6.1 below for each type of calculation: CBS-QB3 gas phase, CPCM stabilization calculated at the gas phase geometries, CBS-QB3 calculated in the polarizable continuum, and those three with explicit hydration by a single water molecule.

We could combine the gas phase and the ΔG solvation energies calculated at the gas phase to get rapidly estimated solution pKa as well. From these, we could determine pKas for the hydrated systems through division by 1.3644 kcal/mol. This data is summarized in the second table.

**TABLE 1: Deprotonation Energetics**

| | gas phase $\Delta G_{\text{CBS-QB3}}$ (kcal/mol) | $\Delta G_{\text{CBS-QB3}} + \Delta G_{\text{CPCM}}$ (for CBS-QB3 and CPCM, handled separately) (kcal/mol) | p$K_a$ (aq) (for CBS-QB3 and CPCM, handled separately) | $\Delta G$ (aq) (CBS-QB3 in CPCM) | p$K_a$ (aq) (CBS-QB3 in CPCM) |
|---|---|---|---|---|---|
| $H_3AsS_4 \rightarrow H_2AsS_4^- + H^+$ | 306.1 | −5.0 | −3.6 | −5.3 | −3.9 |
| $H_2AsS_4^- \rightarrow HAsS_4^{-2} + H^+$ | 407.4 | 11.6 | 8.5 | 10.7 | 7.9 |
| $HAsS_4^{-2} \rightarrow AsS_4^{-3} + H^+$ | 499.5 | 18.3 | 13.4 | 19.2 | 14.1 |
| $H_3AsO_4 \rightarrow H_2AsO_4^- + H^+$ | 325.3 | 8.9 | 6.5 | 8.3 | 6.1 |
| $H_2AsO_4^- \rightarrow HAsO_4^{-2} + H^+$ | 452.3 | 26.8 | 19.6 | 26.3 | 19.3 |
| $HAsO_4^{-2} \rightarrow AsO_4^{-3} + H^+$ | 567.8 | 28.5 | 20.9 | 38.6 | 28.3 |
| $H_3AsS_3 \rightarrow H_2AsS_3^- + H^+$ | 319.3 | 7.4 | 5.5 | 7.4 | 5.4 |
| $H_2AsS_3^- \rightarrow HAsS_3^{-2} + H^+$ | [a] | [a] | [a] | 18.8 | 13.8 |
| $HAsS_3^{-2} \rightarrow AsS_3^{-3} + H^+$ | [a] | [a] | [a] | 26.2 | 19.2 |
| $H_2AsS_3^- \rightarrow AsS_3^{-3} + 2H^+$ | 937.7 | 45.5 | 33.3 | 45.0 | 33.0 |
| $H_3AsO_3 \rightarrow H_2AsO_3^- + H^+$ | 343.1 | 21.0 | 15.4 | 21.5 | 15.7 |
| $H_2AsO_3^- \rightarrow HAsO_3^{-2} + H^+$ | 470.5 | 37.8 | 27.7 | 38.8 | 28.4 |
| $HAsO_3^{-2} \rightarrow AsO_3^{-3} + H^+$ | 574.5 | 37.6 | 27.5 | 49.4 | 36.2 |
| $H_3PO_4 \rightarrow H_2PO_4^- + H^+$ | 327.0 | 8.3 | 6.1 | 6.6 | 4.8 |
| $H_2PO_4^- \rightarrow HPO_4^{-2} + H^+$ | 457.3 | 29.6 | 21.7 | 28.9 | 21.2 |
| $HPO_4^{-2} \rightarrow PO_4^{-3} + H^+$ | 580.9 | 34.1 | 25.0 | 40.7 | 29.8 |
| $H_3AsS_4 \cdot H_2O \rightarrow H_2AsS_4^- \cdot H_2O + H^+$ | 298.9 | −3.6 | −2.6 | −6.3 | −4.6 |
| $H_2AsS_4^- \cdot H_2O \rightarrow HAsS_4^{-2} \cdot H_2O + H^+$ | 402.2 | 10.8 | 7.9 | 11.3 | 8.3 |
| $HAsS_4^{-2} \cdot H_2O \rightarrow AsS_4^{-3} \cdot H_2O + H^+$ | 489.5 | 18.7 | 13.8 | 17.6 | 12.9 |
| $H_3AsO_4 \cdot H_2O \rightarrow H_2AsO_4^- \cdot H_2O + H^+$ | 321.6 | 7.8 | 5.7 | 6.3 | 4.6 |
| $H_2AsO_4^- \cdot H_2O \rightarrow HAsO_4^{-2} \cdot H_2O + H^+$ | 439.7 | 27.7 | 20.3 | 24.1 | 17.7 |
| $HAsO_4^{-2} \cdot H_2O \rightarrow AsO_4^{-3} \cdot H_2O + H^+$ | 551.2 | 29.7 | 21.8 | 39.1 | 28.6 |
| $H_3AsS_3 \cdot H_2O \rightarrow H_2AsS_3^- \cdot H_2O + H^+$ | 313.8 | 5.8 | 4.3 | 6.9 | 5.0 |
| $H_2AsS_3^- \cdot H_2O \rightarrow HAsS_3^{-2} \cdot H_2O + H^+$ | 412.1 | 20.3 | 14.9 | 18.9 | 13.8 |
| $HAsS_3^{-2} \cdot H_2O \rightarrow AsS_3^{-3} \cdot H_2O + H^+$ | 508.1 | 24.8 | 18.2 | 25.3 | 18.5 |
| $H_3AsO_3 \cdot H_2O \rightarrow H_2AsO_3^- \cdot H_2O + H^+$ | 333.8 | 14.1 | 10.3 | 15.8 | 11.5 |
| $H_2AsO_3^- \cdot H_2O \rightarrow HAsO_3^{-2} \cdot H_2O + H^+$ | 458.0 | 41.2 | 30.2 | 41.6 | 30.5 |
| $HAsO_3^{-2} \cdot H_2O \rightarrow AsO_3^{-3} \cdot H_2O + H^+$ | 560.8 | 38.5 | 28.2 | 47.9 | 35.1 |
| $H_3PO_4 \cdot H_2O \rightarrow H_2PO_4^- \cdot H_2O + H^+$ | 322.1 | 8.5 | 6.2 | 6.7 | 4.9 |
| $H_2PO_4^- \cdot H_2O \rightarrow HPO_4^{-2} \cdot H_2O + H^+$ | 443.0 | 27.9 | 20.5 | 27.2 | 19.9 |
| $HPO_4^{-2} \cdot H_2O \rightarrow PO_4^{-3} \cdot H_2O + H^+$ | 562.4 | 35.8 | 26.2 | 40.7 | 29.8 |
| $H_2SO_3 \rightarrow HSO_3^- + H^+$ | 323.6 | 4.1 | 3.0 | 3.3 | 2.4 |
| $HSO_3^- \rightarrow SO_3^{-2} + H^+$ | 466.0 | 29.9 | 21.9 | 31.6 | 23.1 |
| $H_2SO_3 \cdot H_2O \rightarrow HSO_3^- \cdot H_2O + H^+$ | 312.7 | 2.6 | 1.9 | 4.2 | 3.1 |
| $HSO_3^- \cdot H_2O \rightarrow SO_3^{-2} \cdot H_2O + H^+$ | 454.4 | 30.0 | 22.0 | 26.5 | 19.4 |

[a] As noted before, we were unable to find an equilibrium geometry for $HAsS_3^{-2}$ under gas phase CBS-QB3 conditions; these deprotonations could not be evaluated.

Table 6.1: Calculated deprotonation energetics for acid deprotonation reactions.

There was one system, $HAsS_3^{2-}$, which we could not locate a converged geometry for in the gas phase. In this case, we found a converged CPCM-optimized geometry, but as we did not have a gas phase point we do not have the lowest quality pKas. During

the optimization processes for $HAsS_3^{2-}$, we observed that the compound dissociated during optimization into a pair of ions, $AsS_2^-$ and $HS^-$. This only occurred in the presence of the proton; $AsS_3^{3-}$ was easily optimized to a stable geometry. Therefore, we were able to calculate the energy required to doubly deprotonate $H_2AsS_3^-$ to $AsS_3^{3-}$ from our results, but $pKa_2$ and $pKa_3$ were unavailable for $H_xAsS_3$ species.

In the hydrated neutral systems, where we started with a water molecule in contact with the main molecule starting at its optimized gas phase geometry, then conducted optimizations both in the gas phase and in the PCM modeled hydration environment, the water molecule reached a minima with two hydrogen bonds to the main molecule. A typical case is shown in Figure 6.3 of a hydrated $H_3AsO_4 \cdot H_2O$ complex with this cyclic style of hydrogen bonding. Figure 6.4 illustrates the case where hydrogen bonding occurs from the water molecule to the anion. This was true except in rare cases such as for $H_3AsS_4 \cdot H_2O$ when optimized in a CPCM reaction field, where the water molecule sustained only its initial hydrogen bonding interaction.

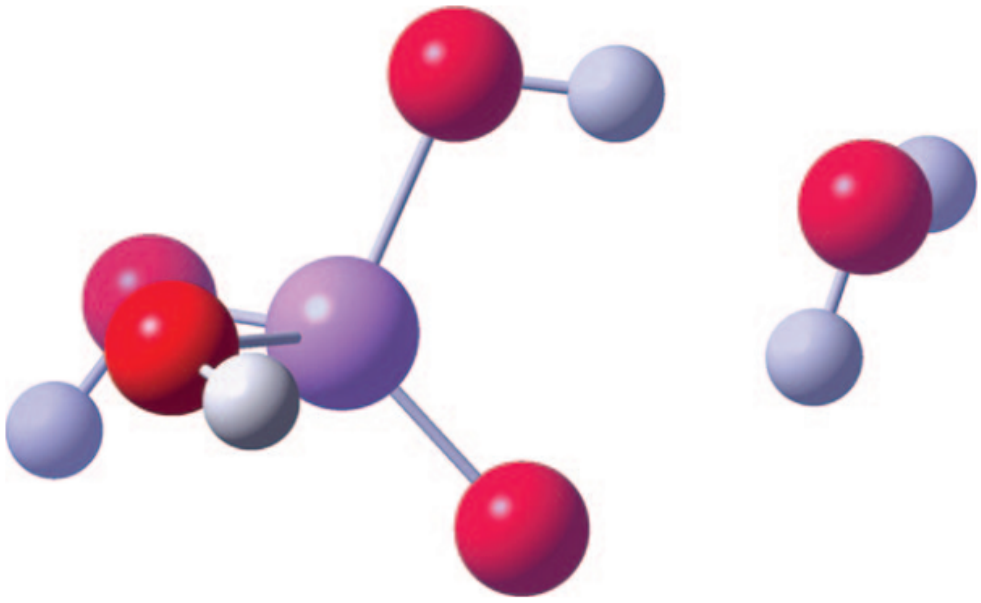

Figure 6.3: $H_3AsO_4$ . $H_2O$ complex optimized CBS-QB3 geometry showing typical cyclic hydrogen-bonding structure seen in singly solvated systems.

The hydrogen bonding does not show proton transfer either from the explicitly solvating water molecule in each calculation to the molecule or from the compound to the water molecule. However, between the most negatively charged anionic species and the least anionic there are differences of about 10% in H-O bond lengths in the water when it is hydrogen bonding. If we compare $H_3AsO_4$ and $AsO_3^{3-}$, the bond length of the hydrogen bonding H atom to the oxygen in its water molecule increases from 0.97A to 1.07A. The length of the hydrogen bond goes from 2.08A to

1.70A between the same two species. The more negatively charged anions have a stronger, shorter hydrogen bond than the neutral species.

There were several different patterns of explicit hydration interaction observed in the two kinds of species, neutral and anionic. When the explicit water molecule interacts with the anion, we note that at equilibrium the $H_2O$ molecule is positioned so that there are one or two hydrogen bonds going from negatively charged oxygen atoms on the anion to the hydrogen atoms on the explicit $H_2O$, such as illustrated in Figure 6.4 below. Uncharged complexes showed hydrogen bonding arrangements where there were both hydrogen bonding interactions going from the uncharged species' protons to the explicit water molecule's oxygen atom and interactions going from the water's hydrogen atoms to the uncharged complex.

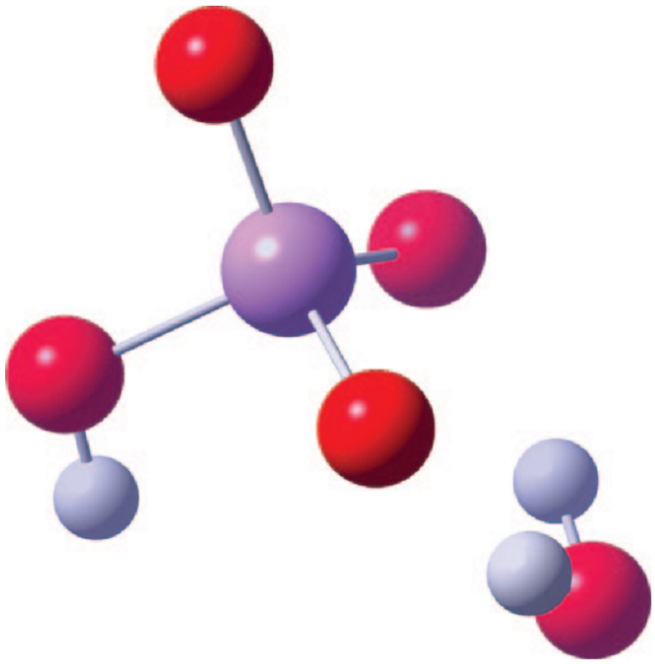

Figure 6.4: Hydrated $HAsO_4^{-2}$ . $H_2O$ complex CBS-QB3 optimized geometry as calculated in the polarizable continuum.

For example, in $H_3AsO_4$ optimized under the CPCM via a CBS-QB3 calculation, we saw the water molecule oriented with one hydrogen bond from one of the complex's protons to the water molecule's oxygen atom while at the same time there was a hydrogen bond going from one of the water molecule's hydrogens to the deprotonated oxygen atom in the complex as seen in Figure 6.3 above. $H_3AsS_4$ differed, however, with an off-axis very long hydrogen bond (see Figure 6.7, below)

The most extensive bonding interaction was seen between the explicit $H_2O$ and the $H_3AsS_3$ cluster. When optimized in the gas phase using CBS-QB3 the system

optimized into an energy minima with three hydrogen bonding interactions, two H atom interactions with the water's oxygen atom, although the third interaction, from a hydrogen atom on the $H_2O$ back to the third sulfur atom in the cluster was very long compared to the other interacting pairs. This pattern was also seen in the explicitly hydrated $H_3AsO_3$ complex shown in Figure 6.6, and the long, off-axis style of hydrogen bond also appeared in the $H_3AsS_4$ . $H_2O$ complex shown in Figure 6.7.

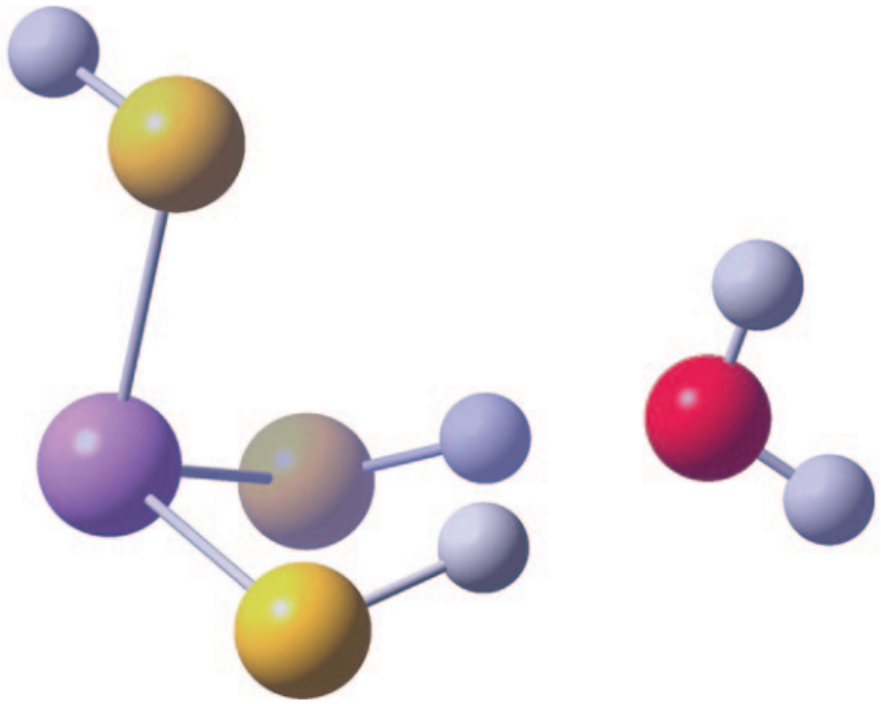

Figure 6.5: Illustration of the most hydrogen-bonding pattern seen in the hydrated $H_3AsS_3$ . $H_2O$ complex found from CBS-QB3 geometry optimization in the polarizable continuum.

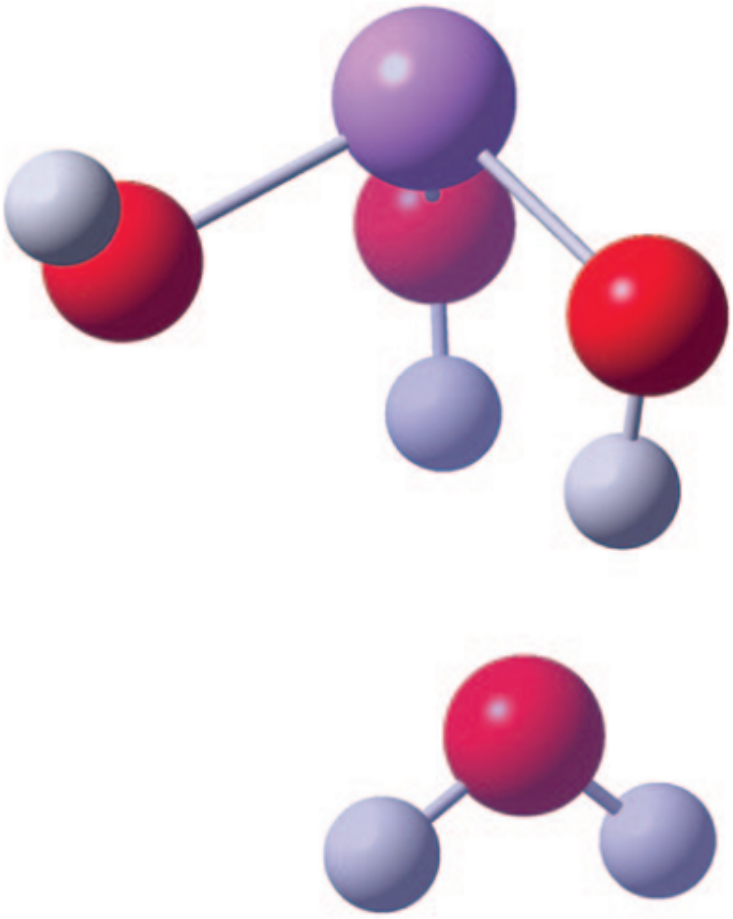

Figure 6.6: Similar multiple hydrogen-bonding interaction seen in $H_3AsO_3$ . $H_2O$ complex calculated under CBS-QB3 method with the CPCM present.

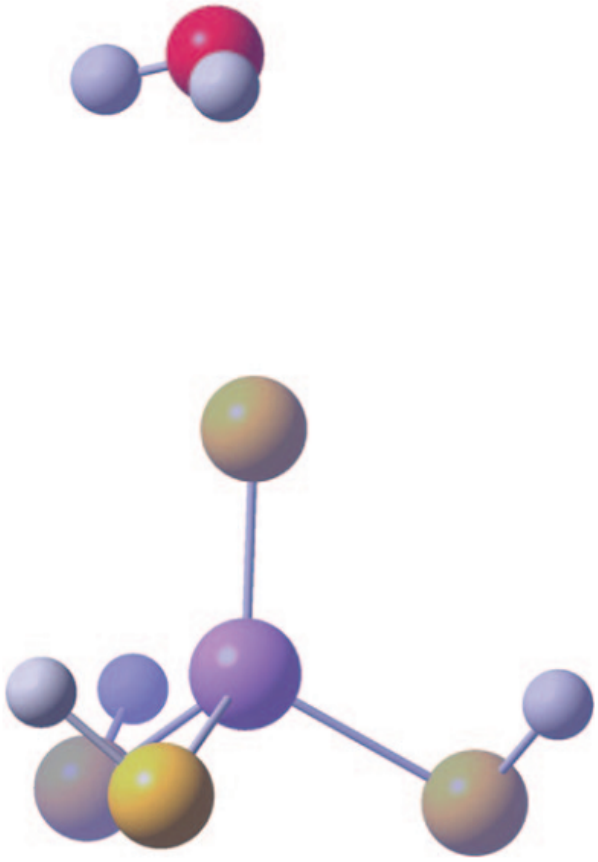

Figure 6.7: Long hydrogen-bonding interaction seen in the CBS-QB3 calculation with the polarizable continuum when optimizing the $H_3AsS_4$ . $H_2O$ explicitly hydrated system.

Having discussed geometries extensively, we move on to examine the acidities calculated with our methods.

The pKa data shows several interesting trends, best explored by examining the different methods in the case of the $H_3AsO_4$ and the $H_3PO_4$ compounds, both of which are well-characterized experimentally.

**TABLE 2: $H_3AsO_4$ and $H_3PO_4$ Comparison between Experiment and Theory**

| | exp. $pK_a$[a] | CBS-QB3 + (gas phase) CPCM $pK_a$ | CBS-QB3 CPCM $pK_a$ (all in PCM) | CBS-QB3 + (gas phase) CPCM w/$H_2O$ | CBS-QB3 CPCM $pK_a$ w/$H_2O$ (all in PCM) |
|---|---|---|---|---|---|
| $H_3AsO_4 \rightarrow H_2AsO_4^- + H^+$ | 2.3 | 6.5 | 6.1 | 5.7 | 4.6 |
| $H_2AsO_4^- \rightarrow HAsO_4^{-2} + H^+$ | 7 | 19.6 | 19.3 | 20.3 | 17.7 |
| $HAsO_4^{-2} \rightarrow AsO_4^{-3} + H^+$ | 13 | 21.0 | 28.3 | 21.8 | 28.6 |
| $H_3PO_4 \rightarrow H_2PO_4^- + H^+$ | 2.2 | 6.1 | 4.8 | 6.2 | 4.9 |
| $H_2PO_4^- \rightarrow HPO_4^{-2} + H^+$ | 7.1 | 21.7 | 21.2 | 20.5 | 19.9 |
| $HPO_4^{-2} \rightarrow PO_4^{-3} + H^+$ | 12.3 | 25.0 | 29.8 | 26.2 | 29.8 |

[a] Experimental $pK_a$s from William L. Jolly, *Modern Inorganic Chemistry*, 2nd edition.

Table 6.2: pKa values for $H_3AsO_4$ and $H_3PO_4$ multiple deprotonations with each CBS-QB3 based method.

**TABLE 3: Calculated $pK_a$s Using CCSD(T) Method**

| | | CCSD(T)/6-311G(2d,p) | | CCSD(T)/aug-cc-pVDZ | | CCSD(T)/CEP-121G | |
|---|---|---|---|---|---|---|---|
| | expt. $pK_a$[a] | gas phase geometry + CPCM solvation energy $pK_a$ | $pK_a$ with CPCM | Gas phase geometry + CPCM solvation energy $pK_a$ | $pK_a$ with CPCM | Gas phase geometry + CPCM solvation energy $pK_a$ | $pK_a$ with CPCM |
| $H_3AsO_4 \rightarrow H_2AsO_4^- + H^+$ | 2.3 | 13.6 | 12.8 | 6.6 | 6.4 | 0.2 | −0.5 |
| $H_2AsO_4^- \rightarrow HAsO_4^{-2} + H^+$ | 7 | 32.6 | 11.0 | 17.6 | 19.7 | 11.8 | 14.1 |
| $HAsO_4^{-2} \rightarrow AsO_4^{-3} + H^+$ | 13 | 50.3 | 43.1 | 19.1 | 29.8 | 23.7 | 33.3 |
| $H_3PO_4 \rightarrow H_2PO_4^- + H^+$ | 2.2 | 12.6 | 27.1 | 5.2 | 4.9 | −2.4 | −1.2 |
| $H_2PO_4^- \rightarrow HPO_4^{-2} + H^+$ | 7.1 | 35.9 | 16.8 | 22.2 | 22.2 | 15.9 | 14.1 |
| $HPO_4^{-2} \rightarrow PO_4^{-3} + H^+$ | 12.3 | 51.1 | 44.1 | 19.7 | 27.8 | 19.1 | 19.6 |

[a] Experimental $pK_a$s from William L. Jolly, *Modern Inorganic Chemistry*, 2nd edition.

Table 6.3: pKa values for $H_3AsO_4$ and $H_3PO_4$ multiple deprotonations with the CCSD(T) method under 6-311G(2d,p), aug-cc-pVDZ, and CEP-121G basis sets.

In most of the records, we observe that the $pKa_3$ is significantly lower in the CBS-QB3 / gas phase with CPCM corrections calulations than in the CBS-QB3 CPCM calculations. For the species with sulfur atoms this difference is generally about 5%, but with oxides we notice a difference around 15-20%. This may be a result of the difference in electronegativities of the two species; with oxygen's significantly higher electronegativity we see a greater effect. The stabilization is a result of the electronic interaction between the self consistent field of electrons arranged around the ion and

the polarizable continuum outside the cavity, so a greater concentration of electron probability would cause a much more intense stabilization effect.

The calculations with the CPCM present reduce the total free energy further for each species.

It can be noted that the energies calculated with CBS-QB3 in the CPCM the total energies are significantly lower for most of the species we studied, except for the most negative, strongly charged anions such as $AsO_4^{3-}$, $AsO_3^{3-}$, and $AsO_3^{3-}$ . $H_2O$. In these cases the energy difference was on the order of only about 10 kcal/mol, which is of the same order of magnitude as our experimental results.

In the case of the fully deprotonated oxide species, including these, $AsO_4^{3-}$, $AsO_3^{3-}$ and the hydrated versions of the same two, we suspect the cause is that the CPCM stabilization energy for the gas phase species is very large, on the order of 500 kcal/mol (400 kcal/mol for sulfides and sulfates). The energies are probably similar because of this large contribution to the energy from solvation. At the same time, the geometries of the highly charged anions are at a deep well in the geometry potential energy surface and do not change much when placed in the CPCM. It is likely that because there is not much of a difference in geometries the CBS-QB3 energies are similar between the different ways of approximating solvation.

However, if we compare the results in Table 6.2 and Table 6.3 with the ones that we find in experimental references, we see that there are some discrepancies, especially for $pKa_2$s and $pKa_3$s. This is to be expected, as the theory is more strained in these cases. The data, however, does show the proper trends for each of the species. This suggests that we can find a relation of some sort between the two.

We therefore prepared Figures 6.8 and 6.9, which illustrate both sets of data, experimental and theoretical.

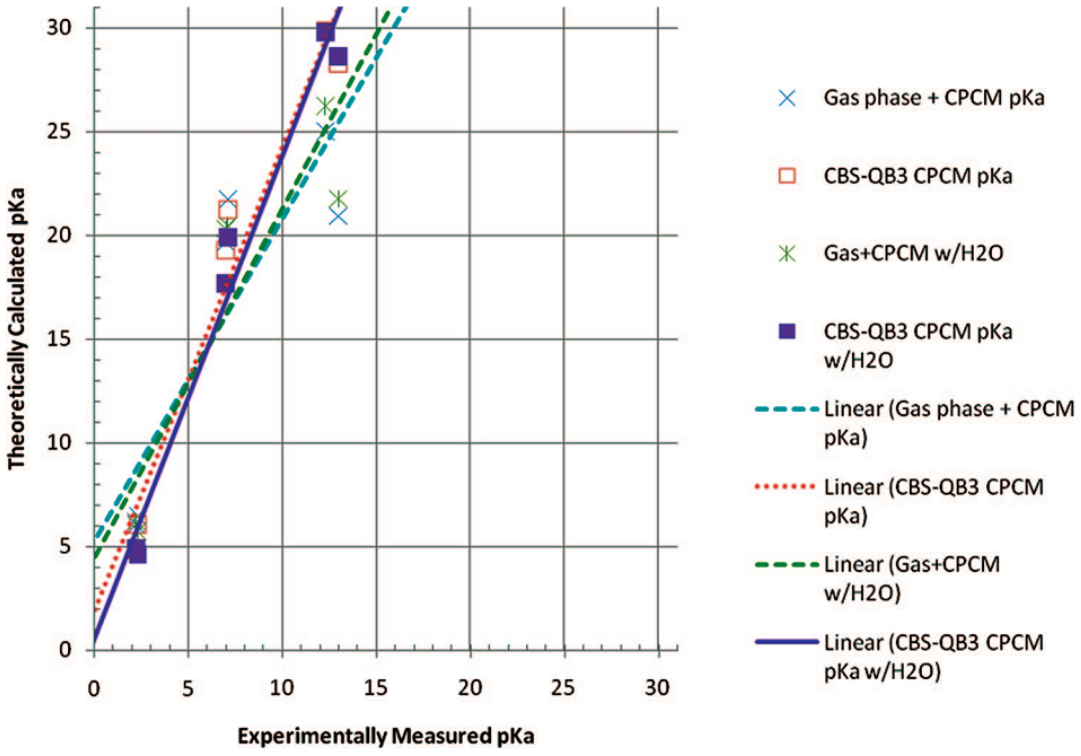


Figure 6.8: Graphs of experimental versus theoretical pKas for As(V) and P(V) systems.

When plotting the experimentally and theoretically determined data against each other, we can see a clear linear relation between the two, as illustrated in Figure 6.8 and Figure 6.9. The difference in these two cases is smallest in magnitude when we compare the CBS-QB3 calculations which were prepared in the polarizable continuum to the experimental ones. These points also had the linear regression fitting the two types of data together, with an $r^2$ value of 0.952 for the non explicitly solvated system and one of 0.974 for the explicitly solvated one.

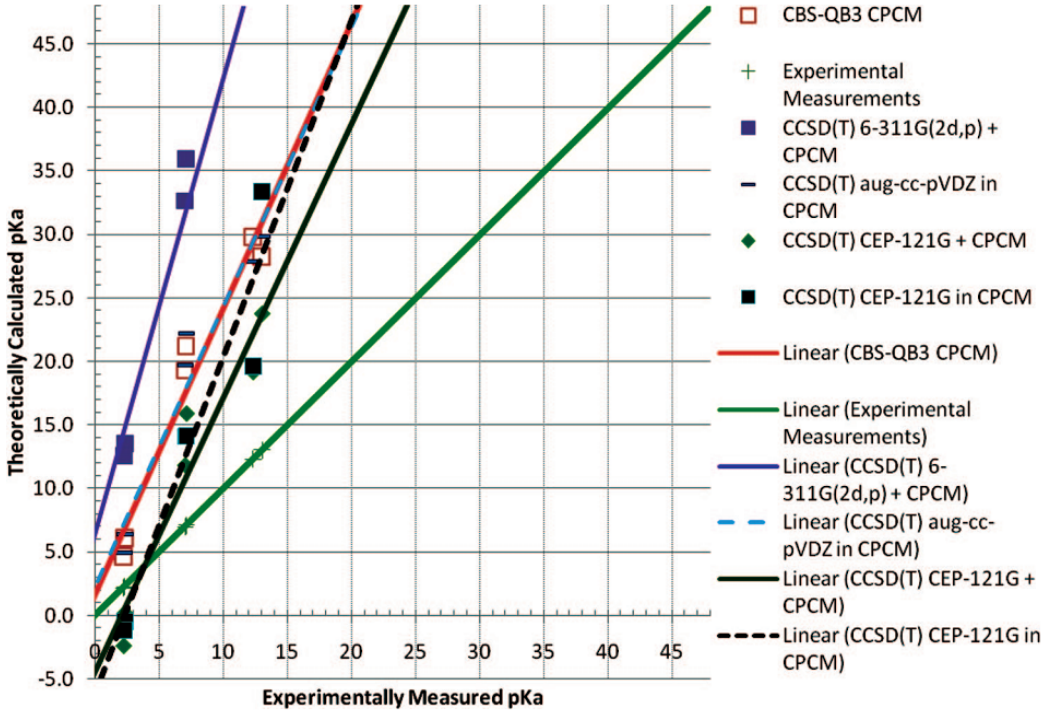


Figure 6.9: Linearity in results calculated with CCSD(T) methods compared to the results from systems calculated via CBS-QB3 in the CPCM.

This linearity was also observed in our high level CCSD(T)/6-311G(2d,p) calculation as well as our CCSD(T)/aug-cc-pVDZ results, although the data spectacularly failed in the former case when optimized in the CPCM, and in the latter when optimized without. These data are summarized in Table 6.4 below.

**TABLE 4: Linear Extrapolation Slope/Intercepts Converting Theoretical Values to Experimental Ones**

| $y = mx + b$ | CBS-QB3 method | | CBS-QB3 with explicit solvation | | CCSD(T)/6−311G(2d,p) | | CCSD(T)/aug-cc-pVDZ | | CCSD(T)/CEP-121G | |
|---|---|---|---|---|---|---|---|---|---|---|
| $y$ = expt. p$K_a$ $x$ = theo. calculated p$K_a$ | CBS-QB3 + (gas phase geometry's) CPCM stabilization p$K_a$ | CBS-QB3 CPCM p$K_a$ (all structures optimized & energy calculated in PCM) | CBS-QB3 + CPCM w/$H_2O$ | CBS-QB3 CPCM p$K_a$ w/$H_2O$ | + CPCM solvation energy | optimized with CPCM | + CPCM solvation energy | optimized with CPCM | + CPCM solvation energy | Optimized with CPCM |
| $m$ | 0.643 | 0.444 | 0.593 | 0.429 | 0.273 | 0.231 | 0.516 | 0.428 | 0.428 | 0.342 |
| $b$ | −3.398 | −0.767 | −2.635 | −0.233 | −1.593 | 1.353 | −0.462 | −0.597 | 2.448 | 2.795 |
| $r^2$ | 0.778 | 0.952 | 0.824 | 0.974 | 0.979 | 0.542 | 0.649 | 0.944 | 0.923 | 0.907 |

Table 6.4: Linear Extrapolations for phosphoric and arsenic acids calculated from previous pKa tables.

As we can see, the results from charged couple theory with the relativistically corrected core effective potential basis set, CCSD(T)/CEP-121G, also compare favorably, although their $r^2$ values are not as good, at 0.923 and 0.907.

Visual observation of the linear extrapolations in Figure 6.8, Figure 6.9 lets us observe the error in CBS-QB3 CPCM with explicit hydration with water is the method with the smallest evident error, and this is confirmed by the data in Table 6.4, where we see that it has an $r^2$ value of 0.974, which is basically equivalent to the CCSD(T)/6-311G(2d,p) result, but with a much flatter slope.

We can use the extrapolations determined from the known $H_3PO_4$ and $H_3AsO_4$ data to fit $pKa_1$, $pKa_2$, and $pKa_3$ values for each of the two types of solvation, CPCM with and without explicit hydration, for $H_3AsO_3$, $H_3AsS_4$, $H_3AsS_3$, and $H_2SO_4$. The results for the CBS-QB3 CPCM pKa's with explicit solvation are tabulated in Table 6.5 below. This corrective extrapolation would account for any systematic differences from other approaches caused by our particular choice of $H^+$ solvated ion energy or our choice of method. This extrapolation therefore appears as Equation 6.2, below:

(6.2) $pKa_{expt} = 0.429\ pKa_{CBS\text{-}QB3\ CPCM\ w/H2O} - 0.233$

**TABLE 5: Fitted CBS-QB3 CPCM p$K_a$s (with Explicit $H_2O$ Molecule Solvation)**

| | | exp. p$K_a$[a] | CBS-QB3 CPCM p$K_a$ w/$H_2O$ | fitted CBS-QB3 CPCM p$K_a$ w/$H_2O$ |
|---|---|---|---|---|
| $H_3AsO_4$ | p$K_{a1}$ | 2.3 | 4.6 | 1.7 |
| | p$K_{a2}$ | 7 | 17.7 | 7.3 |
| | p$K_{a3}$ | 13 | 28.6 | 12.1 |
| $H_3PO_4$ | p$K_{a1}$ | 2.2 | 4.9 | 1.9 |
| | p$K_{a2}$ | 7.1 | 19.9 | 8.3 |
| | p$K_{a3}$ | 12.3 | 29.8 | 12.6 |
| $H_3AsO_3$ | p$K_{a1}$ | 9.2 | 11.5 | 4.7 |
| | p$K_{a2}$ | | 30.5 | 12.9 |
| | p$K_{a3}$ | | 35.1 | 14.8 |
| $H_3AsS_4$ | p$K_{a1}$ | | −4.6 | −2.2 |
| | p$K_{a2}$ | | 8.3 | 3.3 |
| | p$K_{a3}$ | | 12.9 | 5.3 |
| $H_3AsS_3$ | p$K_{a1}$ | | 5.0 | 1.9 |
| | p$K_{a2}$ | | 13.8 | 5.7 |
| | p$K_{a3}$ | | 18.5 | 7.7 |
| $H_2SO_3$ | p$K_{a1}$ | 1.8 | 3.1 | 1.1 |
| | p$K_{a2}$ | 7.2 | 19.4 | 8.1 |

[a] Experimental p$K_a$s from William L. Jolly, Modern Inorganic Chemistry, Second Edition.

Table 6.5: Fitted pKas for each polyprotic acid species using the linear extrapolation.

Of the pKas from the experimental system used to fit the data, we see errors of 0.6, 0.3, and 0.9 pKa units for $H_3AsO_4$, and 0.3, 1.2, and 0.3 pKa units for $H_3PO_4$. Experimental data which we retrieved after producing the extrapolation fared similarly, with errors of 4.5 for the known H3AsO3 point, and 0.7 and 0.9 for $H_2SO_3$, another polyprotic acid system which is well characterized. These errors are on the order of 5 to 30 percent of the raw values, but if we consider the amount of improvement with the fitting than without, the improvement is quite dramatic, with errors in the theoretical pKas around double or triple the magnitudes of the data in the worst cases.

Unfortunately, there was a lack of experimental data for similar polyprotic acids to compare to the $H_3AsO_3$, $H_3AsS_3$, and $H_3AsS_3$. We would therefore expect the results not to be as good as the chemical environment would be different between both oxy- and thio- acids as well as the different oxidation states of arsenic. However, the small polyatomic clusters do have a structural similarity that should allow the extrapolation to be of some help. We see this with our data for $H_3AsO_4$, which shows the largest error of all the known points. The results for $H_2SO_3$, which were not used in constructing the extrapolation are much closer, within one pKa unit of the measured experimental values after applying the correcting factor.

Although the linear relation for the CCSD(T) calculation with the 6-311G(2d,p) basis has a (barely) better $r^2$ value than the explicitly hydrated CBS-QB3 CPCM value we settled upon, a visual examination of the data shows that the latter has definite advantages over the CCSD(T) data. As the slope of the correction is much greater, it indicates that the CCSD(T) method is less correct in this case. However, the CCSD(T)/aug-cc-pVDZ data also shows almost the same quality of result as the CCSD(T)/6-311G(2d,p) one.

*6.4 Conclusions*

Therefore, we would recommend use of the CBS-QB3 CPCM with explicit hydration approach for calculating pKa values in this situation. The results have been shown to be more reliable than calculations done without the correction factor, and though the accuracy is definitely lower for trioxides (and presumably the sulfates and sulfides), it is sufficient for producing semiquantative predictions of second and third pKas.

From our results, we would predict that $H_3AsS_3$ is likely to be deprotonated at least twice for species in solution near pH 7, and it is likely that $H_3AsS_4$ will be fully deprotonated in solutions buffered near the netural point, existing purely as $AsS_4^{3-}$. $H_3AsO_3$ is predicted to exist primarily in singly deprotonated form for most of the neutral range up to pH 12.

Further study of $H_3AsS_3$ would be a reasonable next step. Molecular mechanics calculations could yield an ensemble of average geometries which might be of aid in

finding a distribution of energies in an explicit solvent. From our calculations, we would expect that the presence of more explicit water molecules would lead towards a geometry for the anionic species closer to that of the original, fully protonated species, lowering the cost of dissociation.

We would recommend to laboratories without a dedicated theoretician to do an HF/6-311G optimization calculation in the gas phase first, then follow that up with the CBS-QB3 / CPCM calculation as described in the text. From our experience, the initial Hartree-Fock calculation will quickly yield an optimized geometry sufficiently close to the B3LYP / CBSB7 optimized geometry that the CBS-QB3 calculation will converge quickly and without undue difficulty.

*6.5 Acknowledgements*

NSF Grant EAR0539109 supported the research in this chapter, which is based on the *J. Phys. Chem. A* paper by Zimmermann and Tossell[3] which is part of a trio of works with G. R. Helz who suggested the arsenic system for study. We would like to also acknowledge G. R. Helz for many interesting afternoon discussions of arsenic systems detailed in this work.

*6.6 References*


1. Montgomery, J.A., J.W. Ochterski, and M.J. Frisch, *An improved complete basis set (CBS) model chemistry.* Abstracts of Papers of the American Chemical Society, 1996. **211**: p. 231-PHYS.
2. Barone, V. and M. Cossi, *Quantum calculation of molecular energies and energy gradients in solution by a conductor solvent model.* Journal of Physical Chemistry A, 1998. **102**(11): p. 1995-2001.
3. Zimmermann, M.D. and J.A. Tossell, *Acidities of Arsenic (III) and Arsenic (V) Thio- and Oxyacids in Aqueous Solution using the CBS-QB3/CPCM Method.* Journal of Physical Chemistry A, 2009. **113**(17): p. 5105-5111.
4. Duker, A.A., E.J.M. Carranza, and A. Hale, *Arsenic Geochemistry and Health.* Environ. Int., 2005. **31**.
5. Alexeev, Y., et al., *Accurate heats of formation and acidities for H3PO4, H2SO4, and H2CO3 from ab initio electronic structure calculations.* International Journal of Quantum Chemistry, 2005. **102**(5): p. 775-784.
6. M. J. Frisch, G.W.T., H. B. Schlegel, G. E. Scuseria, M. A. Robb, J. R. Cheeseman, J. A. Montgomery, Jr., T. Vreven, K. N. Kudin, J. C. Burant, J. M. Millam, S. S. Iyengar, J. Tomasi, V. Barone, B. Mennucci, M. Cossi, G. Scalmani, N. Rega, G. A. Petersson, H. Nakatsuji, M. Hada, M. Ehara, K. Toyota, R. Fukuda, J. Hasegawa, M. Ishida, T. Nakajima, Y. Honda, O. Kitao, H. Nakai, M. Klene, X. Li, J. E. Knox, H. P. Hratchian, J. B. Cross, V. Bakken, C. Adamo, J. Jaramillo, R. Gomperts, R. E. Stratmann, O. Yazyev,

A. J. Austin, R. Cammi, C. Pomelli, J. W. Ochterski, P. Y. Ayala, K. Morokuma, G. A. Voth, P. Salvador, J. J. Dannenberg, V. G. Zakrzewski, S. Dapprich, A. D. Daniels, M. C. Strain, O. Farkas, D. K. Malick, A. D. Rabuck, K. Raghavachari, J. B. Foresman, J. V. Ortiz, Q. Cui, A. G. Baboul, S. Clifford, J. Cioslowski, B. B. Stefanov, G. Liu, A. Liashenko, P. Piskorz, I. Komaromi, R. L. Martin, D. J. Fox, T. Keith, M. A. Al-Laham, C. Y. Peng, A. Nanayakkara, M. Challacombe, P. M. W. Gill, B. Johnson, W. Chen, M. W. Wong, C. Gonzalez, and J. A. Pople, *Gaussian 03, Revision C.02*, 2004, Gaussian, Inc., Wallingford CT.

7. Curtiss, L.A., et al., *Gaussian-2 Theory for Molecular-Energies of 1st-Row and 2nd-Row Compounds.* Journal of Chemical Physics, 1991. **94**(11): p. 7221-7230.

8. Curtiss, L.A., et al., *Gaussian-3 (G3) theory for molecules containing first and second-row atoms.* Journal of Chemical Physics, 1998. **109**(18): p. 7764-7776.

9. Becke, A.D., *Density-functional thermochemistry. III. The role of exact exchange.* The Journal of Chemical Physics, 1993. **98**(7): p. 5648-5652.

10. Raghavachari, K., et al., *A fifth-order perturbation comparison of electron correlation theories.* Chemical Physics Letters, 1989. **157**(6): p. 479-483.

11. Krishnan, R. and J.A. Pople, Int. J. Quantum Chem., 1978. **14**: p. 91.

12. Head-Gordon, M., J.A. Pople, and M.J. Frisch, Chem. Phys. Lett., 1988. **153**: p. 503.

13. Ramakrishna, V. and B.J. Duke, J. Chem. Phys., 2003. **118**: p. 6137.

14. Truong, T.N. and E.V. Stefanovich, Chem. Phys. Lett., 1995. **240**: p. 253.

15. Alexeev, Y., et al., Intl. J. Quantum Chem., 2005. **104**: p. 379.

16. Liptak, M.D. and G.C. Shields, Int. J. Quantum Chem., 2001. **85**: p. 727.

17. Camaioni, D., J. Phys. Chem. A, 2005. **109**: p. 10795.

18. Pliego, J.R. and J.M. Riveros, Chem. Phys. Lett., 2000. **332**: p. 597.

19. Pliego, J.R. and J.M. Riveros, Phys. Chem. Chem. Phys., 2002. **4**: p. 1622.

20. Tissandier, M.D., et al., J. Phys. Chem. A, 1998. **102**: p. 7787.

21. Zhan, C.G. and D.A. Dixon, J. Phys. Chem. A, 2001. **105**: p. 11534.

# Chapter 7: HClOx *ab initio* calculations in the CPCM with previously explored fitting and counterions

*In this chapter we examine some properties of different perchloric, chloric, chlorous, and hypochlorous acids using the fitting system developed in the previous chapter. The fit is also shown with counterions present to reduce the total charges in the calculation.*

## *7.1 Introduction*

In this case we are interested in the deprotonation of $HClO_x$ compounds, with x=1 to 4. Perchloric acid, $HClO_4$, is one of the strongest acids, with an experimental pKa of -10[1] at 70% concentration in liquid sulfur dioxide, and a gas phase association energy of 1180 kJ/mol[2]. Our calculations will explore the dissociation chemistry of $HClO_4$, $HClO_3$, $HClO_2$, and HClO from an ab-inito point of view. Chloric acid, $HClO_3$, has an experimental pKa of -1[3], chlorous acid has a pKa of 1.96[4], and hypochlorous acid a pKa of 7.497[5].

Perchloric Acid deprotonation was also examined by another group in 2008[6], who showed that a CBS-QB3 calculation[7-9] was sufficient for calculating pKas for $HClO_4$. In that paper, they use a variety of theoretical approaches, approaching their experimental measurement of pH -10 generally within 1 kcal/mol. Chloric and

perchloric acids heats of formation were also previously reviewed[10] using G2 theory[11], but counter-ions were not used in either case.

*7.2 Methods*

We calculated both gas phase and solvated geometries and energetics with Gaussian 03[12] using MP2[13] and B3LYP[14] with the CBSB7 basis[7], and also conducted CBS-QB3 calculations[7-9] under the same conditions. For each gas phase B3LYP geometry, we calculated the energy of solvation using CPCM[15-17] with Hartree-Fock orbitals determined with the 6-31G, 6-31G**, and 6-31+G** basis sets.

The Gibbs Free Energy of reaction is then calculated for each of the methods for each of the deprotonation reactions. The gas phase calculated energies were combined with the HF/6-31+G** calculated solvation energies, and an $H^+$ (aq) solvation energy of 269.0 kcal/mol was used for the calculations.

No additional basis functions were added to either the CBSB7 basis sets or the 6-31G series basis sets in this calculation.

*7.3 Results and Discussion*

Calculated energies of solvation and sums of electronic and thermal Free Energies (in Hartrees) for each species appears in Table 7.1 below.

| | HF | | | Sum of Electronic and thermal Free Energies (Hartrees) | | | | | |
|---|---|---|---|---|---|---|---|---|---|
| | DeltaG (solvation) (kcal/mol) | | | MP2 | | CBS-QB3 Free Energy | | B3LYP | |
| | 6-31+G** | 6-31G | 6-31G** | SCRF | (no SCRF) | SCRF | (no SCRF) | SCRF | (no SCRF) |
| NaClO | -29.71 | -31.23 | -28.48 | | | -696.820017 | -696.765733 | | |
| HClO | -5.81 | -6.73 | -5.52 | -535.276815 | -535.266005 | -535.456340 | -535.445790 | -536.024040 | -536.012998 |
| ClO- | -70.38 | -71.04 | -71.62 | -534.787752 | -534.672064 | -534.991375 | -534.878292 | -535.543241 | -535.428596 |
| NaClO2 | -22.85 | -23.71 | -21.44 | -771.607165 | -771.566866 | -771.892604 | -771.849173 | -772.969062 | -772.930156 |
| HClO2 | -10.71 | -12.28 | -9.83 | -610.224103 | -610.211089 | -610.507065 | -610.492406 | -611.154246 | -611.139540 |
| ClO2- | -67.47 | -68.49 | -68.27 | -609.752524 | -609.644066 | -610.064243 | -609.958804 | -610.691112 | -610.583528 |
| NaClO3 | -26.76 | -29.08 | -25.72 | -846.619184 | -846.568050 | -847.002461 | -846.940452 | -848.149434 | -848.104492 |
| HClO3 | -9.24 | -12.57 | -8.76 | -685.221764 | -685.210979 | -685.596667 | -685.583420 | -686.320960 | -686.307633 |
| ClO3- | -63.41 | -65.98 | -64.28 | -684.773719 | -684.673270 | -685.178457 | -685.079909 | -685.880324 | -685.779604 |
| NaClO4 | -27.69 | -30.55 | -27.15 | -921.624532 | -921.570212 | -922.097531 | -922.036657 | -923.313772 | -923.261055 |
| HClO4 | -9.69 | -13.82 | -9.57 | -760.213787 | -760.199508 | -760.676010 | -760.659924 | -761.472749 | -923.261055 |
| ClO4- | -56.68 | -57.43 | -57.51 | -759.792178 | -759.700054 | -760.276303 | -760.184317 | -761.058762 | -760.965657 |

Table 7.1: Calculated Gas-phase solvation energies and Free Energies for (H/Na)$ClO_x$ (x=1 to 4). Systems which were CPCM solvated during the calculation on the right are marked SCRF (Self Consistent Reaction Field – CPCM is the type of SCRF we used).

From these data, we can calculate deprotonation energetics for each species with two different types of solvation. Solvation calculated by adding the gas phase solvation energy calculated with the HF method, and solvation calculated at the same time. The results appear in Table 7.2 below:

| | | MP2 | | CBS-QB3 Free Energy | | B3LYP | |
|---|---|---|---|---|---|---|---|
| H+ (aq) | 269 **kcal/mol** | SCRF | **Gas phase +** | SCRF | **Gas phase +** | SCRF | **Gas phase + SCRF** |
| | HClO → H+ + ClO- | 37.89 | 39.13 | 22.77 | 22.53 | 32.70 | 33.14 |
| | HClO2 → H+ + ClO2- | 26.92 | 30.05 | 8.87 | 9.08 | 21.62 | 23.14 |
| | HClO3 → H+ + ClO3- | 12.15 | 14.24 | -6.57 | -7.22 | 7.50 | 8.17 |
| | HClO4 → H+ + ClO4- | -4.44 | -2.58 | -18.18 | -17.55 | -9.22 | -7.52 |

Table 7.2: Deprotonation reaction energies in kcal/mol for solvated system calculated both at SCRF and gas phase geometry with solvation energy added in.

As seen in Table 7.2, the calculated energetics are generally one or two kcal/mol less favorable when done in the faster Gas Phase + SCRF approach.

The most interesting difference here is perhaps the CBS-QB3 energy calculations when compared to the MP2 and B3LYP. With the complete basis set extrapolation, the deprotonation for $HClO_3$ is favorable in solvated conditions. This is as expected, because the experimental pKas are negative as well, although the calculated dissociation is more favorable than the experimental measurements indicate.

| **pKa values** | | MP2 | CBS-QB3 Free Energy | | B3LYP | | |
|---|---|---|---|---|---|---|---|
| Expt. pKa | | SCRF | Gas phase + SCRF | | Gas phase + SCRF | | Gas phase + SCRF |
| 7.5 | HClO → H+ + ClO- | 27.77 | 28.68 | 16.69 | 16.52 | 23.97 | 24.29 |
| 1.96 | HClO2 → H+ + ClO2- | 19.73 | 22.02 | 6.5 | 6.65 | 15.84 | 16.96 |
| -1 | HClO3 → H+ + ClO3- | 8.9 | 10.44 | -4.82 | -5.29 | 5.5 | 5.99 |
| -10 | HClO4 → H+ + ClO4- | -3.25 | -1.89 | -13.33 | -12.86 | -6.76 | -5.51 |

Table 7.3: Calculated pKas for each $HClO_x$ acid. pKa is the change in Gibbs Free Energy / 1.3644.

The calculated pKas in this case are similar to the others which we found for the phosphoric acid in arsenic, and arsenous acids discussed in the previous chapter in that both the favorable and unfavorable pKas were overestimated. However, the basic pKas were relatively close to the experimental measurements in both the $HClO_4$ and HClO cases when using the CBS-QB3 method.

Using the approximation which we calculated for that data set, Equation (7.1) below, we have the following adjusted results in Table 7.4.

(7.1) $pKa_{fitted} = 0.429\ pKa_{CBS\text{-}QB3} - 0.233$

As the fitting was made to be used with CBS-QB3 calculations, and the most applicable columns have been bolded in the table below.

| | Fitted pKa values | MP2 | | CBS-QB3 Free Energy | | B3LYP | |
|---|---|---|---|---|---|---|---|
| Expt. pKa | | SCRF | Gas phase + SCRF | **SCRF** | **Gas phase + SCRF** | SCRF | Gas phase + SCRF |
| **7.5** | **HClO → H+ + ClO-** | 11.66 | 12.05 | **6.9** | **6.83** | 10.03 | 10.16 |
| **1.96** | **HClO2 → H+ + ClO2-** | 8.21 | 9.19 | **2.53** | **2.6** | 6.54 | 7.02 |
| **-1** | **HClO3 → H+ + ClO3-** | 3.56 | 4.22 | **-2.33** | **-2.53** | 2.1 | 2.31 |
| **-10** | **HClO4 → H+ + ClO4-** | -1.66 | -1.07 | **-5.98** | **-5.78** | -3.16 | -2.62 |

Table 7.4: $HClO_x$ pKas as fitted by adjustment method.

In all cases except for $HClO_4$ the results show a decided improvement. The percentage errors for each point are reproduced in Table 7.5 and Table 7.6 below.

| pKa% Error Calculated Values | MP2 | | CBS-QB3 Free Energy | | B3LYP | |
|---|---|---|---|---|---|---|
| | SCRF | Gas phase + SCRF | **SCRF** | **Gas phase + SCRF** | SCRF | Gas phase + SCRF |
| **HClO → H+ + ClO-** | 270% | 283% | **123%** | **120%** | 220% | 224% |
| **HClO2 → H+ + ClO2-** | 906% | 1024% | **232%** | **239%** | 708% | 765% |
| **HClO3 → H+ + ClO3-** | -990% | -1144% | **382%** | **429%** | -650% | -699% |
| **HClO4 → H+ + ClO4-** | -67% | -81% | **33%** | **29%** | -32% | -45% |

Table 7.5: Percent error in unfitted $HClO_x$ pKas

| Fitted pKa value % Error Calculations | MP2 | | CBS-QB3 Free Energy | | B3LYP | |
|---|---|---|---|---|---|---|
| | SCRF | Gas phase + SCRF | **SCRF** | **Gas phase + SCRF** | SCRF | Gas phase + SCRF |
| **HClO → H+ + ClO-** | -55% | -61% | 8% | 9% | -34% | -36% |
| **HClO2 → H+ + ClO2-** | -319% | -369% | -29% | -32% | -234% | -258% |
| **HClO3 → H+ + ClO3-** | 456% | 522% | -133% | -153% | 310% | 331% |
| **HClO4 → H+ + ClO4-** | 83% | 89% | 40% | 42% | 68% | 74% |

Table 7.6: Percent error in fitted pKa values

Although the percentage errors increase in the case of the $HClO_4$ values compared with experiment, in the other cases the quality of the answer improved to well within

an order of magnitude of the correct result. Keeping in mind that the extrapolation was made for CBS-QB3 SCRF calculations, these results are quite satisfactory.

Examining the CBS-QB3 results, with the fitting the error ranges from an absolute value of 8% to 133% in the case of the explicitly solvated calculation, and 9% to 153% for the calculation done separate from the solvation stabilization calculation. At the same time, when the calculations were not fitted the errors went from 33% to 382% for the SCRF stabilized CBS-QB3 calculation, and with the stabilization calculation done separately the absolute error ranged from 29% to 429%. In each case, the maximum error appeared in the $HClO_3$ calculation, although the smallest error was in the $HClO_4$ in the non fitted case and in the HClO calculation in the fitted case (thought the $HClO_4$ results were slightly worse after fitting).

Comparing the different methods, we can easily see from Table 7.5 that the greatest errors occurred in the MP2 calculation, and while the B3LYP calculations were off by less, they were still not as good as the CBS-QB3 calculations.

As an alternative to the equation with unbalanced charges, we also did the same calculations with $Na^+$ counterions. This allowed us to balance the charge difference on each side of the deprotonation equilibrium as follows:

$$Na^+ + HClO_x \rightarrow H^+ + NaClO_x$$

This structural change makes the sum of squares of charges on both sides equal, which should make it easier for the models to handle the reaction energies more effectively, thereby reducing errors in the calculation by a large amount.

| **Reaction Energies** | MP2 | CBS-QB3 Free Energy | | B3LYP | |
|---|---|---|---|---|---|
| H+ (aq) 269 kcal/mol | SCRF | Gas phase | + SCRF | Gas phase | + SCRF |
| Na+ + HClO → NaClO + H+ | 437162.94 | 437132.25 | 21.03 | 24.57 | 437631.82 | 437600.99 |
| Na+ + HClO2 → NaClO2 + H+ | 8.86 | 13.84 | 7.31 | 13.22 | -262.06 | -259.02 |
| Na+ + HClO3 → NaClO3 + H+ | -0.15 | 7.65 | -5.40 | 7.68 | -270.63 | -268.31 |
| Na+ + HClO4 → NaClO4 + H+ | -8.51 | -1.38 | -15.27 | -5.17 | -278.51 | -273.16 |

Table 7.7: $\Delta G_{rxn}$ Reaction energies (kcal/mol) for counterion-assisted calculations.

One of the first things which we notice here is that the additional $Na^+$ ion is causing something to go wrong with our B3LYP calculations. The reaction energetics all appear to have approximately 270 kcal/mol more stability for the products predicted than the other calculations. This extra energy seems to be appearing in the raw energy calculations for the $NaClO_x$ compounds listed in Table 7.1 (1 Hartree is approximately 627.5 kcal/mol), although direct comparison between B3LYP and HF/MP2 methods is not possible.

However, the energetics from the MP2 and CBS-QB3 calculations appear similar to the ones done without the counterion, so we shall focus on those results below.

Next, we will examine the data represented in pKa form both with and without the extrapolation constructed previously for the CBS-QB3 SCRF calculations.

| pKa values | | MP2 | | CBS-QB3 Free Energy | |
|---|---|---|---|---|---|
| Expt. pKa | | SCRF | Gas phase + SCRF | SCRF | Gas phase + SCRF |
| 7.5 | Na+ + HClO → NaClO + H+ | 320406.73 | 320384.24 | 15.41 | 18.01 |
| 1.96 | Na+ + HClO2 → NaClO2 + H+ | 6.5 | 10.15 | 5.36 | 9.69 |
| -1 | Na+ + HClO3 → NaClO3 + H+ | -0.11 | 5.61 | -3.96 | 5.63 |
| -10 | Na+ + HClO4 → NaClO4 + H+ | -6.24 | -1.01 | -11.19 | -3.79 |

Table 7.8: Calculated and experimental pKa values for each counterion-assisted $HClO_x$ calculation.

| Fitted pKa values | | MP2 | | CBS-QB3 Free Energy | |
|---|---|---|---|---|---|
| Expt. pKa | | SCRF | Gas phase + SCRF | SCRF | Gas phase + SCRF |
| 7.5 | Na+ + HClO → NaClO + H+ | 137476.65 | 137467.01 | 6.35 | 7.47 |
| 1.96 | Na+ + HClO2 → NaClO2 + H+ | 2.53 | 4.1 | 2.04 | 3.9 |
| -1 | Na+ + HClO3 → NaClO3 + H+ | -0.3 | 2.15 | -1.96 | 2.16 |
| -10 | Na+ + HClO4 → NaClO4 + H+ | -2.93 | -0.69 | -5.06 | -1.88 |

Table 7.9: $HClO_x$ pKa values fitted by the previously developed linear extrapolation.

The best data is clearly the uncorrected CBS-QB3 predicted pKas. While the trends are reproduced in the MP2 calculation as well, the results aren't as close to the correct answers. The easiest way to compare the results is by examining the percentage errors on each.

| pKa% Error Calculated Values | MP2 | | CBS-QB3 Free Energy | |
|---|---|---|---|---|
| | SCRF | Gas phase + SCRF | SCRF | Gas phase + SCRF |
| Na+ + HClO → NaClO + H+ | 4273699% | 4273399% | 106% | 140% |
| Na+ + HClO2 → NaClO2 + H+ | 231% | 418% | 173% | 394% |
| Na+ + HClO3 → NaClO3 + H+ | -89% | -661% | 296% | -663% |
| Na+ + HClO4 → NaClO4 + H+ | -38% | -90% | 12% | -62% |

Table 7.10: % error in directly calculated $HClO_x$ pKa values versus experimental measurements.

The errors for the MP2 and CBS-QB3 calculations are quite good when done in the SCRF. The uncorrected absolute errors compiled in Table 7.10 range from 231% to

38% for the MP2 calculation done in the SCRF, while the uncorrected error for CBS-QB3 in the SCRF ranges from 296% to 12%. This is less than the corresponding error for the unfitted data calculated without the $Na^+$ counterion shown in Table 7.5; in the MP2 case it ranged from 990% to 67%, and for the CBS-QB3 calculation it went from 382% to 33%.

Unfortunately, for the gas phase ion + stabilization energy calculations the results tell a different story. Although in both cases the counterion calculations showed improvement in overall accuracy, the change isn't as pronounced.

In the direct calculation of the pKa the percent errors from Table 7.5 are similar or a little worse for both of the methods, with an absolute error in the MP2 method of 1144% to 81%, and the CBS-QB3 calculation from 429% to 29%. The results with the counterion are not this good, with absolute errors ranging from 661% to 90% for the MP2 calculation, and 663% to 62% for the CBS-QB3 calculation as shown in Table 7.10.

| **Fitted pKa value % Error Calculations** | MP2 | | CBS-QB3 Free Energy | |
|---|---|---|---|---|
| | SCRF | Gas phase + SCRF | SCRF | Gas phase + SCRF |
| Na+ + HClO → NaClO + H+ | 1833658% | 1833529% | 15% | 0% |
| Na+ + HClO2 → NaClO2 + H+ | -29% | -109% | -4% | -99% |
| Na+ + HClO3 → NaClO3 + H+ | 70% | 315% | -96% | 316% |
| Na+ + HClO4 → NaClO4 + H+ | 71% | 93% | 49% | 81% |

Table 7.11: % error in fitted pKa values compared to experimental measurements.

Although the fitting was not developed with counterions, it performs well in most cases except for the CBS-QB3 gas phase + SCRF energy calculation for this series. The results for the fitted data is in Table 7.11.

Notably, the quality of the results improved slightly with the fit, but not to the extent of the previous calculations. In Table 7.11 the MP2 SCRF results had absolute errors ranging from 29% to 70%, whereas previously the fitted error went from 58% to 472% in Table 7.6, a decided improvement. The CBS-QB3 results were similarly improved, with errors ranging from 6% to 117% in Table 7.6, while the errors with the counterion present went from an absolute error of 4% to 96%.

The calculations done in the gas phase with the SCRF stabilization were not quite as good. The percentage error in the results for MP2 was reduced from 63% to 538% in Table 7.6 to 95% to 331% in Table 7.11. However, the CBS-QB3 calculated results had absolute errors of only 7% to 137% previously in Table 7.6, but when the counterion was introduced the errors on average increased; although the minimum error was reduced to 0% the other errors ranged from 81% to 316%. In the calculation without the counterion the errors were around 40% for the $HClO_4$ and $HClO_2$ pKa calculations, but with the counterion they went from 50% to above 90%.

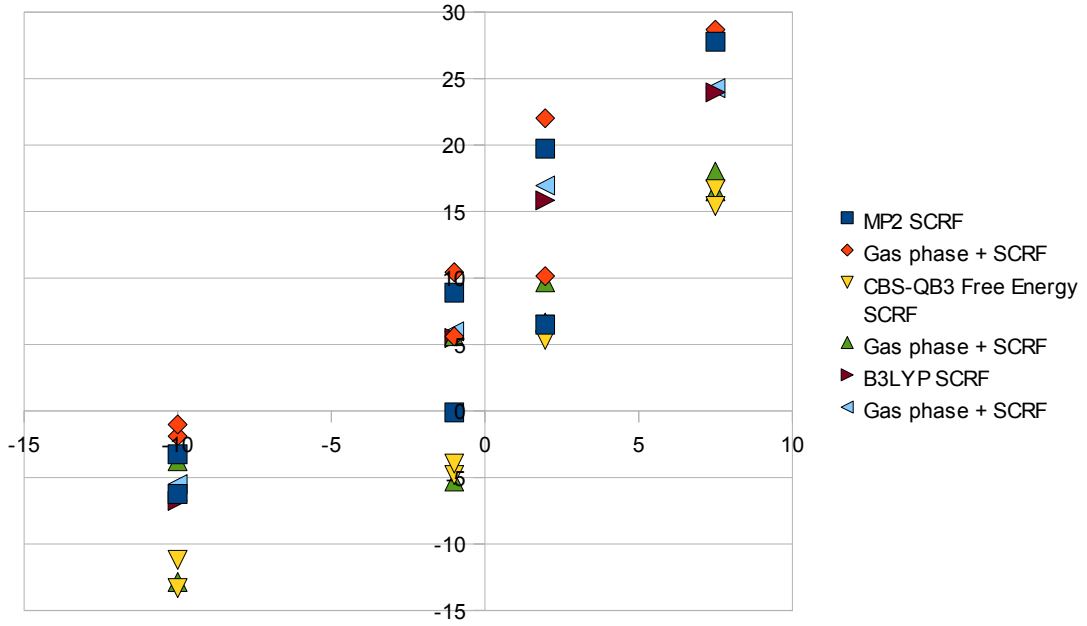


Figure 7.1: pKas for each method (including both direct and counterion assisted calculation results).

In an ideal case, the points would fall on the diagonal of Figure 7.1 if they were equal to the experimental measurements, but we can see that the data is relatively linear in all cases. This is why it is unsurprising that a linear fitting function such as the one we developed is effective.

*7.4 Conclusions*

As we saw, the best results appear in the CBS-QB3 results calculated in the CPCM and corrected by the fitting method. The fitted pKas show the correct trends across

the systems and, except for the $HClO_4$ deprotonation, are within 1 pKa unit of the experimentally measured values.

The addition of $Na^+$ counterions to balance total charge on either side of the reaction, the direct results without fitting showed improvement over the CBS-QB3 CPCM calculated values, with pKas which were closer to the experimental measurements except for the $Na^+ + HClO_4 \rightarrow NaClO_4 + H^+$ reaction. The experimental trends across the series are also reproduced.

The fitting, while not developed with counterions, improved the counterion calculated results except for the case of the $HClO_4$ deprotonation. However, the extreme acidity of HClO4 and the difference in experimental conditions (the commonly cited pKa was measured in liquid sulfur dioxide[1]) may account for some of the difference in our calculated value.

Calculations with explicit solvation would be an interesting topic to explore in this area in the future. It would also be interesting to consider other counterions besides Na+, to see if a different one would improve the accuracy of that approach.

*7.5 References*

1. Brownstein, S. and A.E. Stillman, *Proton Resonance Shifts of Acids in Liquid Sulfur Dioxide.* The Journal of Physical Chemistry, 1959. **63**(12): p. 2061-2062.
2. Marcus, Y., *The thermodynamics of solvation of ions. Part 2.-The enthalpy of hydration at 298.15 K.* Journal of the Chemical Society, Faraday Transactions 1: Physical Chemistry in Condensed Phases, 1987. **83**(2): p. 339-349.
3. Kolthoff, ed. *Treatise on Analytical Chemistry*. 1959, Interscience Encyclopedia, Inc.
4. Atkins, P.W. and J.A. Beran, *General Chemistry*. 2nd ed1990, New York: Scientific American Books.
5. Morris, J.C., *The Acid Ionization Constant of HOCl from 5 to 35°.* The Journal of Physical Chemistry, 1966. **70**(12): p. 3798-3805.
6. Zhang, J., et al., *Theoretical study of pKa for perchloric acid.* Journal of Molecular Structure: THEOCHEM, 2009. **906**(1-3): p. 46-49.
7. Montgomery, J.A., et al., *A complete basis set model chemistry. VI. Use of density functional geometries and frequencies.* Journal of Chemical Physics, 1999. **110**(6): p. 2822-2827.
8. Montgomery, J.A., et al., *A complete basis set model chemistry. VII. Use of the minimum population localization method.* Journal of Chemical Physics, 2000. **112**(15): p. 6532-6542.

9. Montgomery, J.A., J.W. Ochterski, and M.J. Frisch, *An improved complete basis set (CBS) model chemistry.* Abstracts of Papers of the American Chemical Society, 1996. **211**: p. 231-PHYS.

10. Francisco, J.S., *Ab Initio Characterization of HOClO3 and HO4Cl: Implications for Atmospheric Chemistry.* The Journal of Physical Chemistry, 1995. **99**(36): p. 13422-13425.

11. Curtiss, L.A., et al., *Gaussian-2 Theory for Molecular-Energies of 1st-Row and 2nd-Row Compounds.* Journal of Chemical Physics, 1991. **94**(11): p. 7221-7230.

12. M. J. Frisch, G.W.T., H. B. Schlegel, G. E. Scuseria, M. A. Robb, J. R. Cheeseman, J. A. Montgomery, Jr., T. Vreven, K. N. Kudin, J. C. Burant, J. M. Millam, S. S. Iyengar, J. Tomasi, V. Barone, B. Mennucci, M. Cossi, G. Scalmani, N. Rega, G. A. Petersson, H. Nakatsuji, M. Hada, M. Ehara, K. Toyota, R. Fukuda, J. Hasegawa, M. Ishida, T. Nakajima, Y. Honda, O. Kitao, H. Nakai, M. Klene, X. Li, J. E. Knox, H. P. Hratchian, J. B. Cross, V. Bakken, C. Adamo, J. Jaramillo, R. Gomperts, R. E. Stratmann, O. Yazyev, A. J. Austin, R. Cammi, C. Pomelli, J. W. Ochterski, P. Y. Ayala, K. Morokuma, G. A. Voth, P. Salvador, J. J. Dannenberg, V. G. Zakrzewski, S. Dapprich, A. D. Daniels, M. C. Strain, O. Farkas, D. K. Malick, A. D. Rabuck, K. Raghavachari, J. B. Foresman, J. V. Ortiz, Q. Cui, A. G. Baboul, S. Clifford, J. Cioslowski, B. B. Stefanov, G. Liu, A. Liashenko, P. Piskorz, I. Komaromi, R. L. Martin, D. J. Fox, T. Keith, M. A. Al-Laham, C. Y. Peng, A.

Nanayakkara, M. Challacombe, P. M. W. Gill, B. Johnson, W. Chen, M. W. Wong, C. Gonzalez, and J. A. Pople, *Gaussian 03, Revision C.02*, 2004, Gaussian, Inc., Wallingford CT.

13. Head-Gordon, M., J.A. Pople, and M.J. Frisch, *MP2 energy evaluation by direct methods.* Chemical Physics Letters, 1988. **153**(6): p. 503-506.

14. Becke, A.D., *Density-functional thermochemistry. III. The role of exact exchange.* The Journal of Chemical Physics, 1993. **98**(7): p. 5648-5652.

15. Barone, V. and M. Cossi, *Quantum calculation of molecular energies and energy gradients in solution by a conductor solvent model.* Journal of Physical Chemistry A, 1998. **102**(11): p. 1995-2001.

16. Barone, V., M. Cossi, and J. Tomasi, *Geometry optimization of molecular structures in solution by the polarizable continuum model.* Journal of Computational Chemistry, 1998. **19**(4): p. 404-417.

17. Cossi, M., et al., *Energies, structures, and electronic properties of molecules in solution with the C-PCM solvation model.* Journal of Computational Chemistry, 2003. **24**(6): p. 669-681.

# Chapter 8: $Hg(SH)_2$ gas phase formation reactions.

*In this short chapter we examine several reactions showing $Hg(SH)_2$ species formation in the gas phase with a variety of different methods, B3LYP, MP2, CCSD, MP3, and MP4.*

## *8.1 Introduction*

With mercury and sulfur compounds being detected at places with volcanic activity[1, 2], a series of calculations on mercury sulfur compounds seemed like an interesting line of research.

We therefore conducted a variety of calculations on $MeHgS_xH$ (x=1...4, presented with the methylmercury results), $Hg(SH)_2$, and other compounds. In this section we shall discuss the results of our $Hg(SH)_2$ gas phase formation calculations.

## *8.2 Methods*

In this section, we examined reactions of formation for $Hg(SH)_2$. $HgSH^+$, $HgSH^-$, and $Hg(SH_2)$, modeled with both B3LYP[3], MP2[4], MP3[5], CCSD[6], and MP4[7] with a CEP-121G basis set[8-10] sometimes augmented with an extra basis function

for each atom (see below), with single point calculations under the MP4 and CCSD methods.

As previously mentioned, further MeHgSH compounds are also discussed in the following chapter on methylmercury chemistry.

The CEP-121G basis set was used with and without an extra diffuse basis function, as detailed below in Table 8.1, to verify the effects of the extra function on the results. In this calculation we are only dealing with singly charged species with the exception of $Hg^{2+}$, so we would expect that the extra basis function would be less important than in the polyprotic acid anions which we examined elsewhere.

| Atoms | Function Type | Coefficient |
|---|---|---|
| Hg | F | 0.486 |
| C, S | D | 0.700 |
| F, Cl, Br, I | D | 0.650 |

Table 8.1: Extra diffuse functions used in the calculations in this chapter.

*8.3 Results and Discussion*

In some cases, computational limitations prevented the calculations from being completed in a timely fashion. This accounted for the empty entries in Table 8.2(a)

below. However, with the data on hand, we can calculate the energetics for a number of gas phase reactions.

| | B3LYP CEP121G | MP2 CEP121G | CCSD CEP121G | MP3 CEP121G | MP4 CEP121G |
|---|---|---|---|---|---|
| HS- | -10.772981 | -10.575504 | -10.587805 | -10.584092 | -10.587220 |
| HgS | -163.910255 | | | | |
| HgSH- | -164.627721 | -163.620367 | -163.641318 | -163.628021 | |
| HgSH+ | -164.220624 | -163.253038 | -163.269724 | -163.258158 | |
| HgSH2 | -175.305547 | -174.145182 | -174.171829 | -174.156028 | |
| HgS2H- | -174.791619 | -173.636030 | -173.657019 | -173.640733 | -173.667945 |

| | B3LYP CEP121G* | MP2 CEP121G* | CCSD CEP121G* | MP3 CEP121G* | MP4 CEP121G* |
|---|---|---|---|---|---|
| HS- | -10.784490 | -10.655727 | | -10.671206 | |
| HgS | -163.922552 | -163.200566 | -163.195613 | -163.180627 | |
| HgSH- | -164.642643 | -163.886935 | | -163.873446 | -163.911717 |
| HgSH+ | -164.244865 | -163.508380 | -163.516523 | -163.500578 | -163.536769 |
| HgSH2 | -175.348527 | -174.505940 | -174.522862 | -174.505643 | -174.549480 |
| HgS2H- | -174.821540 | -173.985038 | -173.993562 | -173.976121 | -174.025625 |

| | B3LYP CEP121G | MP2 CEP121G | CCSD CEP121G | MP3 CEP121G | MP4 CEP121G |
|---|---|---|---|---|---|
| H + . He | -2.982260 | -2.941150 | -2.946254 | -2.944716 | -2.945727 |
| He (alone) | -2.924981 | -2.884755 | -2.888371 | -2.887456 | -2.888122 |
| Hg2+ | -152.776064 | -152.045051 | -152.046850 | -152.043552 | -152.048519 |
| H+ | -0.057279 | -0.056395 | -0.057883 | -0.057260 | -0.057605 |
| S0 | -10.014929 | -9.859813 | -9.878254 | -9.867174 | -9.870064 |
| S-2 | -9.932134 | -9.740315 | -9.748820 | -9.745876 | -9.748243 |

| | B3LYP CEP121G* | MP2 CEP121G* | CCSD CEP121G* | MP3 CEP121G* | MP4 CEP121G* |
|---|---|---|---|---|---|
| H + . He | -2.982260 | -2.941150 | -2.946254 | -2.944716 | -2.945727 |
| He | -2.924981 | -2.884755 | -2.888371 | -2.887456 | -2.888122 |
| Hg2+ | -152.778206 | -152.161998 | -152.159227 | -152.153976 | -152.168062 |
| H+ | -0.057279 | -0.056395 | -0.057883 | -0.057260 | -0.057605 |
| S0 | -10.016473 | -9.922550 | -9.954233 | -9.940476 | -9.946566 |
| S-2 | -9.932811 | -9.803792 | -9.817432 | -9.815444 | -9.819731 |

Table 8.2(a): HgSH compound free energies of formation.

As expected, the reactions below were all found to be favorable in the gas phase. In cases where charged species were present, the total charge at the end was either the same, but spread over more atoms, or reduced.

Sum of Electronic and Thermal Free Energy Changes for reactions (kcal/mol = 627.5 * Hartrees)

| | B3LYP CEP121G | MP2 CEP121G | CCSD CEP121G | MP3 CEP121G |
|---|---|---|---|---|
| Hg2+ + HS- -> HgSH+ | -421.42 | -396.88 | -398.51 | -395.65 |
| Hg2+ + 2HS- -> HgSH2 | -617.16 | -595.57 | -595.73 | -592.54 |
| HgS + HS- -> HgS2H- | -68.01 | | | |
| HgSH- + S -> HgS2H- | -93.48 | -97.80 | -86.25 | -91.33 |
| HgSH+ + HS- -> HgSH2 | -195.74 | -198.69 | -197.22 | -196.90 |
| HgSH+ + S2- -> HgS2H- | -400.89 | -403.28 | -400.64 | -399.53 |

Sum of Electronic and Thermal Free Energy Changes for reactions (kcal/mol = 627.5 * Hartrees)

| | B3LYP CEP121G* | MP2 CEP121G* | CCSD CEP121G* | MP3 CEP121G* | MP4 CEP121G* |
|---|---|---|---|---|---|
| Hg2+ + HS- -> HgSH+ | -428.06 | -433.39 | | -423.81 | |
| Hg2+ + 2HS- -> HgSH2 | -628.34 | -647.89 | | -633.31 | |
| HgS + HS- -> HgS2H- | -71.85 | -80.79 | | -77.99 | |
| HgSH- + S -> HgS2H- | -101.92 | -110.16 | | -101.78 | -105.01 |
| HgSH+ + HS- -> HgSH2 | -200.28 | -214.50 | | -209.50 | |
| HgSH+ + S2- -> HgS2H- | -404.02 | -422.22 | -413.90 | -414.21 | -419.88 |

Table 8.2(b): HgSH compound gas phase reaction energies with different basis sets.

We can see from Table 8.2(b) above that the most favorable single additions listed are $Hg^{2+} + HS^- \rightarrow HgSH^+$ with an energy going from -395 to -433 kcal/mol, and the $HgSH^+ + S^{2-} \rightarrow HgS_2H^-$ reaction which is predicted to be favorable to the order of 400-422 kcal/mol.

The second addition of $HS^-$ to $Hg^{2+}$, going from $HgSH^+$ to $HgSH_2$, is also extremely favorable, approximately 195 to 215 kcal/mol.

From reactions (2) and (3) we can see that $HgSH^-$ and $S^0$ are about 30 kcal/mol less stable than $HgS^+$ and $HS^-$. If we examine the Lewis electron dot structures of the compounds, we see that this makes sense:

Compare $(Hg::SH)^-$ and $(S:::)^0$ vs Hg:::S and H:S:::$^-$.

Generally, S is represented in calculations by ring structures of $S_5$ or $S_6$, which satisfy the octet rule for each sulfur atom, so the above calculation on the atomic sulfur atom is expected to be less favorable than it might be otherwise. In a future calculation, we might consider calculating the energetics for $S_5$ and $S_6$ with these methods, then have the Hg group extract the single atom from the sulfur moiety.

With the reaction calculations done, we can compare the favorability of each reaction depending on the presence of the diffuse function, and depending on methods. The figures for this comparison are summarized in Table 8.2(c) below:

Additional favorability with additional diffuse basis function.

| | B3LYP | MP2 | CCSD | MP3 | |
|---|---|---|---|---|---|
| Hg2+ + HS- -> HgSH+ | 6.65 | 36.5 | | | 28.16 |
| Hg2+ + 2HS- -> HgSH2 | 11.18 | 52.31 | | | 40.76 |
| HgS + HS- -> HgS2H- | 3.84 | | | | |
| HgSH- + S -> HgS2H- | 8.44 | 12.36 | | | 10.45 |
| HgSH+ + HS- -> HgSH2 | 4.54 | 15.81 | | | 12.6 |
| HgSH+ + S2- -> HgS2H- | 3.14 | 18.94 | | 13.26 | 14.68 |

Table 8.2(c): Additional energy calculated released with additional diffuse basis function present.

We can see that the additional diffuse function makes the largest difference when considering the $Hg^{2+}$ + 2 $HS^-$ reaction, which makes sense because the two $HS^-$ groups would be the most stabilized by the additional function. The total extra favorability when calculated with all three methods that both calculations were conducted with is nearly double that of the single $HS^-$ addition.

We can also compare the energies of reaction for the different methods. This information appears in Figure 8.1 below:

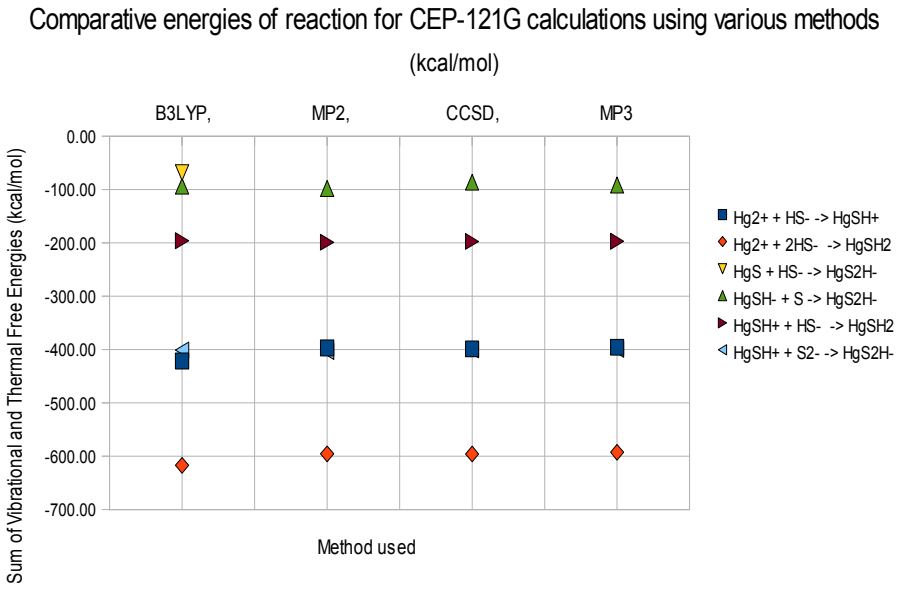


Figure 8.1: Calculated energetics for each reaction using different methods.

From this figure, we see that the energetics for each series of reactions without diffuse functions added to the CEP-121G basis set show the same basic trends for each method, except for B3LYP, where the reactions of HgS + $HS^-$ to form $HgS_2H^-$ and $HgSH^+ + S_2^-$ to make $HgS_2H^-$ are both a bit less favorable than the $HgSH^- + S^0 \rightarrow HgS_2H^-$ reaction and the $Hg^{2+} + HS^- \rightarrow HgSH^+$ reactions respectively.

However, considering Figure 8.2 below, which shows the same reaction energetics with the extra basis functions present, we now see that the MP2 and MP3 methods show the same trend as B3LYP, which retained the same energetic relationships between the different considered reactions as it had without the extra basis functions augmenting the CBS-QB3 basis.

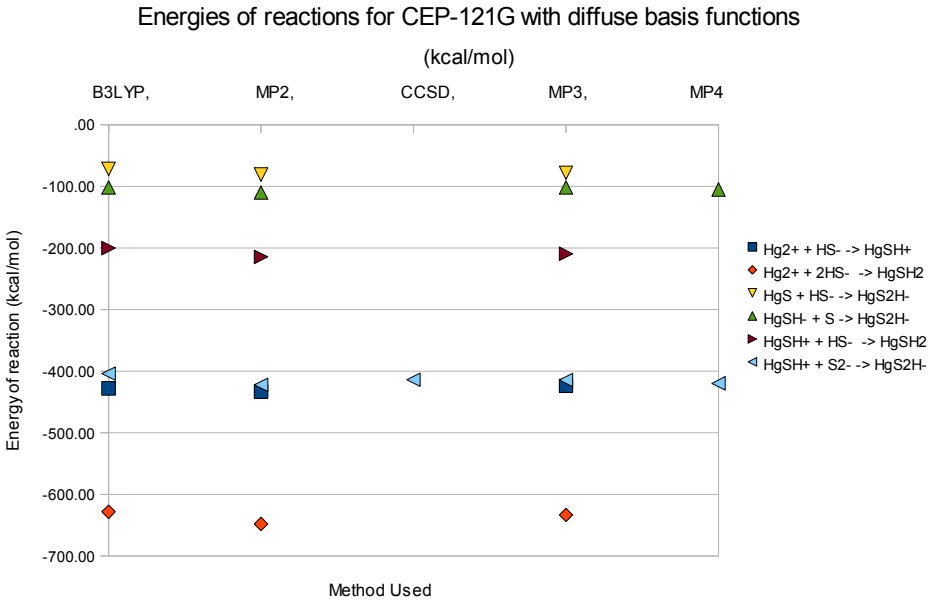


Figure 8.2: Calculated energies of reaction with diffuse basis functions added to the CEP-121G basis used in the previous figure.

In each case the reaction was more favorable with diffuse functions present, although the effect was the smallest for the B3LYP method, in the smallest cases it was 3-4

kcal/mol, but the effect was greatest for $Hg^{2+} + 2\ HS^- \rightarrow Hg(SH)_2$ for the MP2 and MP3 methods, where the difference was 40-50 kcal/mol.

*8.4 Conclusions*

An interesting future calculation would be to see if the relationships between the different levels of favorability are reproduced in different solvation environments. As higher-charged anions and cations are stabilized to different degrees by solvation, the most favorable reactions are often different depending on the solvent. This would also allow us to examine how the reactions behavior changes in undersea conditions as might be observed at volcanic vents.

Further calculations involving methylmercury sulfur compounds are also important, because the pathways that sulfur-reducing bacteria use to deal with sulfur in their environments have been observed to methylate elemental mercury in their neighborhoods[11]. We previously discussed in the introduction how the methylmercury compounds were one of the most hazardous for mankind.

*8.5 References*

1. Cox, M.E., *Summit outgassing as indicated by radon, mercury and pH mapping, Kilauea volcano, Hawaii.* Journal of Volcanology and Geothermal Research, 1983. **16**(1-2): p. 131-151.

2. Ferrara, R., et al., *Atmospheric mercury emission at Solfatara volcano (Pozzuoli, Phlegraean Fields - Italy).* Chemosphere, 1994. **29**(7): p. 1421-1428.

3. Becke, A.D., *Density-functional thermochemistry. III. The role of exact exchange.* J. Chem. Phys., 1993. **98**: p. 5648-52.

4. Head-Gordon, M., J.A. Pople, and M.J. Frisch, *MP2 energy evaluation by direct methods.* Chemical Physics Letters, 1988. **153**(6): p. 503-506.

5. J. A. Pople, J.S.B., and R. Seeger, *Theoretical Models Incorporating Electron Correlation.* Int. J. Quant. Chem, 1976. **S10**.

6. Čížek, J., *On the Use of the Cluster Expansion and the Technique of Diagrams in Calculations of Correlation Effects in Atoms and Molecules*. Advances in Chemical Physics1969: John Wiley & Sons, Inc. 35-89.

7. K. Raghavachari and J. A. Pople, *Approximate 4th-order perturbation-theory of electron correlation energy.* Int. J. Quant. Chem, 1978. **14**: p. 91-100.

8. Cundari, T.R. and W.J. Stevens, *Effective Core Potential Methods for the Lanthanides.* Journal of Chemical Physics, 1993. **98**(7): p. 5555-5565.

9. Stevens, W.J., H. Basch, and M. Krauss, *Compact Effective Potentials and Efficient Shared-Exponent Basis-Sets for the 1st-Row and 2nd-Row Atoms.* Journal of Chemical Physics, 1984. **81**(12): p. 6026-6033.

10. Stevens, W.J., et al., *Relativistic Compact Effective Potentials and Efficient, Shared-Exponent Basis-Sets for the 3rd-Row, 4th-Row, and 5th-Row Atoms.*

Canadian Journal of Chemistry-Revue Canadienne De Chimie, 1992. **70**(2): p. 612-630.

11. Baldi, F., *Microbial transformation of mercury species and their importance in the biogeochemical cycle of mercury.* Metal Ions in Biological Systems, 1997. 34(34): p. 213-257.

# Chapter 9: Methylmercury compound chemistry in Aqueous Solution

*In this chapter we examine a variety of methylmercury chloride and methylmercury thiol compounds, comparing relative energetics over several different methods from Hartree-Fock to CCSD, and both gas phase and CPCM water solvated conditions, and going on to discuss calculated spectra of the species.*

## *9.1 Introduction*

Methylmercury compounds offer a distinct interest for us, as they are dramatically poisonous, acting as a persistent oxidizer which is concentrated in fatty cells such as neural ones, causing permanent and persistent damage to organisms exposed. Methylmercury has been blamed in several severe ecological accidents, including one in Japan[1, 2] and an incident in Iraq[3]. Current and continuing use of coal burning power ensures that the world will have plenty of human-sourced[4] mercury compounds floating around for the foreseeable future.

Therefore, further understanding of these compounds would be quite beneficial.

Using theoretical modeling to study methylmercury compounds via computer software has a dramatic advantage of safety to the researcher over experimental

laboratory studies. By using computational chemistry in this way, we can shortcut the possibility of an unfortunate laboratory accident abruptly ending our line of research[5], and at the same time benefit scientific knowledge.

Our *ab initio* approach has the advantage of safety over more intimate experimental studies, but at the same time it has disadvantages as well. As we can only focus on specific compounds and structures that we have fixed upon in advance, our applicability to experimental results can be affected both by the accuracy of experimental understanding (of which species are important and present during possibly ambiguous measurements) as well as the accuracy of the models.

As previously shown with $H_3PO_4$ and $H_3AsO_4$ calculations in Chapters 5 and 6, the simple and direct use of a CPCM solvation model[6-8], while very useful, has some shortcomings as well. While the pKas calculated for single deprotonations were not too far from the experimentally measured pKas, the raw results for further deprotonations left somewhat to be desired, although the trends were generally good, and we showed how they could be improved. Also, using CPCM solvation prevents any accounting for the interactions that may occur between our compounds of interest and the solvent molecules.

Our results here will address both of these possible possible shortcomings as follows.

We have some initial support for the qualitative quality of these calculations from the results in the previous $H_3PO_4$ and $H_3AsO_4$ series' results, which solidly reproduced trends of the pKas of those species. By focusing on the differences in energetics between the solvated and unsolvated systems, and the relative stabilities of the different compounds, we can avoid the problems which we faced in the acidity calculations where we depended on precise raw energies.

As previously discussed in the mercury chloride NMR calculations in Chapter 4, in $HgCl_2$ and above the effects of explicit hydration on the mercury compounds' NMR shieldings were minimal. This would imply that there are few interactions between the solvent molecules and the mercury proper, so the use of CPCM here instead of explicit solvation should be acceptable. Of course in the future, explict solvation of these compounds would be a reasonable item to investigate as well.

*9.2 Methods*

We conducted calculations on MeHgBr, MeHgCl, MeHgF, MeHgI, MeHgSH, $MeHgS_2H$, $MeHgS_3H$, and $MeHgS_4H$ compounds with four different levels of theory: HF[9], MP2[10], B3LYP[11], and CCSD[12], using the CEP-121G Compact Effective Potential basis set[13-16] with extra diffuse functions (shown in Table 9.1, below):

| Atoms | Function Type | Coefficient |
|---|---|---|
| Hg | F | 0.486 |
| C, S | D | 0.700 |
| F, Cl, Br, I | D | 0.650 |

Table 9.1: Extra diffuse functions used in the calculations in this chapter.

*9.3 Results and Discussion*

| Compound | HF | MP2 | B3LYP | CCSD |
|---|---|---|---|---|
| MeHgF | -183.904536 | -184.559852 | -185.440527 | -184.560058 |
| MeHgCl | -174.768980 | -175.393869 | -176.208113 | -175.405348 |
| MeHgBr | -173.233131 | -173.814946 | -174.671765 | -173.824920 |
| MeHgI | -171.307600 | -171.850547 | -172.735523 | -171.858900 |
| MeHgSH | -170.571453 | -171.183413 | -172.003599 | -171.199811 |
| $MeHgS_2H$ | -180.503454 | -181.234340 | -182.149031 | -181.263312 |
| $MeHgS_3H$ | -190.443152 | -191.295474 | -192.303537 | -191.336711 |
| $MeHgS_4H$ | -200.381167 | -201.355578 | -202.457404 | -201.407340 |

Table 9.2: Sum of Electronic and Thermal Free Energies at 298K (in Hartrees) calculated for each methylmercury species with HF, MP2, B3LYP, and CCSD, calculated with the CEP-121G basis set augmented with our additional functions.

Examination of Table 9.2 results in a graphed form allows us to see the following trends quite easily as shown in Figure 9.1 below.

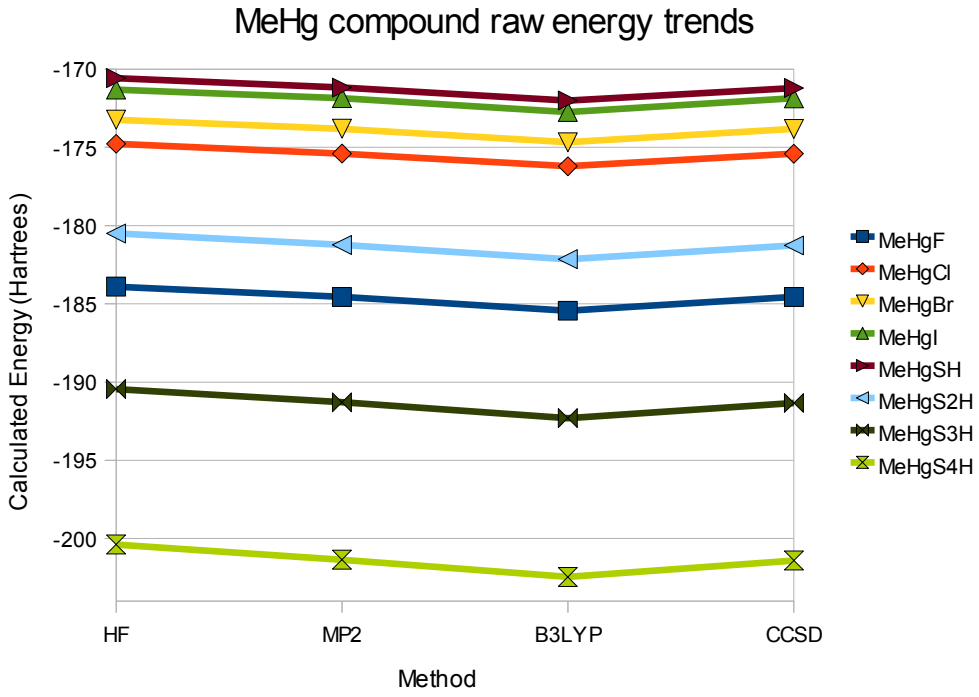


Figure 9.1: Energies calculated from Table 9.2.

We can see the general trend here that the Hartree-Fock raw energies are the highest, while the higher level MP2 and CCSD calculations are slightly lower. This is as expected, because HF is a lower level method that does not take into account some sources of additional stabilization that MP2 and CCSD do.

Note that with this basis, CEP-121G, the energies for the different methylmercury halides are not in order of mass as would be true for other basis sets. This is because the compact effective potential basis only directly models electrons in the valence shell of each atom.

CEP basis sets have advantages because they can account for some relativistic effects which take place in the inner shells of electrons, but as a side effect the energetics cannot be compared directly between different compounds. However, the differences between a variety of compounds can (and shall here) be used to calculate dissociation and reaction energetics for a number of reactions.

With just the data in Table 9.2, we can also look at the results fo the $MeHgS_xH$ series in more detail. Let's examine the differences in each of the $MeHgS_xH$ energies as we add more sulfur atoms.

| | Difference in adding another S to the S-chain (Hartrees) | | | |
|---|---|---|---|---|
| | **HF** | **MP2** | **B3LYP** | **CCSD** |
| **A MeHgSH to MeHgS2H** | -9.93200100E+000 | -1.00509270E+001 | -1.01454320E+001 | -1.00635010E+001 |
| **B MeHgS2H to MeHgS3H** | -9.93969800E+000 | -1.00611340E+001 | -1.01545060E+001 | -1.00733990E+001 |
| **C MeHgS3H to MeHgS4H** | -9.93801500E+000 | -1.00601040E+001 | -1.01538670E+001 | -1.00706290E+001 |
| | **Change in that difference in adding an S atom (Hartrees)** | | | |
| **A -> B** | -7.697E-03 | -1.021E-02 | -9.074E-03 | -9.898E-03 |
| **B -> C** | 1.683E-03 | 1.030E-03 | 6.390E-04 | 2.770E-03 |
| | **Change in difference (kcal/mol 1 Hartree = 627.5 kcal/mol)** | | | |
| **A -> B** | -4.83 | -6.4 | -5.69 | -6.21 |
| **B -> C** | 1.06 | 0.65 | 0.4 | 1.74 |

Table 9.3: Energy differences (Hatrees) in adding additional S atoms to the $MeHgS_xH$ chain.

Examination of Table 9.3 indicate that each addition after the first changed the energy by about 6 kcal/mol favorably through going from the 2nd to 3rd addition was a lot less of a cumulative difference, having changed by only 1 kcal/mol on average. We would therefore expect that the change in stabilization for additional sulfur atoms in

the chain would remain small. The most additional stabilization is gained when going from 2 to 3 sulfurs in the Hg-S-SH chain.

We next turn our attention to some calculations on the same systems in a CPCM solvated environment. CPCM solvation models additional stabilization on polar systems by placing them in a cavity inside a polarizable continuum. The results of these calculations appear in Table 9.4, below.

| | HF/CEP-121G CPCM (Hartrees) | B3LYP/CEP-121G CPCM (Hartrees) |
|---|---|---|
| MeHgF | -183.941568 | -185.467233 |
| MeHgCl | -174.798515 | -176.228814 |
| MeHgBr | -173.256549 | -174.691642 |
| MeHgI | -164.086258 | -172.749289 |
| MeHgSH | -170.593184 | -172.018513 |
| $MeHgS_2H$ | -180.527589 | -182.163634 |
| $MeHgS_3H$ | -190.467892 | -192.320485 |
| $MeHgS_4H$ | -200.405402 | incomplete |

Table 9.4: CPCM Solvated HF and B3LYP energies for MeHgX and $MeHgS_xH$ (X=F, Cl, Br, I,), (x=1...4).

Comparing these results in Table 9.4 calculated under CPCM solvated conditions to the ones calculated in the gas phase, the MeHgF and MeHgCl species are calculated to be lower energy in the solvated conditions, but the MeHgBr and MeHgI compounds are higher energy overall under solvated conditions. This is probably

because the larger Br and I ions are not electronegative enough to overcome the nonpolar methyl group attached to the mercury atom. This would lead to these species preferring solvents which are less polar than water, such as the nonpolar environment of the phospholipid bilayers of cells. This difference in solubility would lead us to predict that MeHgF and MeHgCl would be much safer compounds than MeHgBr and MeHgI.

The methylmercury linked to the sulfur chains show a similar trend as the less polar MeHgBr and MeHgI, with the total free energies of the species pointing to more stability in the gas phase than under solvated conditions. We would therefore predict that these would also prefer nonpolar environments such as found in fatty tissue.

To continue, we shall consider the spectra of the above compounds, reproduced below in Figures 9.2-9.5. Discussion follows.

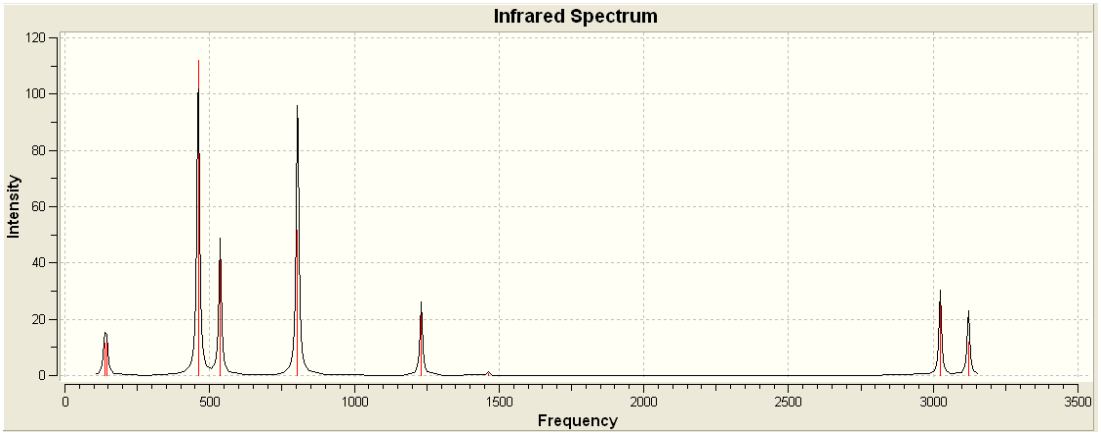


Figure 9.2: B3LYP/CEP-121G CPCM IR Spectrum for MeHgF

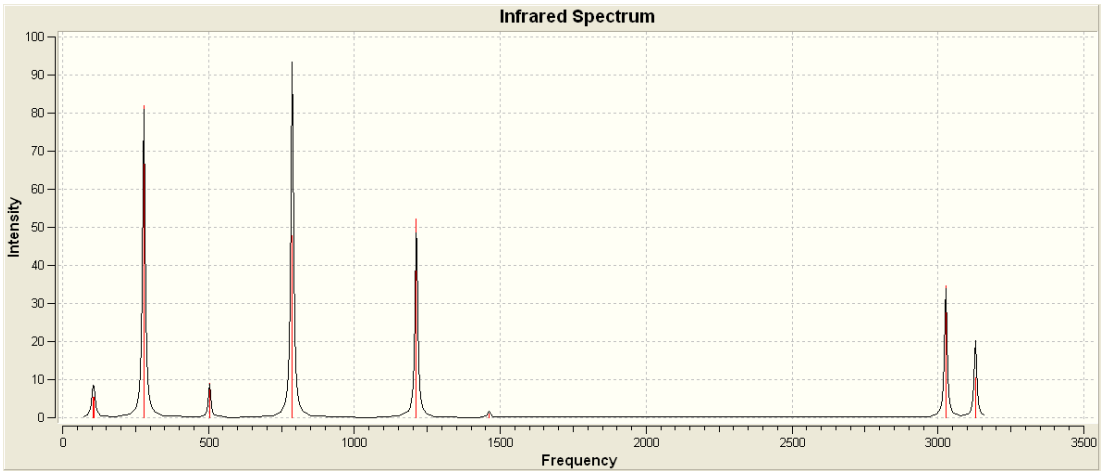


Figure 9.3: B3LYP/CEP-121G CPCM IR Spectrum for MeHgCl

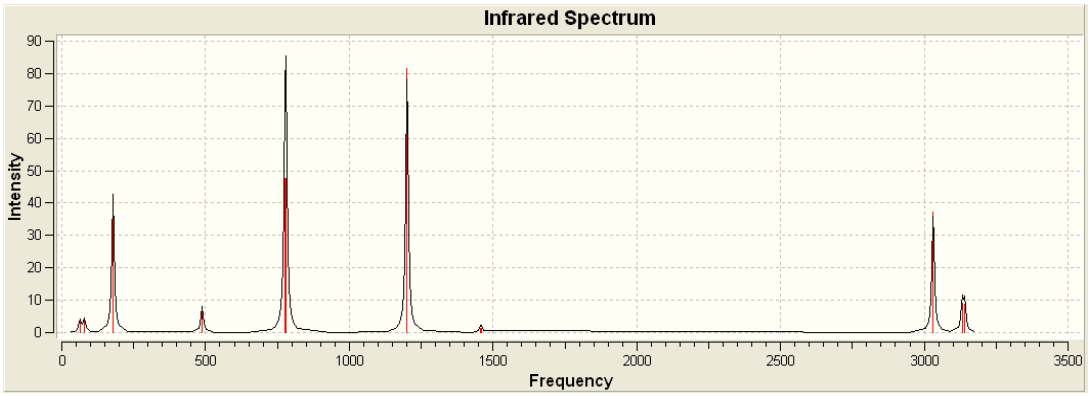


Figure 9.4: B3LYP/CEP-121G CPCM IR Spectrum for MeHgBr

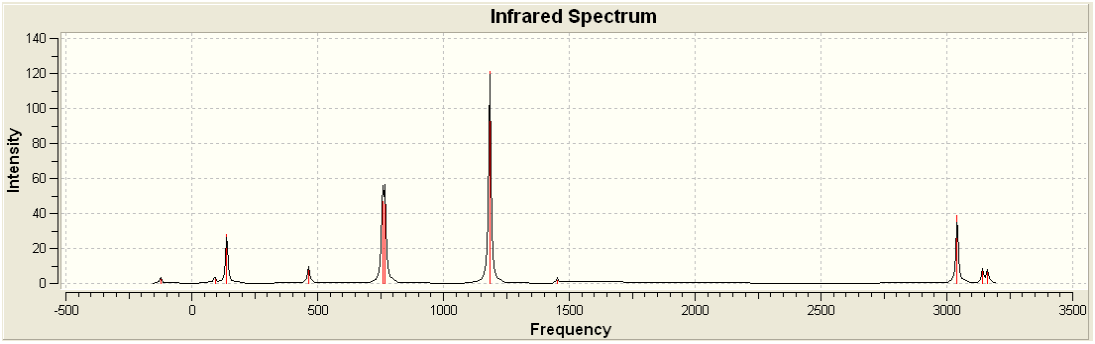


Figure 9.5: B3LYP/CEP-121G CPCM IR Spectrum for MeHgI

These spectra show that the geometry for MeHgI is at a saddle point, and therefore the calculated energy is not the minimum for the species. However, from examining the structure it is clear that the cause of this is the eclipsed geometry between the halogen atom and the H of the methyl group attached to the central mercury atom, as the bond angle between MeHgI is slightly less than 180 degrees, and the I is aligned

to the methyl hydrogen. The vibrational mode is reproduced below in Figure 9.6, and bears out this hypothesis:

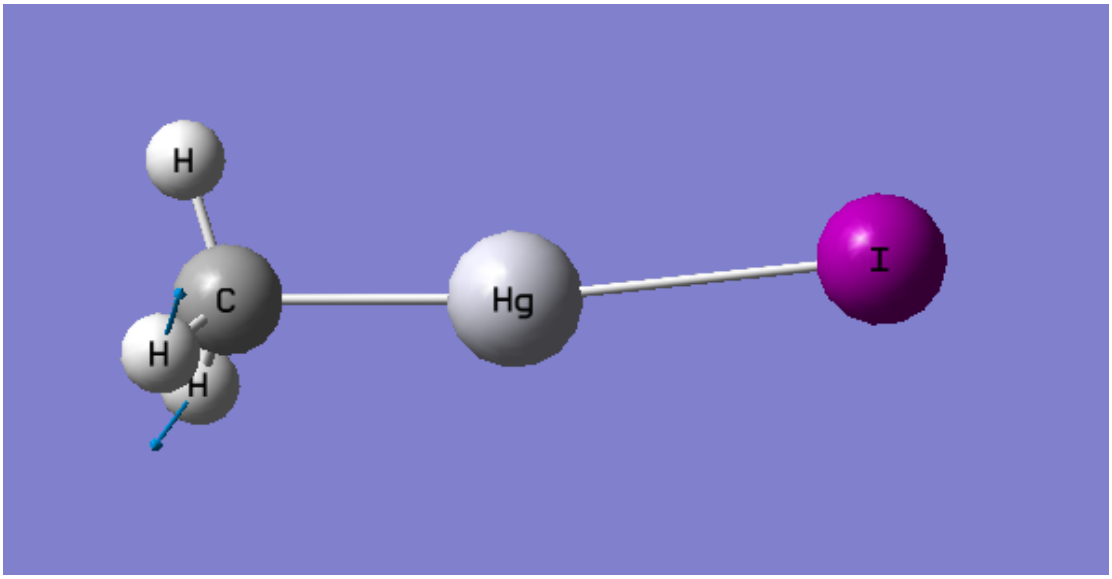


Figure 9.6: B3LYP/CEP-121G CPCM Imaginary Mode for MeHgI.

Several of the $MeHgS_xH$ geometries suffer from the same issue, as seen in the following Figures 9.7 and 9.8. These peaks appear as negative ones in the solvated spectra shown in Figures 9.9 through 9.11 below:

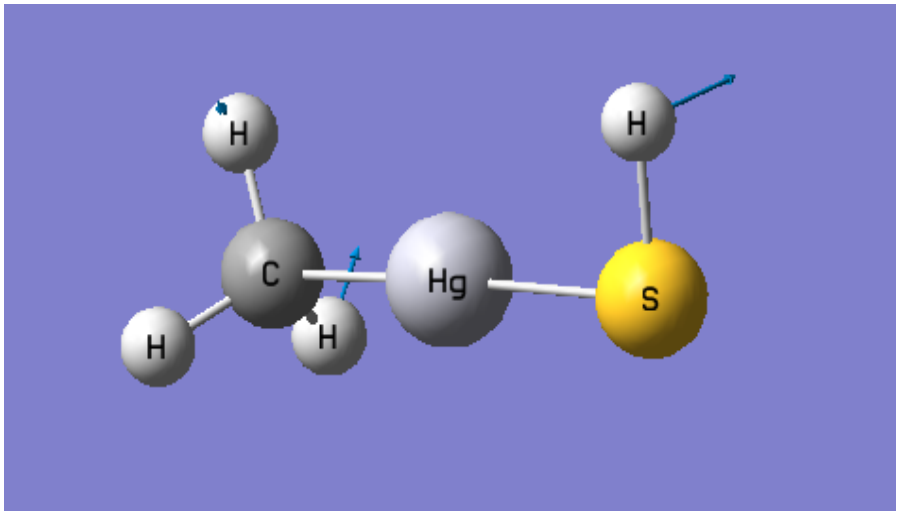


Figure 9.7: Typical imaginary mode for eclipsed conformation of $MeHgS_xH$ as seen in MeHgSH (B3LYP/CEP-121G CPCM)

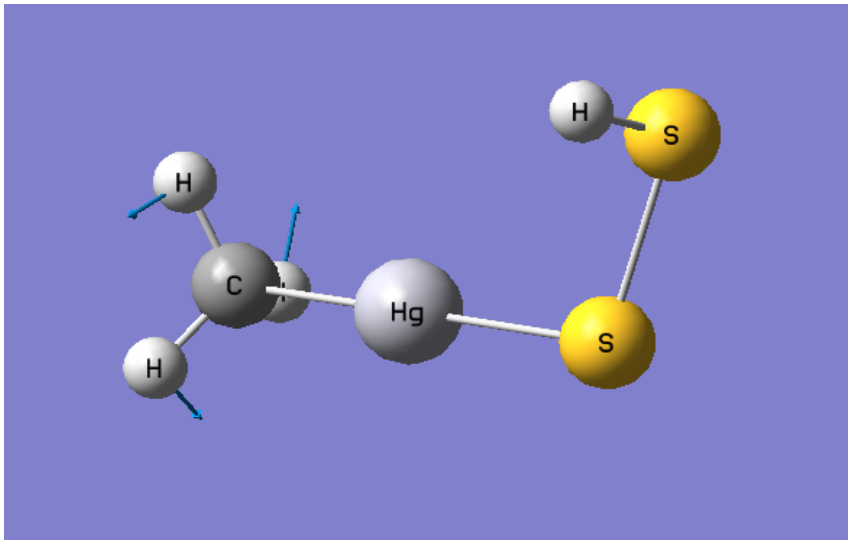


Figure 9.8: Typical imaginary mode for $MeHgS_2H$

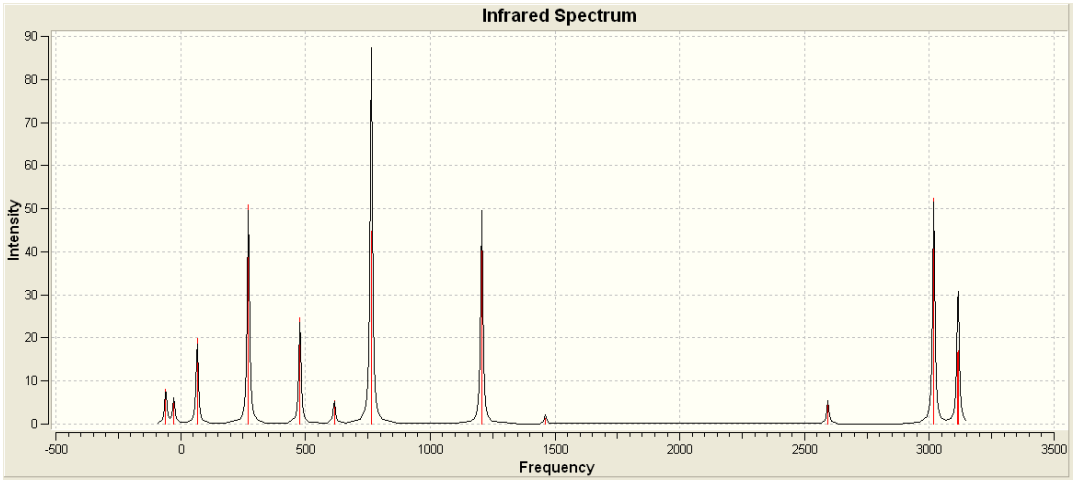


Figure 9.9: MeHgSH IR Spectra (B3LYP/CEP-121G CPCM)

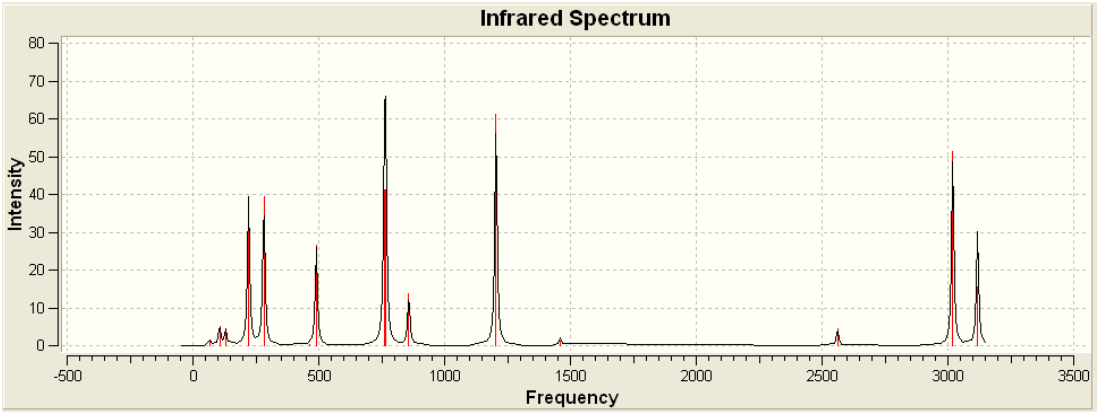


Figure 9.10: $MeHgS_2H$ IR Spectra (B3LYP/CEP-121G CPCM)

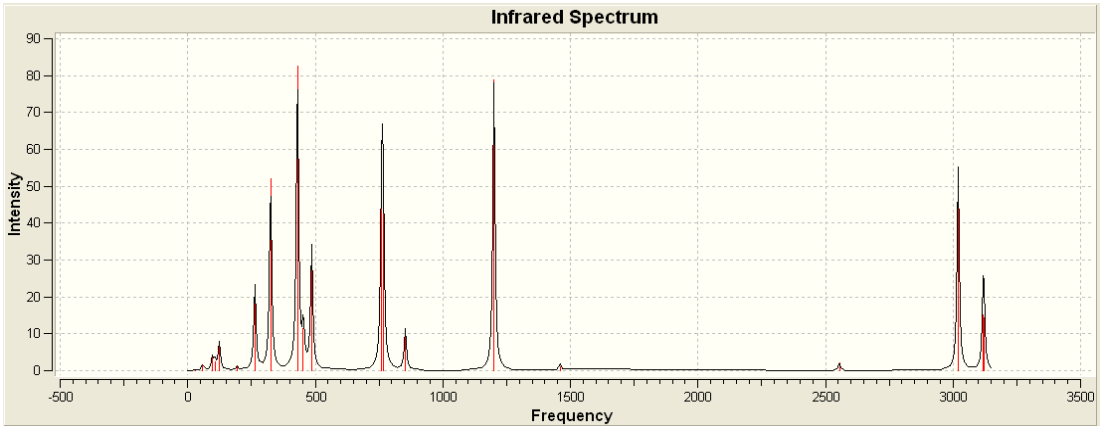


Figure 9.11: $MeHgS_3H$ IR Spectra (B3LYP/CEP-121G CPCM)

Now, let us consider the calculations on the gas-phase species. Having calculated spectra under B3LYP/CEP-121G in the gas phase as well, we see the following in Figures 9.12-9.19:

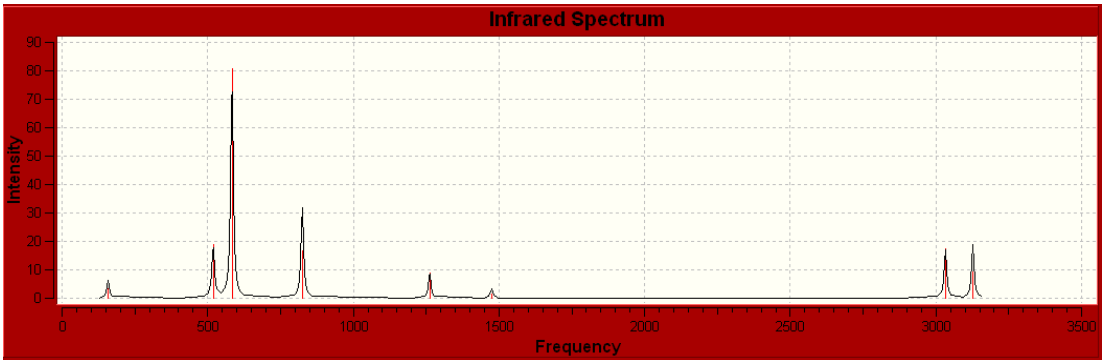


Figure 9.12: MeHgF IR Spectra (B3LYP/CEP-121G)

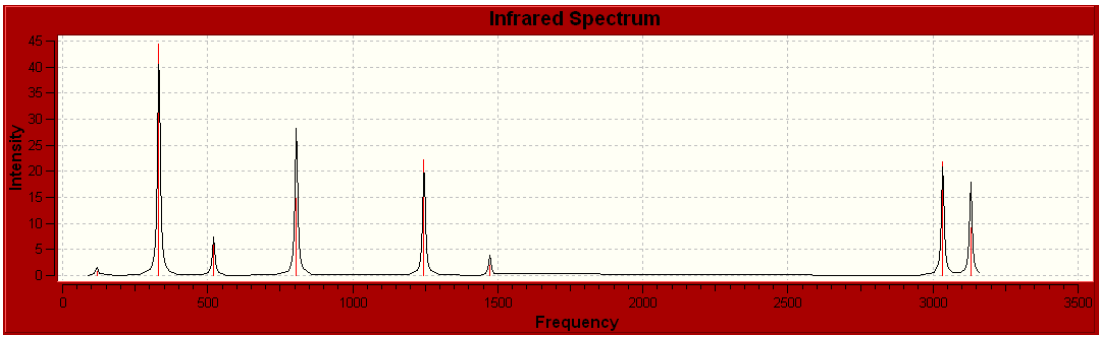


Figure 9.13: MeHgCl IR Spectra (B3LYP/CEP-121G)

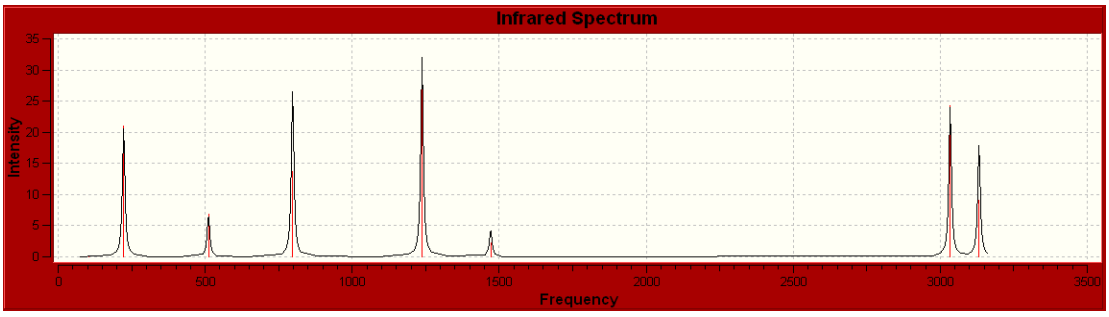


Figure 9.14: MeHgBr IR Spectra (B3LYP/CEP-121G)

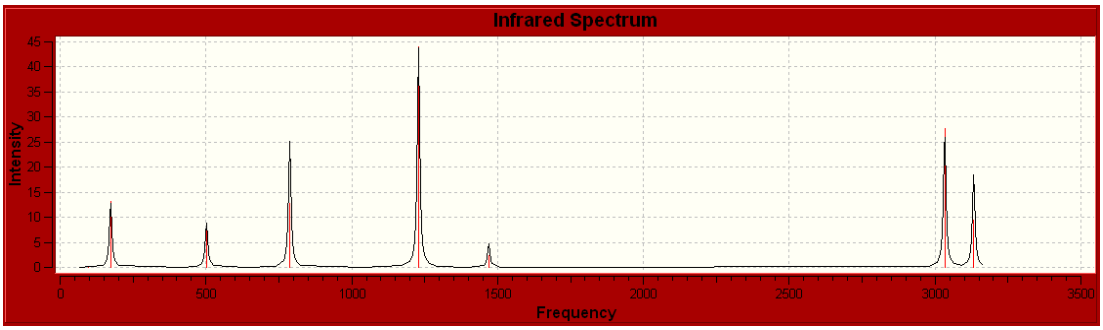


Figure 9.15: MeHgI IR Spectra (B3LYP/CEP-121G)

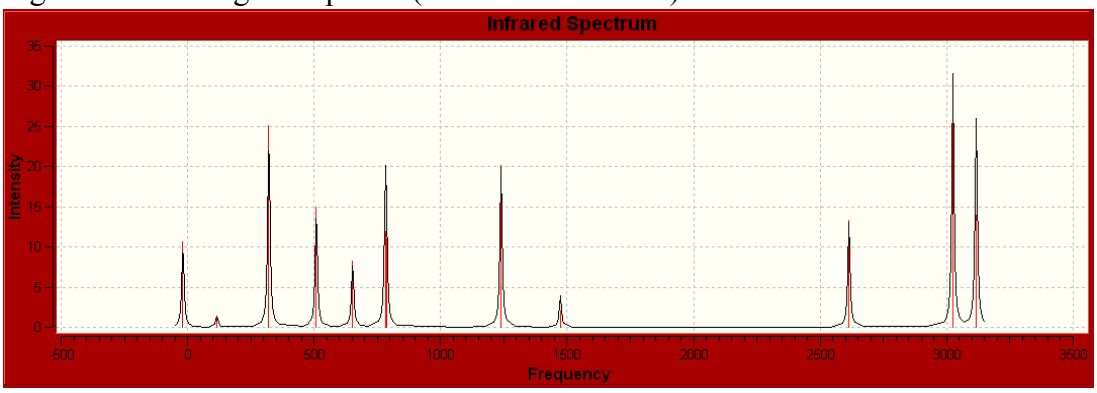


Figure 9.16: MeHgSH Spectra (B3LYP/CEP-121G)

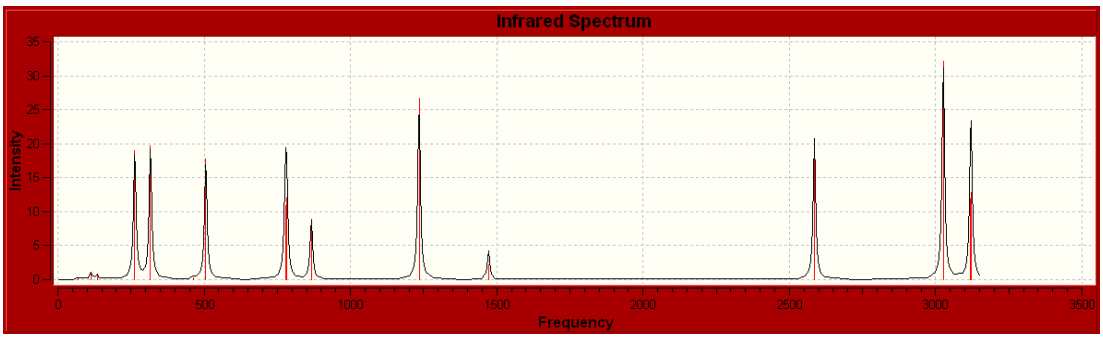


Figure 9.17: $MeHgS_2H$ Spectra (B3LYP/CEP-121G)

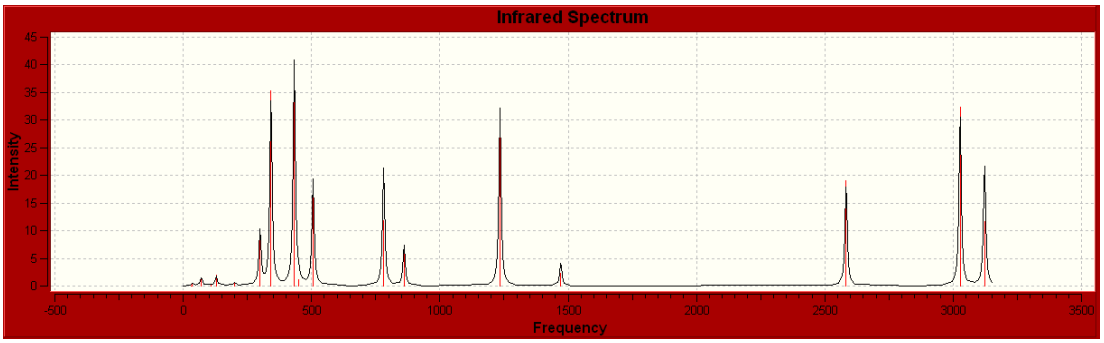


Figure 9.18: $MeHgS_3H$ Spectra (B3LYP/CEP-121G)

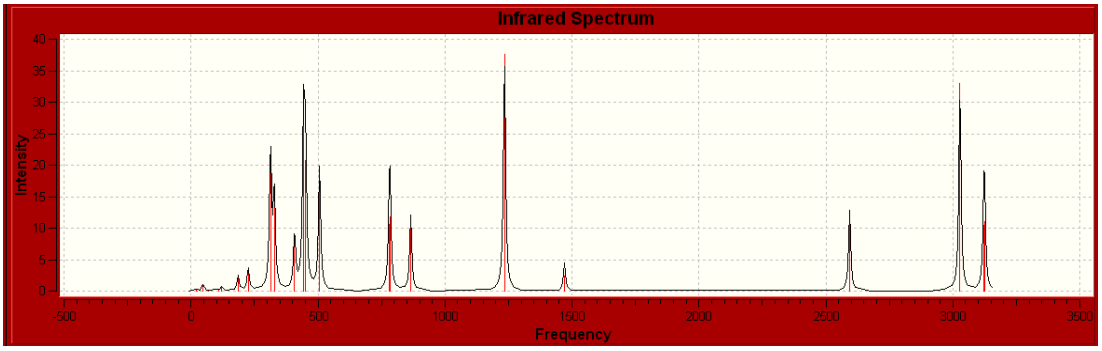


Figure 9.19: $MeHgS_4H$ Spectra (B3LYP/CEP-121G)

Comparing the gas phase and CPCM calculated MeHgF systems in turn in Figure 9.2 and 9.12, we see the most dramatic differences in the stretching mode (see Figure 9.20 below) that appears at 518 $cm^{-1}$ in the gas phase system and at 460 $cm^{-1}$ in the solvated calculation.

The relative intensity of this stretching mode is dramatically larger in the solvated system, with a normalized intensity slightly more than five times larger in the solvated case. This would make sense because as F is very electronegative, we would expect that the stabilization from solvation would make changing the bond length not as expensive, because the Hg-F dipole would be exposed to more of the stabilizing (modeled) solvent.

The asymmetric stretching mode which appeared at 583 $cm^{-1}$ in the gas phase calculation and 536 $cm^{-1}$ in the solvated system was comparatively half as intense in the normalized solvated IR spectrum as the peak was in the gas phase calculation.

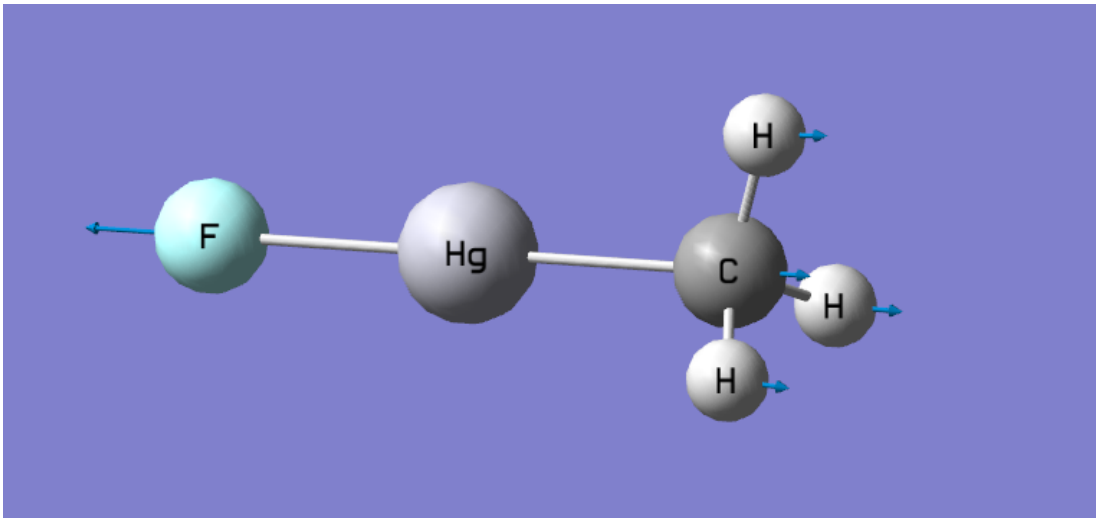


Figure 9.20: MeHgF Symmetric Stretching Mode displacement vectors from B3LYP/CEP-121G CPCM calculation

The other modes of interest involving the Hg atom are the two bending modes, which appear at 158 $cm^{-1}$ in the gas phase and around 140 $cm^{-1}$ in the solvated system. The CPCM solvated system has a relative intensity which is about four times greater than the gas phase calculation's intensity.

Moving on to the MeHgCl calculations shown in Figure 9.3 and 9.13, we see the differences between the solvated and unsolvated gas phase systems are a lot less pronounced. The symmetric stretch which appears at 332 $cm^{-1}$ in the gas phase moves to 278 $cm^{-1}$ in the CPCM solvated system, but the relative intensity is only twice as much in the solvated system compared to the gas phase calculation's normalized intensity. In the MeHgF calculation the difference was a factor of five.

The asymmetric stretch for MeHgCl has nearly the same intensity in both cases, appearing at 520 $cm^{-1}$ in the gas phase calculation and 503 $cm^{-1}$ in the CPCM solvated calculation. Intensities differ by only about 15%.

The bending modes are also much closer together, appearing at 118.5 $cm^{-1}$ in the gas phase calculation and 105 $cm^{-1}$ in the solvated calculation. Here there is a significant intensity difference; in the gas phase the relative normalized intensity is about seven times smaller than the solvated system.

For the MeHgBr system shown in Figure 9.4 and 9.14, the differences are similar to those observed in the MeHgCl calculation. For the symmetric stretch, we see that the expected difference in intensities and base frequencies, with the solvated symmetric stretch at 178 $cm^{-1}$ having just about twice the normalized intensity of the gas phase symmetric stretch that appears at 223 $cm^{-1}$.

The asymmetric stretch, which appears at 511 $cm^{-1}$ in the gas phase and 488 $cm^{-1}$ in the solvated system, is almost entirely the vibration of the $-CH_3$ methyl group towards the central Hg atom, continuing the trend we saw start with the MeHgCl calculation, where as the vibrational modes became more distilled towards the two separate vibrations as opposed to symmetric and asymmetric we saw the difference between the frequencies grow from its initial difference of 65 $cm^{-1}$ for MeHgF to 188 $cm^{-1}$ for MeHgCl and 288 $cm^{-1}$ for MeHgBr.

The bending modes appear for MeHgBr at 106 $cm^{-1}$ in the gas phase, but in the solvated system the modes are at 64 and 79 $cm^{-1}$, although their intensities are significantly greater as well, with the normalized intensities about 60 times larger than the bending mode intensities in the gas phase.

For the MeHgI system which appears in Figure 9.5 and 9.15, we see the former symmetric stretch, which is now almost completely an Hg-I stretch, at 173 $cm^{-1}$ in the gas phase and at 139 $cm^{-1}$ in the solvated system. In this case, the solvated system

was at a saddle point, and the stretching mode for Hg-I also contains a slight amount of I-Hg-Me bending as well. The intensities differ by slightly more than a factor of two, with the mode more intense in the solvated system.

The Hg-Me stretch appears at 501 $cm^{-1}$ in the gas phase calculation and at 465 $cm^{-1}$ in the solvated B3LYP/CEP-121G calculation, with normalized intensities which are basically the same, differing by about 10% (with the solvated system being more intense).

Due to the saddle point in the solvated MeHgI calculation, one of the bending frequencies is not calculated. The remaining one, however, appears at 92 $cm^{-1}$, while in the gas phase the bending appears at 98 $cm^{-1}$. The difference in intensities is even greater here, with the normalized CPCM-solvated aqueous phase intensity being about 65 times greater than the corresponding gas phase intensity.

Turning our attention to the $MeHgS_xH$ series of compounds, we would expect to see a similar trend as the sulfur chain lengthens.

Starting with MeHgSH, and comparing Figure 9.9 and Figure 9.16 we observe that the symmetric and asymmetric stretches appear at about the same places as they did for the MeHgCl system. This makes reasonable sense because the Cl has a molar mass of about 35 g/mol and the -SH group has a similar molar mass of 33 g/mol.

With a bond of similar strength, one would expect that the vibrational modes would be calculated to be the same.

The symmetric stretch for MeHgSH, which mostly consists of the Hg-SH bond stretching, appears at 321 $cm^{-1}$ in the gas phase calculation and 271 $cm^{-1}$ in the solvated calculation. The normalized intensity is about twice as much in the solvated system as it is in the gas phase calculation.

The asymmetric stretch appears at 508 $cm^{-1}$ in the gas phase calculation for MeHgSH, and at 478 $cm^{-1}$ in the solvated calculation. The intensity is about 1.6 times larger in the solvated system than the non-solvated one.

With these $MeHgS_xH$ calculations, there were often minor saddle points that did not significantly affect the overall energy. However, these did affect the predicted vibrational frequencies, leaving us with only one solid bending mode in the predicted spectrum for solvated MeHgSH. This appears at 66 $cm^{-1}$, where in the gas phase the bending modes appear at 117 $cm^{-1}$. The relative intensities are dramatically different, with the solvated system having about 18 times as intense a bending peak on its spectrum as the normalized gas phase calculation's.

In the MeHgSH calculation, there is a bending mode between Hg-S-H which appears at 652 $cm^{-1}$ in the gas phase and 616 $cm^{-1}$ in the solvated calculation. This mode is

relatively more intense in the gas phase calculation, with an intensity about 1.4 times as strong as the normalized solvated bending mode.

Moving on to Figure 9.10 and 9.17, of $MeHgS_2H$, its Hg-S bond stretching mode appears at 316 $cm^{-1}$ in the gas phase and 281 $cm^{-1}$ in the solvated system. The intensities differ by a factor of 2.

The asymmetric stretch of mostly the Me-Hg bond appears at 506 $cm^{-1}$ in the gas phase and 490 $cm^{-1}$ in the solvated system. The relative intensities are similar, with a difference of maybe 1.5 times.

Because the $MeHgS_2H$ system is not axially symmetric, the two bending modes separate quite dramatically, with the gas phase modes appearing at 113 $cm^{-1}$ and 69 $cm^{-1}$, while the solvated ones appear at 106 $cm^{-1}$ and 68 $cm^{-1}$. The relative intensities differ by a factor of slightly more than 5 in each case. The bending mode perpendicular to the Hg-S-S plane at 69 $cm^{-1}$ and 68 $cm^{-1}$ is about 4 times as intense as the in-plane mode (at 113 $cm^{-1}$ and 106 $cm^{-1}$) in both cases.

The S-H bending mode perpendicular to the S-S bond appears at 262 $cm^{-1}$ in the gas phase and 221 $cm^{-1}$ in the solvated system, with a normalized intensity about double the gas phase intensity in the B3LYP/CEP-121G CPCM case. This dramatically lower frequency is probably due to the stabilizing effect of the H atom's interactions

with the previous sulfur in the chain, which was not present in MeHgSH. The S-H bending mode parallel to the S-S bond appears at 866 $cm^{-1}$ in the gas phase calculation and 857 $cm^{-1}$ in the solvated system, confirming this evaluation. It's intensity is half that of the parallel mode in the gas phase case, and a third of the parallel mode in the solvated case.

The S-S stretching mode appears at 463 $cm^{-1}$ in the gas phase calculation and 466 $cm^{-1}$ in the solvated calculation. Although the normalized bond stretching intensities are small, they differ by a factor of two as well.

For the $MeHgS_3H$ calculated spectra, which appear in Figure 9.11 and 9.18, the Hg-S bond stretching mode appears at 299 $cm^{-1}$ in the gas phase and 263 $cm^{-1}$ in the solvated system. In both cases the mode includes vibrations of the H atom attached to the sulfer chain tail as well. The relative normalized intensity for the solvated system is approximately double that of the non-solvated system.

The Me-Hg bond stretching mode appears at 506 $cm^{-1}$ in the gas phase calculation and at 486 $cm^{-1}$ in the solvated calculation. The intensity differs by a factor of about 1.3, with the solvated system having a greater intensity. This mode as it appears here was pretty much unaffected by the additional S atoms in $MeHgS_2H$ and $MeHgS_3H$ compared to MeHgSH, which is somewhat expected, as there should not be much interaction between the Me group and the sulfur chain.

The bending modes for MeHgS more-or-less perpendicular to the first S-S bond appear at 107 $cm^{-1}$ in both the gas phase and the solvated case. For the parallel bending mode, the Me-Hg-S bend appears at 71 $cm^{-1}$ in the gas phase and at 96.5 $cm^{-1}$ in the solvated system. In the perpendicular mode, the difference in intensities is about 17 times, but in the parallel mode the difference is only a factor of two.

The S-H bending mode perpendicular to the S-S bond appears at 342 $cm^{-1}$ in the gas phase calculation and at 325 $cm^{-1}$ in the solvated calculation, with a difference in intensities of a factor of about 1.8 times. This mode appears to have mixed with the Hg-S asymmetric stretching mode which appears at 299 $cm^{-1}$ in the gas phase and 263 $cm^{-1}$ in the solvated system, as that mode also has H motion perpendicular to its immediate S-S bond. The bending modes for S-H parallel to the final S-S bond appear at 861 $cm^{-1}$ and 853 $cm^{-1}$ in the gas phase and solvated systems respectively, with a difference in intensity of about 1.6.

The S-S-S stretching modes become increasingly complex as the S chain lengthens, now appearing similar to the traditional stretching modes of $H_2O$. The S-S-S group has an asymmetric mode appearing at 433 $cm^{-1}$ in the gas phase and 430 $cm^{-1}$ in the solvated calculation's IR spectra. The normalized intensity in the solvated case is approximately double the gas phase intensity. This mode is shown in Figure 9.21 below.

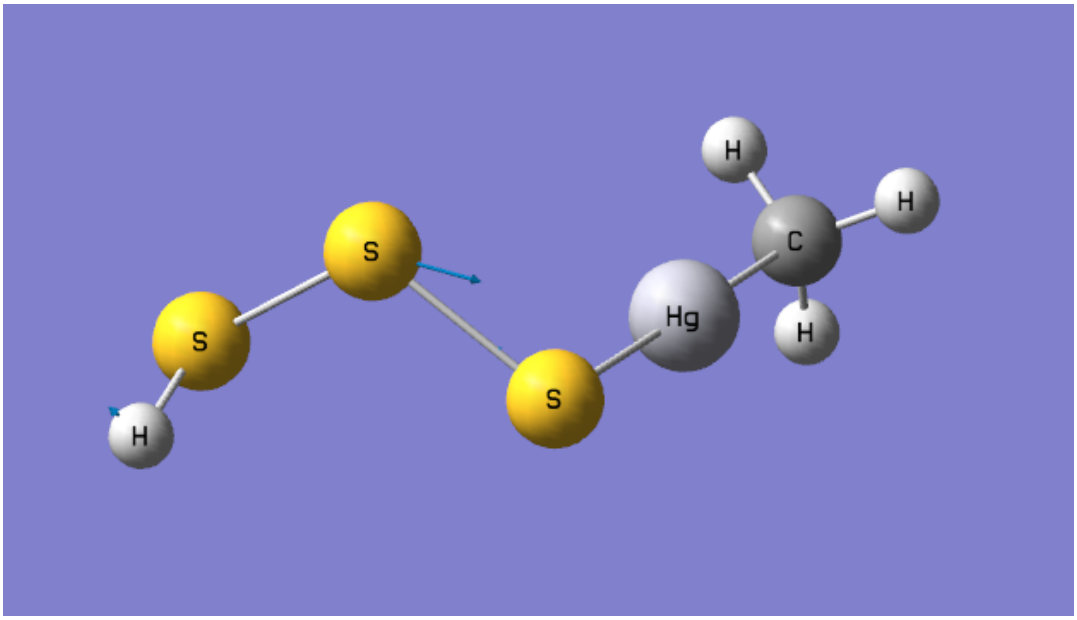


Figure 9.21: $MeHgS_3H$ asymmetric stretching mode calculated in the gas phase under B3LYP/CEP-121G.

For $MeHgS_3H$'s symmetric $S_3$ stretch, shown below in Figure 9.22, which appears at 449 $cm^{-1}$ in the gas phase calculation and at 453 $cm^{-1}$ in the solvated calculation, the intensities differ by a factor of almost ten, with the solvated intensity being the greater.

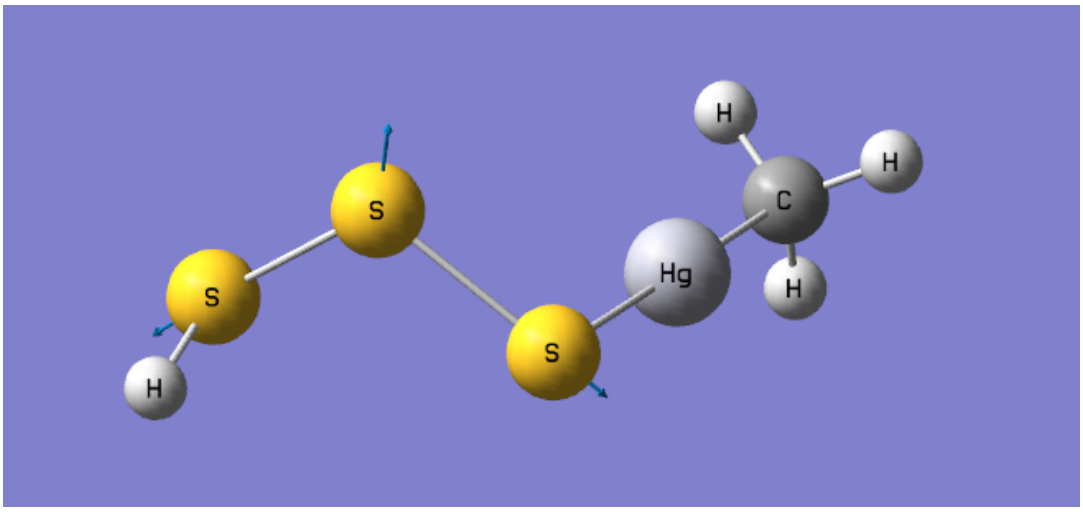


Figure 9.22: $MeHgS_3H$ symmetric stretching mode calculated in the gas phase under B3LYP/CEP-121G.

As the $MeHgS_4H$ calculation ran into difficulties for the solvated system, we will compare the results of the gas phase spectrum in Figure 9.19 to the corresponding gas phase spectrum for $MeHgS_3H$ appearing in Figure 9.18 above.

Hg-S bond stretching appears at 313 $cm^{-1}$, and Me-Hg stretching appears at 506 $cm^{-1}$ with a similar intensity to the Hg-S stretch.

For $MeHgS_4H$ in our gas phase calculation, we observe Me-Hg-S bending modes at 108 $cm^{-1}$ and 121 $cm^{-1}$. The mode bending the molecule perpendicular to the first S-S bond has a normalized gas phase intensity about twice as large as the parallel mode.

The S-H bending modes appear at 328 $cm^{-1}$ for the perpendicular mode which keeps the H distance approximately constant to the second sulfur atom, and at 865 $cm^{-1}$ for the mode parallel to the first S-S bond. Interestingly, the relative intensities of these two gas-phase modes are almost the same, differing by only a factor of 1.3 (though in favor of the perpendicular bending mode as we would expect). The intensities are on the same scale as the Hg-Me stretching peak at 506 $cm^{-1}$.

The S-S bond modes appear at 408 $cm^{-1}$, 444 $cm^{-1}$, and 451 $cm^{-1}$. The mode at 408 $cm^{-1}$ is mostly a stretch of the central two sulfur atoms, and has an intensity about ½ as large as the two modes involving the outer S atoms. The largest peak , at 444 $cm^{-1}$, is about 1.3 times the intensity of the Hg-Me stretching peak at 506 $cm^{-1}$.

*9.4 Conclusions*

Overall, the key observations here were the differing solubilities for the methylmercury halides. Only MeHgF and MeHgCl were polar enough to be calculated more stable in CPCM solvation, indicating that these species would perhaps be less dangerous than -Br or -I substituted analogues. All of the MeHgSH compounds were less stable in water than in the gas phase, so we would predict that they would also prefer nonpolar environments, such as are found in phospholipid bilayers of cells.

In the future, it would be interesting to conduct more calculations with energies of formation in other, less polar solvents, to see at which points the compounds which were destabilized by simulated water were most stabilized. This would shed some light on the types of environments which they would gravitate towards.

*9.5 References*


1. Harada, M., *Minimata Disease - Methylmercury Poisoning in Japan Caused by Environmental-Pollution.* Critical Reviews in Toxicology, 1995. **25**(1): p. 1-24.
2. Takizawa, Y., *Understanding minamata disease and strategies to prevent further environmental contamination by methylmercury.* Water Science and Technology, 2000. **42**(7-8): p. 139-146.
3. Bakir, F. and e. al., *Methylmercury Poisoning in Iraq - Interuniversity Report.* Science, 1973. **181**(4096): p. 230-241.
4. Yan, R., D.T. Liang, and J.H. Tay, *Control of mercury vapor emissions from combustion flue gas.* Environmental Science and Pollution Research, 2003. **10**(6): p. 399-407.
5. Nierenberg, D.W., et al., *Delayed cerebellar disease and death after accidental exposure to dimethylmercury.* New England Journal of Medicine, 1998. **338**(23): p. 1672-1676.

6. Barone, V. and M. Cossi, *Quantum calculation of molecular energies and energy gradients in solution by a conductor solvent model.* Journal of Physical Chemistry A, 1998. **102**(11): p. 1995-2001.

7. Barone, V., M. Cossi, and J. Tomasi, *Geometry optimization of molecular structures in solution by the polarizable continuum model.* Journal of Computational Chemistry, 1998. **19**(4): p. 404-417.

8. Cossi, M., et al., *Energies, structures, and electronic properties of molecules in solution with the C-PCM solvation model.* Journal of Computational Chemistry, 2003. **24**(6): p. 669-681.

9. Roothaan, C.C.J., *New Developments in Molecular Orbital Theory.* Reviews of Modern Physics, 1951. **23**(2): p. 69-89.

10. Head-Gordon, M., J.A. Pople, and M.J. Frisch, *MP2 energy evaluation by direct methods.* Chemical Physics Letters, 1988. **153**(6): p. 503-506.

11. Becke, A.D., *Density-functional thermochemistry. III. The role of exact exchange.* The Journal of Chemical Physics, 1993. **98**(7): p. 5648-5652.

12. Čížek, J., *On the Use of the Cluster Expansion and the Technique of Diagrams in Calculations of Correlation Effects in Atoms and Molecules*. Advances in Chemical Physics1969: John Wiley & Sons, Inc. 35-89.

13. Stevens, W.J., H. Basch, and M. Krauss, *Compact Effective Potentials and Efficient Shared-Exponent Basis-Sets for the 1st-Row and 2nd-Row Atoms.* Journal of Chemical Physics, 1984. **81**(12): p. 6026-6033.

14. Krauss, M., W.J. Stevens, and H. Basch, *Relativistic Effective Potential Scf Calculations of Agh and Auh.* Journal of Computational Chemistry, 1985. **6**(4): p. 287-295.

15. Stevens, W.J., et al., *Relativistic Compact Effective Potentials and Efficient, Shared-Exponent Basis-Sets for the 3rd-Row, 4th-Row, and 5th-Row Atoms.* Canadian Journal of Chemistry-Revue Canadienne De Chimie, 1992. **70**(2): p. 612-630.

16. Cundari, T.R. and W.J. Stevens, Effective Core Potential Methods for the Lanthanides. Journal of Chemical Physics, 1993. 98(7): p. 5555-5565.

# Chapter 10: Ab-Initio modeling of pH dependant Raman Spectra of Myo-Inositol Hexakis Phosphate

*Experimental data from Heighton, L.*

*This chapter discusses calculated Raman spectra of a collection of myo-inositol hexakis phosphates in various states of deprotonation and how this compares to the experimental spectra. The calculated Raman spectra are then dissected, with key peaks examined and the corresponding vibrational modes matched to the features on the experimental spectra. Changes observed in the experimental spectra upon changes in pH are then explained.*

## *10.1 Introduction*

An item of interest in environmental and agricultural chemistry is the behavior of organic and inorganic phosphates in biological systems, as both organic (determined to primarily exist as myo-inositol hexakis phosphate (IHP)) and inorganic phosphates are important environmentally. IHP has been shown to be the a very important, but not well understood form of organic phosphate which is the most common source of phosphate in the enviornment[1]. It is essential to be able to distingush the organic and inorganic forms of phosphates, because plants are unable to use IHP without digestion to remove the phosphate groups from the central carbon ring.

The various species have been studied previously with NMR[2], Mass Spectral[3], and Raman[4, 5] techniques. Although Raman spectra of the different forms of IHP have been demonstrated experimentally to be quite different, prior treatments of the system did not include detailed theoretical studies[4] which could shed additional light on the behavior resulting in the observed experimental changes in the spectra with pH.

The structure of IHP, shown below in Figure 10.1, has twelve acidic protons present that can be removed. In the interest of explaining the experimentally observed Raman spectra[5], this focused our attention to the three main species which would show distinct and different spectral characteristics. We therefore set forward the following calculations to explore the possibilities.

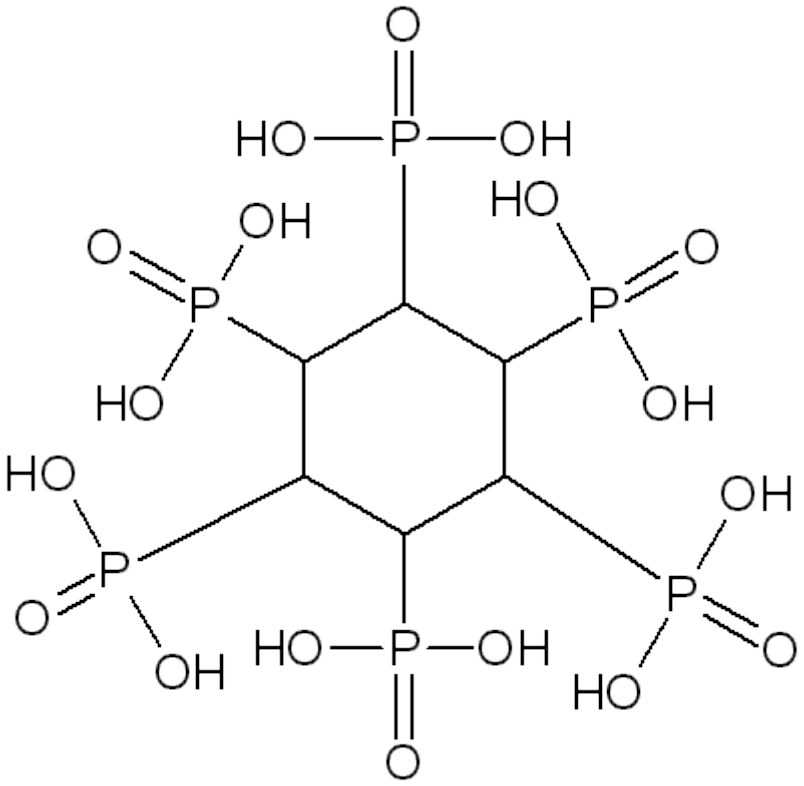

Figure 10.1: IHP structure without stereochemistry. Around a single bonded $C_6H_6$ ring are six $H_2PO_3$ groups.

*10.2 Methods*

As the IHP system was relatively large, we started with a Hartree Fock[6] calculation with a smaller basis set, 6-31G, than we used in previous calculations. Because we were more interested in the spectral and vibrational information rather than energetics, we expected the lower level of theory to be acceptable. We also

performed B3LYP[7] calculations on the same systems to confirm the stability of the HF spectral results. Calculations were conducted with Gaussian 03[8].

The main three compounds which we examined were $H_{12}IHP$ (fully protonated), $H_6IHP^{6-}$ (half deprotonated), and $IHP^{12-}$ (fully deprotonated). These three were chosen to cover the three main states of the phosphonic acid groups, fully protonated $[H_2PO_3\text{-}]^0$, $[HPO_3\text{-}]^-$, and $[PO_3\text{-}]^{2-}$. As these particular species show the most differentiation in their experimental spectra as well as populations in vivo systems, they should allow us to cast the most light on the experimental results.

Initial calculations were gas phase only, followed by explicit hydration with 6 water molecules in each system. This was done successfully for $H_6IHP^{6-}$ . 6 $H_2O$.

Although CPCM solvation calculations were initially considered, because the phosphate groups were expected to exhibit hydrogen bonding interactions which would affect the spectra, conducting a CPCM investigation was left to a future date.

*10.3 Results and Discussion*

Below appear the optimized geometries: HF/6-31G first, as shown in Figure 10.2, then B3LYP/6-31G, in Figure 10.3. As the species are complex, the figures appear as crosseyed stereograms for ease of examination.

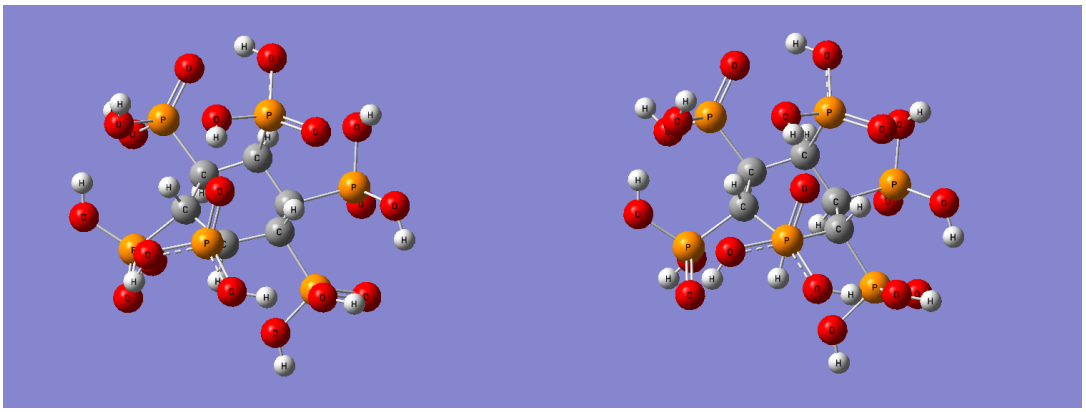

Figure 10.2: $H_{12}$IHP HF optimized structure (3d, crosseyed stereogram)

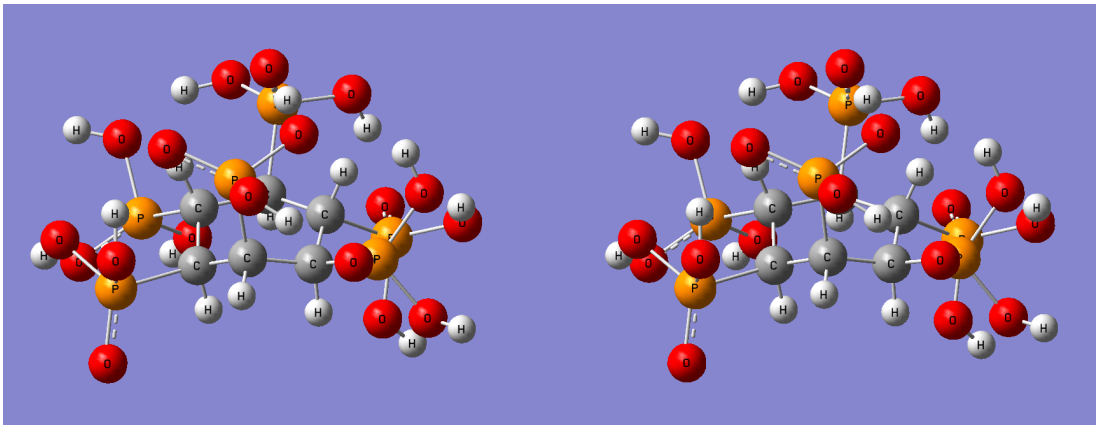

Figure 10.3: $H_{12}$IHP B3LYP re-optimized structure (3d, crosseyed stereogram)

In each case, an initial optimization was first conducted from our structure with simple molecular mechanics methods (not reproduced here), then using that geometry as our first guess, with HF/6-31G. After a stable geometry was found, B3LYP was used to re-optimize and calculate vibrational frequencies as well. This gave us IR peaks for both methods for comparison, and Raman peaks for the HF calculations.

The optimized geometries for the half-deprotonated species appear below in Figure 10.4 and Figure 10.5.

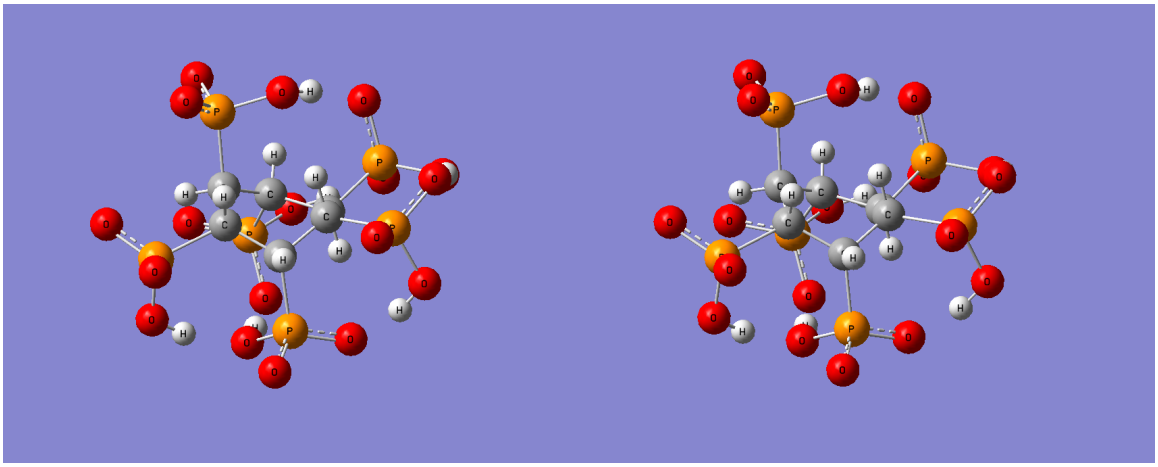

Figure 10.4: $H_6IHP^{6-}$ HF structure (3d, crosseyed stereogram)

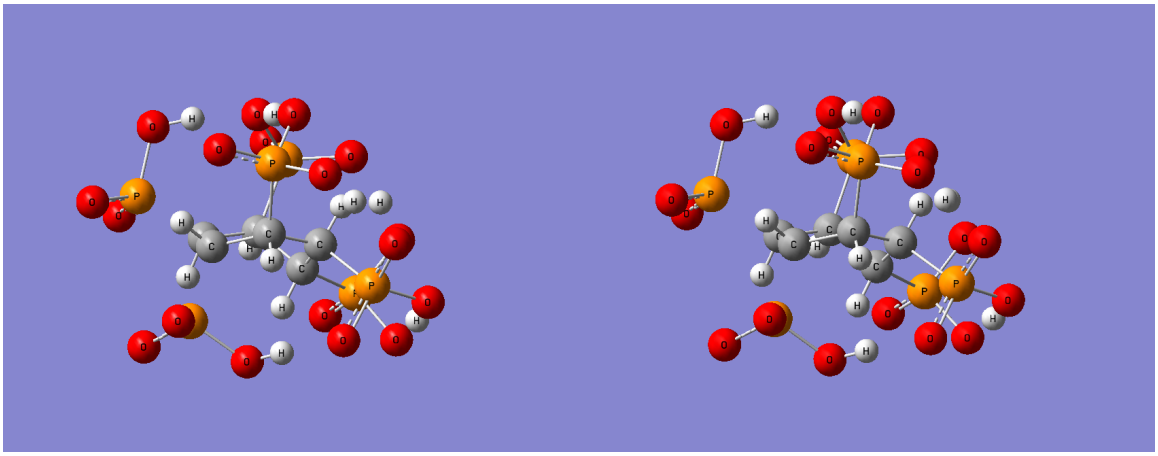

Figure 10.5: $H_6IHP^{6-}$ B3LYP structure (3d, crosseyed stereogram)

We then calculated the structure of an explicitly hydrated system, the half-deprotonated $H_6IHP^{6-}$ , with water molecules positioned to hydrogen bond with each

of the phosphonic acid groups present. The stable minima which we found appears in Figure 10.6, below.

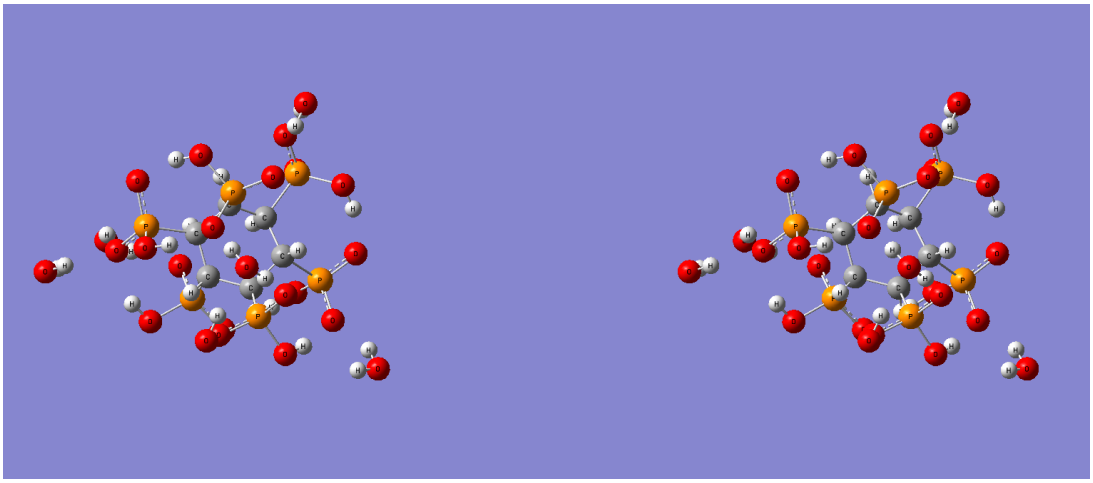

Figure 10.6: $H_6IHP^{6-}$ HF structure, explicitly solvated explicitly by 6 $H_2O$ molecules (3d, crosseyed stereogram)

As the anions became progressively more negatively charged, the optimization steps began taking increasing lengths of time to reach a stable energy minima. The last set of calculations on the fully deprotonated $IHP^{12-}$ system was, as expected, the most difficult to stabilize; pure gas phase calculations upon it are still in progress, as well explictly solvated calculations for $H_{12}IHP$.

Let's look at the spectra of each species in turn. First, we shall examine the synthetic HF spectra of the fully protonated, neutral species $H_{12}IHP$, which includes both IR and Raman peaks, as shown in Figure 10.7.

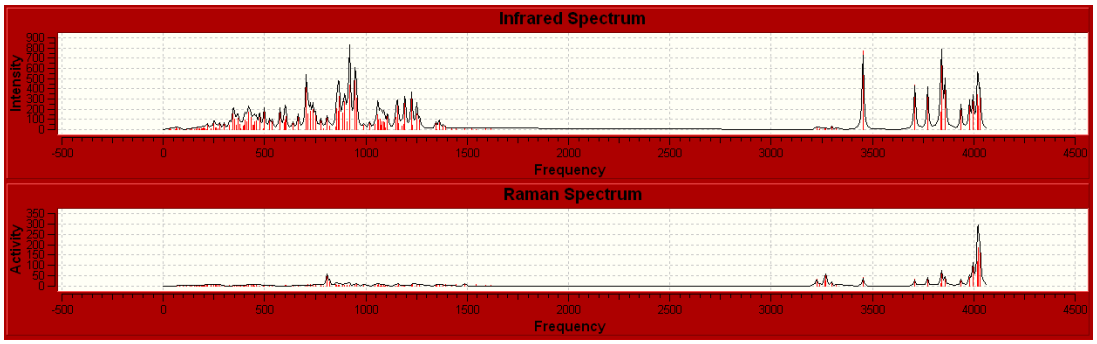


Figure 10.7: HF synthetic IR and Raman spectra for $H_{12}IHP$ calculated with the 6-31G basis set.

As we can see, with the many IR peaks, the largest seen at 3453 $cm^{-1}$, 3841 $cm^{-1}$, 705 $cm^{-1}$, 946 $cm^{-1}$, 3858 $cm^{-1}$, 919 $cm^{-1}$, 3709 $cm^{-1}$, 3772 $cm^{-1}$, 4019 $cm^{-1}$, and the primary Raman peaks showing around 4015 $cm^{-1}$, with four peaks at 4021 $cm^{-1}$, 4030 $cm^{-1}$, and 4019 $cm^{-1}$, and 3996 $cm^{-1}$ having the highest intensities overall, with a smaller one at 809 $cm^{-1}$. The experimental Raman spectra, which we will cover below, run from 500 $cm^{-1}$ to 2000 $cm^{-1}$, and we shall discuss this area of the spectra in more detail later.

Our focus here in telling the differences between the different states of the IHP system will be the phosphate groups, as they become deprotonated and behave differently in the different cases. However, before we address those, lets examine the spectra overall and look at the differences between the HF and B3LYP calculations.

In our B3LYP calculation, shown in Figure 10.8, we have the primary IR peaks appearing at 2643 $cm^{-1}$, 3083 $cm^{-1}$, 3275 $cm^{-1}$, 772 $cm^{-1}$, 3325 $cm^{-1}$, 948 $cm^{-1}$, 3262 $cm^{-1}$, 793 $cm^{-1}$, and 836 $cm^{-1}$. For the higher frequency modes, the frequencies changed little, for example the vibrational modes at 948 $cm^{-1}$ and 946 $cm^{-1}$ in the HF calculation. These modes correspond with vibrations of hydrogen-bonding H atoms between the phosphate groups which are vibrating perpendicular to the O-H-O bonding axis.

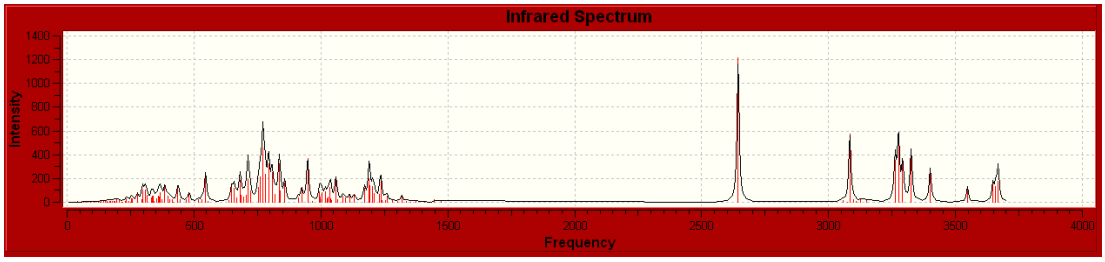


Figure 10.8: B3LYP synthetic IR spectrum for $H_{12}IHP$ calculated with the 6-31G basis set.

A peak at 780 $cm^{-1}$ corresponds to a stretching distortion of the $C_6$ ring in the B3LYP calculation also appears in the HF calculation, although the additional bond stiffness seen in HF makes the intensity of the peak much weaker.

The largest difference here is in the vibration at 2643 $cm^{-1}$ in the B3LYP calculation, which turns out to correspond with the peak at 3453 $cm^{-1}$ in the HF calculation. This vibrational mode is for an especially well shared hydrogen atom, and is shown in Figure 10.9, which illustrates the mode in the B3LYP case. We would expect that the

hydrogen-bonding H atoms would show lower frequency vibrational modes in the B3LYP calculation because it is well known that in HF calculations hydrogen bonds are much stiffer and ionic than they are in reality.

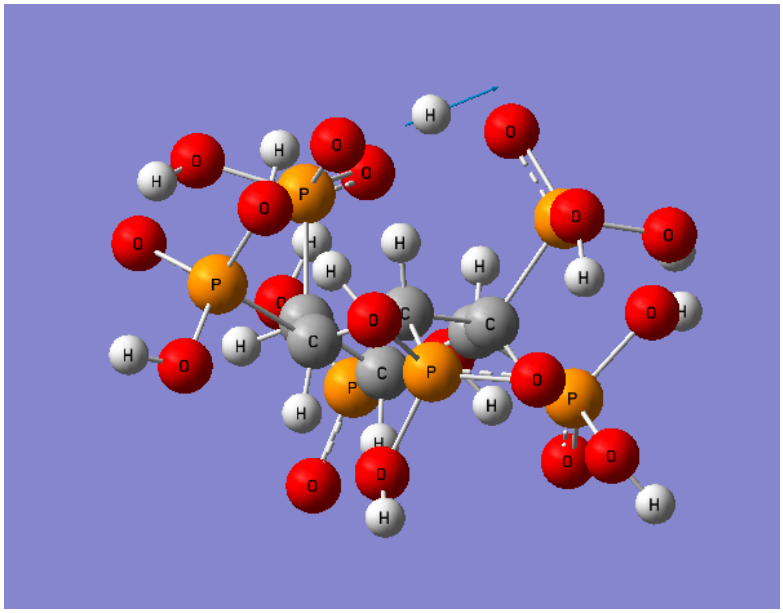

Figure 10.9: B3LYP vibrational mode at at 2644 $cm^{-1}$. Note the displacement vector for the H atom at the top shares it between the two nearby O atoms.

The vibrational spectra for the half-deprotonated system in the gas phase appears below in Figure 10.10 for the HF calculation and Figure 10.11 for the B3LYP calculation. We shall discuss both briefly at the same time, as the experimental characterization was done in aqueous conditions and the results do not particularly apply to our overall discussion.

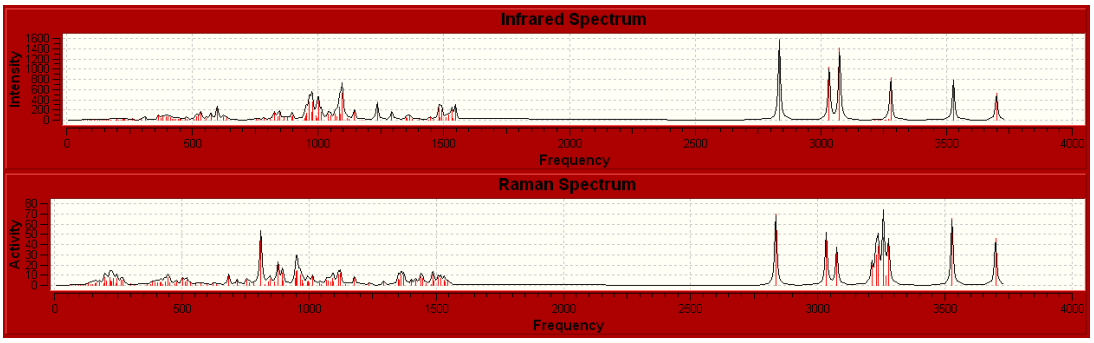


Figure 10.10: HF synthetic IR and Raman spectra for gas phase $H_6IHP^{-6}$ calculated with the 6-31G basis set.

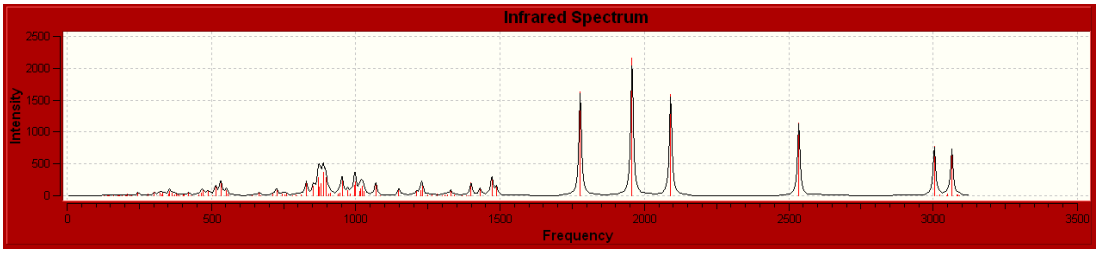


Figure 10.11: B3LYP synthetic IR spectrum for gas phase $H_6IHP^{-6}$ calculated with the 6-31G basis set.

Taking both together, we can see that the general shape of both IR spectra are nearly the same, showing that the HF method is sufficient in this case for modeling $H_6IHP^{-6}$ in the gaseous phase. However, the Raman spectra has little resemblance to the experimental spectra shown later in Figure 10.14, as it was calculated in the gas phase, so we shall pass over these results to focus on the explicitly solvated system, which goes much farther in explaining the experimental results.

Our calculation of the same system with six explicit water molecules using HF, as shown in Figure 10.12, shows the expected behavior in its Raman spectra, with peaks appearing at 832 $cm^{-1}$, at 960-970 $cm^{-1}$, and around 1100 $cm^{-1}$ and 1162 $cm^{-1}$.

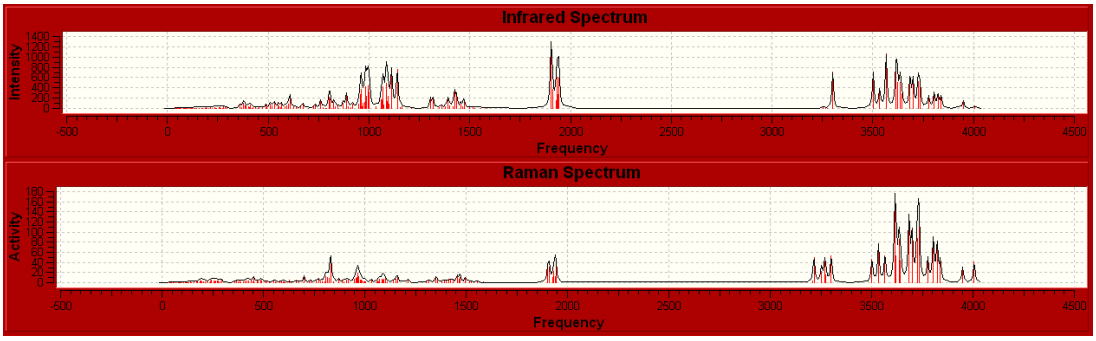


Figure 10.12: HF synthetic IR and Raman spectra for $H_6IHP^{6-}$ . $6H_2O$ calculated with the 6-31G basis set.

The primary vibrational mode at 832 $cm^{-1}$ is the hydrogen-bonding phosphate H atoms moving perpendicular to the axis of hydrogen bonding between adjacent phosphate groups. The primary mode at 967 $cm^{-1}$ appears to be a symmetric stretch that appeared when the phosphate was deprotonated as shown in Figure 10.13, while the mode at 1100 $cm^{-1}$ corresponds to an asymmetric stretch of the same groups. The peaks near 1500 appear to be H atom bending modes mostly on the central carbon atoms.

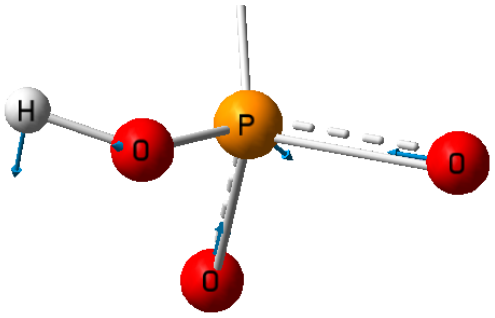


Figure 10.13: Phosphate group symmetric stretch observed in HF/6-31G calculated Raman spectrum for $H_6IHP^{6-}$ . 6 $H_2O$ at 967 $cm^{-1}$.

The peaks around 1162 $cm^{-1}$ correspond to various vibrational modes of the $C_6$ ring in the center of the compound.

We can now compare our Raman data to experimental spectra[5] taken under various pH conditions, as shown in Figure 10.14.

Looking between the peaks seen experimentally at low (acidic) pH 3, where the fully protonated $H_{12}IHP$ would be predominant, and the peaks seen in more neutral solutions near pH 7, we can first observe in the experimental data that there is a trend where the peak at 850 $cm^{-1}$ shrinks, and a peak appears near 1000 $cm^{-1}$. This trend is duplicated in our theoretical data for the explicitly solvated $H_6IHP^{-6}$ . 6 $H_2O$ anion as calculated with the HF/6-31G, which is a good sign.

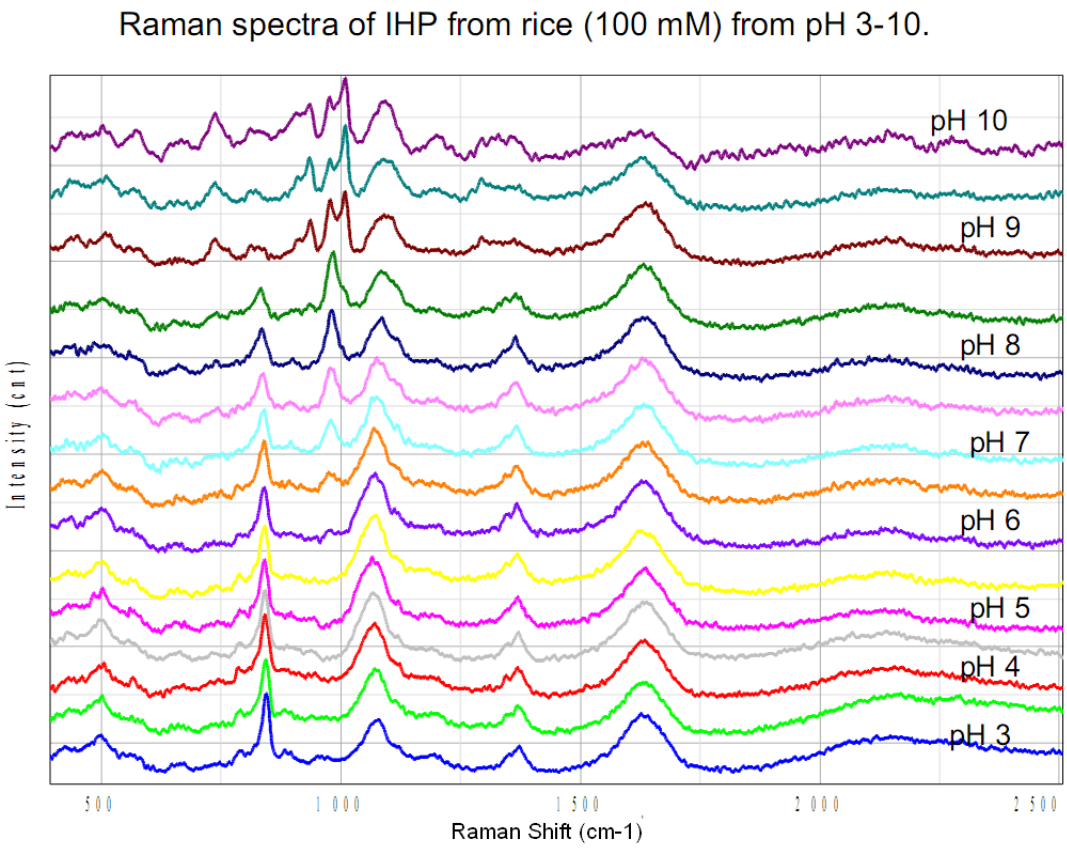


Figure 10.14: Experimentally Measured Raman Spectra under various pH conditions as measured by L. Heighton[5].

Let's use our calculations to interpret the Raman peaks seen on the experimental spectra, identifying them as follows.

The peak slightly below 1000 $cm^{-1}$ in the experimental spectra is probably the phosphate symmetric stretching mode shown by the singly deprotonated $HPO_3$-R groups in our calculation and shown in Figure 10.13. The peak further down is the vibrational modes of the intramolecularly hydrogen bonding protons on the phosphate

groups vibrating perpendicular to the bonds. This would explain the near disappearance of the peak in the most basic conditions, where the acidic groups would be fully deprotonated and this kind of mode would no longer be possible.

Finally, the peak just above 1000 $cm^{-1}$ is related to the vibrational modes of the central $C_6H_6$ ring, which is why it remains for the most part unchanged regardless of the external pH. The modes between 1450 and 1600 $cm^{-1}$ on our spectrum appear to correspond to different bending modes of nonbonding H atoms, mostly on the central $C_6$ ring, although they also include some motion of phosphate H atoms in unfavorable directions. This might explain why the peaks seen on the experimental spectrum in this area become subdued under the most basic pH conditions.

*10.4 Conclusions*

We have shown that the HF/6-31G method is sufficient in this case, with IR spectra with similar shapes in the area of interest between 500-2000 $cm^{-1}$ as the higher level B3LYP method. Although predictive peak positions were not necessarily achieved with this approach, the clear trends of where the Raman absorptions are with relation to each other correspond closely to the experimental results, confirming the identities of the species suspected by the experimenter. Theoretical vibrational modes provided additional insight into the sources of each observed peak in the experimental measurement.

In the future, it would be interesting to explore energetics calculations on these compounds.

The large charges would probably make the calculation difficult, but a clear starting point would be to do a single point CCSD(T) calculation at the final B3LYP geometry, and possibly some calculations on the anions with larger basis sets. As we observed explicit solvation was essential for the spectra to correspond with experimental measurement, either explicit water molecules or a modeled solvent will be essential, with all the additional computational costs which that implies.

Currently, further efforts continue to model the solvated, fully deprotonated $IHP^{-12}$ system, and this additional information will be presented in a future paper. Future calculations on explicitly solvated molecules of the fully deprotonated $IHP^{-12}$ should shed further light on the area of the experimental spectrum in the 1200-1700 $cm^{-1}$ area as well, as changes were observed there compared to the $H_{12}IHP$ and $H_6IHP^{-6}$ systems examined here.

Another good future effort would be to do a vibrational calculation including anharmonic contributions could provide corrections to the measured frequencies, possibly allowing us to predict the experimental spectrum directly. This type of calculation would also still be possible even if full optimization under the higher level

method was inaccessible. These could be added as corrections to the IR and Raman spectral lines of interest to improve the raw accuracy theoretical results.

## *10.5 Acknowledgements*

We would like to acknowledge Heighton, L. for several entertaining afternoons discussing IHP and possible applications of theoretical chemistry, for patience while the calculations were being conducted, and for assistance in finding good references.

## *10.6 References*

1. Turner, B.L., et al., *Inositol phosphates in the environment.* Philos Trans R Soc Lond B Biol Sci., 2002. **357**(1420): p. 449-469.
2. Heighton, L., W.F. Schmidt, and R.L. Siefert, *Kinetic and Equilibrium Constants of Phytic Acid and Ferric and Ferrous Phytate Derived from Nuclear Magnetic Resonance Spectoscopy.* Journal of Agricultural and Food Chemistry, 2008. **56**: p. 9543-9547.
3. Heighton, L., et al., *Electrospray ionization mass spectroscopy shows speciation of phytate to be pH dependent.* Journal of Food, Agriculture & Environment, 2008. **6**(2): p. 401-407.

4. Yang, H.-F., et al., *Electrochemical and Surface Enhanced Raman Scattering Spectroelectrochemical Study of Phytic Acid on the Silver Electrode.* J. Phys. Chem. B., 2004. **108**: p. 17412-17417.

5. Heighton, L.P. and W.F. Schmidt. *Raman spectra of organic (myo-inositol hexakis phosphate) and inorganic P sepctra show pH dependence.* in *Proceedings of American Chemical Society National Meeting*. 2009. Washington, D.C.

6. Roothaan, C.C.J., *New Developments in Molecular Orbital Theory.* Reviews of Modern Physics, 1951. **23**(2): p. 69-89.

7. Becke, A.D., *Density-functional thermochemistry. III. The role of exact exchange.* The Journal of Chemical Physics, 1993. **98**(7): p. 5648-5652.

8. M. J. Frisch, G.W.T., H. B. Schlegel, G. E. Scuseria, M. A. Robb, J. R. Cheeseman, J. A. Montgomery, Jr., T. Vreven, K. N. Kudin, J. C. Burant, J. M. Millam, S. S. Iyengar, J. Tomasi, V. Barone, B. Mennucci, M. Cossi, G. Scalmani, N. Rega, G. A. Petersson, H. Nakatsuji, M. Hada, M. Ehara, K. Toyota, R. Fukuda, J. Hasegawa, M. Ishida, T. Nakajima, Y. Honda, O. Kitao, H. Nakai, M. Klene, X. Li, J. E. Knox, H. P. Hratchian, J. B. Cross, V. Bakken, C. Adamo, J. Jaramillo, R. Gomperts, R. E. Stratmann, O. Yazyev, A. J. Austin, R. Cammi, C. Pomelli, J. W. Ochterski, P. Y. Ayala, K. Morokuma, G. A. Voth, P. Salvador, J. J. Dannenberg, V. G. Zakrzewski, S. Dapprich, A. D. Daniels, M. C. Strain, O. Farkas, D. K. Malick, A. D. Rabuck, K. Raghavachari, J. B. Foresman, J. V. Ortiz, Q. Cui, A. G. Baboul,

S. Clifford, J. Cioslowski, B. B. Stefanov, G. Liu, A. Liashenko, P. Piskorz, I. Komaromi, R. L. Martin, D. J. Fox, T. Keith, M. A. Al-Laham, C. Y. Peng, A. Nanayakkara, M. Challacombe, P. M. W. Gill, B. Johnson, W. Chen, M. W. Wong, C. Gonzalez, and J. A. Pople, Gaussian 03, Revision C.02, 2004, Gaussian, Inc., Wallingford CT.

# Chapter 11: Conclusions and Future Work

*In which we summarize the overall results from each section of the research and offer suggestions for further study.*

## *11.1 Introduction*

In conclusion, we have examined a number of different chemical systems using a variety of theoretical methods.

Systems examined included the series of mercury chlorides, methylmercury chlorides and other mercuric halides discussed previously, as well as a variety of inorganic polyprotic acids, whose acidities were explored in detail. We also studied the Raman spectra of myo-inositol hexakis phosphate (IHP) in a joint project with an experimental group.

The theories applied ranged from Hartree-Fock[1] to CCSD(T)[2], CBS-QB3[3, 4], and complete basis set extrapolations[5]. Calculations included geometry and stability calculations, which were used in both the gas phase and in solvated systems (simulated by CPCM solvation[6-8] and explicit hydration with $H_2O$, consisting of single and multiple water molecules), and NMR shielding calculations[9-11] done with ADF[12-14] , and infrared spectra calculated with Gaussian 03[15].

*11.2 Results and Discussion*

Results were generally successful.

In the case of the mercury chlorides, we calculated energetics and structures, and NMR data for $HgCl^{+}$ through $HgCl_6^{4-}$. Energetics results were shown to be stable between B3LYP / CEP-121G+ and the higher level CCSD and CCSD(T) complete basis set extrapolations, so B3LYP is sufficient for calculations on these compounds. The overall NMR results showed trends for the NMR with decreasing shielding running from approximately 10000 $cm^{-1}$ to 6700 $cm^{-1}$ with increasing substitution.

In our polyprotic acid study, we examined the behavior of a set of polyprotic acids including $H_3PO_4$, $H_3AsO_4$, $H_3PO_3$, $H_3AsO_3$, $H_3AsS_4$, $H_3AsS_3$, and $H_2SO_3$. Each species of these, both unexplicitly and explicitly solvated, was calculated for stable geometries and the energetics were predicted using both gas phase CBS-QB3 and CPCM solvated CBS-QB3. We then had graphed the predicted pKa values against the experimental measurements, discovering a linear relation between the two. A linear extrapolation was determined to adjust the calculated pKa values, which improved the results to theoretical quality, reproduced below as Equation 11.1.

(11.1) $pKa_{expt} = 0.429\ pKa_{CBS\text{-}QB3\ CPCM\ w/H2O} - 0.233$

The acidity calculation results done with CBS-QB3 in the CPCM were uniformly reasonable for the first deprotonation, as expected, though the second and third deprotonations were not as good (also as expected). With the extrapolation we developed, however, the results became theoretical quality; within 2 kcal/mol of the experimental measurements.

The results with the extrapolation were also tested on an $H_2SO_3$ system which we did not include in the original results used to make the system, and were then used to explore a series of $HClO_x$ compounds (x=1...4) with counter-ions present (described in Chapter 7). These calculations yielded results that showed the correct trends of increasing acidity in the series, although they overestimated the experimental acidity of the $HClO_4$ dramatically.

The methylmercury structures, which we previously discussed as being responsible for the instances of mercury poisoning in Japan (as Minamata Disease)[16] and in Iraq (from repurposed mercury-treated grain)[17] were also explored in detail, showing the expected trends of decreasing solubility with the softer halogens Br and I. The IR spectra and differences in them between solvated and unsolvated conditions were also examined in detail.

At the suggestion of Lynne Heighton, an experimentalist, we did a series of Raman Spectra calculations on partly depronated myo-inositol hexakis phosphate (IHP), the

most common organic phosphate compound seen in nature, to compare and shed further light on the experimental data previously presented at ACS[18]. We calculated both Raman spectra with HF and IR spectra with HF and B3LYP for both the nondeprotonated $H_{12}IHP$ system and the partly deprotonated $H_6IHP^{6-}$ systems, the latter with explicit hydration, and the spectra showed the expected trends, confirming the experimental results and casting light on the vibrational modes responsible for several of the observed peaks.

In the future, we can see that its important to check over even unexpected results visually to see if an obscured relation exists. The good results found in the case of the polyprotic acids are a clear indication that this approach is effective.

Throughout our explorations, we observed that the largest challenge in applied theoretical chemistry is probably determination of the geometries corresponding to the energy minima. This was especially true when dealing with edge cases that stressed the theory, such as hydrated ionic species. In many cases, much of the CPU time was spent on geometry optimization rather than other parts of the calculations.

We addressed this somewhat by applying a stair-step method, optimizing the geometries with a quickly-minimizing HF calculation with a small basis set to get a better starting geometry than could be determined by hand, followed by higher level calculations. Although the HF geometries were not very accurate, they provided an

easy to reach geometric springboard for the future calculations which stood closer than our initial guesses as to the geometries.

The most difficult conditions we observed when reaching geometric equilibrium was modeling anionic systems with the B3LYP method with CPCM solvation. Under these three conditions, it was often the case that the geometry began oscillating slowly around a stable geometry on the multidimensional free energy surface instead of straightforwardly reaching a final geometry. This is because the presence of CPCM flattens the potential energy surface and B3LYP tends to be one of the slower methods to reach equilibrium. A strongly charged system will be deeply stabilized whatever the geometry by the presence of the CPCM, which makes it more difficult to reach a final geometry regardless of the method.

We found that the best thing to do in this case was to solve for a stable geometry in the gas phase first, and follow that preliminary calculation with the CPCM calculation. In troublesome cases, a HF calculation in the gas phase followed by an MP2 calculation in the CPCM allowed for a starting geometry for B3LYP which was effective in a timely fashion. This was also helpful in our CBS-QB3 calculations with anions because of the initial B3LYP optimization step.

Future steps which would correspond with our group's focus on environmental and geochemical applications of computational chemistry could likely include

calculations on other Hg systems. For example, when we examined our methylmercury calculation results, we saw that solvation actually destabilized some of the compounds. It would be exciting to test a variety of different solvents to allow us to determine what solvent polarity would be necessary to make MeHgBr more stable when solvated, for example. Of course, another group might set forwards to do this same type of calculation on other, better characterized systems, such as protonated or ionic clusters where precise physical measurements are already available.

We also did a number of calculations which focused on the behavior of $HgCl_x$ compounds, both in the gas phase and in solvation. Further calculations of this sort could be done with other simulated solvents. With increasing interest in ionic liquids for separations because of their environmental friendliness and reusability, for example, it would be interesting to explore the possible behaviors of the mercury compounds in a more ionic liquid.

*11.3 Acknowledgements*

We would like to acknowledge S. Vinnikova for her great assistance in preparing this section and offering helpful suggestions and encouragement during its writing.

*11.4 References*

1. Roothaan, C.C.J., *New Developments in Molecular Orbital Theory.* Reviews of Modern Physics, 1951. **23**(2): p. 69-89.

2. Pople, J.A., et al., *Electron Correlation Theories and Their Application to Study of Simple Reaction Potential Surfaces.* International Journal of Quantum Chemistry, 1978. **14**(5): p. 545-560.

3. Montgomery, J.A., et al., *A complete basis set model chemistry. VI. Use of density functional geometries and frequencies.* Journal of Chemical Physics, 1999. **110**(6): p. 2822-2827.

4. Montgomery, J.A., et al., *A complete basis set model chemistry. VII. Use of the minimum population localization method.* Journal of Chemical Physics, 2000. **112**(15): p. 6532-6542.

5. Halkier, A., et al., *Basis-set convergence of the energy in molecular Hartree-Fock calculations.* Chemical Physics Letters, 1999. **302**(5-6): p. 437-446.

6. Barone, V. and M. Cossi, *Quantum calculation of molecular energies and energy gradients in solution by a conductor solvent model.* Journal of Physical Chemistry A, 1998. **102**(11): p. 1995-2001.

7. Barone, V., M. Cossi, and J. Tomasi, *Geometry optimization of molecular structures in solution by the polarizable continuum model.* Journal of Computational Chemistry, 1998. **19**(4): p. 404-417.

8. Cossi, M., et al., *Energies, structures, and electronic properties of molecules in solution with the C-PCM solvation model.* Journal of Computational Chemistry, 2003. **24**(6): p. 669-681.

9. Wolff, S.K., et al., *Density functional calculations of nuclear magnetic shieldings using the zeroth-order regular approximation (ZORA) for*

*relativistic effects: ZORA nuclear magnetic resonance.* Journal of Chemical Physics, 1999. **110**: p. 7689

10. Schreckenbach, G. and T. Ziegler, *The calculation of NMR shielding tensors using GIAO's and modern density functional theory.* Journal of Physical Chemistry, 1995. **99**.
11. Schreckenbach, G. and T. Ziegler, *The calculation of NMR shielding tensors based on density functional theory and the frozen-core approximation.* International Journal of Quantum Chemistry, 1996. **60**.
12. Baerends, E.J., et al., *ADF2004.01, SCM, Theoretical Chemistry, Vrije Universiteit, Amsterdam, The Netherlands,* http://www.scm.com. 2004.
13. Velde, G.t., et al., *Chemistry with ADF.* Journal of Compututational Chemistry, 2001. **22**: p. 931.
14. Guerra, C.F., et al., *Towards an order-N DFT method.* Theoretical Chemistry Accounts, 1998. **99**.
15. M. J. Frisch, G.W.T., H. B. Schlegel, G. E. Scuseria, M. A. Robb, J. R. Cheeseman, J. A. Montgomery, Jr., T. Vreven, K. N. Kudin, J. C. Burant, J. M. Millam, S. S. Iyengar, J. Tomasi, V. Barone, B. Mennucci, M. Cossi, G. Scalmani, N. Rega, G. A. Petersson, H. Nakatsuji, M. Hada, M. Ehara, K. Toyota, R. Fukuda, J. Hasegawa, M. Ishida, T. Nakajima, Y. Honda, O. Kitao, H. Nakai, M. Klene, X. Li, J. E. Knox, H. P. Hratchian, J. B. Cross, V. Bakken, C. Adamo, J. Jaramillo, R. Gomperts, R. E. Stratmann, O. Yazyev, A. J. Austin, R. Cammi, C. Pomelli, J. W. Ochterski, P. Y. Ayala, K.

Morokuma, G. A. Voth, P. Salvador, J. J. Dannenberg, V. G. Zakrzewski, S. Dapprich, A. D. Daniels, M. C. Strain, O. Farkas, D. K. Malick, A. D. Rabuck, K. Raghavachari, J. B. Foresman, J. V. Ortiz, Q. Cui, A. G. Baboul, S. Clifford, J. Cioslowski, B. B. Stefanov, G. Liu, A. Liashenko, P. Piskorz, I. Komaromi, R. L. Martin, D. J. Fox, T. Keith, M. A. Al-Laham, C. Y. Peng, A. Nanayakkara, M. Challacombe, P. M. W. Gill, B. Johnson, W. Chen, M. W. Wong, C. Gonzalez, and J. A. Pople, *Gaussian 03, Revision C.02*, 2004, Gaussian, Inc., Wallingford CT.

16. Takizawa, Y., *Understanding minamata disease and strategies to prevent further environmental contamination by methylmercury.* Water Science and Technology, 2000. **42**(7-8): p. 139-146.

17. Bakir, F. and e. al., *Methylmercury Poisoning in Iraq - Interuniversity Report.* Science, 1973. **181**(4096): p. 230-241.

18. Heighton, L.P. and W.F. Schmidt. Raman spectra of organic (myo-inositol hexakis phosphate) and inorganic P sepctra show pH dependence. in Proceedings of American Chemical Society National Meeting. 2009. Washington, D.C.

# Glossary

| | |
|---|---|
| ADF | Amsterdam Density-Functional theory software (by Scientific Computing and Modeling). |
| B3LYP | Hybrid HF-DFT method with similar quality results as MP2 |
| CBS-QB3 | Complete Basis Set Extrapolation Model Chemistry computational method |
| CCSD | Coupled Cluster Theory (high level) computational method (with single and double excitations) |
| CCSD(T) | Coupled Cluster Theory (very high level) computational method (with some triple excitations as well) |
| CEP-121G | Compact Effective Potential basis set with |
| CEP-31G | Compact Effective Potential basis set |
| CPCM | Polarizable Continuum Method computational method for simulating solvation (with water or other solvents) |
| DFT | Density-functional Theory |
| G03 | Gaussian 03 computational chemistry software (from Gaussian, Inc). |
| G2 | GAUSSIAN-2 Model Chemistry computational method |
| G3 | GAUSSIAN-3 Improved Model Chemistry computational method |
| HF | Hartree-Fock (low level) *ab initio* computational method. |

| | |
|---|---|
| MP2 | Moller-Plesset Perturbation Theory (second order) computational method. |
| NMR | Nuclear Magnetic Resonance |
| pH | Measure of Acidity (in water solutions, ranges from 0 – acidic, to 14 – basic, pH = - log([H+])) |
| pKa | Measure of Acid Strength, related to pH |
| polyprotic acid | In this case, acids with more than one acidic proton which can be removed in aqueous solution |

# Bibliography

## Chapter 1


1. Frisch, M.J., et al., *Gaussian 03, Revision B.03*. 2003, Gaussian, Inc.: Wallingford CT.
2. Nierenberg, D.W., et al., *Delayed cerebellar disease and death after accidental exposure to dimethylmercury.* New England Journal of Medicine, 1998. **338**(23): p. 1672-1676.
3. Goodsite, M.E., J.M.C. Plane, and H. Skov, *A theoretical study of the oxidation of Hg-0 to HgBr2 in the troposphere.* Environmental Science & Technology, 2004. **38**(6): p. 1772-1776.
4. Tossell, J.A., *Calculation of the energetics for oxidation of gas-phase elemental Hg by Br and BrO.* Journal of Physical Chemistry A, 2003. **107**(39): p. 7804-7808.
5. Khalizov, A.F., et al., *A theoretical study on the reactions of Hg with halogens: Atmospheric implications.* Journal of Physical Chemistry A, 2003. **107**(33): p. 6360-6365.
6. Ariya, P.A. and A. Ryzhkov, *Atmospheric transoformation of elemental mercury upon reactions with halogens.* Journal De Physique Iv, 2003. **107**: p. 57-59.

7. Lindberg, S.E., et al., *Dynamic oxidation of gaseous mercury in the Arctic troposphere at polar sunrise.* Environmental Science & Technology, 2002. **36**(6): p. 1245-1256.

8. Schroeder, W.H., et al., *Arctic springtime depletion of mercury.* Nature, 1998. **394**(6691): p. 331-332.

9. Jitaru, P. and F. Adams, *Toxicity, sources and biogeochemical cycle of mercury.* Journal De Physique Iv, 2004. **121**: p. 185-193.

10. Grigg, J., *Environmental toxins; their impact on children's health.* Archives of Disease in Childhood, 2004. **89**(3): p. 244-250.

11. Bisinoti, M.C. and W.F. Jardim, *Behavior of methylmercury in the environment.* Quimica Nova, 2004. **27**(4): p. 593-600.

12. Tchounwou, P.B., et al., *Environmental exposure to mercury and its toxicopathologic implications for public health.* Environmental Toxicology, 2003. **18**(3): p. 149-175.

13. Clarkson, T.W., L. Magos, and G.J. Myers, *The toxicology of mercury - Current exposures and clinical manifestations.* New England Journal of Medicine, 2003. **349**(18): p. 1731-1737.

14. Ullrich, S.M., T.W. Tanton, and S.A. Abdrashitova, *Mercury in the aquatic environment: A review of factors affecting methylation.* Critical Reviews in Environmental Science and Technology, 2001. **31**(3): p. 241-293.

15. Sweet, L.I. and J.T. Zelikoff, *Toxicology and immunotoxicology of mercury: A comparative review in fish and humans.* Journal of Toxicology and Environmental Health-Part B-Critical Reviews, 2001. **4**(2): p. 161-205.

16. Takizawa, Y., *Understanding minamata disease and strategies to prevent further environmental contamination by methylmercury.* Water Science and Technology, 2000. **42**(7-8): p. 139-146.

17. Satoh, H., *Occupational and environmental toxicology of mercury and its compounds.* Industrial Health, 2000. **38**(2): p. 153-164.

18. Morel, F.M.M., A.M.L. Kraepiel, and M. Amyot, *The chemical cycle and bioaccumulation of mercury.* Annual Review of Ecology and Systematics, 1998. **29**: p. 543-566.

19. Harada, M., *Minamata Disease - Methylmercury Poisoning in Japan Caused by Environmental-Pollution.* Critical Reviews in Toxicology, 1995. **25**(1): p. 1-24.

20. Boffetta, P., E. Merler, and H. Vainio, *Carcinogenicity of Mercury and Mercury-Compounds.* Scandinavian Journal of Work Environment & Health, 1993. **19**(1): p. 1-7.

21. Bakir, F., et al., *Methylmercury Poisoning in Iraq - Interuniversity Report.* Science, 1973. **181**(4096): p. 230-241.

22. Lohman, K., et al., *Sensitivity analysis of mercury human exposure.* Science of the Total Environment, 2000. **259**(1-3): p. 3-11.

23. *CPMD, Copyright IBM Corp 1990-2006, Copyright MPI für Festkörperforschung Stuttgart 1997-2001.*

24. Bartlett, R.J. and G.D. Purvis, *Many-body perturbation theory, coupled-pair many-electron theory, and the importance of quadruple excitations for the correlation problem.* Int. J. Quant. Chem., 1978. **14**(5): p. 561-581.

25. Stevens, W.J., H. Basch, and M. Krauss, *Compact effective potentials and efficient shared-exponent basis sets for the first- and second-row atoms.* J. Chem. Phys., 1984. **81**(12): p. 6026-6033.

26. Stevens, W.J., et al., *Relativistic compact effective potentials and efficient, shared-exponent basis sets for the third-, fourth-, and fifth-row atoms.* Can. J. Chem./Rev. can. chim., 1992. **70**(2): p. 612-630.

27. Becke, A.D., *Density-functional thermochemistry. III. The role of exact exchange.* J. Chem. Phys., 1993. **98**(7): p. 5648-5652.

28. Pople, J.A., M. Head-Gordon, and D.J. Fox, *Gaussian-1 theory: A general procedure for prediction of molecular energies.* J. Chem. Phys., 1989. **90**(10): p. 5622-5629.

29. Riedel, S., M. Straka, and M. Kaupp, *Validation of density functional methods for computing structures and energies of mercury(IV) complexes.* Physical Chemistry Chemical Physics, 2004. **6**(6): p. 1122-1127.

30. van Lenthe, E., E.J. Baerends, and J.G. Snijders, *Relativistic regular two-component Hamiltonians.* J. Chem. Phys., 1993. **99**(6): p. 4597-4610.

31. Perdew, J.P., et al., *Prescription for the design and selection of density functional approximations: More constraint satisfaction with fewer fits.* The Journal of Chemical Physics, 2005. **123**(6): p. 062201.

35. Perdew, J.P., et al., *Atoms, molecules, solids, and surfaces: Applications of the generalized gradient approximation for exchange and correlation.* Phys. Rev. B, 1992. **46**(11): p. 6671-6687.

36. Nierenberg, D.W., et al., *Delayed cerebellar disease and death after accidental exposure to dimethylmercury.* New England Journal of Medicine, 1998. **338**(23): p. 1672-1676.

37. Guerra, C.F., et al., *Towards an order-N DFT method.* Theoretical Chemistry Accounts, 1998. **99**.

35. Velde, G.t., et al., *Chemistry with ADF.* Journal of Compututational Chemistry, 2001. **22**: p. 931.

36. Baerends, E.J., et al., ADF2004.01, SCM, Theoretical Chemistry, Vrije Universiteit, Amsterdam, The Netherlands, http://www.scm.com. 2004.

37. Wolff, S.K., et al., *Density functional calculations of nuclear magnetic shieldings using the zeroth-order regular approximation (ZORA) for relativistic effects: ZORA nuclear magnetic resonance.* Journal of Chemical Physics, 1999. **110**: p. 7689

38. Schreckenbach, G. and T. Ziegler, *The calculation of NMR shielding tensors based on density functional theory and the frozen-core approximation.* International Journal of Quantum Chemistry, 1996. **60**.

39. Schreckenbach, G. and T. Ziegler, The calculation of NMR shielding tensors using GIAO's and modern density functional theory. Journal of Physical Chemistry, 1995. **99**.

## Chapter 2

1. Nierenberg, D.W., et al., *Delayed cerebellar disease and death after accidental exposure to dimethylmercury.* New England Journal of Medicine, 1998. **338**(23): p. 1672-1676.
2. Clarkson, T.W., L. Magos, and G.J. Myers, *The toxicology of mercury - Current exposures and clinical manifestations.* New England Journal of Medicine, 2003. **349**(18): p. 1731-1737.
3. Schroeder, W.H., et al., *Arctic springtime depletion of mercury.* Nature, 1998. **394**(6691): p. 331-332.
4. Ariya, P.A., et al., *The Arctic: a sink for mercury.* Tellus Series B-Chemical and Physical Meteorology, 2004. **56**(5): p. 397-403.
5. Ebinghaus, R., et al., *Antarctic springtime depletion of atmospheric mercury.* Environmental Science & Technology, 2002. **36**(6): p. 1238-1244.
6. Bottenheim, J.W., et al., *Ozone in the Arctic lower troposphere during winter and spring 2000 (ALERT2000).* Atmospheric Environment, 2002. **36**(15-16): p. 2535-2544.

7. Sumner, A.L., et al., *Atmospheric chemistry of formaldehyde in the Arctic troposphere at Polar Sunrise, and the influence of the snowpack.* Atmospheric Environment, 2002. **36**(15-16): p. 2553-2562.

8. Ariya, P.A., A. Khalizov, and A. Gidas, *Reactions of gaseous mercury with atomic and molecular halogens: Kinetics, product studies, and atmospheric implications.* Journal of Physical Chemistry A, 2002. **106**(32): p. 7310-7320.

9. Boudries, H. and J.W. Bottenheim, *Cl and Br atom concentrations during a surface boundary layer ozone depletion event in the Canadian high Arctic.* Geophysical Research Letters, 2000. **27**(4): p. 517-520.

10. Platt, U. and G. Honninger, *The role of halogen species in the troposphere.* Chemosphere, 2003. **52**(2): p. 325-338.

11. Calvert, J.G. and S.E. Lindberg, *A modeling study of the mechanism of the halogen-ozone-mercury homogeneous reactions in the troposphere during the polar spring.* Atmospheric Environment, 2003. **37**(32): p. 4467-4481.

12. Tossell, J.A., *Calculation of the energetics for oxidation of gas-phase elemental Hg by Br and BrO.* Journal of Physical Chemistry A, 2003. **107**(39): p. 7804-7808.

13. Shepler, B.C. and K.A. Peterson, *Mercury monoxide: A systematic investigation of its ground electronic state.* Journal of Physical Chemistry A, 2003. **107**(11): p. 1783-1787.

14. Goodsite, M.E., J.M.C. Plane, and H. Skov, *A theoretical study of the oxidation of Hg-0 to HgBr2 in the troposphere.* Environmental Science & Technology, 2004. **38**(6): p. 1772-1776.

15. Khalizov, A.F., et al., *A theoretical study on the reactions of Hg with halogens: Atmospheric implications.* Journal of Physical Chemistry A, 2003. **107**(33): p. 6360-6365.

16. Sheu, G.R. and R.P. Mason, *An examination of methods for the measurements of reactive gaseous mercury in the atmosphere.* Environmental Science & Technology, 2001. **35**(6): p. 1209-1216.

17. Skov, H., et al., *Fate of elemental mercury in the arctic during atmospheric mercury depletion episodes and the load of atmospheric mercury to the arctic.* Environmental Science & Technology, 2004. **38**(8): p. 2373-2382.

18. Fitzgerald, W.F., et al., *Modern and historic atmospheric mercury fluxes in northern Alaska: Global sources and Arctic depletion.* Environmental Science & Technology, 2005. **39**(2): p. 557-568.

19. Dommergue, A., C.P. Ferrari, and C.F. Boutron, *First investigation of an original device dedicated to the determination of gaseous mercury in interstitial air in snow.* Analytical and Bioanalytical Chemistry, 2003. **375**(1): p. 106-111.

20. Dommergue, A., et al., *Diurnal cycles of gaseous mercury within the snowpack at Kuujjuarapik/Whapmagoostui, Quebec, Canada.* Environmental Science & Technology, 2003. **37**(15): p. 3289-3297.

21. Dommergue, A., et al., *The fate of mercury species in a sub-arctic snowpack during snowmelt.* Geophysical Research Letters, 2003. **30**(12).

22. Ferrari, C.P., et al., *Profiles of Mercury in the snow pack at Station Nord, Greenland shortly after polar sunrise.* Geophysical Research Letters, 2004. **31**(3).

23. Lyons, W.B., K.A. Welch, and J.C. Bonzongo, *Mercury in aquatic systems in Antarctica.* Geophysical Research Letters, 1999. **26**(15): p. 2235-2238.

24. Muir, D.C.G., et al., *Arctic Marine Ecosystem Contamination.* Science of the Total Environment, 1992. **122**(1-2): p. 75-134.

25. Schroeder, W., et al., *Volatilization of Mercury from Lake Surfaces.* Science of the Total Environment, 1992. **125**: p. 47-66.

26. Morel, F.M.M., A.M.L. Kraepiel, and M. Amyot, *The chemical cycle and bioaccumulation of mercury.* Annual Review of Ecology and Systematics, 1998. **29**: p. 543-566.

27. Hsu, H. and D.L. Sedlak, *Strong Hg(II) complexation in municipal wastewater effluent and surface waters.* Environmental Science & Technology, 2003. **37**(12): p. 2743-2749.

28. Bisinoti, M.C. and W.F. Jardim, *Behavior of methylmercury in the environment.* Quimica Nova, 2004. **27**(4): p. 593-600.

29. Baldi, F., *Microbial transformation of mercury species and their importance in the biogeochemical cycle of mercury.* Metal Ions in Biological Systems, Vol 34, 1997. **34**: p. 213-257.

30. Warner, K.A., E.E. Roden, and J.C. Bonzongo, *Microbial mercury transformation in anoxic freshwater sediments under iron-reducing and other electron-accepting conditions.* Environmental Science & Technology, 2003. **37**(10): p. 2159-2165.

31. Tossell, J.A., *Theoretical study of the photodecomposition of methyl Hg complexes.* Journal of Physical Chemistry A, 1998. **102**(20): p. 3587-3591.

32. Hedgecock, I.M. and N. Pirrone, *Chasing quicksilver: Modeling the atmospheric lifetime of Hg-(g)(0) in the marine boundary layer at various latitudes.* Environmental Science & Technology, 2004. **38**(1): p. 69-76.

33. Laurier, F.J.G., et al., *Reactive gaseous mercury formation in the North Pacific Ocean's marine boundary layer: A potential role of halogen chemistry.* Journal of Geophysical Research-Atmospheres, 2003. **108**(D17).

34. Lalonde, J.D., et al., *Photoinduced oxidation of Hg-0 (aq) in the waters from the St. Lawrence estuary.* Environmental Science & Technology, 2004. **38**(2): p. 508-514.

35. Kraepiel, A.M.L., et al., *Sources and variations of mercury in tuna.* Environmental Science & Technology, 2003. **37**(24): p. 5551-5558.

36. Gonzalez, P., et al., *Comparative Effects of Dietary Methylmercury on Gene Expression in Liver, Skeletal Muscle, and Brain of the Zebrafish (Danio rerio).* Environmental Science & Technology, 2005. **ASAP Web Release**.

37. Satoh, H., *Occupational and environmental toxicology of mercury and its compounds.* Industrial Health, 2000. **38**(2): p. 153-164.

38. Bakir, F., et al., *Methylmercury Poisoning in Iraq - Interuniversity Report.* Science, 1973. **181**(4096): p. 230-241.

39. Harada, M., *Minamata Disease - Methylmercury Poisoning in Japan Caused by Environmental-Pollution.* Critical Reviews in Toxicology, 1995. **25**(1): p. 1-24.

40. Takizawa, Y., *Understanding minamata disease and strategies to prevent further environmental contamination by methylmercury.* Water Science and Technology, 2000. **42**(7-8): p. 139-146.

41. Rajar, R., et al., *Application of three-dimensional mercury cycling model to coastal seas.* Ecological Modelling, 2004. **171**(1-2): p. 139-155.

42. Yan, R., D.T. Liang, and J.H. Tay, *Control of mercury vapor emissions from combustion flue gas.* Environmental Science and Pollution Research, 2003. **10**(6): p. 399-407.

43. Tang, S., et al., *Mercury speciation in the flue gas of a small-scale coal-fired boiler in Guiyang, PR China.* Journal De Physique Iv, 2003. **107**: p. 1287-1290.

44. Granite, E.J. and H.W. Pennline, *Photochemical removal of mercury from flue gas.* Industrial & Engineering Chemistry Research, 2002. **41**(22): p. 5470-5476.

45. Sommar, J., O. Lindqvist, and D. Stromberg, *Distribution equilibrium of mercury (II) chloride between water and air applied to flue gas scrubbing.*

Journal of the Air & Waste Management Association, 2000. **50**(9): p. 1663-1666.

46. Abu-Daabes, M.A. and N.G. Pinto, *Synthesis and characterization of a nano-structured sorbent for the direct removal of mercury vapor from flue gases by chelation.* Chemical Engineering Science, 2005. **60**(7): p. 1901-1910.

47. Galbreath, K.C. and C.J. Zygarlicke, *Mercury transformations in coal combustion flue gas.* Fuel Processing Technology, 2000. **65**: p. 289-310.

48. Seigneur, C., et al., *Modeling the atmospheric fate and transport of mercury over North America: power plant emission scenarios.* Fuel Processing Technology, 2004. **85**(6-7): p. 441-450.

49. Fang, F.M., et al., *Atmospheric particulate mercury in Changchun City, China.* Atmospheric Environment, 2001. **35**(25): p. 4265-4272.

50. Friedli, H.R., et al., *Mercury in the atmosphere around Japan, Korea, and China as observed during the 2001 ACE-Asia field campaign: Measurements, distributions, sources, and implications.* Journal of Geophysical Research-Atmospheres, 2004. **109**(D19).

51. Tossell, J.A. and D.J. Vaughan, *Relationships between Valence Orbital Binding-Energies and Crystal-Structures in Compounds of Copper, Silver, Gold, Zinc, Cadmium, and Mercury.* Inorganic Chemistry, 1981. **20**(10): p. 3333-3340.

52. Stromberg, D., O. Gropen, and U. Wahlgren, *Non-Relativistic and Relativistic Calculations on Some Zn, Cd and Hg Complexes.* Chemical Physics, 1989. **133**(2): p. 207-219.

53. Stromberg, D., M. Sandstrom, and U. Wahlgren, *Theoretical Calculations on the Structure of the Hexahydrated Divalent Zinc, Cadmium and Mercury Ions.* Chemical Physics Letters, 1990. **172**(1): p. 49-54.

54. Stromberg, D. and U. Wahlgren, *1st-Order Relativistic Calculations on Au2 and Hg-2(2+).* Chemical Physics Letters, 1990. **169**(1-2): p. 109-115.

55. Stromberg, D., A. Stromberg, and U. Wahlgren, *Relativistic Quantum Calculations on Some Mercury Sulfide Molecules.* Water Air and Soil Pollution, 1991. **56**: p. 681-695.

56. Xiao, Z.F., D. Stromberg, and O. Lindqvist, *Influence of Humic Substances on Photolysis of Divalent Mercury in Aqueous-Solution.* Water Air and Soil Pollution, 1995. **80**(1-4): p. 789-798.

57. Tossell, J.A., *Theoretical studies on the formation of mercury complexes in solution and the dissolution and reactions of cinnabar.* American Mineralogist, 1999. **84**(5-6): p. 877-883.

58. Tossell, J.A., *Calculation of the structures, stabilities, and properties of mercury sulfide species in aqueous solution.* Journal of Physical Chemistry A, 2001. **105**(5): p. 935-941.

59. Balabanov, N.B. and K.A. Peterson, *A systematic ab initio study of the structure and vibrational spectroscopy of HgCl2, HgBr2, and HgBrCl.* Journal of Chemical Physics, 2003. **119**(23): p. 12271-12278.

60. Balabanov, N.B. and K.A. Peterson, *Mercury and reactive halogens: The thermochemistry of Hg+{Cl-2, Br-2, BrCl, ClO, and BrO}*. Journal of Physical Chemistry A, 2003. **107**(38): p. 7465-7470.

61. Filatov, M. and D. Cremer, Revision of the dissociation energies of mercury chalcogendies - Unusual types of mercury bonding. Chemphyschem, 2004. 5(10): p. 1547-1557.

## Chapter 3

1. Schrodinger, E., *An Undulatory Theory of the Mechanics of Atoms and Molecules.* Physical Review, 1926. **28**(6): p. 1049.

2. Pauli, W., *Über das Wasserstoffspektrum vom Standpunkt der neuen Quantenmechanik.* Zeitschrift für Physik A Hadrons and Nuclei, 1926. **36**(5): p. 336-363.

3. Adams, W.H., *Solution of Schrodinger Equation for H2 in Terms of a Wave-Function Least Distorted from a Product of Atomic Wave-Functions.* International Journal of Quantum Chemistry, 1973: p. 127-133.

4. Kolos, W. and Wolniewi.L, *IMPROVED THEORETICAL GROUND-STATE ENERGY OF HYDROGEN MOLECULE.* Journal of Chemical Physics, 1968. **49**(1): p. 404-&.

5. Roothaan, C.C.J., *New Developments in Molecular Orbital Theory.* Reviews of Modern Physics, 1951. **23**(2): p. 69-89.

6. Slater, J.C., *Atomic Shielding Constants.* Physical Review, 1930. **36**(1): p. 57.

7. Harris, F.E. and H.H. Michels, *Multicenter Integrals in Quantum Mechanics. II. Evaluation of Electron-Repulsion Integrals for Slater-Type Orbitals.* The Journal of Chemical Physics, 1966. **45**(1): p. 116-123.

8. Hehre, W.J., R.F. Stewart, and J.A. Pople, *Self-Consistent Molecular-Orbital Methods .I. Use of Gaussian Expansions of Slater-Type Atomic Orbitals.* Journal of Chemical Physics, 1969. **51**(6): p. 2657-&.

9. M. J. Frisch, G.W.T., H. B. Schlegel, G. E. Scuseria, M. A. Robb, J. R. Cheeseman, J. A. Montgomery, Jr., T. Vreven, K. N. Kudin, J. C. Burant, J. M. Millam, S. S. Iyengar, J. Tomasi, V. Barone, B. Mennucci, M. Cossi, G. Scalmani, N. Rega, G. A. Petersson, H. Nakatsuji, M. Hada, M. Ehara, K. Toyota, R. Fukuda, J. Hasegawa, M. Ishida, T. Nakajima, Y. Honda, O. Kitao, H. Nakai, M. Klene, X. Li, J. E. Knox, H. P. Hratchian, J. B. Cross, V. Bakken, C. Adamo, J. Jaramillo, R. Gomperts, R. E. Stratmann, O. Yazyev, A. J. Austin, R. Cammi, C. Pomelli, J. W. Ochterski, P. Y. Ayala, K. Morokuma, G. A. Voth, P. Salvador, J. J. Dannenberg, V. G. Zakrzewski, S. Dapprich, A. D. Daniels, M. C. Strain, O. Farkas, D. K. Malick, A. D. Rabuck, K. Raghavachari, J. B. Foresman, J. V. Ortiz, Q. Cui, A. G. Baboul, S. Clifford, J. Cioslowski, B. B. Stefanov, G. Liu, A. Liashenko, P. Piskorz, I. Komaromi, R. L. Martin, D. J. Fox, T. Keith, M. A. Al-Laham, C. Y. Peng, A.

Nanayakkara, M. Challacombe, P. M. W. Gill, B. Johnson, W. Chen, M. W. Wong, C. Gonzalez, and J. A. Pople, *Gaussian 03, Revision C.02*, 2004, Gaussian, Inc., Wallingford CT.

10. Moller, C. and M.S. Plesset, *Note on an Approximation Treatment for Many-Electron Systems.* Physical Review, 1934. **46**(7): p. 618.
11. Head-Gordon, M., J.A. Pople, and M.J. Frisch, *MP2 energy evaluation by direct methods.* Chemical Physics Letters, 1988. **153**(6): p. 503-506.
12. Čížek, J., *On the Use of the Cluster Expansion and the Technique of Diagrams in Calculations of Correlation Effects in Atoms and Molecules*. Advances in Chemical Physics1969: John Wiley & Sons, Inc. 35-89.
13. Pople, J.A., et al., *Electron Correlation Theories and Their Application to Study of Simple Reaction Potential Surfaces.* International Journal of Quantum Chemistry, 1978. **14**(5): p. 545-560.
14. Becke, A.D., *Density-functional thermochemistry. III. The role of exact exchange.* J. Chem. Phys., 1993. **98**: p. 5648-52.
15. Montgomery, J.A., et al., *A complete basis set model chemistry. VII. Use of the minimum population localization method.* Journal of Chemical Physics, 2000. **112**(15): p. 6532-6542.
16. Montgomery, J.A., et al., *A complete basis set model chemistry. VI. Use of density functional geometries and frequencies.* Journal of Chemical Physics, 1999. **110**(6): p. 2822-2827.

17. Velde, G.t., et al., *Chemistry with ADF.* Journal of Compututational Chemistry, 2001. **22**: p. 931.

18. Guerra, C.F., et al., *Towards an order-N DFT method.* Theoretical Chemistry Accounts, 1998. **99**.

19. Baerends, E.J., et al., *ADF2004.01, SCM, Theoretical Chemistry, Vrije Universiteit, Amsterdam, The Netherlands,* http://www.scm.com. 2004.

20. Lenthe, E.v. and E.J. Baerends, *Optimized Slater-type basis sets for the elements 1-118.* Journal of Computational Chemistry 2003. **24**.

21. Schreckenbach, G. and T. Ziegler, *The calculation of NMR shielding tensors using GIAO's and modern density functional theory.* Journal of Physical Chemistry, 1995. **99**.

22. Schreckenbach, G. and T. Ziegler, *The calculation of NMR shielding tensors based on density functional theory and the frozen-core approximation.* International Journal of Quantum Chemistry, 1996. **60**.

23. Lenthe, E.v., A.E. Ehlers, and E.J. Baerends, *Geometry optimization in the Zero Order Regular Approximation for relativistic effects.* Journal of Chemical Physics, 1999. **110**.

24. Wolff, S.K., et al., *Density functional calculations of nuclear magnetic shieldings using the zeroth-order regular approximation (ZORA) for relativistic effects: ZORA nuclear magnetic resonance.* Journal of Chemical Physics, 1999. **110**: p. 7689

25. J. A. Pople, J.S.B., and R. Seeger, *Theoretical Models Incorporating Electron Correlation.* Int. J. Quant. Chem, 1976. **S10**.

26. K. Raghavachari and J. A. Pople, *Approximate 4th-order perturbation-theory of electron correlation energy.* Int. J. Quant. Chem, 1978. **14**: p. 91-100.

27. Yang, R.G.P.a.W., *Density-functional theory of atoms and molecules.*1989, Oxford: Oxford Univ. Press.

28. Curtiss, L.A., et al., *Gaussian-2 Theory for Molecular-Energies of 1st-Row and 2nd-Row Compounds.* Journal of Chemical Physics, 1991. **94**(11): p. 7221-7230.

29. Curtiss, L.A., et al., *Gaussian-3 (G3) theory for molecules containing first and second-row atoms.* Journal of Chemical Physics, 1998. **109**(18): p. 7764-7776.

30. Curtiss, L.A., et al., *Assessment of Gaussian-2 and density functional theories for the computation of ionization potentials and electron affinities.* Journal of Chemical Physics, 1998. **109**(1): p. 42-55.

31. Curtiss, L.A., et al., *Assessment of Gaussian-2 and density functional theories for the computation of enthalpies of formation.* Journal of Chemical Physics, 1997. **106**(3): p. 1063-1079.

32. Curtiss, L.A., P.C. Redfern, and K. Raghavachari, *Assessment of Gaussian-3 and density-functional theories on the G3/05 test set of experimental energies.* Journal of Chemical Physics, 2005. **123**(12): p. -.

33. Curtiss, L.A., et al., *Assessment of Gaussian-3 and density functional theories for a larger experimental test set.* Journal of Chemical Physics, 2000. **112**(17): p. 7374-7383.

34. Redfern, P.C., et al., *Assessment of Gaussian-3 and density functional theories for enthalpies of formation of C-1-C-16 alkanes.* Journal of Physical Chemistry A, 2000. **104**(24): p. 5850-5854.

35. Xiu-Juan, Q., et al., *Assessment of Performance of G3B3 and CBS-QB3 Methods in Calculation of Bond Dissociation Energies.* Chinese Journal of Chemistry, 2005. **23**(2): p. 194-199.

36. Pickard Iv, F.C., et al., *Comparison of CBS-QB3, CBS-APNO, G2, and G3 thermochemical predictions with experiment for formation of ionic clusters of hydronium and hydroxide ions complexed with water.* The Journal of Chemical Physics, 2005. **122**(2): p. 024302-7.

37. Barone, V. and M. Cossi, *Quantum calculation of molecular energies and energy gradients in solution by a conductor solvent model.* Journal of Physical Chemistry A, 1998. **102**(11): p. 1995-2001.

38. Barone, V., M. Cossi, and J. Tomasi, *Geometry optimization of molecular structures in solution by the polarizable continuum model.* Journal of Computational Chemistry, 1998. **19**(4): p. 404-417.

39. Cossi, M., et al., *Energies, structures, and electronic properties of molecules in solution with the C-PCM solvation model.* Journal of Computational Chemistry, 2003. **24**(6): p. 669-681.

40. Frisch, M.J., J.A. Pople, and J.S. Binkley, *Self-Consistent Molecular-Orbital Methods .25. Supplementary Functions for Gaussian-Basis Sets.* Journal of Chemical Physics, 1984. **80**(7): p. 3265-3269.

41. Hehre, W.J., Ditchfie.R, and J.A. Pople, *Self-Consistent Molecular-Orbital Methods .12. Further Extensions of Gaussian-Type Basis Sets for Use in Molecular-Orbital Studies of Organic-Molecules.* Journal of Chemical Physics, 1972. **56**(5): p. 2257-&.

42. Ditchfie.R, W.J. Hehre, and J.A. Pople, *Self-Consistent Molecular-Orbital Methods .9. Extended Gaussian-Type Basis for Molecular-Orbital Studies of Organic Molecules.* Journal of Chemical Physics, 1971. **54**(2): p. 724-&.

43. Mclean, A.D. and G.S. Chandler, *Contracted Gaussian-Basis Sets for Molecular Calculations .1. 2nd Row Atoms, Z=11-18.* Journal of Chemical Physics, 1980. **72**(10): p. 5639-5648.

44. Stevens, W.J., et al., *Relativistic Compact Effective Potentials and Efficient, Shared-Exponent Basis-Sets for the 3rd-Row, 4th-Row, and 5th-Row Atoms.* Canadian Journal of Chemistry-Revue Canadienne De Chimie, 1992. **70**(2): p. 612-630.

45. Stevens, W.J., H. Basch, and M. Krauss, *Compact Effective Potentials and Efficient Shared-Exponent Basis-Sets for the 1st-Row and 2nd-Row Atoms.* Journal of Chemical Physics, 1984. **81**(12): p. 6026-6033.

46. Cundari, T.R. and W.J. Stevens, *Effective Core Potential Methods for the Lanthanides.* Journal of Chemical Physics, 1993. **98**(7): p. 5555-5565.

47. Wilson, A.K., et al., *Gaussian basis sets for use in correlated molecular calculations. IX. The atoms gallium through krypton.* Journal of Chemical Physics, 1999. **110**(16): p. 7667-7676.

48. Woon, D.E. and T.H. Dunning, *Gaussian-Basis Sets for Use in Correlated Molecular Calculations .3. The Atoms Aluminum through Argon.* Journal of Chemical Physics, 1993. **98**(2): p. 1358-1371.

49. Dunning, T.H., *Gaussian Basis Functions for Use in Molecular Calculations . 1. Contraction of (9s5p) Atomic Basis Sets for First-Row Atoms.* Journal of Chemical Physics, 1970. **53**(7): p. 2823-&.

50. Spitznagel, G.W., et al., *Efficient Diffuse Function-Augmented Basis-Sets for Anion Calculation .4. An Evaluation of the Performance of Diffuse Function-Augmented Basis-Sets for 2nd-Row Elements, Na-Cl.* Journal of Computational Chemistry, 1987. **8**(8): p. 1109-1116.

51. Clark, T., et al., *Efficient Diffuse Function-Augmented Basis-Sets for Anion Calculations .3. The 3-21+G Basis Set for 1st-Row Elements, Li-F.* Journal of Computational Chemistry, 1983. **4**(3): p. 294-301.

52. Halkier, A., et al., *Basis-set convergence of the energy in molecular Hartree-Fock calculations.* Chemical Physics Letters, 1999. **302**(5-6): p. 437-446.

53. Davidson, E.R. and S.J. Chakravorty, *A possible definition of basis set superposition error.* Chemical Physics Letters, 1994. **217**(1-2): p. 48-54.

54. Tossell, J.A., *Calculation of the energetics for oxidation of gas-phase elemental Hg by Br and BrO.* Journal of Physical Chemistry A, 2003. **107**(39): p. 7804-7808.

55. Tossell, J.A., *Calculation of reaction energies in solution: Successes and conundrums.* Abstracts of Papers of the American Chemical Society, 2005. **229**: p. U710-U710.

56. Tossell, J.A. and M.D. Zimmermann, *Calculation of the structures, stabilities, and vibrational spectra of arsenites, thioarsenites and thioarsenates in aqueous solution.* Geochimica Et Cosmochimica Acta, 2008. **72**(21): p. 5232-5242.

57. Boys, S. F., *Electronic Wave Functions. I. A General Method of Calculation for the Stationary States of Any Molecular System*. Proc. R. Soc. Lond. A, 1950, **200**(1063) p. 542-554.

58. Levine, I. N. *Quantum Chemistry*, 3rd ed.; Allyn and Bacon: Massachusetts, 1970.

## Chapter 4

1. Sheu, G.R. and R.P. Mason, *An examination of methods for the measurements of reactive gaseous mercury in the atmosphere.* Environmental Science & Technology, 2001. **35**(6): p. 1209-1216.

2. Sillen, L.G., *Electrometric Investigation of Equilibria between Mercury and Halogen Ions .8. Survey and Conclusions.* Acta Chemica Scandinavica, 1949. **3**(5): p. 539-553.

3. M. J. Frisch, G.W.T., H. B. Schlegel, G. E. Scuseria, M. A. Robb, J. R. Cheeseman, J. A. Montgomery, Jr., T. Vreven, K. N. Kudin, J. C. Burant, J. M. Millam, S. S. Iyengar, J. Tomasi, V. Barone, B. Mennucci, M. Cossi, G. Scalmani, N. Rega, G. A. Petersson, H. Nakatsuji, M. Hada, M. Ehara, K. Toyota, R. Fukuda, J. Hasegawa, M. Ishida, T. Nakajima, Y. Honda, O. Kitao, H. Nakai, M. Klene, X. Li, J. E. Knox, H. P. Hratchian, J. B. Cross, V. Bakken, C. Adamo, J. Jaramillo, R. Gomperts, R. E. Stratmann, O. Yazyev, A. J. Austin, R. Cammi, C. Pomelli, J. W. Ochterski, P. Y. Ayala, K. Morokuma, G. A. Voth, P. Salvador, J. J. Dannenberg, V. G. Zakrzewski, S. Dapprich, A. D. Daniels, M. C. Strain, O. Farkas, D. K. Malick, A. D. Rabuck, K. Raghavachari, J. B. Foresman, J. V. Ortiz, Q. Cui, A. G. Baboul, S. Clifford, J. Cioslowski, B. B. Stefanov, G. Liu, A. Liashenko, P. Piskorz, I. Komaromi, R. L. Martin, D. J. Fox, T. Keith, M. A. Al-Laham, C. Y. Peng, A. Nanayakkara, M. Challacombe, P. M. W. Gill, B. Johnson, W. Chen, M. W. Wong, C. Gonzalez, and J. A. Pople, *Gaussian 03, Revision C.02*, 2004, Gaussian, Inc., Wallingford CT.

4. Halkier, A., et al., *Basis-set convergence of the energy in molecular Hartree-Fock calculations.* Chemical Physics Letters, 1999. **302**(5-6): p. 437-446.

5. Feller, D. and J.A. Sordo, *A CCSDT study of the effects of higher order correlation on spectroscopic constants. I. First row diatomic hydrides.* The Journal of Chemical Physics, 2000. **112**(13): p. 5604-5610.

6. Becke, A.D., *Density-functional thermochemistry. III. The role of exact exchange.* The Journal of Chemical Physics, 1993. **98**(7): p. 5648-5652.

7. Wolff, S.K., et al., *Density functional calculations of nuclear magnetic shieldings using the zeroth-order regular approximation (ZORA) for relativistic effects: ZORA nuclear magnetic resonance.* Journal of Chemical Physics, 1999. **110**: p. 7689

8. Schreckenbach, G. and T. Ziegler, *The calculation of NMR shielding tensors based on density functional theory and the frozen-core approximation.* International Journal of Quantum Chemistry, 1996. **60**.

9. Schreckenbach, G. and T. Ziegler, *The calculation of NMR shielding tensors using GIAO's and modern density functional theory.* Journal of Physical Chemistry, 1995. **99**.

10. Guerra, C.F., et al., *Towards an order-N DFT method.* Theoretical Chemistry Accounts, 1998. **99**.

11. Velde, G.t., et al., *Chemistry with ADF.* Journal of Compututational Chemistry, 2001. **22**: p. 931.

12. Baerends, E.J., et al., ADF2004.01, SCM, Theoretical Chemistry, Vrije Universiteit, Amsterdam, The Netherlands, http://www.scm.com. 2004.

## Chapter 5

1. Moller, C. and M.S. Plesset, *Note on an Approximation Treatment for Many-Electron Systems.* Physical Review, 1934. **46**(7): p. 618.
2. Montgomery, J.A., J.W. Ochterski, and M.J. Frisch, *An improved complete basis set (CBS) model chemistry.* Abstracts of Papers of the American Chemical Society, 1996. **211**: p. 231-PHYS.
3. Lopez, X., et al., *Theoretical Evaluation of pKa in Phosphoranes: Implications for Phosphate Ester Hydrolysis.* Journal of the American Chemical Society, 2002. **124**(18): p. 5010-5018.
4. Alexeev, Y., et al., *Accurate heats of formation and acidities for H3PO4, H2SO4, and H2CO3 from ab initio electronic structure calculations.* International Journal of Quantum Chemistry, 2005. **102**(5): p. 775-784.
5. Jolly, W.L., *Modern Inorganic Chemistry*. 2nd ed 1991, New York: McGraw Hill. 655.
6. Tsuchida, E., *Ab initio molecular-dynamics simulation of concentrated phosphoric acid.* Journal of the Physical Society of Japan, 2006. **75**(5): p. -.
7. Chesnut, D.B., *A Theoretical Study of 31P NMR Chemical Shielding Models for Concentrated Phosphoric Acid Solution.* The Journal of Physical Chemistry A, 2005. **109**(51): p. 11962-11966.
8. M. J. Frisch, G.W.T., H. B. Schlegel, G. E. Scuseria, M. A. Robb, J. R. Cheeseman, J. A. Montgomery, Jr., T. Vreven, K. N. Kudin, J. C. Burant, J. M. Millam, S. S. Iyengar, J. Tomasi, V. Barone, B. Mennucci, M. Cossi, G.

Scalmani, N. Rega, G. A. Petersson, H. Nakatsuji, M. Hada, M. Ehara, K. Toyota, R. Fukuda, J. Hasegawa, M. Ishida, T. Nakajima, Y. Honda, O. Kitao, H. Nakai, M. Klene, X. Li, J. E. Knox, H. P. Hratchian, J. B. Cross, V. Bakken, C. Adamo, J. Jaramillo, R. Gomperts, R. E. Stratmann, O. Yazyev, A. J. Austin, R. Cammi, C. Pomelli, J. W. Ochterski, P. Y. Ayala, K. Morokuma, G. A. Voth, P. Salvador, J. J. Dannenberg, V. G. Zakrzewski, S. Dapprich, A. D. Daniels, M. C. Strain, O. Farkas, D. K. Malick, A. D. Rabuck, K. Raghavachari, J. B. Foresman, J. V. Ortiz, Q. Cui, A. G. Baboul, S. Clifford, J. Cioslowski, B. B. Stefanov, G. Liu, A. Liashenko, P. Piskorz, I. Komaromi, R. L. Martin, D. J. Fox, T. Keith, M. A. Al-Laham, C. Y. Peng, A. Nanayakkara, M. Challacombe, P. M. W. Gill, B. Johnson, W. Chen, M. W. Wong, C. Gonzalez, and J. A. Pople, *Gaussian 03, Revision C.02*, 2004, Gaussian, Inc., Wallingford CT.

9. Head-Gordon, M., J.A. Pople, and M.J. Frisch, *MP2 energy evaluation by direct methods.* Chemical Physics Letters, 1988. **153**(6): p. 503-506.

10. Cossi, M., et al., *Energies, structures, and electronic properties of molecules in solution with the C-PCM solvation model.* Journal of Computational Chemistry, 2003. **24**(6): p. 669-681.

11. Barone, V., M. Cossi, and J. Tomasi, *Geometry optimization of molecular structures in solution by the polarizable continuum model.* Journal of Computational Chemistry, 1998. **19**(4): p. 404-417.

12. Barone, V. and M. Cossi, *Quantum calculation of molecular energies and energy gradients in solution by a conductor solvent model.* Journal of Physical Chemistry A, 1998. **102**(11): p. 1995-2001.
13. Roothaan, C.C.J., *New Developments in Molecular Orbital Theory.* Reviews of Modern Physics, 1951. **23**(2): p. 69-89.
14. Car, R. and M. Parrinello, *Unified Approach for Molecular Dynamics and Density-Functional Theory.* Physical Review Letters, 1985. **55**(22): p. 2471.

## Chapter 6

1. Montgomery, J.A., J.W. Ochterski, and M.J. Frisch, *An improved complete basis set (CBS) model chemistry.* Abstracts of Papers of the American Chemical Society, 1996. **211**: p. 231-PHYS.
2. Barone, V. and M. Cossi, *Quantum calculation of molecular energies and energy gradients in solution by a conductor solvent model.* Journal of Physical Chemistry A, 1998. **102**(11): p. 1995-2001.
3. Zimmermann, M.D. and J.A. Tossell, *Acidities of Arsenic (III) and Arsenic (V) Thio- and Oxyacids in Aqueous Solution using the CBS-QB3/CPCM Method.* Journal of Physical Chemistry A, 2009. **113**(17): p. 5105-5111.
4. Duker, A.A., E.J.M. Carranza, and A. Hale, *Arsenic Geochemistry and Health.* Environ. Int., 2005. **31**.

5. Alexeev, Y., et al., *Accurate heats of formation and acidities for H3PO4, H2SO4, and H2CO3 from ab initio electronic structure calculations.* International Journal of Quantum Chemistry, 2005. **102**(5): p. 775-784.

6. M. J. Frisch, G.W.T., H. B. Schlegel, G. E. Scuseria, M. A. Robb, J. R. Cheeseman, J. A. Montgomery, Jr., T. Vreven, K. N. Kudin, J. C. Burant, J. M. Millam, S. S. Iyengar, J. Tomasi, V. Barone, B. Mennucci, M. Cossi, G. Scalmani, N. Rega, G. A. Petersson, H. Nakatsuji, M. Hada, M. Ehara, K. Toyota, R. Fukuda, J. Hasegawa, M. Ishida, T. Nakajima, Y. Honda, O. Kitao, H. Nakai, M. Klene, X. Li, J. E. Knox, H. P. Hratchian, J. B. Cross, V. Bakken, C. Adamo, J. Jaramillo, R. Gomperts, R. E. Stratmann, O. Yazyev, A. J. Austin, R. Cammi, C. Pomelli, J. W. Ochterski, P. Y. Ayala, K. Morokuma, G. A. Voth, P. Salvador, J. J. Dannenberg, V. G. Zakrzewski, S. Dapprich, A. D. Daniels, M. C. Strain, O. Farkas, D. K. Malick, A. D. Rabuck, K. Raghavachari, J. B. Foresman, J. V. Ortiz, Q. Cui, A. G. Baboul, S. Clifford, J. Cioslowski, B. B. Stefanov, G. Liu, A. Liashenko, P. Piskorz, I. Komaromi, R. L. Martin, D. J. Fox, T. Keith, M. A. Al-Laham, C. Y. Peng, A. Nanayakkara, M. Challacombe, P. M. W. Gill, B. Johnson, W. Chen, M. W. Wong, C. Gonzalez, and J. A. Pople, *Gaussian 03, Revision C.02*, 2004, Gaussian, Inc., Wallingford CT.

7. Curtiss, L.A., et al., *Gaussian-2 Theory for Molecular-Energies of 1st-Row and 2nd-Row Compounds.* Journal of Chemical Physics, 1991. **94**(11): p. 7221-7230.

8. Curtiss, L.A., et al., *Gaussian-3 (G3) theory for molecules containing first and second-row atoms.* Journal of Chemical Physics, 1998. **109**(18): p. 7764-7776.

9. Becke, A.D., *Density-functional thermochemistry. III. The role of exact exchange.* The Journal of Chemical Physics, 1993. **98**(7): p. 5648-5652.

10. Raghavachari, K., et al., *A fifth-order perturbation comparison of electron correlation theories.* Chemical Physics Letters, 1989. **157**(6): p. 479-483.

11. Krishnan, R. and J.A. Pople, Int. J. Quantum Chem., 1978. **14**: p. 91.

12. Head-Gordon, M., J.A. Pople, and M.J. Frisch, Chem. Phys. Lett., 1988. **153**: p. 503.

13. Ramakrishna, V. and B.J. Duke, J. Chem. Phys., 2003. **118**: p. 6137.

14. Truong, T.N. and E.V. Stefanovich, Chem. Phys. Lett., 1995. **240**: p. 253.

15. Alexeev, Y., et al., Intl. J. Quantum Chem., 2005. **104**: p. 379.

16. Liptak, M.D. and G.C. Shields, Int. J. Quantum Chem., 2001. **85**: p. 727.

17. Camaioni, D., J. Phys. Chem. A, 2005. **109**: p. 10795.

18. Pliego, J.R. and J.M. Riveros, Chem. Phys. Lett., 2000. **332**: p. 597.

19. Pliego, J.R. and J.M. Riveros, Phys. Chem. Chem. Phys., 2002. **4**: p. 1622.

20. Tissandier, M.D., et al., J. Phys. Chem. A, 1998. **102**: p. 7787.

21. Zhan, C.G. and D.A. Dixon, J. Phys. Chem. A, 2001. **105**: p. 11534.

## Chapter 7

1. Brownstein, S. and A.E. Stillman, *Proton Resonance Shifts of Acids in Liquid Sulfur Dioxide.* The Journal of Physical Chemistry, 1959. **63**(12): p. 2061-2062.
2. Marcus, Y., *The thermodynamics of solvation of ions. Part 2.-The enthalpy of hydration at 298.15 K.* Journal of the Chemical Society, Faraday Transactions 1: Physical Chemistry in Condensed Phases, 1987. **83**(2): p. 339-349.
3. Kolthoff, ed. *Treatise on Analytical Chemistry*. 1959, Interscience Encyclopedia, Inc.
4. Atkins, P.W. and J.A. Beran, *General Chemistry*. 2nd ed1990, New York: Scientific American Books.
5. Morris, J.C., *The Acid Ionization Constant of HOCl from 5 to 35°.* The Journal of Physical Chemistry, 1966. **70**(12): p. 3798-3805.
6. Zhang, J., et al., *Theoretical study of pKa for perchloric acid.* Journal of Molecular Structure: THEOCHEM, 2009. **906**(1-3): p. 46-49.
7. Montgomery, J.A., et al., *A complete basis set model chemistry. VI. Use of density functional geometries and frequencies.* Journal of Chemical Physics, 1999. **110**(6): p. 2822-2827.
8. Montgomery, J.A., et al., *A complete basis set model chemistry. VII. Use of the minimum population localization method.* Journal of Chemical Physics, 2000. **112**(15): p. 6532-6542.

9. Montgomery, J.A., J.W. Ochterski, and M.J. Frisch, *An improved complete basis set (CBS) model chemistry.* Abstracts of Papers of the American Chemical Society, 1996. **211**: p. 231-PHYS.

10. Francisco, J.S., *Ab Initio Characterization of HOClO3 and HO4Cl: Implications for Atmospheric Chemistry.* The Journal of Physical Chemistry, 1995. **99**(36): p. 13422-13425.

11. Curtiss, L.A., et al., *Gaussian-2 Theory for Molecular-Energies of 1st-Row and 2nd-Row Compounds.* Journal of Chemical Physics, 1991. **94**(11): p. 7221-7230.

12. M. J. Frisch, G.W.T., H. B. Schlegel, G. E. Scuseria, M. A. Robb, J. R. Cheeseman, J. A. Montgomery, Jr., T. Vreven, K. N. Kudin, J. C. Burant, J. M. Millam, S. S. Iyengar, J. Tomasi, V. Barone, B. Mennucci, M. Cossi, G. Scalmani, N. Rega, G. A. Petersson, H. Nakatsuji, M. Hada, M. Ehara, K. Toyota, R. Fukuda, J. Hasegawa, M. Ishida, T. Nakajima, Y. Honda, O. Kitao, H. Nakai, M. Klene, X. Li, J. E. Knox, H. P. Hratchian, J. B. Cross, V. Bakken, C. Adamo, J. Jaramillo, R. Gomperts, R. E. Stratmann, O. Yazyev, A. J. Austin, R. Cammi, C. Pomelli, J. W. Ochterski, P. Y. Ayala, K. Morokuma, G. A. Voth, P. Salvador, J. J. Dannenberg, V. G. Zakrzewski, S. Dapprich, A. D. Daniels, M. C. Strain, O. Farkas, D. K. Malick, A. D. Rabuck, K. Raghavachari, J. B. Foresman, J. V. Ortiz, Q. Cui, A. G. Baboul, S. Clifford, J. Cioslowski, B. B. Stefanov, G. Liu, A. Liashenko, P. Piskorz, I. Komaromi, R. L. Martin, D. J. Fox, T. Keith, M. A. Al-Laham, C. Y. Peng, A.

Nanayakkara, M. Challacombe, P. M. W. Gill, B. Johnson, W. Chen, M. W. Wong, C. Gonzalez, and J. A. Pople, *Gaussian 03, Revision C.02*, 2004, Gaussian, Inc., Wallingford CT.

13. Head-Gordon, M., J.A. Pople, and M.J. Frisch, *MP2 energy evaluation by direct methods.* Chemical Physics Letters, 1988. **153**(6): p. 503-506.
14. Becke, A.D., *Density-functional thermochemistry. III. The role of exact exchange.* The Journal of Chemical Physics, 1993. **98**(7): p. 5648-5652.
15. Barone, V. and M. Cossi, *Quantum calculation of molecular energies and energy gradients in solution by a conductor solvent model.* Journal of Physical Chemistry A, 1998. **102**(11): p. 1995-2001.
16. Barone, V., M. Cossi, and J. Tomasi, *Geometry optimization of molecular structures in solution by the polarizable continuum model.* Journal of Computational Chemistry, 1998. **19**(4): p. 404-417.
17. Cossi, M., et al., *Energies, structures, and electronic properties of molecules in solution with the C-PCM solvation model.* Journal of Computational Chemistry, 2003. **24**(6): p. 669-681.

## Chapter 8

1. Cox, M.E., *Summit outgassing as indicated by radon, mercury and pH mapping, Kilauea volcano, Hawaii.* Journal of Volcanology and Geothermal Research, 1983. **16**(1-2): p. 131-151.

2. Ferrara, R., et al., *Atmospheric mercury emission at Solfatara volcano (Pozzuoli, Phlegraean Fields - Italy).* Chemosphere, 1994. **29**(7): p. 1421-1428.

3. Becke, A.D., *Density-functional thermochemistry. III. The role of exact exchange.* J. Chem. Phys., 1993. **98**: p. 5648-52.

4. Head-Gordon, M., J.A. Pople, and M.J. Frisch, *MP2 energy evaluation by direct methods.* Chemical Physics Letters, 1988. **153**(6): p. 503-506.

5. J. A. Pople, J.S.B., and R. Seeger, *Theoretical Models Incorporating Electron Correlation.* Int. J. Quant. Chem, 1976. **S10**.

6. Čížek, J., *On the Use of the Cluster Expansion and the Technique of Diagrams in Calculations of Correlation Effects in Atoms and Molecules*. Advances in Chemical Physics1969: John Wiley & Sons, Inc. 35-89.

7. K. Raghavachari and J. A. Pople, *Approximate 4th-order perturbation-theory of electron correlation energy.* Int. J. Quant. Chem, 1978. **14**: p. 91-100.

8. Cundari, T.R. and W.J. Stevens, *Effective Core Potential Methods for the Lanthanides.* Journal of Chemical Physics, 1993. **98**(7): p. 5555-5565.

9. Stevens, W.J., H. Basch, and M. Krauss, *Compact Effective Potentials and Efficient Shared-Exponent Basis-Sets for the 1st-Row and 2nd-Row Atoms.* Journal of Chemical Physics, 1984. **81**(12): p. 6026-6033.

10. Stevens, W.J., et al., *Relativistic Compact Effective Potentials and Efficient, Shared-Exponent Basis-Sets for the 3rd-Row, 4th-Row, and 5th-Row Atoms.*

Canadian Journal of Chemistry-Revue Canadienne De Chimie, 1992. **70**(2): p. 612-630.

11. Baldi, F., *Microbial transformation of mercury species and their importance in the biogeochemical cycle of mercury.* Metal Ions in Biological Systems, 1997. 34(34): p. 213-257.

## Chapter 9

1. Harada, M., *Minimata Disease - Methylmercury Poisoning in Japan Caused by Environmental-Pollution.* Critical Reviews in Toxicology, 1995. **25**(1): p. 1-24.
2. Takizawa, Y., *Understanding minamata disease and strategies to prevent further environmental contamination by methylmercury.* Water Science and Technology, 2000. **42**(7-8): p. 139-146.
3. Bakir, F. and e. al., *Methylmercury Poisoning in Iraq - Interuniversity Report.* Science, 1973. **181**(4096): p. 230-241.
4. Yan, R., D.T. Liang, and J.H. Tay, *Control of mercury vapor emissions from combustion flue gas.* Environmental Science and Pollution Research, 2003. **10**(6): p. 399-407.
5. Nierenberg, D.W., et al., *Delayed cerebellar disease and death after accidental exposure to dimethylmercury.* New England Journal of Medicine, 1998. **338**(23): p. 1672-1676.

6. Barone, V. and M. Cossi, *Quantum calculation of molecular energies and energy gradients in solution by a conductor solvent model.* Journal of Physical Chemistry A, 1998. **102**(11): p. 1995-2001.

7. Barone, V., M. Cossi, and J. Tomasi, *Geometry optimization of molecular structures in solution by the polarizable continuum model.* Journal of Computational Chemistry, 1998. **19**(4): p. 404-417.

8. Cossi, M., et al., *Energies, structures, and electronic properties of molecules in solution with the C-PCM solvation model.* Journal of Computational Chemistry, 2003. **24**(6): p. 669-681.

9. Roothaan, C.C.J., *New Developments in Molecular Orbital Theory.* Reviews of Modern Physics, 1951. **23**(2): p. 69-89.

10. Head-Gordon, M., J.A. Pople, and M.J. Frisch, *MP2 energy evaluation by direct methods.* Chemical Physics Letters, 1988. **153**(6): p. 503-506.

11. Becke, A.D., *Density-functional thermochemistry. III. The role of exact exchange.* The Journal of Chemical Physics, 1993. **98**(7): p. 5648-5652.

12. Čížek, J., *On the Use of the Cluster Expansion and the Technique of Diagrams in Calculations of Correlation Effects in Atoms and Molecules*. Advances in Chemical Physics1969: John Wiley & Sons, Inc. 35-89.

13. Stevens, W.J., H. Basch, and M. Krauss, *Compact Effective Potentials and Efficient Shared-Exponent Basis-Sets for the 1st-Row and 2nd-Row Atoms.* Journal of Chemical Physics, 1984. **81**(12): p. 6026-6033.

14. Krauss, M., W.J. Stevens, and H. Basch, *Relativistic Effective Potential Scf Calculations of Agh and Auh.* Journal of Computational Chemistry, 1985. **6**(4): p. 287-295.

15. Stevens, W.J., et al., *Relativistic Compact Effective Potentials and Efficient, Shared-Exponent Basis-Sets for the 3rd-Row, 4th-Row, and 5th-Row Atoms.* Canadian Journal of Chemistry-Revue Canadienne De Chimie, 1992. **70**(2): p. 612-630.

16. Cundari, T.R. and W.J. Stevens, *Effective Core Potential Methods for the Lanthanides.* Journal of Chemical Physics, 1993. **98**(7): p. 5555-5565.

## Chapter 10

1. Turner, B.L., et al., *Inositol phosphates in the environment.* Philos Trans R Soc Lond B Biol Sci., 2002. **357**(1420): p. 449-469.

2. Heighton, L., W.F. Schmidt, and R.L. Siefert, *Kinetic and Equilibrium Constants of Phytic Acid and Ferric and Ferrous Phytate Derived from Nuclear Magnetic Resonance Spectoscopy.* Journal of Agricultural and Food Chemistry, 2008. **56**: p. 9543-9547.

3. Heighton, L., et al., *Electrospray ionization mass spectroscopy shows speciation of phytate to be pH dependent.* Journal of Food, Agriculture & Environment, 2008. **6**(2): p. 401-407.

4. Yang, H.-F., et al., *Electrochemical and Surface Enhanced Raman Scattering Spectroelectrochemical Study of Phytic Acid on the Silver Electrode.* J. Phys. Chem. B., 2004. **108**: p. 17412-17417.

5. Heighton, L.P. and W.F. Schmidt. *Raman spectra of organic (myo-inositol hexakis phosphate) and inorganic P sepctra show pH dependence.* in *Proceedings of American Chemical Society National Meeting*. 2009. Washington, D.C.

6. Roothaan, C.C.J., *New Developments in Molecular Orbital Theory.* Reviews of Modern Physics, 1951. **23**(2): p. 69-89.

7. Becke, A.D., *Density-functional thermochemistry. III. The role of exact exchange.* The Journal of Chemical Physics, 1993. **98**(7): p. 5648-5652.

8. M. J. Frisch, G.W.T., H. B. Schlegel, G. E. Scuseria, M. A. Robb, J. R. Cheeseman, J. A. Montgomery, Jr., T. Vreven, K. N. Kudin, J. C. Burant, J. M. Millam, S. S. Iyengar, J. Tomasi, V. Barone, B. Mennucci, M. Cossi, G. Scalmani, N. Rega, G. A. Petersson, H. Nakatsuji, M. Hada, M. Ehara, K. Toyota, R. Fukuda, J. Hasegawa, M. Ishida, T. Nakajima, Y. Honda, O. Kitao, H. Nakai, M. Klene, X. Li, J. E. Knox, H. P. Hratchian, J. B. Cross, V. Bakken, C. Adamo, J. Jaramillo, R. Gomperts, R. E. Stratmann, O. Yazyev, A. J. Austin, R. Cammi, C. Pomelli, J. W. Ochterski, P. Y. Ayala, K. Morokuma, G. A. Voth, P. Salvador, J. J. Dannenberg, V. G. Zakrzewski, S. Dapprich, A. D. Daniels, M. C. Strain, O. Farkas, D. K. Malick, A. D. Rabuck, K. Raghavachari, J. B. Foresman, J. V. Ortiz, Q. Cui, A. G. Baboul,

S. Clifford, J. Cioslowski, B. B. Stefanov, G. Liu, A. Liashenko, P. Piskorz, I. Komaromi, R. L. Martin, D. J. Fox, T. Keith, M. A. Al-Laham, C. Y. Peng, A. Nanayakkara, M. Challacombe, P. M. W. Gill, B. Johnson, W. Chen, M. W. Wong, C. Gonzalez, and J. A. Pople, *Gaussian 03, Revision C.02*, 2004, Gaussian, Inc., Wallingford CT.

## Chapter 11

1. Roothaan, C.C.J., *New Developments in Molecular Orbital Theory.* Reviews of Modern Physics, 1951. **23**(2): p. 69-89.
2. Pople, J.A., et al., *Electron Correlation Theories and Their Application to Study of Simple Reaction Potential Surfaces.* International Journal of Quantum Chemistry, 1978. **14**(5): p. 545-560.
3. Montgomery, J.A., et al., *A complete basis set model chemistry. VI. Use of density functional geometries and frequencies.* Journal of Chemical Physics, 1999. **110**(6): p. 2822-2827.
4. Montgomery, J.A., et al., *A complete basis set model chemistry. VII. Use of the minimum population localization method.* Journal of Chemical Physics, 2000. **112**(15): p. 6532-6542.
5. Halkier, A., et al., *Basis-set convergence of the energy in molecular Hartree-Fock calculations.* Chemical Physics Letters, 1999. **302**(5-6): p. 437-446.

6. Barone, V. and M. Cossi, *Quantum calculation of molecular energies and energy gradients in solution by a conductor solvent model.* Journal of Physical Chemistry A, 1998. **102**(11): p. 1995-2001.

7. Barone, V., M. Cossi, and J. Tomasi, *Geometry optimization of molecular structures in solution by the polarizable continuum model.* Journal of Computational Chemistry, 1998. **19**(4): p. 404-417.

8. Cossi, M., et al., *Energies, structures, and electronic properties of molecules in solution with the C-PCM solvation model.* Journal of Computational Chemistry, 2003. **24**(6): p. 669-681.

9. Wolff, S.K., et al., *Density functional calculations of nuclear magnetic shieldings using the zeroth-order regular approximation (ZORA) for relativistic effects: ZORA nuclear magnetic resonance.* Journal of Chemical Physics, 1999. **110**: p. 7689

10. Schreckenbach, G. and T. Ziegler, *The calculation of NMR shielding tensors using GIAO's and modern density functional theory.* Journal of Physical Chemistry, 1995. **99**.

11. Schreckenbach, G. and T. Ziegler, *The calculation of NMR shielding tensors based on density functional theory and the frozen-core approximation.* International Journal of Quantum Chemistry, 1996. **60**.

12. Baerends, E.J., et al., *ADF2004.01, SCM, Theoretical Chemistry, Vrije Universiteit, Amsterdam, The Netherlands,* http://www.scm.com. 2004.

13. Velde, G.t., et al., *Chemistry with ADF.* Journal of Compututational Chemistry, 2001. **22**: p. 931.

14. Guerra, C.F., et al., *Towards an order-N DFT method.* Theoretical Chemistry Accounts, 1998. **99**.

15. M. J. Frisch, G.W.T., H. B. Schlegel, G. E. Scuseria, M. A. Robb, J. R. Cheeseman, J. A. Montgomery, Jr., T. Vreven, K. N. Kudin, J. C. Burant, J. M. Millam, S. S. Iyengar, J. Tomasi, V. Barone, B. Mennucci, M. Cossi, G. Scalmani, N. Rega, G. A. Petersson, H. Nakatsuji, M. Hada, M. Ehara, K. Toyota, R. Fukuda, J. Hasegawa, M. Ishida, T. Nakajima, Y. Honda, O. Kitao, H. Nakai, M. Klene, X. Li, J. E. Knox, H. P. Hratchian, J. B. Cross, V. Bakken, C. Adamo, J. Jaramillo, R. Gomperts, R. E. Stratmann, O. Yazyev, A. J. Austin, R. Cammi, C. Pomelli, J. W. Ochterski, P. Y. Ayala, K. Morokuma, G. A. Voth, P. Salvador, J. J. Dannenberg, V. G. Zakrzewski, S. Dapprich, A. D. Daniels, M. C. Strain, O. Farkas, D. K. Malick, A. D. Rabuck, K. Raghavachari, J. B. Foresman, J. V. Ortiz, Q. Cui, A. G. Baboul, S. Clifford, J. Cioslowski, B. B. Stefanov, G. Liu, A. Liashenko, P. Piskorz, I. Komaromi, R. L. Martin, D. J. Fox, T. Keith, M. A. Al-Laham, C. Y. Peng, A. Nanayakkara, M. Challacombe, P. M. W. Gill, B. Johnson, W. Chen, M. W. Wong, C. Gonzalez, and J. A. Pople, *Gaussian 03, Revision C.02*, 2004, Gaussian, Inc., Wallingford CT.

16. Takizawa, Y., *Understanding minamata disease and strategies to prevent further environmental contamination by methylmercury.* Water Science and Technology, 2000. **42**(7-8): p. 139-146.

17. Bakir, F. and e. al., *Methylmercury Poisoning in Iraq - Interuniversity Report.* Science, 1973. **181**(4096): p. 230-241.

19. Heighton, L.P. and W.F. Schmidt. *Raman spectra of organic (myo-inositol hexakis phosphate) and inorganic P sepctra show pH dependence.* in *Proceedings of American Chemical Society National Meeting*. 2009. Washington, D.C.